XXXIII OSTIV CONGRESS

8 - 13 January 2017
Benalla, Victoria, Australia

Congress Program and Proceedings

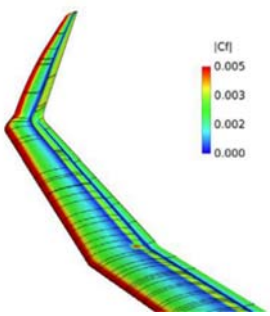

Die Deutsche Bibliothek – CIP Einheitsaufnahme

Die Deutsche Nationalbibliothek verzeichnet diese Publikation in der Deutschen Nationalbibliografie; detaillierte bibliografische Daten sind im Internet unter http://dnb.d-nb.de abrufbar.

Rolf Radespiel (Ed.)

XXXIII OSTIV Congress – Congress Program and Proceedings

ISBN 978-3-928628-85-3

Publisher of OSTIV Conference Proceedings:

TU Braunschweig – Niedersächsisches Forschungszentrum für Luftfahrt
Hermann-Blenk-Straße 27 • 38108 Braunschweig • Germany
Tel: 0531-391-9822 • Fax: 0531-391-9804
Mail: nfl@tu-braunschweig.de
Internet: www.tu-braunschweig.de/nfl

NFL
am Campus Forschungsflughafen

PapatyaBilim Yayınevi (DaisyScience Publishing House)
Ankara Cad. Prof. Dr. F. Kerim Gökay İşhanı Girişi No: 11/3
Cağaloğlu (Fatih) • İstanbul • Turkey
Sertifa No: 11218
Tel: +90 212 527 52 06
Internet: www.papatyabilim.com.tr

Welcome to the OSTIV Congress 2017 in Australia. Every two years the Congress offers new information and latest research results in soaring and sailplane technology to scientists and engineers from all over the world. The meeting presents unique opportunities for scientific exchange and coordination of future activities.

This year the Congress is hosted by the Gliding Federation of Australia, along with the 34th FAI World Gliding Championships, in Benalla, Victoria. We are thankful that the OSTIV Congress can take place in the Benalla Performing Arts Centre (BPACC) near the club house at Benalla Airfield.

We thank our industrial sponsors, Alexander Schleicher Segelflugzeugbau, GP Gliders, Jonker Sailplanes, and Schempp-Hirth Flugzeugbau, who made it possible for us to offer free access to the Congress and give special support to participating students.

The Call for Abstracts issued by OSTIV generated response by engineers and scientists from 11 countries worldwide. The received extended abstracts were reviewed, and they are published in this proceeding booklet. We believe that a varied program has been generated this way. For their efforts in recruiting high-quality contributions we acknowledge the members of the Program Committee:

Zafer Aslan, Turkey	Götz Bramesfeld, Canada	Helmut Fendt, Germany
Mark Maughmer, USA	Judah Milgram, USA	Ian Oldaker, Canada
Lukáš Popelka, Czech Republic	Rolf Radespiel, Germany	Gerard Robertson, New Zealand

Preparing the Congress took endless hours of work by the Organizing Team, consisting of Murray Stimson, Australia, Stu Smith, Australia, Rolf Radespiel, Germany and Britta Schlenker, Germany. We are very thankful for their efforts. Our thanks also go to Alexander Barklage and Tim Landa of Technische Universität Braunschweig for booklet editing.

The OSTIV Congress is the perfect setting to bestow the OSTIV Prize 2017 and the OSTIV Best Student Paper Awards. We look forward to the Opening Ceremony and the Congress Closing Dinner for presenting the Award Winners.

We wish all Congress participants an exciting and rewarding week in Benalla.

Prof. Rolf Radespiel — OSTIV President

Prof. Mark Maughmer — OSTIV Vice President

OSTIV acknowledges support provided by

Welcome to Benalla for the XXXIII OSTIV Congress

Benalla is a town of around 10,000 people situated 200km NE of Melbourne on the main Melbourne-Sydney train line and freeway (the "Hume"). It has been a significant regional town since European settlement the 1840s. The original inhabitants are the Taungurong people, who must have had abundant resources with the rivers, swamps, plains and hills in this rich area. Today Benalla's resources for eating, entertainment and accommodation are greater than a town of its size due to it having a major Motor Racing circuit at Winton used most weekends except mid-summer, and Australia's premier gliding club, GCV, to keep it busy over the summer. Benalla also boasts a major regional Art Gallery, many fine parks, a "must-see' local museum, 2 Golf Clubs, a wide range of shops, cafés, restaurants and hotels.

The Great OSTIV BUS TOUR of North East Victoria **Wednesday 11th Jan. 2017**

OSTIV delegates are invited to join in on this fun tour. Doug Hamilton of Precision Airmotive at Wangaratta has generously offered to allow us a special viewing of his Warbird Restoration business. Current aircraft include P-40 Kittyhawk, PT-22 Ryan, Lockheed 12, Harvard and many others in and around his business. P-40 construction is in progress. Doug expects to soon offer P-40 rides too!

From "Wang" the tour continues east to Milawa for a morning tea stop at this village bakery (user pays, not included in price). Passing through Myrtleford (quickstop) we head up to the Alpine plateau of Mt Buffalo for cool air and a scenic spot for lunch. You'll get a good view of the alpine soaring conditions in the WGC contest area. We then descend and head to the Warby Ranges for wine tasting of our best Reds, Muscat, Tokay and Port, at a personal favourite, Baileys of Glenrowan, est. 1870. After a leisurely tipple, the tour picks up again and heads for the Winton Wetlands, a natural depression with much Australian birdlife. From there we'll have you back at the airfield in time to see the finishing gliders.

Cost: $30 per person includes lunch and wine tasting.

Departs: Benalla Airfield near BPACC. Meet 8.45am for a strict 9:00am departure

Please pay at registration time. OSTIV wishes to thank our Tour Partners:

Precision Airmotive & Classic Air Adventures – Doug Hamilton
Absolutely Delicious – lunch cuisine from Sue & Kelly
Baileys of Glenrowan
Benalla Bus & Coach Lines

OSTIV Congress Dinner @ North Eastern Hotel **Friday 13th January 2017**

After the fascination of a solid week of technical presentations, all OSTIV Speakers, Delegates, family and friends of OSTIV are invited to enjoy a relaxed and friendly dinner together at the North Eastern Hotel in Benalla. (1Nunn St, near the Benalla Railway Station) from about 7:00 for 7:30 pm. This is really a lovely restaurant, disguised as a classic old Aussie country hotel. You'll find excellent quality cuisine and a great range of wines. Drinks from the bar, pay as you go, and order meals off the menu, so you can eat light, or have couple of courses, or have 3 or more. No set fee, you pay for what you order. We'll almost take over the whole place, so it could go late! It is centrally located and therefore walking distance to most accommodation. You can spend $20 eating very light or $100, but allowing $50-60 each would be roughly two courses with a couple of drinks.

Please advise attendance and numbers at Registration desk when you register.

Stu Smith and Murray Stimson

	Sunday, 8 January 2017
	Rotunda in the Rose Garden, Botantical Gardens, Bridge St, Benalla VIC 3672
15:45 - 16:30	Opening Ceremony and Presentation of OSTIV-Prize 2017

	Monday, 9 January 2017
	Benalla Performing Arts Centre (BPACC), 57 Samaria Rd, Benalla VIC 3672
08:00 - 10:00	registration BPACC Room 3
	Aging Sailplane Structures BPACC Room 1+2 Chair: Helmut Fendt
09:00 - 09:30	PIK-20D GLIDER FATIGUE REVIEW. E. Soinne , Helsinki, Finland.
09:30 - 10:00	RISK OF FLUTTER IN AGING SAILPLANES. U. Kopp, J. Gross, Braunschweig, Germany.
10:00 - 10:30	A CASE STUDY IN GELCOAT CRACK PROPAGATION BELOW PU PAINT. R. Hanbury, Broadmeadows, Australia.
10:30 - 11:00	coffee break
	Sailplane Safety BPACC Room 1+2 Chair: Helmut Fendt
11:00 - 11:30	IS IT NECESSARRY TO UPDATE SPIRAL DIVE REQUIREMENTS? G. Waibel, Bad Hindelang, Germany.
11:30 - 12:00	PERCEPTUAL ERRORS IN THE TURN FROM BASE TO FINAL. D. Johnson, Menomonie, Wisconsin, USA.
12:00 - 12:30	COMPARATIVE STATISTICAL ANALYSIS OF FATAL SPIN ACCIDENTS FOR TRAINING GLIDERS. S. Smith, M. G. Stimson, Melbourne, Australia.
12:30 - 14:00	lunch break / registration
	Electric Propulsion BPACC Room 1+2 Chair: Helmut Fendt
14:00 - 14:30	ELECTRIC PROPULSION FOR GLIDING - STATE OF THE ART AND FUTURE. A. Lange, Zweibrücken, Germany. (withdrawn)
14:30 - 15:00	SIDE-BY-SIDE FLYING WITH E-POWER: INDEPENDENT AND SAFE. L. Muth, Wildau, Germany.
15:00 - 15:30	coffee break
	Medical Factors BPACC Room 1+2 Chair: Stu Smith
15:30 - 16:00	FIELD PHYSIOLOGY: INFLIGHT MEASUREMENTS TO MONITOR OXYGEN SATURATIONS OF PILOTS DURING HIGH-ALTITUDE GLIDER FLIGHTS OF THE MOUNTAIN WAVE PROJECT IN THE HIMALAYAN REGION AND THE FRENCH ALPS. C. Ledderhos, R. Heise, Ch. Gamel, A. Gens, Fürstenfeldbruck, Germany.
16:00 - 16:30	LOW-ALTITUDE HYPOXIA. D. Johnson, Menomonie, Wisconsin, USA.
	Evening Session BPACC Auditorium Chair: Stu Smith
20:00 - 20:30	FES TECHNOLOGY DEVELOPMENT MILESTONES. L. Žnidaršič, Logatec, Slovenia.
20:30 - 21:30	INITIATIVE PROSEGELFLIEGER - A PACKAGE OF MEASURES FOR THE EFFECTIVE ENHANCEMENT OF PASSIVE SAFETY OF SAILPLANES. M. Volck, Wiener Neustadt, Austria.

	Tuesday, 10 January 2017
	Benalla Performing Arts Centre (BPACC)
08:00 - 09:00	registration BPACC Room 3
	Boundary Layers BPACC Room 1+2 Chair: Mark Maughmer
09:00 - 09:30	INFLUENCE OF ZIGZAG-TAPE ON PROFILE DRAG AT LOW REYNOLDS NUMBERS. T. Hofmacher, P. Scholz, Braunschweig, Germany.
09:30 - 10:00	LAMINAR-TURBULENT TRANSITION ON WINGS WITH 3D FLOW EFFECTS. F. Muñoz, M. Kruse, R. Petzold, R. Radespiel, Braunschweig, Germany.
10:00 - 10:30	VALIDATION OF NUMERICAL MODELS FOR TRANSITIONAL FLOWS ON AIRFOILS. J. Příhoda, P. Straka, J. Fürst, L. Popelka, D. Šimurda, Praha, Czech Republic.
10:30 - 11:00	EFFECTS OF STRUCTURAL MOTION ON SEPARATION AND SEPARATION CONTROL: AN INTEGRATED INVESTIGATION USING NUMERICAL SIMULATIONS, THEORY, WIND-TUNNEL AND FREE-FLIGHT EXPERIMENTS. H. Fasel, S. Hosseinverdi, J. Little, A. Gross, Tucson, USA.
11:00 - 11:30	coffee break
	Sailplane Performance BPACC Room 1+2 Chair: Murray Stimson
11:30 - 11:50	SPEED-TO-FLY THEORY #1: INSIGHTS ON THE IMPLICATIONS OF FLYING INCORRECT SPEEDS WITH QUADRATIC AND NON-QUADRATIC POLARS. M. Steckner, Beachwood, USA.
11:50 - 12:10	SPEED-TO-FLY THEORY #2: IMPLICATIONS OF FLIGHT TEST DATA VARIABILITY. M. Steckner, Beachwood, USA.
12:10 - 12:30	SPEED-TO-FLY THEORY #3: POTENTIAL ISSUES WITH MODERN SAILPLANES WITH NON-QUADRATIC POLARS. M. Steckner, Beachwood, USA.
12:30 - 14:00	lunch break
	Atmospheric Waves BPACC Room 1+2 Chair: Zafer Aslan
14:00 - 14:30	USING DATA FROM HIGH-ALTITUDE SAILPLANE FLIGHTS TO STUDY ATMOSPHERIC MOUNTAIN WAVES. R. Millane, N. Zhang, E. Enevoldson, J. Murray, Christchurch, New Zealand and Edwards, USA.
14:30 - 15:00	THE HARZ-FOEHN-PROJECT - EMPIRICAL RESEARCH ON MOUNTAIN WAVES IN AN NORTHERN GERMAN LOW MOUNTAIN RANGE. K.-H. Dannhauer, Leipzig, Germany.
15:00 - 15:30	coffee break
	Atmospheric Convection BPACC Room 1+2 Chair: Rick Millane
15:30 - 16:00	HEAT TRANSFER BY CONVECTION FROM THE GROUND TO A TYPICAL AUSTRALIAN THERMAL. D. M. Wilson , Glen Iris, Australia.
16:00 - 16:30	INVESTIGATION OF THE VEGETATION EFFECTS ON CONVECTION BY USING COSMO-CLM. N. Akataş, S. Yeşilköy, Z. Aslan , Istanbul, Turkey.

	Wednesday, 11 January 2017
08:00 - 09:00	registration BPACC Room 3
	Departing Benalla Air Field, Carpark BPACC
09:30 - 17:00	**Excursion to North East Victoria region**
	Wangaratta Warbirds, Mt Buffalo / Victorian Alps, Baileys Winery, Winton Wetlands
	Benalla Performing Arts Centre (BPACC)
	Evening Session BPACC Auditorium Chair: Rolf Radespiel
20:00 - 21:30	FUTURE OF THE OPEN CLASS. Panel Discussion: Loek Boermans, Tilo Holighaus, Atti Jonker, Axel Lange, Gerhard Waibel.

	Thursday, 12 January 2017
	Benalla Performing Arts Centre (BPACC)
	Configuration Aerodynamics BPACC Room 1+2 Chair: Rolf Radespiel
09:00 - 09:30	SAILPLANE WINGLETS: HOW MANY TIPS ARE TOO MANY TIPS? T. Krebs, G. Bramesfeld, Toronto, Canada.
09:30 - 10:00	INVESTIGATING DESIGNS OF AUTONOMOUS GLIDER EXPLORATION OF OUTER SOLAR SYSTEM ATMOSPHERES. C. Colletti, R. P. LeBeau, G. Bramesfeld, Saint Louis, USA.
10:00 - 10:30	THE USE OF COMPUTATIONAL FLUID DYNAMICS ANALYSIS IN WING-WINGLET DESIGN. M. D. Maughmer, J. G. Coder, University Park, PE, USA.
10:30 - 11:00	coffee break
	Sailplane Loads BPACC Room 1+2 Chair: Götz Bramesfeld
11:00 - 11:30	ON THE GUST LOAD OF SAILPLANES. L. M. M. Boermans, Delft, Netherlands.
11:30 - 12:00	LIFETIME CONSIDERATIONS ON SAILPLANES. C. Kensche, J. Wassenaar, Bruchsal, Germany.
12:00 - 13:30	lunch break

	Soaring in Atmosphere BPACC Room 1+2 Chair: Zafer Aslan
13:30 - 14:00	DO NOT GET CAUGHT-ON-TOP! E. Hindman, Wurtsboro, USA.
14:00 - 14:30	GRAVITY WAVE OVER FLAT TERRAIN. D. Johnson, Menomonie, Wisconsin, USA.
	Meteorology Poster Session BPACC Room 1+2 Chair: Edward Hindman
14:30 - 14:40	COMPARISON OF FIELD MEASUREMENTS AND MODIS ALBEDO DATA AND ITS EFFECT ON LATENT HEAT FLUX. S. Yeşilköy, N. Akataş, L. Şaylan, F. Bakanoğulları, Z. Aslan, Istanbul, Turkey.
14:40 - 14:50	ATMOSPHERIC CONVECTION AND SEA SURFACE TEMPERATURE. İ. Osanmaz, Istanbul, Turkey.
14:50 - 15:00	CLIMATE CHANGE, AVIATION AND GLIDING. A. Tokgözlü, K. Temurçin, K. Yasdıman Uysal, İnönü-Eskişehir, Turkey.
15:00 - 15:10	HIGH EVAPOTRANSPIRATION AND HUMIDITY ON THE AVIATION AND SOARING. F. Dökmen, Z. Aslan, Kocaeli, Turkey.
15:10 - 15:30	Poster Discussions
15:30 – 16:00	coffee break
	OSTIV Meteorology Panel Meeting Chair: Zafer Aslan
16:00 - 18:00	Contributions by Edward Hindman; Loek M. M. Boerman; René Heise, Thorsten Reinhardt, Peter Frei, Ralph Paul; Bruno Neininger, David Braig, René Heise and Frank Janser; Rick Millane and Morgan Sandercock; Fred Kucharski, Zafer Aslan, Uğur Şener; Ramazan Çağlar, Serhat Şeker, Jelena Dikun, T. Çetin Akıncı, Emel Önal, Emine Ayaz.
	New developments in weather forecasting models for soaring flights, new trends in mountain wave analyses, short - term forecasting of soaring parameters, wind speed, wind shear, turbulence, high altitude sailplane flights, ABL.
	Evening Session BPACC Auditorium Chair: Murray Stimson
20:00 - 21:30	THE FIRST YEAR IN ARGENTINA WITH THE PERLAN 2 GLIDER. M. Sandercock, Bend, USA.

	Friday, 13 January 2017
	Benalla Performing Arts Centre (BPACC)
	Sailplane Propulsion BPACC Room 1+2 Chair: Götz Bramesfeld
09:00 - 09:30	ELECTRIC PROPULSION IN GLIDERS IS MORE THAN AN ALTERNATIVE TO TRADITIONAL COMBUSTION ENGINES. R. Klein, Mosbach, Germany.
09:30 - 10:00	INVESTIGATIONS INTO THE DESIGN OF A TWO-SEAT SELF-LAUNCHING MOTOR GLIDER. R. Taouk, K.C. Wong, Sydney, Australia.
10:00 - 10:30	SOARING MEETS CRUISING – OPTIMAL STRATEGIES IN POWERED FLIGHT. T. Mörsel, P. Scheffel, Strausberg, Germany. (withdrawn)
10:30 - 11:00	MEASUREMENT AND SIMULATION OF POTENTIAL ELECTROMAGNETIC INTERFERENCE SOURCES IN SMALL AIRCRAFT. M. Fröhner, R. Geise, B. Neubauer, Braunschweig, Germany.
11:00 - 11:30	coffee break
	Simulation BPACC Room 1+2 Chair: Bernald Smith
11:30 - 12:00	THE USE OF SIMULATION IN GLIDING: CURRENT STATE AND FUTURE DIRECTIONS. G. Robertson, New Zealand.
12:00 - 13:30	lunch break
	Performance and FAI Class BPACC Room 1+2 Chair: Mark Maughmer
13:30 - 14:00	FLIGHT PERFORMANCE MEASUREMENT OF GLIDERS WITH GNSS-SYSTEM. K. Rohde-Brandenburger, Braunschweig, Germany.
14:00 - 14:30	REINFORCEMENT LEARNING ALGORITHMS FOR SOARING FLIGHT IN TURBULENT ENVIRONMENTS G. Reddy, J. Wong-Ng, A. Celani, T. Sejnowski, M. Vergassola, La Jolla, California, USA.
14:30 - 15:00	ASPECTS OF FAI 13.5M CLASS. H. Fendt, Braunschweig, Germany.
	North Eastern Hotel, 1 Nunn Street, Benalla
19:00	**Congress Closing Dinner**

PIK-20D Glider Fatigue Review

Erkki Soinne[1]
[1]*Finnish Transport Safety Agency, erkki.soinne@trafi.fi*

Abstract: A critical review is made on the fatigue calculations of the PIK-20D glider based on the methodology used at Saab on commercial and military aircraft. The method is applied on the composite wing spar cap and web fatigue calculations. The results are transformed to be consistent with the Kossira-Reinke spectrum. Also the effect of aerobatic flight is investigated. The effect of the stress levels in the performed static and fatigue tests is assessed. The fatigue of the primary metal brackets is calculated using the Saab method. Finally, the factors influencing the inspection program are described.

***Keywords*:** fatigue, composites, metal, inspections

Introduction

Fatigue is a common question for all aging aircraft and it is wise to plan in advance for possible actions. The European Aviation Safety Agency EASA has requested the Finnish Transport Safety Agency Trafi to suggest a fatigue inspection program for the PIK-20D glider, shown in Figure 1. As a basis for the inspection objects and inspection interval the stress calculations, fatigue and material tests were reviewed and new fatigue calculations were made for the primary metal brackets.
Fatigue of composite gliders has been studied in several countries such as Australia and Germany. Kossira and Reinke[1] performed flight measurements in the 1980s to establish an envelope spectrum covering all types of glider flights. To enable the extension of fatigue life of gliders Patching and Wood[2] performed in the 1990s flight load measurements and a fatigue test on a Janus wing. Kensche[3] has published several papers on composite structure life time prediction and certification. Waibel[4] has written a valuable summary on the subject.

The following factors have an influence on composite structure fatigue:
- load spectrum
- aerobatic flight
- resin system and fiber type
- material survivability and confidence limits
- application adjustment
- scatter factors for life and cumulative damage sum

and have been taken into account in the analysis. This extended abstract presents examples of the analyses performed on composite structure, metal brackets and the inspection program.

Methodology

In the calculation method, used at Saab on fatigue of civil and military aircraft, the cumulative damage sum is determined according to the classical Miner-Palmgren rule

$$D = \sum_{i=1}^{k} \frac{n_i}{N_i}$$

where n_i is the number of load cycles and N_i the number of allowable load cycles at a certain stress level.

The method contains five steps:
- derivation of limit loading spectrum
- normal correction of the coupon fatigue tests
- application adjustment
- scatter factors for life and stress
- choice of the cumulative damage sum limit

which are explained in detail in the paper. The results are based on the Kossira-Reinke spectrum with 12,5% aerobatic flight added. Aerobatics has a noticeable effect on fatigue.

In the wing spar web the stress state at the neutral axis is pure shear loading. The pure shear stress τ is equivalent to a state of acting stresses in the fiber directions

$$\sigma_1 = \tau$$
$$\sigma_2 = -\tau$$

in the +45° and -45° directions. The strain in fiber direction in this biaxial stress state can be derived as

$$\varepsilon = \frac{\sigma_1}{E_1} - \nu_{12}\frac{\sigma_2}{E_2}$$

where the first term is the strain due to the stress σ_1 in the principal 45° direction and the second term is the contraction due to the stress σ_2 in the perpendicular -45° direction. E_1 and E_2 are the moduli of elasticity in the fiber directions and ν_{12} is the Poisson number indicating contraction in direction 1 due to the stress acting in the perpendicular direction 2. The stress state is such that in the principal fiber direction the strain is ε and in the perpendicular direction the strain is -ε. This enables to estimate the fatigue shear loading with a normal stress fatigue coupon.

When selecting the inspection objects for the inspection program the consequences of the failure of a part were assessed. The failure of a primary part would cause a loss of the aircraft and at low altitude also the loss of the pilot's life. In the choice of the inspection objects it was taken into account the performed analysis of maximum stress areas, strain gage surveys, static test results, fatigue test results, stresses in adjacent elements, stress concentrations and service experience. Also the consequences on flutter were studied. The inspection program was divided into mandatory and voluntary objects to put the emphasis on critical issues. The voluntary objects serve as a guide for good care of the glider.

Results

Wing spar caps. The spar caps on PIK-20D were fabricated from Courtaulds Grafil A-S carbon fiber and Rütapox L02/SL resin system. A bundle of tows was pulled through a resin basin and a nozzle and placed into the spar cap tool, where pressure was applied with screws on the material during curing. The method guaranteed a 60% fiber volume and a void free even quality. The entire glider structure was post cured at 70° C temperature permitting the use of colored external surface paint. An important factor in composite material fatigue is the used resin and fiber. Fatigue tests at DFVLR and Helsinki University of Technology have shown that the Rütapox L20/SL resin system has very good fatigue properties.
The spar cap fatigue calculation using the Miner–Palmgren rule was based on the maximum spar cap strain slightly outboard of the wing root rib. This strain was derived with a FEM calculation using the grid shown in Figure 2 and a calibration to experimentally measured strains. The computed strain peak of ε=0,5393% at limit load is lower than the value 0,61%, quoted in ref. Kensche[3] and ref. Waibel[4] as a common design level (limit strain) on a sailplane wing spar.
The fatigue calculation in ref. Soinne[5] using the Miner–Palmgren rule gave for the spar cap of PIK-20D a fatigue life of $4{,}829*10^{20}$ FLH, based on the Kossira-Reinke load spectrum, with 12,5% aerobatic flight added, the scatter reduced S-N curve of Courtaulds Grafil A-S carbon fiber and Rütapox L02/SL66 resin system, a conservative stress ratio of R=-1, a life factor of 8 and a cumulative fatigue limit sum of D=0,1.
Only the highest load level at n=6,62 contributed to fatigue. The result is still conservative due to the conservative choice of the limit value D and the conservative approximation in the stress ratio R. Also the aerobatic flight spectrum was handled conservatively as it was based on the maximum take-off weight of 450 kg, whereas aerobatics is flown without water ballast at a maximum weight of 360 kg.

Wing fatigue test. A development fatigue test on the PIK-20D wing was performed after the certification. The spectrum was derived by analysis and was not intended to cover aerobatics. The gust loads were derived using power spectral density analysis. Consequently, the spectrum was less severe than the Kossira-Reinke spectrum. However, the testing contained very high static load cases at an elevated load factor n=6,62+20%=7,944. Considering the static tests as the critical part of the Kossira-Reinke spectrum with 12,5% aerobatics added they cover a life of $2{,}893\cdot10^{14}$ FLH, based on the spar cap cumulative damage sum transformed with the Miner-Palmgren rule.

Wing spar web. Kensche[3] has studied fatigue of shear webs and his results indicate, that a wing spar web might be more critical than a spar cap. The pure shear loading in the wing web can be transformed into a biaxial normal strain state as described above.
Strain measurements on the PIK-20D fatigue test wing indicated a higher strain on the forward side of the spar web than on the aft side. This was probably due to a locally asymmetric reaction to the wing spar end pin load in the root rib. The highest strain in 45° fiber direction at limit load n=6,62 at the spar neutral axis was ε=0,492%. The fatigue calculation in ref. Soinne[5] gave for the wing spar web of PIK-20D a fatigue life of 938156 FLH, based on the Kossira-Reinke load spectrum, with 12,5% aerobatic flight added, the reduced S-N curve of Interglas glass fiber weave and Rütapox L02/SL resin system with a stress ratio of R=0,15, a life factor of 8 and a cumulative fatigue sum of D=0,1. The largest contributions to the fatigue emerge from low load levels at n=1,1…1,47 where

aerobatic flight is not a factor. The estimate is very conservative due the log-linear extrapolation of the S-N curve to very high number of cycles, where the log-linear line unphysically crosses the zero strain level.

Metal brackets. Fatigue calculations have not been required in the airworthiness requirements for glider metal parts, but the primary brackets were checked with the method utilized at Saab for commercial and military aircraft. The primary parts at the wing spar end main fitting bracket, wing root bevel pins for the attachment of the fuselage and the tailplane and fin forward and aft fitting brackets were studied. The fatigue calculation using the Miner–Palmgren rule gave for the wing spar end main fitting a fatigue life of 67607 FLH, based on the Kossira-Reinke load spectrum with 12,5% aerobatic flight added, the scatter reduced S-N curve of AISI 4130 alloy steel, a scatter factor of 8 in life and 1,8 in stress and a cumulative fatigue sum limit of D=0,7. Without aerobatics the fatigue life was 265655 FLH. There was no cumulative fatigue on the other primary brackets.

Inspection program. On the composite structure primary parts are for example the wing spar root, aft fuselage and elevator. On the fuselage quite large damage can be tolerated without losing the aircraft, but not on the wing spar root or the elevator. Also the metal brackets and the control systems were assessed. The wing spar end main fitting bracket pin, wing bevel pins for the attachment of the fuselage and the tailplane and fin forward and aft fitting brackets are primary parts as well as some of the control system parts. However, for example the elevator actuator bracket is not strictly speaking a primary part as the elevator push rod acts on the elevator from underneath and the pilot can deflect the elevator upwards and perform a landing. This has been demonstrated several times when pilots have forgotten in rigging to connect the elevator push rod.
The inspection program was divided into mandatory and voluntary objects to put the emphasis on critical issues. It was proposed that for a normal condition aircraft the fatigue inspections are started at 10000 FLH with an interval of 5000 FLH until 65000 FLH is reached. The inspection program is requested in the EASA.SAS.A.024.PIK-20D and is found on Trafi's web page

http://www.trafi.fi/en/aviation/airworthiness/pik-20_support

At 65000 FLH a renewed review, using future state of the art methods, shall be made by the future competent authority to check if this original program needs a clampdown or can be relaxed. With an annual flight time of approximately 100 FLH reaching the 65000 FLH may take about 500 years. An electronic magnifying glass, indicating the structural fatigue life with six digits, would be great.

Conclusions

The review shows on PIK-20D a long fatigue life and that there are no known fatigue problems. Reaching a long usage time depends more on the good care of the glider. For this reason, the metal parts shall be kept free of corrosion, the paint in good condition to protect the structure against UV- radiation and humidity and the glider shall be stored in dry conditions.

References

[1]Kossira H., Reinke W., 1984: Festigkeit von modernen GFK-Konstruktionen für Segelflugzeuge - Bestimmung eines Belastungskollektives, IFL-IB 84-01 Technische Universität Braunschweig, 234 p.
[2]Patching C.A., Wood L.A., 1991: Fatigue Test of a GFRP Glider Wing, XXII OSTIV Congress.
[3]Kensche C.W., 2002: Lifetime of GFRP in a shear web and in the girder of a sailplane wing spar, Technical Soaring, April 2002, pp. 51-55.
[4]Waibel G., 2002: Safe life substantiation for a FRP-sailplane, Technical Soaring, April 2002, pp. 56-61.
[5]Soinne E., 2015: PIK-20D Fatigue Evaluation, Trafi Research Reports 7/2015, Finnish Transport Safety Agency, Helsinki, p. 94

Figure 1. PIK-20D in flight.

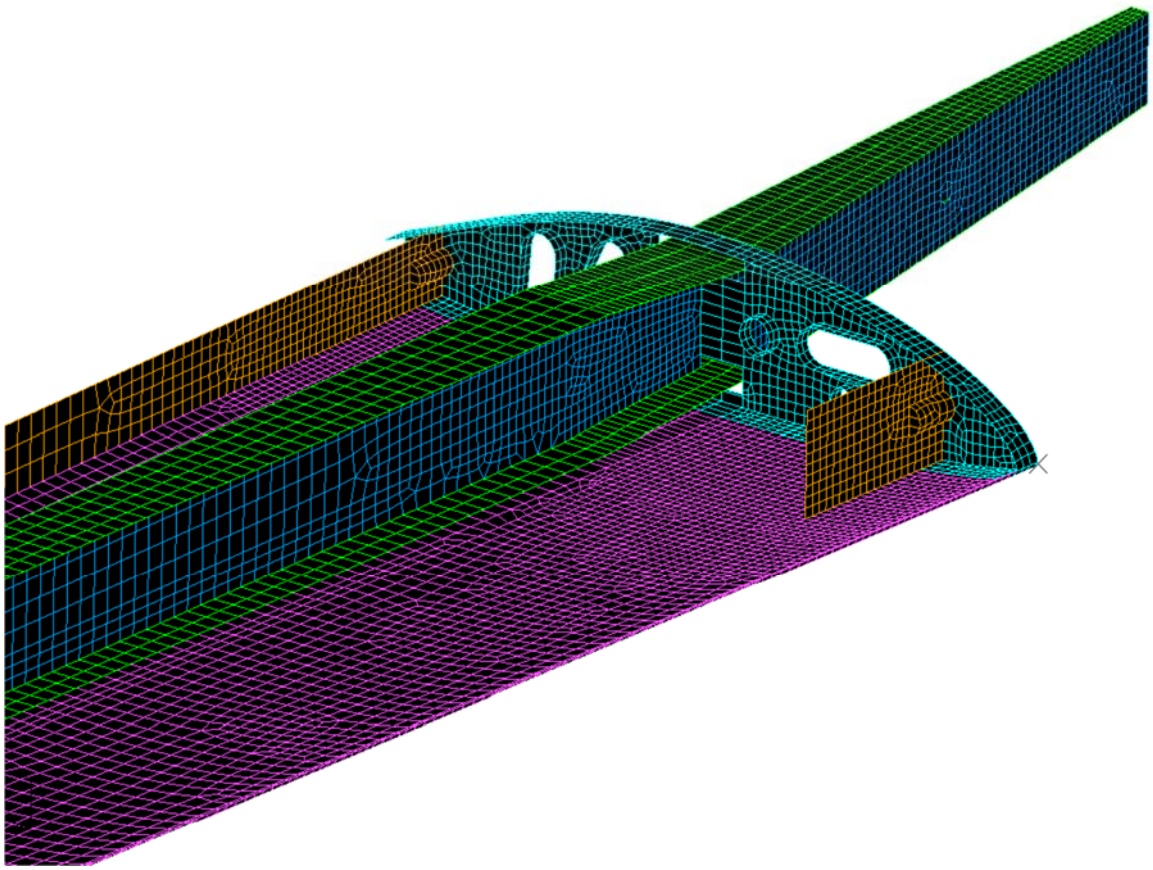

Figure 2. PIK-20D wing

Risk of Flutter in Aging Sailplanes

Kopp, Ullrich
Luftfahrt-Bundesamt, ullrich.kopp@lba.de
Gross, Joseph, Dr.-Ing.
formerly Technical University Hamburg-Harburg

Abstract: The effect of aging on the aeroelastic behavior of fiber-reinforced composite aircraft structures was investigated by the Hamburg University of Technology (TUHH) by ground vibration tests as well as flutter calculation. The investigation aimed to detect the presence of aging effects (structural degradation, stiffness reduction, etc.) in test aircraft and, if present, quantify their overall influence on aeroelastic safety. In conclusion, this study has not found any relation between aircraft age and flutter speed due to structural degradation or fatigue. However, control system weakening with respect to age has been shown to affect the aeroelastic safety of the aircraft investigated. Control surface eigenfrequencies decreasing with time can advance coupling between control and structural modes resulting in a lower flutter speed.

Keywords**:** *Aeroelasticity, flutter, composite aircraft, ground vibration test, control system.*

Introduction

The effect of aging on the aeroelastic behavior of fiber-reinforced composite aircraft structures was investigated by the Hamburg University of Technology (TUHH) during recent years. The study "**Flutter in aging Sailplanes 50.0338/2009 - Improvements in aeroelastic assessment procedures"**[1] was initiated by the German Luftfahrt-Bundesamt (LBA), and financed by the Federal Ministry of Transport and Digital Infrastructure (BMVI).
Freedom of flutter must be shown before a new Sailplane or powered sailplane can be certified by the authorities. This is done by ground vibration tests, flutter calculations as well as test flights with new aircraft. The assumption is that the results of this investigation will be valid lifelong assuming fair quality maintenance. This worldwide assumption should be verified by this investigation.
The investigation aimed to detect the presence of aging effects (structural degradation, stiffness reduction, etc.) in test aircraft and, if present, quantify their overall influence on aeroelastic safety.

Methodology

Two aircraft types, both fiber-reinforced motorized sailplanes, were considered in this investigation. These were the ASH25-EB28 with a 28 m wingspan from the company, Binder Motorenbau, and the Stemme S10-VT with a 23 m wingspan from the company, Stemme AG. Of each aircraft type, two aircraft were analyzed, one in new and one in an aged condition. The aircraft in new condition had, in both cases, a negligible number of flight hours (less than 100 h). The aged-condition S10-VT had approximately 2 500 flight hours and was ready for a major overhaul (3000 h life-time extension). The aged ASH25-EB28 had over 8 000 hours and passed already 2 major overhauls.
To collect comparable data, new and aged sailplanes constructed from composite material were subjected to ground vibration tests and aeroelastic flutter analysis according to the airworthiness requirements (JAR 22 and CS 22, § 22.251, § 22.603, and mainly § 22.629). Aircraft with large wingspans and high aspect ratios were selected for the tests as these were expected to have undergone more significant stress during flight operation.
For both tests, a single-shaker excitation approach was applied using both random white noise and sinusoidal excitation signal types for each of 15 measurement configurations. The test configurations used in both tests can be seen in Fig.1. The aircraft structures were excited using electromagnetic actuators capable of ±75N at 0.5 Hz−7 kHz. For this GVT, the frequency range was limited to 1 − 75 Hz, and force amplitudes above approximately 20 N were not required. Structural response data was collected using 79 and 94 piezo-electric accelerometers for the Stemme S10-VT and the ASH25-EB28, respectively. These were attached at predetermined measurement nodes with 1 force transducer between the electromagnetic exciter and driving point.
Measurement data was evaluated using the commercial software package, MATLAB, converting real-time data into the frequency domain via fast Fourier transformations. Using the spectral averaging method, discrete frequency response functions were computed from the numerous excitation loops run for each measurement configuration. Modal parameters were then extracted from the frequency response data using a modal analysis technique, the global singular value decomposition [2].
The flutter calculations on the modal data of both powered sailplanes were performed using the commercial software package ZAERO from Zona Technologies, Inc. The program utilizes the doublet-lattice method [3] (DLM) to compute unsteady aerodynamic influence coefficients resulting from modal structural-dynamic oscillations. The complex eigenvalue problem posed by the aeroelastic equation of motion is solved with both the k and the g methods (modified p-k method) [4], yielding modal frequencies and damping terms as a function of increasing air-speed. The flutter solution in this investigation was computed using ZAERO's linear module for subsonic flutter analysis, ZONA6, for international standard atmospheric conditions at 0.3 MACH.

A comparison of the results served to evaluate the influence of age on the flutter speed of the aircraft type under investigation. Primarily, the flexible vibration modes representing the aircraft structures as well as the control modes were excited, investigated and analysed. Due to the end of the research project and bad weather conditions, flight tests with the aged powered sailplanes were canceled.

Results

The results of the ground vibration tests for both aircraft types showed little difference between the flexible vibration modes of the aircraft structures (with some exceptions due to aircraft modifications and measurement error). The overall flutter speed was seen to be affected by these differences only for the case of the ASH25-EB28, however, the flutter safety of the aircraft was not compromised. In general, a trend between aircraft age and modal parameters of flexible modes was not found in any of the cases examined.
Examination of the control modes (rigid body rotational oscillations of control surfaces) suggested a trend between aircraft age and eigenfrequency reduction for the case of the S10-VT. This is likely to have been caused by the weakening of the control system over time combined with an increase in control surface free play. These age related factors, in combination, lead to a reduced effective rotational stiffness of control surfaces.
In summary, deviations were found in results of the ground vibration test for both structural and control surface rotation modes. These led to differences in the computed aeroelastic behavior of the aircraft type; however, a flutter mode was not found for either case. Differences in structural vibration modes were less significant, did not show a definite tendency with respect to aircraft age, and could still be attributable to measurement error and production deviation. Resonant frequencies of control surfaces, however, were shown to decrease with respect to aircraft age. The significance of these differences suggests an inverse relationship between control surface rotational eigenfrequencies and aircraft age for this case.

Conclusions

In conclusion, this study has not found any relation between aircraft age and flutter speed due to structural degradation or fatigue. However, control system weakening with respect to age has been shown to affect the aeroelastic safety of the aircraft investigated. Control surface eigenfrequencies decreasing with time can advance coupling between control and structural modes resulting in a lower flutter speed.
Recommendations for minimizing this flutter risk are:

1) During aeroelastic testing prior to certification of an aircraft, the rotational stiff ness of each control surface should be measured (with the control stick and pedals constrained) and documented. A linear method would be sufficient for the rotational stiffness measurement.
2) Aeroelastic safety analysis should account for realistic rotational stiffness tolerances of control surfaces. Tolerance values could be recommended by the manufacturer based on expected deviations in the control system between the control stick and the trailing edge of the control surface. If no expected values are available, experience has shown ±10% to be a reasonable starting point for the flutter analysis.
3) Periodic inspection of control surface rotational stiffnesses should be performed to ensure these remain within analyzed tolerances. This inspection could be performed using the same method described in Point (1). It is important to ensure that rotational stiffness deviation has not exceeded tolerances set in Point (2). Should these tolerances be exceeded, the control system would need to be repaired to ensure the validity of the original aeroelastic flutter analysis and, as such, the flutter safety of the aircraft.

The implementation of these safety measures – along with measures already in place pertaining to mass and residual torque tolerances for control surfaces – would improve consistency between the aeroelastic behavior of aircraft in new and aged conditions, ultimately maintaining the flutter safety of an aircraft as it ages.

References

[1] Gross, Joseph, Dr.-Ing.; Weltin, Uwe, Prof. Dr.-Ing.; Verbesserung der aeroelastischen Beurteilungsverfahren für die allgemeine
Luftfahrt (LBA-BMVI-PROG-3 Issue: A.01), Institute of Reliability Engineering; Hamburg University of Technology, Hamburg
April 2016
[2] D.J. Ewins, Modal Testing: Theory, Practice, and Application, Research Studies Press, Ltd., 2000.
[3] E. Albano and W. Rodden, A doublet-lattice method for calculating lift distributions on oscillating surfaces in subsonic flows. AIAA, vol. 7 no. 2, Feb. 1969.
[4] P.C. Chen, Damping perturbation method for flutter solution: the g method, AIAA, vol. 38 no. 9, Sept. 2000.

Figure 1. The test conditions during the ground vibration tests. (above Stemme S10-VT; bottom ASH25-EB28

A Case Study in Gelcoat Crack Propagation below PU Paint

Rob Hanbury
[1]*Gliding Federation of Australia, hanbury.rob@gmail.com*

Abstract: A case study of a glider which has gelcoat cracks occurring under PU paint. It had been recoated with polyurethane paint over gelcoat after removing all the cracked gelcoat. It is clear that the recent gelcoat cracks caused damage to the glass and carbon FRP structure in as little as a year. The conclusion is that gelcoat that may crack is a high risk to gliders and if the gelcoat starts cracking all of it must be removed. The best would be that glider manufacturers stop applying gelcoat that may crack.

***Keywords*:** Gelcoat, Crack, Paint, Sailplane, Glider

Introduction

Gelcoat use on gliders is critical and cracking issues have caused major risk to gliders and caused millions of dollars of unnecessary costs to owners. This paper aims to assist proving a ruling in Australia from 1987 - all gelcoat that may crack must be removed and not over-sprayed with paint. This should influence manufacturing processes at many European factories that still use gelcoat. Gelcoat that cracks is a high risk to structures in the longterm, if it is to be repaired it is a high risk to the structure in removal and a high cost to the owner. The best solution is no gelcoat.

Gelcoat has advantages and disadvantages over paint. The issue is if it cracks due to aging. Some Gelcoat obviously cracks more. Others have a long history of not cracking. Gelcoat that may crack must not be used in manufacture. It is not necessary – some manufacturers stopped using gelcoat – eg Stemme in 1998. Some manufacturers still insist on using it and over-coat it with paint in the belief this delays cracking. It does but in the end it cracks and the damage is a high risk and cost to repair.

If cracks occur then damage starts to occur to the structure under the crack. This has been unclear but other cases of damage are well known. This case study furthers the proof that cracks cause damage, probably chemically, to the structure under the crack. The gelcoat cracks have to be repaired promptly.

My main references are the Gliding Federation of Australia (GFA) Airworthiness Directive GFA AD 278 and GFA AN 69 first written in 1987. The cracking on Fibre Reinforced Plastic (FRP) gliders started in early 1980 and was already a major issue in Australia, South Africa and elsewhere. It was extensively researched by GFA and the AD and AN already defined the problems and the solutions in 1987. This was lost in intervening years, even in Australia, as owners and refinishers tried to save cost, risk and effort. Many refinished gliders have had to be redone at great expense. It appears painting does help slow the cracking but if the paint becomes thin then the gelcoat cracks.

This is a case study of a particular glider that is cracking and has had the structure damaged by cracking since refinishing. It is to provide data to convince others to take action. It is based upon monitoring, repairs, photos and microscopic examination by me.

My conclusion is manufacturers must stop using gelcoat that may crack and, if refinishing, all gelcoat that may crack must be removed. If not there is a high risk that cracking will re-occur and cause damage.

Methodology

The Case:

The glider is a Stemme S10 manufactured in Germany in 1992. The manufacturing process was to spray gelcoat in the mould and then layup FRP structure on that. The shells were joined and then the joins oversprayed with the same gelcoat and the whole profiled. This is the standard German process of glider manufacture still used by most German companies.

By about 2000 the gelcoat was yellowing and only the after mould gelcoat was cracking badly. It was repaired by well respected Australian professionals but to save cost and effort the uncracked gelcoat was left and only the cracked gelcoat was removed and replaced. The whole glider was then oversprayed with polyurethane paint (common high quality Australian sourced.)

A few years ago I noticed and started monitoring and repairing a number of gelcoat failures:

1. Small pits broke out mainly on the wing upper surfaces. These were caused by gelcoat over air-bubbles from manufacture trapped between the gelcoat and the FRP or in the FRP. They were often about 2 mm deep and usually <5mm long. The structure is full of these bubbles and so there are many more waiting to happen.
2. Later a few 10 to 30mm long cordwise cracks appeared in one wing, outer upper surface, forward D-box. The Stemme has 4 wing panels and only the one wing has ever cracked like this.
3. But the tailplane is now also cracking, but spanwise.
4. And a similar but <10mm long frequent crack is occurring along trailing edges on both wingtips and ailerons, cordwise, possibly aggravated by edge effects and stress. See Figure 4.

5. The cracks in 2, 3, 4 are aligned in one direction in a structure but some cordwise and others spanwise. Probably stress and strain related.
6. Later # pattern cracking was noticed nearby in the wing. # pattern cracking is a well known gelcoat crack pattern and is obviously different to the cracks in 2. These are prominent but short spanwise cracks with cordwise shorter cracks at right angles in an otherwise random pattern. See Figure 3. These also occur in cowling panels on the fuselage. In all cases wherever the paint was thin. The paint was not sanded or cut so thinning was mainly from thin application. These are probably caused by gelcoat shrinkage and embrittlement over time.
7. On all types of cracks the gelcoat seemed to have curled up and so it was probably detached from the FRP to the width of the visible line on the FRP, ie 1mm wide. I believe this curling up is tension in the gelcoat. Curling up only occurs after a few months – initially the cracks are fine and flat.
8. The wing cracks are shown in the following Figure 1. This shows where the # cracks, the inner, the middle, but not the outer cracks occurred – this was a little to the right. Most cracks were two in a line as shown. Some were two parallel. All are considered as a single occurrence.

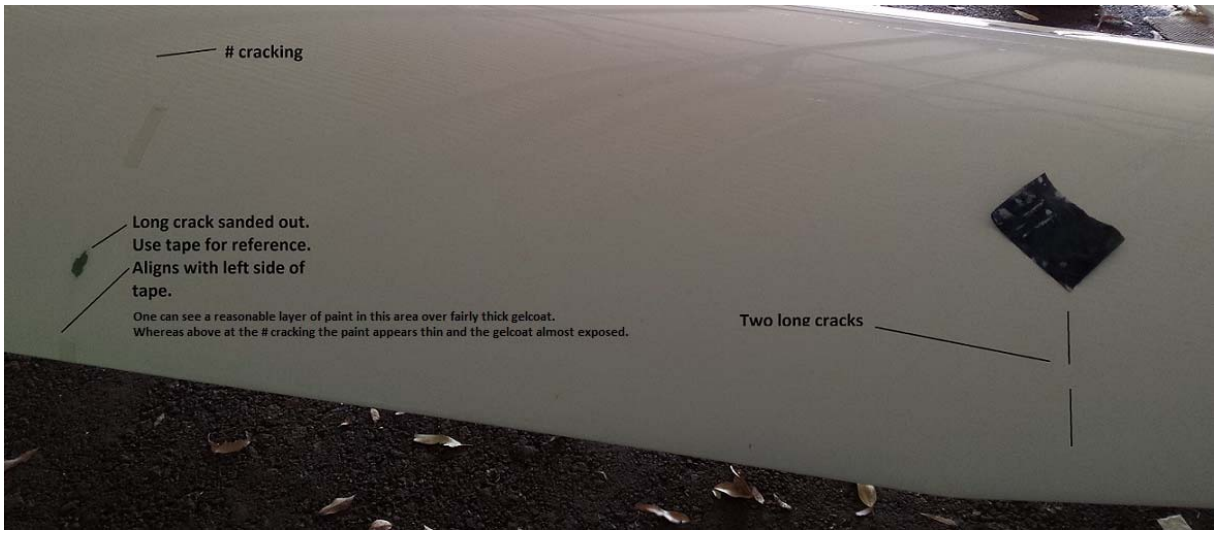

Figure 1. Left outer wing – Top Surface

Examination of the wing cracks:

After sanding away the paint and gelcoat from the cracks closest to the tip I cut out a sample of the upper skin to the foam core. I had avoided sanding the FRP as much as possible. And damaging the sample by bending. The sample came out intact, clearly showing the line of the crack. It is not manually weaker on the line of the crack and is available as removed.

On the inner and middle cracks I sanded to remove the gelcoat. After inspection and photos, I continued to sand through the layers of FRP in stages. I could still see the line of the crack all the way to the foam, i.e. it penetrated both the 92110 and the 92125 layers of fibreglass cloth. It was not clear at depth and has not come out clearly in photos.

All three cracks appeared similar and so I expect observation on one applies to all.

Examination of the sample:

The sample was viewed under a 45X stereo microscope. It is very clear and the following can be seen. Generally, this can be less clearly seen in the photos:

1. The sanding probably touched the top of the weave but had only damaged a small proportion of the fibres. It may be possible to carefully sand away most of the gelcoat like this and do a small percentage of damage. How much?
2. The FRP has a high proportion of air bubbles entrained in the resin. This has formed pockets in the weave. It probably makes little difference to strength but more vacuum and better layup would have been achievable. It is noticeable on the aircraft that these air-pockets are causing bits of gelcoat to separate and form pits. Also the other wing is even worse and although it has not cracked it has noticeable high frequency of large air pockets that can be seen under the paint and gelcoat even after the refinish. I think this shows the pockets are not the cause of the cracks but cause the first failure mode.

Figure 2. A crack area after gelcoat removal over glass FRP

3. The line of the damage was visible but less clear when wet. It varied with each strand of the weave but appeared to be more related to the resin, i.e. it was more clear where the resin was thicker.
4. There were cracks on the line but only the length of the width of one strand. The rest of the line and 90% of it was not cracked.
5. It appeared that the resin was leached out of the strands on the line as is clear in Figure 2. Possibly the cloth before layup had a chemical defect that had stopped the resin wetting it out properly. Maybe a fold in the cloth. The line is diagonal to the weave and approximately perpendicular to the wing leading edge. Maybe this caused the cracks and it could be a reason but seems odd to fold diagonal to the weave?
6. The other possibility is the strands seem to be semidetached along the line. See Figure 2. Maybe water got into the air bubbles through the gelcoat crack and froze on high flights. I have flown in moist conditions in wave to -19C but prior to the cracks appearing. With the cracks visible I have flown to below zero degrees, i.e. freezing could have expanded the water and damaged the resin and strands. This seems possible. But I believe all cracks have not frozen wet, whereas all cracks caused damage. I suggest freezing is not the cause.
7. Some flakes of resin appear more frequent along the line. In fact, after sanding the lines are hard to see and feel. But a few days later they can be felt and I think this is the flakes curling and standing up rather than fibres sticking up.

Examination of the # cracks:

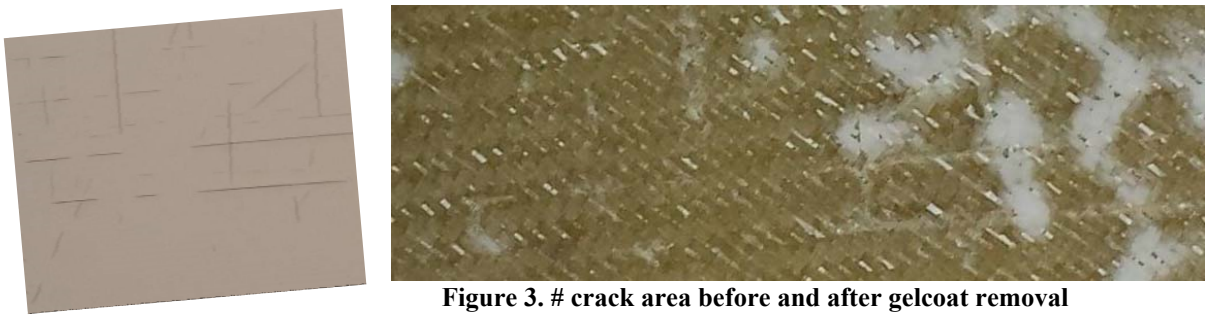

Figure 3. # crack area before and after gelcoat removal

The # cracking is the normal pattern of discontinuous cracks of varying length, predominantly in one direction but also at 90 degrees as shown in Figure 3. But the predominant direction is spanwise and so perpendicular to the 3 main cracks. They appear obviously unrelated. But the # cracks are definitely related to the thin paint. They stopped when the paint was thicker, i.e. I sanded the patches bigger until no gelcoat cracks were visible and in all cases the paint over gelcoat was visibly thicker.
These cracks also caused a line on the FRP which appeared the same as the main crack lines, see Figure 3 right. I.e. the damage to the FRP is the same. This means the gelcoat crack causes the damage and not the damage results in cracks! The same is true on stress cracks and on fibreglass or carbon fibre.

Figure 4. Crack damage in carbon fibre trailing edge.

In one case the main cracks were actually two parallel cracks as shown in Figure 2. One can see the same line on the FRP for both. I.e. there was always a mark on the FRP for every crack.

Results

The wing damage was repaired and repainted. All cracked areas were sanded away and a standard repair was done replacing the layup. But only the cracked patches. I plan to remove all gelcoat in time and repaint the whole glider. I continue to research and monitor as follows.

1. All cracks are kept sealed normally with white tape until repaired. Initially they were not as they were very fine and obscure. But I now know they cause damage and hope sealing slows this.
2. I left a fourth recent major crack and the gelcoat. I filled it with paint and it has disappeared for now under the paint which was replaced for the whole wing upper surface. I will monitor for its return and will eventually expose the FRP to determine the extent of damage.

Conclusions

1. By examining these cracks, I can see that gelcoat cracks can cause damage to the underlying FRP structure whether it is glass or carbon.
2. It appears to be the resin rather than the cloth that suffers chemical degradation.
3. Some gelcoat cracks are definitely resulting due to thin paint not protecting gelcoat whereas others may be stress related under thick paint.
4. Initially I was unsure if the damage was causing cracks or the cracks were causing damage. By comparing the three types of crack they all have the same damage underneath and I conclude the cracks cause the damage. Even in as little as a year period. Probably not due to freezing but chemical weathering of the resin.
5. The cracks and gelcoat deterioration is increasing exponentially. For about 8 years after refinishing no cracking was noticed. One crack appeared within 10 years. Now large areas of cracking have occurred and new cracks are found every month.

Others in Australia have reported similar clear damage in both glass and carbon due to gelcoat cracks. Some say damage does not occur in carbon but I contend that based on this study where glass and carbon occurs in one aircraft and the damage appears the same.

I have not researched whether modern gelcoat from the same supplier still cracks. But modern gliders are still cracking even in a few years. Obviously the handling of the gelcoat in manufacture is a factor – the same gelcoat cracks after a different period on the same glider. But in the end it cracks if it is of the type that cracks.

I conclude that gelcoat cracking is a serious problem that has been clear since the 1980s. It has been less of a problem in cooler countries and so the manufacturers of Europe could ignore it more easily. But even there the problem is now common and causing high cost. I have personally removed the gelcoat and refinished a few gliders, it is a difficult, unpleasant, costly, and high risk job that can leave damage and hide it with a nice shiny paint. Australia has clear directives that must be followed. Buyers should refuse any gelcoat on their new gliders. Some manufacturers have solved the problem, like Stemme don't use gelcoat any longer, whereas most still do.

References

[1]GFA, 2016: GFA AD 278, Quality control of the process of external finish removal and replacement. http://doc.glidingaustralia.org

[2]GFA, 1997: GFA AN 69, Gelcoat failure. http://doc.glidingaustralia.org

Is it necessary to update Spiral Dive Requirements?

Gerhard Waibel
Hindelanger Straße 6, 87541 Bad Hindelang, Germany, GuM.Waibel@t-online.de

***Abstract**:* According to personal experience spiral dive accidents have happened. It is the goal of this paper to improve the knowledge and competence of the pilots in order to avoid structural overload accidents**.**

***Keywords*:** OSTIV TSP,Test-Pilot-Interviews, Flight-Manuals,V-n-Diagram.

Introduction

During recent OSTIV SDP meetings the problems of unsuccessful spiral dive recoveries was discussed, see the minutes. It quickly turned out that the OSTIV TSP (Training and Safety Panel) must be contacted. It was also apparent, that the knowledge of restricted strength of the sailplanes exists, when the speed of V_A is exceeded in flight. Interviews with pilots having flight test experience were taken and are summarized to improve flight manual information.

Methodology

In addition to a brainstorming in two recent OSTIV-SDP-Meetings many personal and telephone interviews were held on the subject. Literature besides the current versions of OSTIVAS and EASA CS-22 was kindly supplied by interview partners, see chapter ***References*** below. The author has summarized the inputs from 17 competent pilots of which 5 are professional test pilots.

Results

The interviews for this paper had two results: More pilot information is needed to show reduced sailplane strength limits at speeds above V_A for Category Utility sailplanes and a vast majority of test pilots on the method to recover from a spiral dive.

Conclusions

The subjects of this paper are not finally agreed. Discussion with the OSTIV-TSP is strongly desired.
The OSTIV-SDP has already agreed to improve Flight Manual instructions for spiral dive recoveries in particular, that the airbrakes should not be used at high load factors. Also all control inputs must be moderate at speed approaching V_{NE}. The interviews of the test pilots showed, that the knowledge about the V-n-Diagram is poor among pilots flying Category U sailplanes. Aerobatic pilots are better informed. So the OSTIV-SDP proposes to improve Flight Manual instructions on reduced structural strength at speeds between V_A and V_{NE} for airbrake operation, control inputs and against gust loads. The author wants to add an example for a coloured V-n-diagram and the important fact, that for Category U the combination of two or more maximum load cases like full control maneuvers at the maximum gust or highest maneuver loads are not covered. This is so to save structural weight. In Category A for aerobatics the structures are remarkably stronger and heavier.

References

[1]OSTIV-SDP Meeting Wasserkuppe, Minutes 2015
[2]OSTIV-SDP Meeting at FOCA Bern, Minutes 2016
[3]OSTIVAS issud 1997, amended 1999 and 2001
[4]EASA: Certificatin Specifications for Sailplanes and Powered Sailplanes, issued 14 September 2003
[5]Extracts form Darrol Stinton: The Anatomy of the Aeroplane, p.209, The Design of the Aeroplane, p.459f, Fying Qualities and Flight Testing of the Aeroplane, p.486ff and p.506, all provided by Hans-Ludwig Meyer.

Interviews with competent pilots as: Dr. Wolfgang Ambros, Paul Anklam, Walter Binder, Helmut Fendt, Michael Greiner, Martin Heide, Wolf Lemke, Hans-Ludwig Meyer, Heiner Neumann, Jannes Neumann, Guenter Schapka, Markus Scherdel, Werner Schott, Werner Scholz, Peter Stagge, Gerhard Stich and the author.

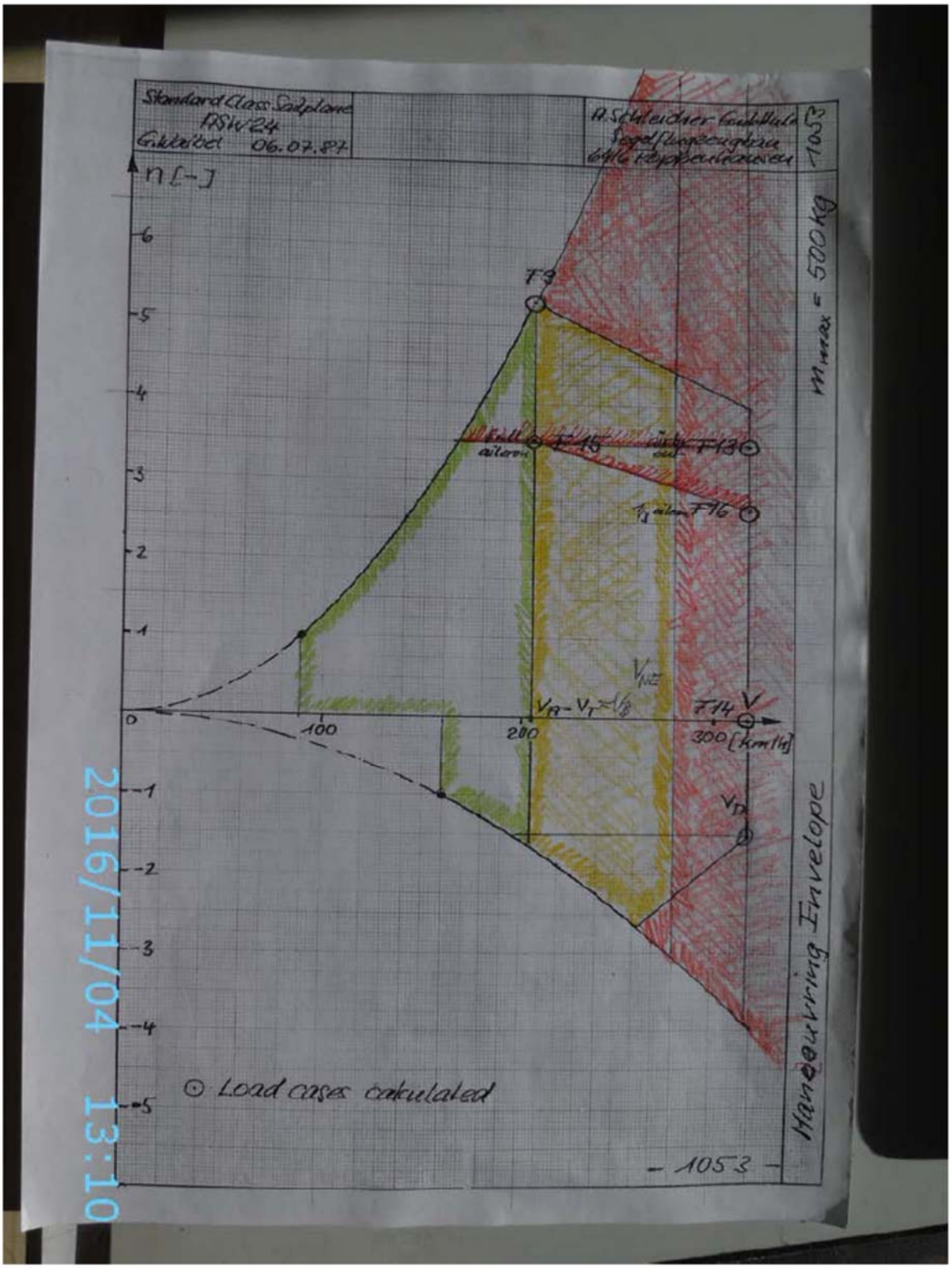

Figure 1. Example of a coloured V-n-diagram

Perceptual errors in the turn from base to final

Daniel L. Johnson (MD)
Mayo Clinic Health System, Menomonie, Wisconsin, USA drdan@wwt.net

Abstract: One of the most frequent fatal glider accidents is a stall during the turn to final. There are several perceptual distortions that may contribute to this. The best prevention is to actually glance at the airspeed indicator frequently to stay comfortably above turning stall speed, and to make a coordinated or slipping turn. This presentation summarizes ways in which the human perceptual system is prone to error.

Keywords: pattern accidents, low stalls, misperceptions at low altitude, circuit stalls, pilot illusion.

Introduction

Every action pilots take depends on their synthesis information, involving selection, perception, and comprehension of information. If this is erroneous, training and skill may be competently applied to wrong information.

Our perceptions are not reality. They are a finely detailed cartoon of reality, one that we believe, because it's normally reliable. However, perception's reliability and accuracy depends on a constant flow of redundant and overlapping information, especially from visual fixation on known objects.

Selection: Researchers are keenly aware that *selection bias* jeopardizes all observation. The turn to final is an experience, not an experiment. It is important to attend to the most relevant information – and to deprecate unimportant or misleading observations, in order to correctly interpret dynamically the status of pilot and glider in the three-dimensional environment, and to avoid embarrassment or catastrophe at the ground, which is uncompromisingly stiff.

Perception: False perception of the glider's dynamic status in the three dimensions of the air (perceptual illusion) of course yields a false notion of how to manipulate the controls to make right actions (cognitive illusion). The important point is that the glider pilot *cannot* be aware of error until *perceptual conflict* occurs. The result is quaintly called an Undesired Aircraft State.

Eventually the pilot with illusory perceptions, because they're wrong, will sense something contradictory. This does *not* immediately correct the illusion. There are good reasons for this:
- The clashing information or sensation is displaced from consciousness, ignored, or misinterpreted (incorporated into the cognitive illusion).
- The clashing information is attended to, but the pilot cannot integrate it into the incorrect gestalt. The pilot feels *confused*, for this is not The Voice of Mother. The confusion is useful, because it causes the pilot to seek additionally confirmatory information (such as a quick glance at the airspeed indicator).

There are two key challenges at this point: One is that, when very low to the ground, there may not be time for a reflective moment to resolve the confusion. The other is that the moment of confusion is an *interruption* and *distraction*. Any such may bump a planned action out of the *prospective memory* queue.

Prospective memory refers to the fact that in all activities, we often must line up a sequence of actions, all of which are deferred until their time. Interruption and distraction can bump actions items out of the queue, especially the next in line.

An item may also be bumped from prospective memory due to illusion – for example, if the expected consequences of an action are perceived. For instance, if the glider enters sink during a distraction that occurs just as the pilot reaches the time to extend landing gear or spoilers, the subconscious brain may pass a “job done” token to consciousness, and the pilot may emerge from one illusion only to enter another.

More experienced pilots may be more prone to this because action sequences are often done habitually, as a single item, like a musician playing a scale, chord, or arpeggion.

Training: Training does not prevent illusion, but it should teach the pilot *where to focus attention*. For example, the airspeed indicator, the rudder position, the yaw string or ball, and the runway of intended landing must be repeatedly and frequently checked. Anything that hinders the pilot from continually re-checking on these important sources of perceptual information is a distraction during the turn to final.

Formal named illusions that may be in play:
Vection illusion: This is the name for "false motion." When an aircraft turns above 300 meters/1000 ft or so, the ground hardly seems to move, and it seems to pivot in the air even during a fairly broad turn. This is a vection illusion that may hinder the pilot from effectively center a thermal, but creates no danger.

The *pivot altitude* is that altitude at which an aircraft, in making a coordinated turn, seems to the pilot to pivot about a point on the ground that's just at the wingtip. Above that altitude, there is the false sense of a small turn and slow speed. Below that altitude there is a sense of a broad turn and high speed – at the same aircraft velocity. The turn to final is below pivot altitude for most aircraft.

The fact that gliders normally stay high, well above pivot altitude, habituates perception to a slow-speed illusion. As the pilot flies a circuit/pattern to land, the sense of speed steadily increases during descent even though the aircraft is often actually slowing. This creates an illusion of increased speed, which can be corrected cognitively only by checking the airspeed indicator.

Speed constancy: We tend to interpret the apparent movement of external objects as always representing the same speed. This is the heart of the vection illusion above. Errors of memory, or errors of integrating memory into today's perception, exacerbate this illusion.

Size constancy: We tend to interpret all similar-appearing things as being of the size of the one with which we're most familiar. This is particularly important when landing off-field or at a novel field.

False horizon: When there are hills or mountains nearby, this is serious. While we're above everything, we see the real horizon. As soon as we descend below any hump of earth, any ridge line becomes a false horizon.

Neglect: We commonly fail to discipline ourselves to attend to all the clues that can correct illusion. Tom Knauff's famous didactic presentation, The Five Signs of a Stall, regularly reminds us that we do not train ourselves to use all the information available to us in order to correct the cognitive illusions that are inevitable.

Conclusion

We may forget, through the familiarity of success, that we can fly only because of speed. An aircraft is designed to stay in the air safely only within limits, bounded on the upper end by flutter, where control surfaces might snap off, and at the lower end by the stall speed, below which we fall out of the air. The airspeed indicator stands by to correct speed illusions.

Awareness of illusions and misperceptions is important, if only to teach us that we must continually seek redundant information, to verify our status in the three-dimensional dynamic environment we occupy as a pilot. We cannot be smug during the turn to final; we must always check the basics: airspeed, attitude, yawstring or ball.

It's airspeed we want, and we put the nose at -whatever attitude keeps the airspeed where it's meant to be: 1.3 VSO + % the gust velocity (more, if it's really gusty).

References

Dismukes, R., Berman, B. 2010. Checklists and Monitoring in the Cockpit: Why Crucial Defenses Sometimes Fail. http://human-factors.arc.nasa.gov/publications/NASA-TM-2010-216396.pdf
Dismukes, R. 2015. Cognition, Aging, and the Soaring Pilot. Soaring Magazine, October 2015, 35-37.
Dismukes, R. 2016. Why Do Pilots (and everyone else) Sometimes Forget to Perform Critical Tasks? Soaring magazine, October, 2016, 38-41.
Johnson, D. 2013. Why We Blunder in the Turn. Soaring Magazine, March, 2013, 13-15
Johnson, D. 2014. How to Spin Unintentionally. Soaring magazine, May, 2014, 8-11
Knauf, T. 2014. Developing a discipline. Soaring magazine, May, 2014, 3-4

Comparative Statistical Analysis of Fatal Spin Accidents for Training Gliders

Stuart Smith, Murray G. Stimson
Melbourne, Australia

Introduction

Debate raged in previous decades regarding whether a glider should be designed to be easy to spin or not. Pro-spin design centered on the argument that all pilots should be taught to recognize and avoid a spin in a training glider which would spin easily. Against was the argument that a glider design should be as resistant as possible to routine mishandling, especially under high-stress or abnormal situations near the ground. Over and above those arguments was the question of whether engaging in spin training exposed pilots to much greater risk than would be the case if they did not. A routine literature search did not uncover definitive research to answer these questions.

Methodology

The Aviation Safety Network (ASN) now provides a searchable database of worldwide accident and incident reports dating back many decades. These data were not otherwise available for all soaring nations although in recent years new reporting systems have been introduced in some countries. ASN was examined for fatal accidents since 1980 involving the five most common training glider types made from Glass Fibre Reinforced Plastic (GFRP). The accidents were categorized by degree of certainty that loss of control or spinning was the primary contribution to the fatal accident based on the brief reports included. Identification of accidents or incidents involving loss-of-control or spinning was not always clear, and some known accidents were not listed in ASN. The ASN wiki-database was privately run and volunteer driven in terms of contributed reports from around the world.

Comparison between different glider designs only on the basis of raw numbers of fatal accidents was considered only part of the picture. Accident rates have traditionally been calculated by dividing mishap numbers or number of fatalities by some measure of exposure to risk, such as flight hours or number of flights. As useful as these safety research and management data might be, no readily available and reliable data of that type was found across global fleets of these gliders, or indeed for any single nation. Consequently, we chose to calculate accident rates based on estimated Aircraft Service Years (ASY). ASY represented the cumulative total of the number of aircraft in service each year since first flight. As a first approximation of ASY, internet media reports on production milestones were used to estimate production rates for various types over the years since first flight. Fleet size was reduced by reported write-offs in ASN.

Results

Our results in Table 1 indicated that the SZD-50 Puchacz fleet far exceeded all other types in the number and rate of fatal accidents. Even using wide uncertainty bounds the data showed that this was largely due to fatal accidents that could be classed as definitely or probably resulting from loss of control resulting in a spin. The ASN wiki may have been heavily biased to preferentially report spins involving the SZD-50, but where media reports on the accidents were available loss of control or a spin was confirmed. Over two-thirds of the fatal accidents involving the SZD-50 occurred since the type ceased production in 1997, indicating that owners continue to operate the type in-spite of a much higher rate of fatal accidents than comparable aircraft. The remaining four types showed accident rates due to loss of control less than one tenth of that for the SZD-50 Puchacz. Of the seven total fatal accidents for the ASK-21, none could be attributed to spinning. Five were reported to involve collision with another aircraft, which removed loss of control as a primary contributory cause for those accidents.

Table 1. Comparison of fatal accidents and accident rates to 2016 for common GFRP two-seat training gliders, based on the ASN on-line database.

Type	Number Built to 2016 (Est)	Aircraft Service Years	Reported Fatal Accidents (Aviation Safety Network)					
			Definite Spin		Probable Spin		All Fatal	
		(ASY)	Acc.	Rate	Acc.	Rate	Acc.	Rate
SZD-50 Puchacz	343	8373	23	2.75	8	0.96	34	4.06
ASK-21	994	18718	0	0.00	0	0.00	7	0.37
G103 Twin Astir	904	30615	6	0.20	1	0.03	13	0.42
Duo Discus	772	9194	1	0.11	0	0.00	3	0.33
DG-500/1000	363	6093	1	0.16	1	0.16	7	1.15

Note: Accident Rate given as: Fatal Accidents per 1000 ASY

In all of the 64 accident reports examined none of the fatalities were reported to result from loss of control during spin training exercises. In so far as the reported phase of flight was accurate, launch and landing approach appeared to be the most commonly represented phases of flight in fatal accidents. Winch launch failure was the most common reported activity.

In future, collection of risk exposure data such as flight hours, number of flights, and flight purpose should be undertaken by each National Aviation Authority and the results made publically available for safety research. For every accident, an authoritative report that includes phase of flight, primary contributory factors and other relevant details should be submitted to each NAA and made publically available on a global website. Prior experience in safety research and this study strongly suggest that exposure data and accident reports should be prepared to an internationally agreed standard format.

Common GFRP training gliders were shown by this study to occupy two distinct risk groups in regard to fatal accident rates.

Side-by-Side Flying with E-Power: Independent and Safe

Lars Muth
REINER STEMME Utility Air Systems, l.muth@RS-UAS.com

***Keywords*:** Electric, Motorglider, Stemme, Two seater, 20m wingspan

Introduction

Beginning with a competitive sailplane in the FAI two seater class (20 m wingspan), the target specification of the SK10.e project will use the advantages an electric propulsion system has to offer. Additionally, the plane will have a side-by-side configuration of the pilot seats.
This results in a self-launching sailplane with a glide ratio of 1:48 with flaps and 180 kg of water ballast.

Methodology

A Federal Ministry of Economics-funded project to develop innovations for the development of the SK10.e was started in January 2016. The Technische Hochschule Wildau teams up with Reiner Stemme Utility Air Systems to fulfil the standards set by the guidelines for a funded project.

Reducing empty weight

To enable the wide range of wing loads, the structural weight has to be reduced by 25%. In addition to numerous small improvements in the structure derived from many lessons learned, there are many more improvements required to compensate for the additional weight that comes with the electric propulsion system and its batteries.
To reach the goals prepreg technology will be introduced to the world of certified sailplanes. To reduce costs and to avoid the need for an autoclave, low temperature prepregs will be used. They cure under vacuum with a temperature of less than 150 °C and therefore do not need the autoclave. Much tighter tolerances can be achieved with this technology, combined with additional improvements concerning weight.

Improved efficiency of the propulsion system.

To provide the necessary power for takeoff and climb an electric motor with 70 kW peak power is required. The motor will be located in the front of the fuselage behind a non-rotating nose cone, which will move forward to provide the gap required for a folding propeller to be deployed.
Reducing the gap between the nose cone and the fuselage will decrease the losses induced due to this configuration. The fuselage will work as an end plate for the propeller. Making the intersection between the nose cone and the fuselage more circular rather than elliptical will improve the efficiency even further.
To quantify these improvements, research using computational fluid dynamics is being conducted by the Technische Hochschule Wildau. With the proof-of-concept-plane these calculations will be verified.
The propeller blades are a customized design, optimized for the SK10.e. They are also being developed by the Technische Hochschule Wildau.

Improving the aerodynamics

The wing features a profile family which varies over the wing span to ensure best possible soaring performance. The wing-fuselage junction will be optimized and the fuselage tapering increased.

Ergonomics

Ensuring comfortable seating for extended periods to help reducing physical fatigue for pilots from 1,60 m to 2 m tall is achieved by a slightly enlarged fuselage and cockpit. Tests with a mockup of the cockpit are used to verify the comfortable position of the seats.

Range extender

Expanding the range will be made possible with a range extender. This will be a pod which is mountable under the wing. It will contain an internal combustion engine, a generator and a fuel tank which will expand the range of the Sk10.e. by nearly 1000 km. It will also enable charging of the batteries on the ground if there is no infrastructure available.

Results

Initial calculations show that a 25% weight reduction is within our reach.

With new batteries that will be available when the series production is planned to start, 1 h flight time on batteries is possible.

The preliminary design is completed in loop zero. It assures the feasibility of our ambitious project and shows that the SK10.e will be a force to be reckoned with in the 20m Two Seater Class.

Conclusions

With the outer wings, the first components are due to be manufactured at the end of 2016. These will be stress tested to verify the manufacturing processes as well as the calculations and simulations that have been completed.

Figure 1. SK10.e elfin

Field Physiology: Inflight Measurements to Monitor Oxygen Saturations of Pilots During High-Altitude Glider Flights of the Mountain Wave Project in the Himalayan Region and the French Alps

Carla Ledderhos[1], Rene Heise[2], Christine Gammel[1], André Gens[1]
[1]*Center of Aerospace Medicine German Air Force, CarlaLedderhos@bundeswehr.org*
[2]*OSTIV-Mountain Wave Project, Rene.Heise@mountain-wave-project.com*

Abstract: Recent F-22 fleet incidents show that unnoticed oxygen deprivation is still an issue during high-altitude flights. Currently, aircrews are trained in altitude simulation set-ups to recognize their individual symptoms, hoping that they would recognize them in a real-life scenario. Oxygen deficiency sensors are not commonly used.

Earlier work of our group showed that various pulse oximeters are accurate enough to be used as warning systems for oxygen deprivation in pilots and that the sensors' signal quality degrades only negligibly in tests on vibration platforms and in flight.

The objective of this study was to evaluate the failure rate of these systems at different measuring points (forehead, sternum, shin) in high-altitude flights with heavy turbulences and wide-ranging ambient temperatures and to optimize the crew's oxygen management.

Keywords**:** oxygen saturation, detection of hypoxia inflight, high altitude physiology, non-invasive physiological monitoring, risk management

Introduction

After two expeditions to the Andes, the OSTIV-Mountain Wave Project (MWP) Team carried out a research campaign to the Himalayas in 2013/2014. Based on a motor glider-bound (STEMME S10VT) multidisciplinary approach, the team amongst others realized scientific measurements of the distribution and transport of atmospheric pollutants in Nepal as well as new digital aerial imageries of exceptional resolution and highest accuracy to create a 3D terrain model of glaciers close to the Mount Everest and Aconcagua.
Within the project, members of the MWP worked together with scientists of the German Aerospace Center (DLR, Institute of Optical Sensor Systems), the Aerospace Technology Faculty of the University of Applied Sciences Aachen and the research team of the German Air Force Center of Aerospace Medicine.
Firstly, participating pilots wanted to explore the Himalayas and the Mt. Everest region, feared for their bad weather conditions in pioneer flights. There was only one former Himalayan soaring expedition in 1985 by Alvaro de Orleans Borbon, but never before a pilot succeeded to fly up to the height of the Mt. Everest with a motor-glider.
Secondly, the project served to enhance the knowledge in turbulence research and improvement of weather forecast models.
Thirdly aerosol measurements were conducted in order to record the vertical distribution of particulate matter and their optical properties for source apportionment in Nepal.
Fourthly, digital aerial imagery with a resolution, as high as never used before, should be taken in this region to enhance the geographical knowledge about this region, draw conclusions regarding global warming, predict flood impacts and produce documentations of natural or cultural heritage.
And last but not least, concomitant aeromedical aspects of human performance and limitations with a special focus on an early detection of hypoxic hypoxia in pilots under these uniquely extreme environmental conditions (high altitude, low temperature, turbulences) were of particular interest.
Historically oxygen deprivation was one of the first environmental challenges Aerospace medicine had to deal with. As recent F-22 fleet incidents have demonstrated impressively, it is still an issue this field of medicine is engaged in. Worldwide, aircrews are trained in altitude simulation set-ups to become familiar with their individual symptoms, hoping that they would recognize them in a real-flight scenario. Till now, sensors to detect oxygen deficiencies in flight are not in common use.
With the introduction of pulse oximetry (SpO_2), an easy-to-use method to quantify oxygen deprivation of individuals was established in clinical routine. However, and this is surprising, not much effort regarding this technology in the field of Aerospace Medicine was made so far. Earlier work of our group of the GAF CAM could demonstrate that several of those pulse oximetry systems, used in clinical routine, are accurate enough to be also considered as warning systems for pilots. Trials on vibration platforms as well as in-flight tests with different types of aircraft have confirmed that the signal quality of the devices tested is degraded only negligibly. Therefore, with the due degree of prudence, these sensors can be considered to suit the intended purpose of an early warning system in flight.

With this in mind a reflectance pulse oximetry system was tested in the environment of high-altitude glider flying with its expected heavy turbulences and wide-ranging ambient temperatures. In addition, the intended measurements were tailored to optimize the crew's oxygen management during those high-altitude flights.

Methodology

In preparation of the Himalaya campaign pilots completed a comprehensive theoretical and practical training in the hypobaric chamber of the GAF CAM in Koenigsbrueck. Among other things, the curriculum was meant to familiarize the pilots with the handling of oxygen equipment and the advantages and limitations of the technique of pulse oximetry. During the campaign the signal failure rate of pulse oximetry sensors was determined in 28 high-altitude glider flights (up to FL 290) in the Himalaya including the Mt. Everest region and (to enhance the number of flights) in the French Alps. All 7 individuals were equipped with three Nonin, bicolor reflectance sensors and the associated WristOx 3100 system. The sensors were fitted at three different measuring points (forehead, sternum and shin). In addition to oxygen saturation, the heart rate and altitude values were also recorded during the flights.

Results

In total, 19 complete data sets with readings from all sensor locations used could be gathered. SpO_2 values recorded at different measuring points showed distinct differences: the highest values were observed at the forehead (95.39 $\pm$ 2.11%) (Mean $\pm$ standard deviation), the values detected at the sternum were the lowest (84.38 $\pm$ 6.74%). Furthermore, the failure rate was highest at the sternum (26.51 $\pm$ 18.56% of the measuring time). At the shin, the mean SpO_2 was 93.93 $\pm$ 4.24% with a failure rate of 11.67 $\pm$ 19,74% of the measuring time. Measurements at the forehead were most robust, showing a failure rate of 3.28 $\pm$ 6.29% of the measuring time. The mean duration of failures was 12,8 $\pm$ 4,7 s at the forehead, 15,5 $\pm$ 12,8 s at the sternum and 13,7 $\pm$ 11,0 s at the shin.

Conclusions

Without any question, the use of pulse oximetry added to enhance flight safety in this campaign to the Himalayas. However, the results also clearly reveal the difficulties of obtaining robust signals that reliably reflect inflight blood oxygen saturation that have to be overcome. This is particularly true for the shortfalls anyway inherent to the method itself. Nevertheless, in this day and age, the objective continuous detection of a pilot´s oxygen deprivation is inevitable with respect to flight safety. Among the application points for the sensors tested, the forehead appears to be most suitable.

References

Acharya S, Rajasekar A, Shender BS, Hrebien L, Kam M, 2015: Pulse oximeter signal fusion for robust hypoxia detection. Aerosp Med Hum Perform 86 (5), 495-496.

Aoyagi T and K. Miyasaka, 2002: Pulse oximetry: its invention, contribution to medicine, and future tasks. Anesth Analg,, 94 (Suppl), 1-3.

Aviation Hypoxia Monitor. US Patent 5372134; 1994: www.google.com/patents/US5372134 (last accessed on 2 July 2015).

DeJarnette R, Holleran R, von Rotz NP, Downing C, Willhite J, Storer, 1993: D. Pulse oximeter during helicopter transport. Air Med J., 1(4), 93-96.

Severinghaus JW, Astrup P, Murray JF. Blood gas analysis and critical care medicine. Am J Respir Crit Care Med, 157(4 Pt 2), S114-S122

Severinghaus JW. History and recent developments in pulse oximetry, 1993: Scand J Clin Lab Invest (Suppl), 214, 105-111

Figure 1: High altitude measurement flights with the motor glider Stemme S10VTX with the crew Keimer/Heise over the Kali Gandaki Gorge and Annapurna region on the 27th of January 2014

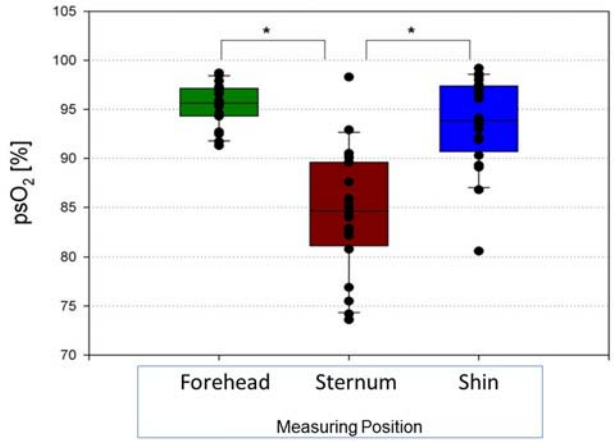

Figure 2: Comparison of the oxygen saturations measured at the forehead, sternum and shin

Low-Altitude Hypoxia

Daniel L. Johnson,
MD Mayo Clinic Health System, Menomonie, WI USA drdan@wwt.net

***Abstract**:* Using oxygen at altitudes below that required by regulations can improve performance and mitigate the likelihood of cognitive pilot error. Portable oximetry is useful in estimating individual need and benefit, if used with understanding.

Introduction

"Lack of oxygen dulls the mind and judgment, slows the reflexes, weakens the muscles, and takes away our higher faculties. The higher one goes, the more serious are these effects. Too many people forget this exactly at a time when they should be most responsive to the danger." (Houston)

There is little data (that I can find) on cognitive impairment from mild hypoxemia – but plenty of anecdotes, and each person has unique experiences. See **Figure 1** for a summary of saturation, altitude, and cognitive change.

We are far more sensitive to hypoxia than the regulations recognize. They are concerned with incapacitation, and flying is usually such a simple, straightforward task that pilots have often returned to brag from flights without oxygen above 6 km (20,000 ft.) MSL. However, none of them could have worked a calculus problem up there, or subtracted a compass heading (it wouldn't have seemed important, anyway; lethargy being a symptom of hypoxia).

Anyone who's donned oxygen while flying at night at 1.5 – 2 km (5-7k ft.) MSL can tell you how quickly the lights on the ground went to 'bright.' (They don't mention that the brain also went to 'bright.')

It's known that smokers function as if they are 1-1.5 km (3-5k ft.) higher than the altitude on the altimeter. In this regard, it's important that carbon monoxide is a problem is several ways.
- It ties up, generally, 3-10% of hemoglobin and permanently prevents it from transporting oxygen to the brain.
- It decreases the ability of hemoglobin to release oxygen into the tissues where it's needed.
- It interferes in all tissues with metabolism even at low concentrations (5-9%) by interfering with the heme-containing proteins that are centrally important in energy transport.
- It makes the oximeter read falsely high. Carboxyhemoglobin levels in nonsmokers are less than 2%, while they may be as high as 10-20% in heavy smokers. COHb resemble[s] oxyhemoglobin in the red range, and thus looks like oxyhemoglobin, causing the pulse oximeter to over-read. For every 1% of circulating carboxyhemoglobin, the pulse oximeter over-reads by 1%. Fifty percent of cigarette smokers have a Carboxyhemoglobin concentration of 6%. Thus, the most important limitation of pulse oximeters is that they are inaccurate when pilots need them the most.

The net of this is that smokers should always carry oxygen, and should always use it beginning at about 1.5 – 2 km (5-7k ft.) above their home airport elevation, and the regulatory limits should be decreased by 1-1.5 km (3-5k ft.). Pilots who've smoked for more than about 20 years, do have impaired lung function, and should plan on using oxygen at lower altitudes – a finger oximeter is the best guide to just when to use it, keeping saturation in the mid-nineties or above for peak performance.

It's important to realize that respiratory physiology is that of a young, healthy body. In my clinical experience, mild (often undiagnosed) asthma is common. Any lung disease will likely cause some deficiency of oxygen absorption, Anemia is common in older people and results in impaired oxygen transport to tissues.

A challenge for understanding oxygen need and effect is that our bodies have no oxygen detector. Breathing is driven by carbon dioxide level and by acid-base balance.

Shortness of breath is not caused by low oxygen – but by whatever increases the work of breathing (resistance to airflow, lung stiffness from asthma, fibrotic tissue, infection, or venous congestion), alters the blood acid-base balance, or alters the
carbon dioxide content.

Pulse oximetry:

Finger pulse oximeter readings are often inaccurate and misleading – but they are useful! One must understand the conditions in which they are prone to error, and make allowance.

Every electronic measuring device will display numbers if powered up. The question is, what is the relationship between reality and the displayed number? This is the main question of metrology, the science of measurement, which really is the science of measurement error.

In looking at measurements, we need to keep in mind that precision (the number of digits after the decimal) does not indicate accuracy (the connection of the number to reality). Oximeters get less accurate when the readings are more important - lower than normal because signal may be eclipsed by noise.

Manufacturers claim their readings are +/- 2% or +/- 3% in the range of 70-100% saturation. This means that when the oximeter reads precisely 87%, your actual blood oxygen saturation is probably in the range of 84- 90% for the less accurate, 85-89% for the more accurate – in the best laboratory conditions, which your cockpit is not! What can delude this instrument?
- Sunlight can "overpower" the unit's own spectrophotometric light source. Some models have better shielding than others.
- Pigmented skin yields lower saturation readings when actual values are in the 80% range.
- Fidgeting degrades their accuracy by 5-20% (that is, with a true O2 saturation of 95%, the meter may read 75-90%)
- The oximeter is measuring the oxygenation of the blood in the fingertip. What really matters is the oxygenation of the blood flowing through the brain.
- Cold fingers have low blood flow, so readings will be low. Only measure warm fingers. Yes, this is a problem for wave flights.
- Carbon monoxide falsely elevates saturation readings due the color of carboxyhemoglobin.
- Hyperventilation which typically happens with altitude, increases peripheral oxygenation while decreasing brain oxygenation, so readings are spuriously high.

With these limitations, oximeters are most useful to reassure you that your oxygenation is OK (90+%), or that you should don oxygen or troubleshoot the situation (85% or below).

They are also useful for self-assessment – for any give reading below about 95% saturation, how do you feel? How well is your brain working? Can you subtract compass headings? Re-program your flight computer adroitly? Do you feel enthusiasm and energy for the task at hand?

If you sense any cognitive clouding for complex mental tasks, turn on the oxygen, and correlate your brain's function with oximeter readings.

The most important reason to evaluate your personal oxygen need is the "I feel fine" problem. Our brilliant minds and superb motor skills depend, for excellence, on our neurochemistry working just right. However, our bodies' impairment-detector is pretty much a near-death detector, and ignores and compensates for mild annoyances (to do otherwise would create continual distractions).

Don't assume that what you need one week will be correct for you the next. The respiratory system normally acclimates and de-acclimates to altitude in just days; respiratory infection, exposure to smoke or fumes, or variable activity of asthma may change your day-to-day oxygen physiology and need.

Pulse oximeters are readily available at prices from $15 to $300. I cannot find comparative performance and reliability data; Nonin was the first to market, if that means anything.

Conclusion

The rapid ascent of aircraft does not permit any acclimatization to altitude. It is the experience of many pilots that subtle hypoxia causes small but noticeable loss of acuity, motivation, or alertness. The pilot who needs peak performance will benefit from using low-flow supplemental oxygen at altitudes much lower than required by regulation to prevent impairment.

Smokers should always carry oxygen, and should always use it beginning at about 1.5 – 2 km (5-7k ft.) above their home airport elevation, and 1-1.5 km (3-5k ft.) before reaching the regulatory altitude, due to carbon monoxide impairment of oxygen absorption and transport.

References

Houston CS. 1996. What price a summit? Wilderness Environ Med 1996; 7:287-8.
Johnson, D. 2012. How Oxygenation Works. Soaring Magazine, 2012 January, 14-16.
http://www.danlj.org/~danlj/Soaring/SoaringRx/2012-01-How-Oxygen-Works-P14-15-16.pdf
Johnson, D. 2012. Does Your Pulse Oximeter Mean What it Says? Soaring Magazine, 2012 June, 18-20.
http://www.danlj.org/~danlj/Soaring/SoaringRx/2012-06-Pulse-Ox-Accuracy-p18-20-22.pdf
Jubran A. 1999. Pulse Oximetry. Crit. Care 1999, R11-R17.

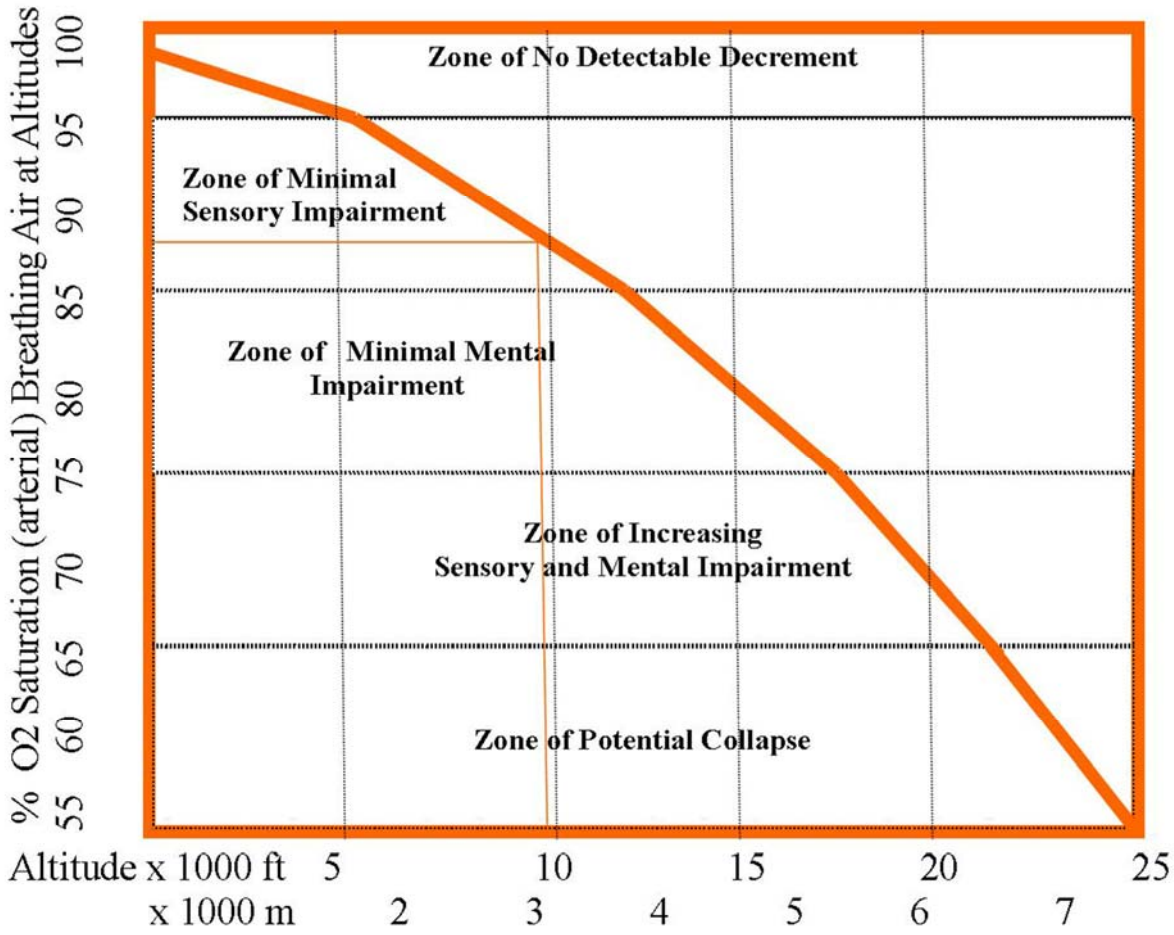

Figure 1: Cognitive function v. altitude v. oxygen saturation

Source: http://www.altitudemouthpiece.com/AMP-and-Altitude-Sickness-Research-Science.html, 2010, Dr. Mike Williams Adapted from McFarland, R.A., "Psychophysiological Implications of Life at Altitude and Including the Role of Oxygen in the Process of Aging", in Yousef, M.K. et al, ed, Physiological Adaptations, pub. Academic Press, New York, Chap. 11, 157-182, 1972. Used under non-commercial “fair use” provisions of Copyright law

Initiative ProSegelflieger - a Package of Measures for the effective Enhancement of passive Safety of Sailplanes

Martin Volck
Diamond Aircraft, M.Volck@diamond-air.at

Abstract: In the several fields of mobilization a lot of knowledge about passive safety has been gained and successfully implemented within the last decades. An important element is the knowledge of the survivable loads of the human body during a crash.
By analyzing the scenarios of sailplane accidents, it can be shown that in typical sailplane accidents most of the severe and fatal injuries could be avoided if this knowledge would consequently be implemented in the sailplane design.

A package of technical measures is proposed.

A moderate increase in weight and costs and a small impact on gliding performance will be the downside effects of this measures.
The goal of the initiative is a significant reduction in the consequences of glider accidents, for this reason: ProSegelflieger*.
The chances for all involved groups, including the sailplane manufacturers, are shown.

(**German:* Segelflieger = *English*: glider pilot)

***Keywords*:** Crash scenarios, Passive safety, Survival cell, Energy absorbing elements, Spinal loads.

Introduction

In the several fields of mobilization a lot of knowledge about passive safety has been gained and successfully implemented within the last decades with a significant positive effect on the respective statistics of traffic victims. In spite of this the yearly number of fatal victims in gliding is constantly growing.
Several publications, such as the work from Dipl. Ing. Martin Sperber, TÜV Rheinland[1] or from Dr. Anthony Segal[2] did not yet have much impact on the sailplane design.

Methodology

By analyzing the scenarios of sailplane accidents, it is shown that in typical sailplane accidents most of the severe and fatal injuries could be avoided if the knowledge regarding the survivable loads of the human body during a crash body would consequently be implemented in the sailplane design.

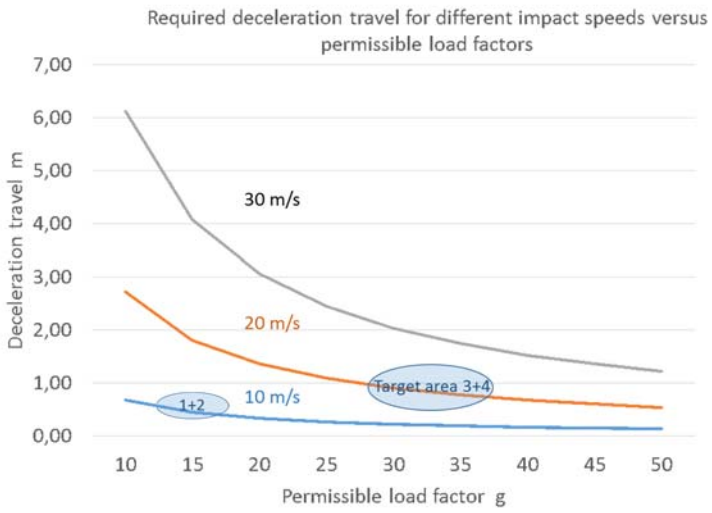

The goal of the initiative is a significant reduction in the consequences of glider accidents. In order to achieve this, a package of technical measures is proposed:

1. Survival cell
2. Energy absorbing fuselage nose
3. Adapted seat belt attachment points
4. Landing gear with increased energy absorption
5. Seat with energy absorbing elements

A forward pointing new standard is presented. This standard will as well help to market safety!

Results

The goal of the Initiative ProSegelflieger is the reduction of the risk of fatal and severe injuries in an accident with a sailplane by a factor of 10. For a sailplane of the 15 m class the additional mass for the package of measures is summing up to 16 kg, the additional costs are summing up to 2500 €.

Conclusions

The reduction of the risk of fatal and severe injuries in an accident with a sailplane requires a package of measures. For an effective enhancement it is necessary to rise the existing standards by a factor of two or even more. The down side is, a statistical effect on the rate of fatal accidents will be very, very slow due to the slow rejuvenation of the fleet.

References

[1]Sperber, M., 1998: Crashworthiness Tests on Glider Cockpits
[2]Segal, A.M., 2004: Survivable Loads on the Pilot and Crashworthiness of Glider Cockpits

Influence of zigzag-tape on profile drag at low Reynolds numbers

Thiemo Hofmacher[1], Peter Scholz[2]
[1] *Institut für Strömungsmechanik, TU Braunschweig, t.hofmacher@tu-bs.de*
[2] *Institut für Strömungsmechanik, TU Braunschweig, p.scholz@tu-bs.de*

Abstract: The contribution discusses the additional drag of 2D transition fixing and zigzag-tape on airfoils at low Reynolds numbers Re=100'000 and Re=200'000 (as typically found e.g. on Winglets), as well as different criteria to estimate the minimum thickness for such tapes. Wind tunnel experiments were conducted in order to determine lift and drag of different airfoils with different thicknesses of zigzag-tape. Two methods to estimate the required thickness of the tape have been compared to the experimental results. The results show that the so-called Re_k-criterion is well able to predict the required tape thickness, although it has been proposed only for larger Re. Nevertheless, also the second criterion seems useful.

***Keywords*:** laminar-turbulent transition, fixed transition, zigzag-tape, airfoil drag, low Reynolds number airfoil

Introduction

The drag of airfoil at low Reynolds numbers is of interest for a variety of applications, not at least sailplanes. It is a standard approach to apply transition fixing tapes to such airfoils in order to prevent laminar separation bubbles, decrease drag and increase lift. For such fixing tapes it is of interest to estimate the required tape thickness to trigger transition, because applying a tape with an oversized thickness will increase drag. In the contribution we review two different criteria: An estimation based on a critical Reynolds number Re_k, as originally proposed by Eppler[1], and a minimum Re_Θ criterion has been published by Preston[2]. For a comprehensive overview also refer to Boermanns[3].

The first criterion is that a minimum Re_k of 200, calculated with the thickness k and the velocity u_k inside the boundary-layer, should be achieved for a zigzag-tape to trigger transition. Originally, this criterion has been proposed for Re>300'000; with the simplicity of this criterion it is of interest, if it is suitable also for Reynolds numbers below 300'000, which also Boermanns[3] suggested as the lowest working Reynolds number for this criterion. Below a Reynolds number of 300'000 he proposes to use a second criterion, which is that a Re_Θ of 320 should be achieved, where the concept is that the zigzag-tape increases Re_Θ. Re_Θ is calculated with the free stream velocity U_∞ and the momentum loss thickness Θ, and the criterion is motivated by the finding that a minimum Re_Θ is required for the existence of a turbulent boundary layer[2]. This was however a study on a flat plate.

If a too large transition tape is used, the drag of the airfoil increases. Beside the criteria, also this aspect was studied. The total drag of an airfoil with zigzag-tape was estimated as the basic drag of the airfoil without the zigzag-tape, minus the drag of the laminar separation bubble plus the drag of the zigzag-tape and the additional friction drag of the longer turbulent boundary layer. The drag of the zigzag-tape has been calculated like the drag of a simple wire as described in Preston[2]: A specific drag coefficient c_D* of 0.75 of a wire was used for the zigzag-tape in the first calculations. Also in the contribution, an attempt will be presented to formulate c_D* for zigzag-tape as a function of Re_k.

Methodology

Wind tunnel tests with different airfoils with chord of around c=138 mm and thicknesses of zigzag-tape (between k=0.11 mm and k=0.66 mm) were made in a small Eiffel wind tunnel. Lift was measured with an electronic scale, which holds the airfoil at one side. The total drag was measured with the momentum loss method by measuring the total pressure distribution in the wake. The experimental setup has been validated by comparing the experimental results with results from the airfoil design code XFoil[4] for various airfoils and it was found to be well able to represent the drag variations of interest. Three different airfoils were used to make the results more independent from the individual airfoil contour. All airfoils however feature a large laminar separation bubble on the suction side. The zigzag-tape was placed just upstream of the separation line, which was found by oilflow-visualization.

The properties of the boundary layers required to estimate Re_k and Re_Θ have been taken from accompanying simulations also using the XFoil code.

Results

The characteristic plot of total airfoil drag over Re_k of different zigzag-tape thicknesses is shown in Fig. 1 for the NACA4412 airfoil, which is taken here as an example. The data for the other airfoils are very similar. All airfoils feature a large laminar separation bubble and, thus, increasing tape thickness decreases drag, because the bubble is more and more disturbed and it's pressure drag contribution decreases. At some point, minimum drag is achieved. Oilflow-vizualizations highlight, that at this point the bubble is heavily disturbed, but not yet fully prevented. If the tape thickness, and thus Re_k, is further increased, drag increases. This is mainly due to the additional drag of

the zigzag-tape itself, but also the additional drag of the turbulent boundary layer contributes. In Fig. 1 minimum drag is below Re_k=200. The oilflow visualizations have shown that a bubble could not be observed at Re_k=200 and above. Thus, Re_k seems to be a suitable criterion to estimate the minimum required tape thickness, also in the regime of Re tested here. It should be noted that the results are very similar for all airfoils tested.
For the Re_Θ criterion the results are also similar, but the variations are larger due the fact, that the specific drag c_D^* of 0.75 of a wire is used to estimate the additional Re_Θ of the zigzag-tape. A function for c_D^* for zigzag-tape was found by fitting the theoretical total drag of the airfoil with "thick" zigzag-tapes (which is the minimum drag of the airfoil plus the additional drag, which is assumed to be completely due to the zigzag-tape) to the experimental drag values. It was found that c_D^* depends on Re_k; it becomes larger for lower Re_k. A best fit curve was found to estimate c_D^* as

$$c_D^* = 300 \cdot Re_k^{-0.935} + 0.585 \quad (1)$$

This approach might hold for similar problems (i.e. Re between 100'000 and 300'000 and thin airfoils with medium camber), but to formulate a more general estimation, the additional drag must be split into the contribution of the fixing tape and the additional drag of the turbulent boundary layer.

Conclusions

As based on the drag data acquired with small airfoils in a Eiffel-type windtunel, the Re_k criterion to estimate minimum tape thickness for zigzag-tape is useful even at Reynolds numbers below 300'000. Though the data is somewhat limited and drag breakdown is only possible by some assumptions and comparisons to XFoil-results, it can be said, that practically using the Re_k-criterion in an application with these airfoils would have been a good choice with respect to drag.
The Re_Θ criterion seems to be reasonable, too, and leads to a similar solution. However, it is based on some assumptions (most important the c_D^* of the tape), which probably makes it more fragile. A first approach to estimate the c_D^* of zigzag-tape has been made, but further work is necessary to account for additional effects/contributions such as the friction drag of the larger (longer) turbulent boundary layer. Currently, LES-simulations are conducted to gain such insight.

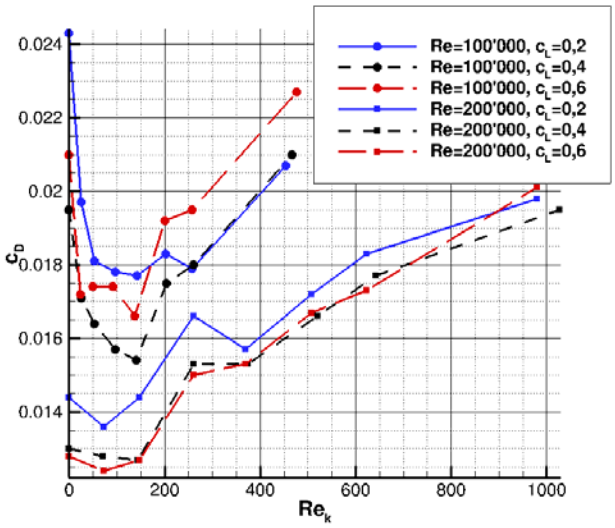

References

[1]Eppler, R., 1979: The effect of disturbance on a wing. The Science and Technology of Low Speed and Motorless Flight, Pt. 1, pp. 81-92
[2]Preston, J.H.., 1958: The minimum Reynolds number for a turbulent boundary layer and the selection of transition device. .Journal of Fluid Mechanics, Vol. 3, pp. 373-384.
[3]Boermanns, L.M.M., 2015: Turbulators in practice. Symposium für Segelflugzeugentwicklung, 19.-20. Nov. 2015, Darmstadt, Germany
[4]Drela, M., 1989: XFoil: An Analysis and Design System for low Reynolds number Airfoils, In: Mueller, T.J. (Ed.,), Low Reynolds number Aerodynamics, Springer Verlag, 1989

Laminar-turbulent transition on wings with 3D flow effects

Federico Muñoz[1], Martin Kruse[2], Rouven Petzold[1], Rolf Radespiel[1]
[1]*Technische Universität Braunschweig, Institute of Fluid Mechanics, Germany,* r.radespiel@tu-bs.de
[2]*DLR, Institute of Aerodynamics and Flow Technology, Braunschweig, Germany*

Abstract: Boundary layer transition on a 3D wing with strong variations of instability along the span is measured in two low-speed wind tunnels. The measurements include pressure distributions, infrared imaging and hot film signals. Comparisons with linear stability computation and N-factors at transition location are also reported. The results display various regions of the model dominated by different transition scenarios. Representing obeserved transition by prediction approaches may require advanced models beyond N-Factor methods based on linear local stability.

***Keywords*:** 3D boundary layers, boundary layer transition, stability anaylsis.

Introduction

For the development of laminar-flow high-performance aircraft it is necessary to have reliable numerical methods that allow predicting where and how laminar-turbulent boundary layer (BL) transition occurs. Methods based on local linear stability theory (LST) and the e^N-method are still widely employed. Founded on the parallel flow assumption, local stability methods neglect effects of stream- and spanwise boundary layer variations [1]. Spanwise pressure gradients can be found in regions of wing fuselage interaction, at connections between wing sections with different sweep and taper, and around intersections of wing and winglet. We note that there is a significant lack of knowledge on the effects of surface-tangential flow gradients on transition. The present work aims at closing this knowledge gap by performing new transition experiments and corresponding flow simulations.

Methodology

Therefore, a special wind tunnel model was carefully designed and manufactured. The model is a wing with varying sweep along its span as shown in Figure 1. The airfoil was specially defined so that Tollmien-Schlichting (TS) instability waves and crossflow (CF) waves are present on the model with different relative amplification rates in different regions [2]. This results in transition scenarios that are TS dominated, CF dominated, and mixed transition scenarios exist as well. By introducing a special layered skin structure of the wind tunnel model high-resolution infrared images needed to determine transition location over the whole surface in an automated fashion are obtained, see Figure 2. The high-resolution infrared images could be also used to determine the wave length of stationary crossflow vortices on the wing. Unsteady instability waves were characterized by using hot films glued to the model skin. The measurements were obtained in two wind tunnels. These were the 1.3m wind tunnel MUB of the Technische Universität Braunschweig and the 3m wind tunnel NWB of the German-Dutch Wind Tunnels.

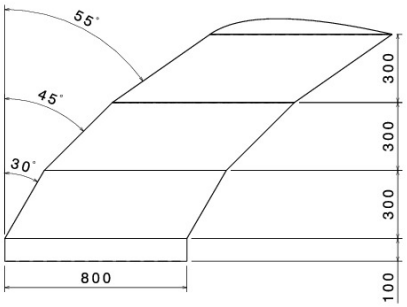

Figure 1. Planform of sickle wing

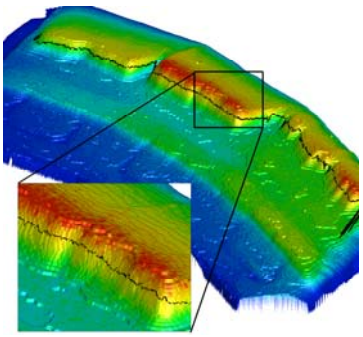

Figure 2. Surface temperature measured by IR-thermography and extracted transition line

These measurements were compared to the results of a LST-method. Boundary layer flow was computed by solving 3D Navier-Stokes equations in laminar flow regions and RANS-equations in turbulent parts of the wing. The simulations employed dense computational meshes in order to fully resolve the 3D wing BL with locally large spanwise variations. Static pressure distributions confirm that pressure-gradient driven BL mean flow agrees very well in computations and experiments [3]. LST applied along BL edge streamlines resulted in N-factors for TS and stationary CF instabilities. The comparison with surface measurements performed using hot-film sensors showed the presence of TS waves and stationary as well as travelling CF instabilities.

Results

The results of the project quantify the effect of wind tunnel environment, the effect of transition scenario and the effects of locally large changes of instability on transition and transition N-factors. Typical differences of transition location measured in the two tunnels are displayed in Figure 3.

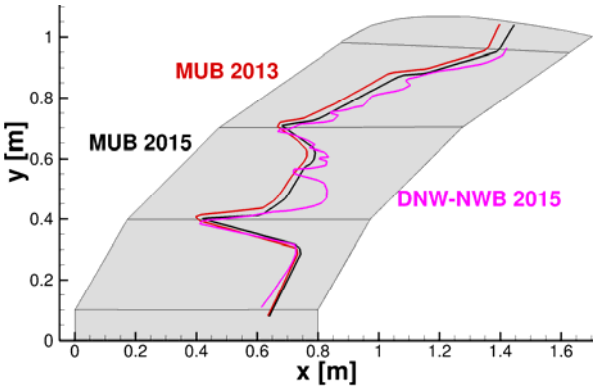

Figure 3. Transition lines on upper wing for different tunnel entries in MUB and DNW-NWB, α=-2.6 deg, Re=2.75·10^6

Figure 4 displays a typical result of measured transition lines at an intermediate Reynolds number, along with the corresponding N-factor computations. It is seen that the inboard wing shows TS-dominated transition where increased turbulence levels towards the wing root reduce transition N-factors. The mid-span upper surface is dominated by stationary crossflow instabilities, whereas the outer wing segment displays a gradual change from travelling CF to dominating TS waves. Interesting are the regions of sweep angle change. These are characterized by locally reduced extent of laminar flow due to strong CF which is only partially explained by LST. Note that there exist flow conditions for which this local behavior is reversed (not shown). We also note that N-factor scatter in Figure 4 (right) is significantly reduced if only data from regions with quasi 2d flow is retained. The amplitudes of hot film data in TS-dominated regions are in good agreement with LST, whereas saturation effects are observed for travelling cross flow waves present at the outer wing section (not shown either).

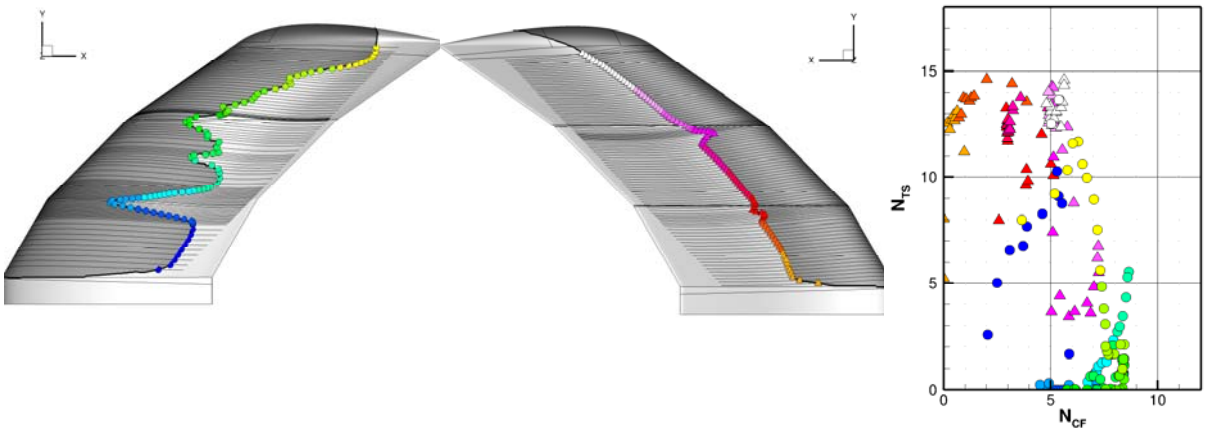

Figure 4. Transition lines on wing upper (left) and lower (middle) sides along with BL edge streamlines shown in black and corresponding N-factors (right), DNW-NWB 2015 data, α=-2.6 deg, Re=2.75·10^6

References

[1]Reed, H. L., Saric, W., Arnal, D., 1996: Linear Stability Theory applied to Boundary Layers, Ann. Rev. Fluid. Mech., 281, pp 389-428.

[2]Petzold, R., Radespiel, R., and Kruse, M., 2011: Entwurf eines Validierungsexperimentes für die 2N-Faktor Transitionsvorhersage, Proceedings of the Deutscher Luft- und Raumfahrtkongress 2011, DGLR.

[3]Petzold, R., Radespiel, R., 2014: Transition on a wing with spanwise varying crossflow and linear stability analysis, AIAA Journal, 53, pp. 321-335.

Validation of Numerical Models for Transitional Flows on Airfoils

Jaromír Příhoda[1], Petr Straka, Jiří Fürst, Lukáš Popelka, David Šimurda
[1] *Institute of Thermomechanics AS CR, v.v.i., Dolejškova 5, 182 00 Praha 8, Czech Republic, prihoda@it.cas.cz*

Abstract: Transition models based on various approaches were tested for transitional flows at relatively low free-stream turbulence on airfoils. The modified algebraic model of Fürst et al. (2013) connected with the EARSM model of Hellsten (2005) gives acceptable results in all tested cases. The k-kL-ω model predicts in some cases the transition onset shift downstream which leads to the laminar separation in the decelerated flow and to the transition in the separation bubble. Moreover, comparison with XFOIL program was drawn: it provides the transition prediction using the e^n method, which gives the adequate transition onset, provided that the appropriate value of parameter n is chosen.

***Keywords*:** CFD, Transition, Separation Bubble, Airfoils

Mathematical models

The Reynolds-averaged Navier-Stokes equations are closed partly by the explicit algebraic Reynolds stress turbulence model (EARSM) according to *Hellsten (2004)* connected with the algebraic transition model modified by *Straka and Příhoda (2010)* and partly by the three-equation k-k_L-ω model of *Walters and Cokljat (2008)*.

The algebraic model was implemented into the in-house numerical code. The code is based on the finite volume method of the cell-centered type with the Osher's-Solomon's approximation of the Riemann solver and a two-dimensional linear reconstruction with the Van Albada's limiter. The governing equations are discretized using a multi-block quadrilateral structured grid with a block overlapping implementation.

The free accessible program OpenFOAM with the own implementation of the k-k_L-ω model was used for the simulation of the transitional flows. The system of governing equations was solved by the SIMPLE algorithm for the incompressible flow. The convective terms were discretized by the upwind method with the reconstruction of the second degree and the viscous terms by means of the central scheme.

The k-k_L-ω model of *Walters and Cokljat (2008)* can be applied for the simulation of complex shear flows on unstructured grids without any restriction. On the other hand, the algebraic transition model was adapted for local variables only but structured grids are preferred near walls.

2.1 Algebraic transition model

The algebraic transition model was used together with the EARSM model proposed by *Hellsten (2004)*. The Reynolds stress is given by the anisotropy tensor defined by the relation

$$a_{ij} = \frac{\overline{u_i u_j}}{k} - \frac{2}{3}\delta_{ij}$$

The anisotropy tensor is expressed by the polynomial

$$a_{ij} = \beta_1 S_{ij} + \beta_3(\Omega_{ik}\Omega_{kj} - \frac{1}{3}\delta_{ij} II_\Omega) + \beta_4(S_{ik}\Omega_{kj} - \Omega_{ik}S_{kj})$$
$$+\beta_6(S_{ik}\Omega_{kl}\Omega_{lj} + \Omega_{ik}\Omega_{kl}S_{lj} - \frac{2}{3}\delta_{ij} IV) \qquad (1)$$
$$+\beta_9(\Omega_{ik}S_{kl}\Omega_{lm}\Omega_{mj} - \Omega_{ik}\Omega_{kl}S_{lm}\Omega_{mj})$$

where non-dimensional strain-rate and vorticity tensors are defined by relations

$$S_{ij} = \tau\frac{1}{2}\left(\frac{\partial U_i}{\partial x_j} + \frac{\partial U_j}{\partial x_i}\right) \text{ and } \Omega_{ij} = \tau\frac{1}{2}\left(\frac{\partial U_i}{\partial x_j} - \frac{\partial U_j}{\partial x_i}\right)$$

The time scale τ is given by the relation

$$\tau = \max\left(\frac{1}{\beta^*\omega}; C_\tau\sqrt{\frac{\nu}{\beta^*\omega k}}\right)$$

where the Kolmogorov time scale is used near the wall with constants $\beta^* = 0.09$ and $C_\tau = 6$. Coefficients β in Eq. (1) are functions of invariants $II_S = S_{kl}S_{lk}$, $II_\Omega = \Omega_{kl}\Omega_{lk}$, $III_S = S_{kl}S_{lm}S_{mk}$, and $IV = S_{kl}\Omega_{lm}\Omega_{mk}$.

The transport equations for the turbulent energy k and the specific dissipation rate ω in presented calculation are used in the two-layer form with two sets of model coefficients and with the blending function similarly as the SST model proposed by *Menter (1994)*. The detailed description of the EARSM model is given by *Hellsten (2004)*. For the prediction of the transitional flows, the production and destruction terms in the k-equation are multiplied by the intermittency coefficient γ.

The algebraic transition model is based on the concept of different values of the intermittency coefficient in the boundary layer γ_i and in the free stream γ_e. The intermittency coefficient in the boundary layer is given by the relation proposed by *Narasimha (1957)*.

The onset and the length of the transition region is given by empirical correlations for the momentum Reynolds number $Re_{\theta t}$ and parameters characterizing the generation and the growth of turbulent spots. Most of transition models are proposed for modelling of the bypass transition where free stream turbulence induces so called bypass transition by the diffusion of turbulent fluctuations across the shear layer. The lower limit of empirical relations for the bypass transition onset is about $Tu \approx 0.15$-0.2 %.

The often used approach to the transition modelling at low turbulence level is the so called e^n method based on the linear stability analysis. The solution of the Orr-Sommerfeld equation for a given velocity profile is applied for the estimation of the spatial growth rate of disturbances and the transition onset occurs when the amplification of the most unstable disturbance reaches a critical value. However, results of stability analysis cannot be directly used for the estimation of the transition onset as the e^n method is based on the disturbance ratio rather than on the actual disturbance amplitude.

On the basis of the stability analysis, *Mack (1977)* proposed the correlation $n = -8.43-2.4 \ln (Tu/100)$ giving the link between the stability analysis and experimental data. For the determination of the maximum amplifi-cation factor by means of boundary layer parameters, *Gleyzes et al. (1985)* proposed a simple empirical relation giving for the similar solution of *Falkner and Skan (1930)* the linear relation between the maximum amplification factor and the momentum Reynolds number. This approach was modified for non-similar flows as well, and so the maximum amplification factor can be determined without the solution of the Orr-Sommerfeld equation, see *Drela and Giles (1987)*.

The scatter of experimental data is for low free-stream turbulence $Tu < 0.1$ % much greater because the transition in this region is influenced by other factors especially by acoustic disturbances.

The typical turbulence level $Tu \approx 0.5$ % was established by the in-flight CTA measurement of velocity fluctuations in the thermal convection atmosphere, this being typical sailplane operating environment, see *Popelka et al. (2014)*.

The effect of various disturbances especially acoustic noise on the transition at very low free-stream turbulence was firstly studied by *Govindarajan and Narasimha (1991)*. In this region, the transition is caused by so-called residual disturbances specific to the used facility. *Govindarajan and Narasimha (1991)* expressed these disturbances by the equivalent turbulence level Tu_o and modified the criterion for the transition to the relation $Re_{\theta to} = 110 + 340 / (Tu^2+Tu_o^2)^{1/2}$.

Similarly, the correlation proposed by *Straka et al. (2012)* for the transition onset on the flat plate can be modified for $Tu \le 0.25$ % according to experiments of *Schubauer and Skramstad (1948)* in the form:

$$Re_{\theta to} = 900 + 215\left\{1 - \exp\left[-4\left(\frac{0.25 - Tu}{0.17}\right)^2\right]\right\}$$

where the parameter $A = 215$ depends on other disturbances than free-stream turbulence. This modified criterion follows up smoothly to the relation:

$$Re_{\theta to} = 975.8 - 497.2Tu + \frac{11.4}{Tu} \quad \text{for } 0.25 \le \mathrm{Tu} \le 1\%$$

$$Re_{\theta to} = 96.7 + \frac{340}{Tu} + \frac{53.3}{Tu^2} \quad \text{for } Tu > 1\%$$

The general criterion for the transition onset is still given by the relation:

$$Re_{\theta t} = Re_{\theta to}\left[1 + \mathrm{F}(Tu)\frac{1 - \exp(-40\lambda_t)}{1 + 0.4\exp(-40\lambda_t)}\right]$$

where is:

$$\mathrm{F}(Tu) = 0.29\left[1 - 0.54\exp(-3.5Tu)\right]\exp(-Tu)$$

The present correlation was compared partly with experimental data of *Schubauer and Skramstad (1948)* and *Wells (1967)* where $A = 575$ and partly with empirical correlations of *Govindarajan and Narasimha (1991)* and results of *Gleyzes et al. (1985)* for the flat plate flow.

The length of the transition region given by the spot generation rate $\hat{n}$ and the spot propagation rate σ is expressed by the parameter N introduced by *Narasimha (1985)*. The effect of the free-stream turbulence and the pressure gradient on the parameter N is correlated by an empirical relation $N = \mathrm{f}(Tu, \lambda_t)$ proposed for the attached flow by *Solomon et al. (1996)*. This correlation agrees with experiments *Schubauer and Skramstad (1948)* at low free-stream turbulence as well.

The onset of transition in separated flow is given by the correlation proposed by *Mayle (1991)* in the form:

$$Re_{xt} = 300Re_{\theta s}^{0.7} + Re_{xs}$$

where $Re_{\theta s}$ is the momentum Reynolds number at the separation and Re_{xs} is the Reynolds number related to the distance of the separation position from the leading edge. The transition length is expressed in the form: $\hat{n}\sigma = 2.28\times10^{-5}\, Re_{\theta s}^{-1.4}$

and so the same approach can be applied as in the attached flow.

To avoid the application of local variables, the maximum of the vorticity Reynolds number Re_{vmax} is used instead of the momentum Reynolds number Re_θ according to *Langtry and Menter (2009)*. The vorticity Reynolds number is given for complex flows by the relation: $Re_v = y^2 |\Omega| / \nu$

where y is the distance from the wall and Ω is the absolute value of the vorticity tensor. This link is expressed by the relation $Re_\theta = Re_{vmax}/C$ where the parameter C depends on the pressure gradient. Free-stream turbulence was taken at the boundary layer thickness δ estimated by means of the position of the maximum vorticity Reynolds number using the similar solutions of *Falkner and Skan (1930)*. The algebraic transition model is described in detail by *Straka et al. (2012)*.

2.2 k-k_L-ω model

The three-equation model proposed by *Walters and Leylek (2004)* and later modified by *Walters and Cokljat (2008)* is based on the assumption that velocity fluctuations before the transition can be divided into small vortices contributing to the production of turbulence and large mainly longitudinal vortices near the wall contributing to the production of non-turbulent fluctuations.

The used version of the three-equation model is in detail described by *Fürst et al. (2013)*. The transfer of energy between non-turbulent and turbulent vortices is modelled in these equations by terms R_{BP} and R_{NAT} expressing the effect of the decay of laminar fluctuations during the natural and bypass transition, see also *Prihoda et al (2014)*.

Results

Out from numerous reference cases a sailplane relevant selection on airfoils is presented. It involves a LWK-designed XIS40MOD airfoil experiencing both separation-bubble coupled transition and also natural transition in attached flow, in order to cover typical scenarios on sailplane wing sections, given low operating Reynolds number. Comparison with experimental data is provided on the Figures 1 and 2.

Conclusions

Transition models based on various approaches were tested for transitional flows at relatively low free-stream turbulence. The modified algebraic model of *Fürst et al. (2013)* connected with the EARSM model of *Hellsten (2005)* gives acceptable results in all tested cases. The k-k_L-ω model predicts in some cases the transition onset shift downstream which leads to the laminar separation in the decelerated flow and to the transition in the separation bubble. The XFOIL program with the transition predicted by the e^n method gives the adequate transition onset provided that the appropriate value of parameter n is chosen, which requires ad hoc validation for each calculation.

Presented models provide a viable option of accurate calculation of pressure and viscous contribution to sailplane airfoil drag.

References

1. R. Langtry, F.R. Menter, AIAA J., 47, 2894-2906 (2009)
2. K. Lodefier, E. Dick, Flow, Turbulence and Combustion, **76**, 103-132 (2005)
3. P. Straka, J. Příhoda, *Proc. Conf. Experimental Fluid Mechanics 2010*, Liberec, 636-641 (2010)
4. M. Drela, M.B. Giles, AIAA J., **23**, 1347–1355 (1987)
5. H.W. Stock, W. Haase, AIAA J., **38**, 2059-2066 (2000)
6. D.K. Walters, J.H. Leylek, J. Turbomachinery, **126**, 193–202 (2004)
7. H. Lee, S.-H. Kang, J. Fluids Engineering, **122**, 522-532 (2000)
8. W. Würz, *Hitzdrahtmessungen zum laminar-turbu-lenten Strömungsumschlag in anliegenden Grenz-schichten und Ablöseblasen sowie Vergleich mit der linearen Stabilitätstheorie und empirischen Um-schlagskriterien*, Dissertation, Universität Stuttgart (1995)
9. A. Hellsten, *New two-equation turbulence model for aerodynamics applications*, PhD Thesis, Helsinki University of Technology (2004)
10. A. Hellsten: New advanced k-omega turbulence model for high-lift aerodynamics, *AIAA Jour.*, 43, 9, 1857-1869, 2005
11. D.K. Walters, D. Cokljat, J. Fluids Engineering, **130**, 121401/1-121401/14 (2008)
12. F.R. Menter, AIAA J., **32**, 1598-1605 (1994)
13. R. Narasimha, J. Aerospace Science, **24**, 711-712 (1957)
14. L.M. Mack, *AGARD Conference Proc.*, **224**, 1/1-1/22 (1977)
15. C. Gleyzes, J. Cousteix, J.L. Bonnet, *Proc. Conf. on Low Reynolds Number Airfoil Aerodynamics*, University of Notre Dame Press, 137-152 (1985)
16. V.M. Falkner, S.W. Skan, Phil. Mag., **12**, 865-896 (1930)
17. R. Govindarajan, R. Narasimha, J. Fluids Engi-neering, **113**, 147-149 (1991)

18. P. Straka, J. Příhoda, D. Šimurda, EPJ Web of Conferences **25**, 01091 (2012)
19. G.B. Schubauer, H.K. Skramstad, *NACA Report No. 909* (1948)
20. C.S. Wells Jr., AIAA J., **5**, 172-174 (1967)
21. R. Narasimha, Progress in Aerospace Science, **22**, 29-80 (1985)
22. W.J. Solomon, G.J. Walker, J.P. Gostelow, J. Turbo-machinery, **118**, 744-751 (1996)
23. R.E. Mayle, J. Turbomachinery, **113**, 509-537 (1991)
24. J. Fürst, J. Příhoda, P. Straka, Computing, **95**, S163-S182 (2013)
25. J. Windte, R. Radespiel, U. Scholz, B. Eisfeld B, *Meeting on Enhancement of NATO Military Flight Vehicle Performance by Management of Interacting Boundary Layer Transition and Separation*, RTO-MP-AVT-111-P-03, Prague (2004)
26. J. Příhoda, P. Straka, J. Fürst, L. Popelka, *Proc. Conf. AEaNMiFMaE 2014, University of Žilina (2014)*
27. J. Fürst, P. Straka, J. Příhoda,: Modelling of natural and bypass transition in aerodynamics, *Proc. Conf. Experimental Fluid Mechanics 2013*, Liberec, 217-222, 2013
28. L. Popelka, M. Matějka, L. Zelený, V. Uruba: CTA measurement of longitudinal velocity fluctuation and its spectra in thermal convection atmosphere and lee-wave condition using sailplane in-flight experiment, *Proc. Conf. Topical Problems of Fluid Mechanics*, Prague, 105-108, 2014

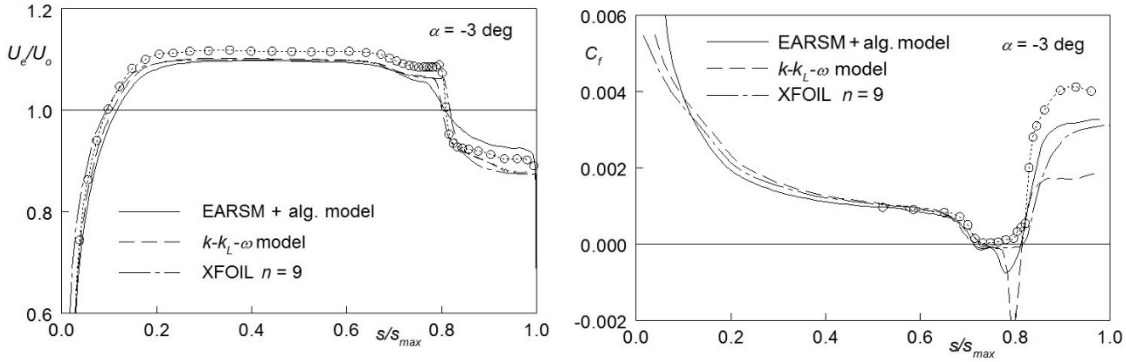

Fig. 1 Velocity distribution (left) and the friction coefficient C_f (right) on the XIS40MOD airfoil, AoA α = -3 deg, comparison with experimental data

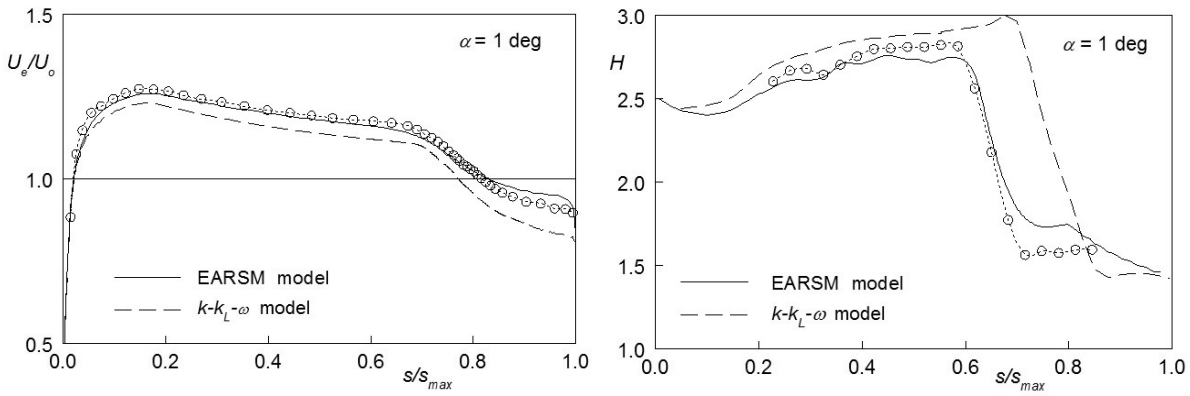

Fig. 2 Velocity distribution (left) and the form parameter H (right) on the XIS40MOD airfoil, AoA α = 1 deg, comparison with experimental data

Effects of Structural Motion on Separation and Separation Control: An Integrated Investigation using Numerical Simulations, Theory, Wind-Tunnel and Free-Flight Experiments

Hermann F. Fasel[1], Shirzad Hosseinverdi[1], Jesse Little[1], and Andreas Gross[2]
[1]*Aerospace & Mechanical Engineering Department, University of Arizona, Tucson, AZ 85718*
[2]*Mechanical & Aerospace Engineering Dept., New Mexico State Univ., Las Cruces, NM 88003*
Email Contact: faselh@email.arizona.edu

Abstract: A combined investigative approach which employs high-fidelity numerical simulations, wind & water-tunnel and free-flight experiments is taken to investigate the fundamental flow physics of separation and separation control for wing sections undergoing temporal motions. Detailed investigations of the underlying unsteady flow physics have been carried out for the X-56A airfoil at nominal angles of attack of 10 and 12 degrees for Re = 200k. The reduced frequency of the structural motion is k=0.7 and the plunging amplitude is 3.2% and 4.8% of the chord length. For 10deg AoA, the agreement between the measurements, simulations, and Theodorsen's theory is good even though the instantaneous angles of attack during the airfoil oscillations are outside the linear $C_L - AoA$ regime and extend into the region associated with static stall. As the angle of attack is increased to 12deg, the flow over the suction surface of the wing begins to intermittently separate and Theodorsen's theory fails. Experiments and simulations show strong qualitative agreement and both capture "bursting" of the laminar separation bubble near the leading edge of the airfoil. Furthermore, highly resolved Direct Numerical Simulations (DNS) were performed in order to investigate the hydrodynamic instability mechanisms and transition to turbulence in swept laminar separation bubbles.

Keywords: Unsteady boundary-layer separation, laminar-turbulent transition, wing motion, swept wings.

Introduction

For most of the published research addressing separation for wing sections the effect of wing motion on the fluid dynamics is neglected. In the near-stall and/or full-stall regime some degree of wing movement is always present. With the current trend towards aerodynamically more efficient flexible high-aspect-ratio composite wings, this effect will become even more relevant in the future. Therefore, the consideration of the wing motion is crucially required for the successful implementation of flow control strategies in future advanced military and civilian aircraft. Our combined research approach addresses this critical issue by employing CFD simulations, wind-tunnel and free-flight experiments for investigating the fundamental flow physics of separation and its control for wing sections that are undergoing temporal (oscillatory, or impulse) motions resulting from fluid-structure interactions, atmospheric unsteadiness, engine vibrations, etc. By directly describing the wing movement in the investigations, the proposed research sets itself apart from existing fluid-structure interaction research. The focus here is not on the fluid-structure interaction per se, but rather on the effect of the airfoil motion on the fundamental flow physics of separation and its control. The parameter space for this (w.r.t., Reynolds number, pitching and/or plunging amplitude and frequency) is very different from flapping wing research and is therefore highly relevant for larger UAVs and/or full-size aircraft. The objective of the current research is to provide a fundamental physics-based understanding of how unsteady wing motion affects separation and its control for lifting surfaces. This improved understanding will ultimately lead to guidelines for the design of novel flexible composite wings with reduced fatigue loads or tailored elastic properties, such that the structural motion can be exploited for flow control.

Despite the large amount of research carried out for laminar-turbulent transition in laminar separation bubbles (LSBs) and considerable advances made in the understanding of the relevant mechanisms, our knowledge regarding swept separation bubbles is quite limited. To contribute towards a better understanding of the highly complex flow physics of LSBs in three-dimensional boundary layers, highly resolved 3D DNS are carried for a LSBs developing on a flat plate generated by a strong favorable-to-adverse pressure gradient for different sweep angles.

Methodology

To investigate the interaction of structural motion and separation, with support from the Air Force Office of Scientific Research (AFOSR) a collaborative research program was initiated at the University of Arizona (UA) and New Mexico State University (NMSU). Free-flight experiments are being carried out at the University of Arizona (UA) to map out the relevant parameter space (amplitudes, frequencies and Reynolds numbers) which will then be used for the CFD simulations and wind-tunnel experiments. Two different dynamically scaled models of the X-56A have been designed for scientific flight experiments. The X-56A, also known as the MUTT flight demonstrator, is a product of the AFRL-led Multi-Utility Aeroelastic Demonstration (MAD) program as shown in Fig. 1a. The airplane was designed and constructed by Lockheed Martin's Skunk Works. At the University of

Arizona, a 1:3 dynamically scaled model of the X-56A has been designed and built (see Fig. 1b) and its flight readiness was demonstrated. The aircraft is currently waiting to be instrumented for scientific flight tests.

The X-56A airfoil is investigated in the new low free-stream turbulence subsonic wind tunnel at the UA. A plunging apparatus was designed and built for subjecting wing sections to plunging motions up to 20Hz (see Fig. 2a). It consists of an electric motor and a system of linkages that convert the rotational motion of the motor to a linear motion of the model (Mertens et al.[1]). A 1ft chord X-56A airfoil (AR=3) was instrumented with pressure taps near midspan and mounted vertically in the wind tunnel. The model is connected to a custom plunging apparatus that operates near the eigen-frequency of the flight-test model. In parallel, Implicit Large Eddy Simulations (ILES) are performed at NMSU. This multi-tiered approach allows for the cross-validation of the different investigative tools (free-flight & wind-tunnel experiments, simulations) and thus increases chances for breakthroughs in this difficult field of research. A research Computational Fluid Dynamics (CFD) code that solves the compressible Navier-Stokes equations in curvilinear coordinates was employed for the present wing section simulations.[2] Rigid grid movement is accomplished through a time-dependent coordinate transformation.[3] The convective terms of the Navier-Stokes equations were discretized with a ninth-order-accurate van Leer scheme[4] and a fourth-order-accurate discretization was employed for the viscous terms. An implicit second-order-accurate Adams-Moulton method was used for time integration. An O-grid with high orthogonality and smoothness was generated with a Poisson grid generator (Fig. 2b). The number of cells in the circumferential, wall-normal, and spanwise direction is 400x100x32. The grid extent in the radial and spanwise direction is 10c and 0.2c, respectively.

A 3-D incompressible Navier-Stokes code using high-order accurate finite-difference approximations was employed for the DNS of LSBs. This code was developed in our CFD Laboratory and validated for numerous investigations of boundary-layer transition and LSBs (Meitz & Fasel[5], Hosseinverdi et al.[6], Balzer & Fasel[7], Hosseinverdi & Fasel[8]). For details see Meitz & Fasel.[5] The simulation setup is guided by water-tunnel experiments that are being carried out at the Hydrodynamics Laboratory of the University of Arizona. The setup of the simulations for the swept LSB simulations is illustrated in Fig. 2c (separation is generated on a flat plate as in the experiments).

Results

The wing section experiments and simulations for Re=200k are discussed first. The phase-averaged lift coefficient for α=10deg, k=0.7, and h=0.032 is presented in Fig. 3a. A slight phase shift is observed between simulation and Theodorsen's theory. Compared to the experiment, the simulation data is almost perfectly harmonic and lacks the slight experimental lift increase near φ=270deg which is a consequence of flow separation. For α=12deg, k=0.7, and h=0.048 both experiment and simulation deviate from theory (Fig. 3b) mostly with respect to the phase. Near φ=300deg the drag coefficient becomes very large indicating a significant amount of flow separation. For 270deg<φ<45deg the lift coefficient for the simulation is lower than for the experiment. During the upstroke, for φ=75deg the drag coefficient attains a minimum indicating flow reattachment. Instantaneous flow visualizations (Fig. 4a) reveal a progressing trailing edge separation during the downstroke (90deg<φ<270deg) that persists into the first half of the upstroke (270deg<φ<360deg). Both experiment and simulation capture the laminar separation bubble at the leading edge, however, a more aggressive trailing edge separation is observed in the experiment (see Fig. 4b).

Building on our previous research for unswept laminar separation bubbles[6,7,8], highly resolved DNS were employed to investigate the effect of crossflow on LSBs. From a technical application point of view, an elevated free-stream turbulence intensity (FSTI) is often responsible for laminar-turbulent transition and has thus to be considered when investigating laminar-to-turbulent transition in LSBs. In the simulations, isotropic grid turbulence was introduced at the inflow boundary (see Hosseinverdi et al.[6] and Balzer & Fasel[7] for details). The chordwise variation of the time- and spanwise-averaged skin-friction coefficient for different sweep angles are plotted in Fig. 5 for both the natural quiet scenario (FSTI=0) and for a scenario with an elevated FSTI of 0.1%. For FSTI=0, preliminary results show that the mean separation length is essentially independent of the sweep angle. Major differences for the unswept and swept flow become visible when a FSTI of 0.1% is introduced in the simulations. The mean separation length is reduced by 66.1% for 45deg sweep compared to the zero FST case. The reductions are 48% and 37.3% for the 30deg swept and unswept case, respectively. Iso-surfaces of the λ_2-criterion[9] are shown in Fig. 6. For FSTI=0%, large spanwise coherent structures are forming because of shear layer instability. These structures are commonly called 'spanwise rollers' or Kelvin-Helmholtz vortices. For a FSTI of 0.1%, the free-stream turbulence induces low-frequency u-velocity distortions inside the laminar approach boundary-layer and disturbances with a wide range of wavelengths and frequencies (including steady disturbances) are strongly amplified.

Conclusions

Wind tunnel experiments and implicit large eddy simulations for a plunging wing section for 10 and 12deg angle of attack were found to be in good qualitative agreement. For α=10deg the lift coefficient followed Theodorsen's theory closely and the experimental and numerical data revealed minimal flow separation and a periodic thickening

and thinning of the suction side boundary layer. For 12deg angle of attack intermittent flow separation from the suction surface is observed during the downstroke and the first half of the upstroke and the lift coefficient deviates from Theodorsen's theory mainly with respect to the phase. Although quantitative agreement between experiment and simulation was achieved only over part of the plunging period, both data sets reveal a periodic bursting of the laminar leading edge bubble. The effect of wing sweep was investigated for a representative model geometry. From DNS, it was found that wing sweep considerably amplifies the effect of FST on the structure of laminar separation bubbles.

Acknowledgements

This research was funded by the Air Force Office of Scientific Research (AFOSR) (Program Manager: Dr. Douglas Smith, grant number: FA9550-14-1-0184).

References

[1]Mertens C, Pineda S, Agate M, Little J, Gross A, Fasel, H. F., 2016: Effects of Structural Motion on the Aerodynamics of the X-56A Airfoil. AIAA Paper 2016-2073.
[2]Gross, A., and Fasel, H., 2008: High-Order Accurate Numerical Method for Complex Flows. AIAA J., 46(1), pp. 204-214.
[3]Gross, A., Zhou, J., and Fasel, H.F., 2015: Numerical Simulation of Circular Cylinder and Wing Sections in Unsteady Motion. AIAA-paper AIAA-2015-3069.
[4]Gross, A., Little, J.C., and Fasel, H.F., 2016: Numerical Simulation of Wing Section Near Stall. AIAA 2016-3947.
[5]Meitz, H. & Fasel, H. F., 2000: A compact-difference scheme for the Navier-Stokes equations in vorticity-velocity formulation. J. Comp. Phys, 157, 371–403.
[6]Hosseinverdi, S., Balzer, W., and Fasel, H. F., 2012: Direct Numerical Simulations of the Effect of Free-Stream Turbulence on 'Long' Laminar Separation Bubbles. AIAA Paper 2012-2972, New Orleans, LA.
[7]Balzer, W. & Fasel, H. F., 2010: Direct numerical simulation of laminar boundary layer separation and separation control on the suction side of an airfoil at low Reynolds number conditions. AIAA Paper 2010-4866.
[8]Hosseinverdi, S and Fasel H. F., 2013: Direct Numerical Simulations of Transition to Turbulence in Two-Dimensional Laminar Separation Bubbles. AIAA Paper 2013-0264.
[9]Jeong, J. & Hussain, F., 1995: On the identification of a vortex. J. Fluid Mech, 285, 69–94.

Figures

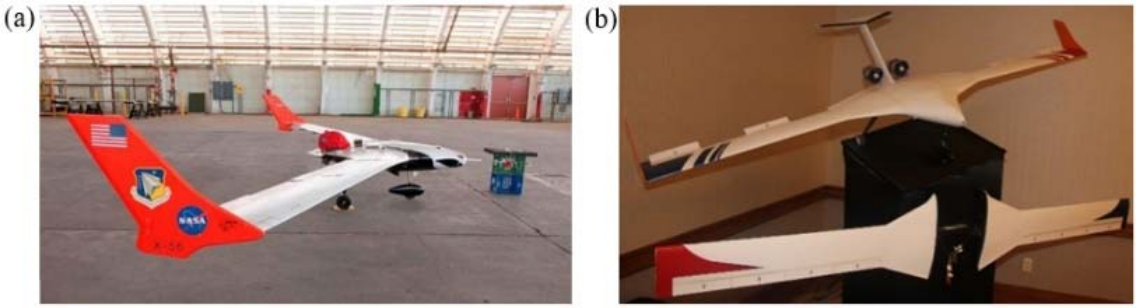

Figure 1. X-56A: a) Full size (NASA Armstrong); b) 1:3 dynamically scaled model (University of Arizona).

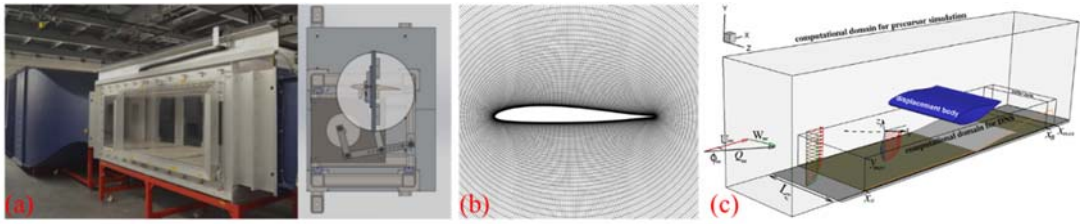

Figure 2. a) Wind tunnel and plunging mechanism, b) O-grid for wing section simulations; c) computational setup for simulating swept laminar separation bubble on flat plate.

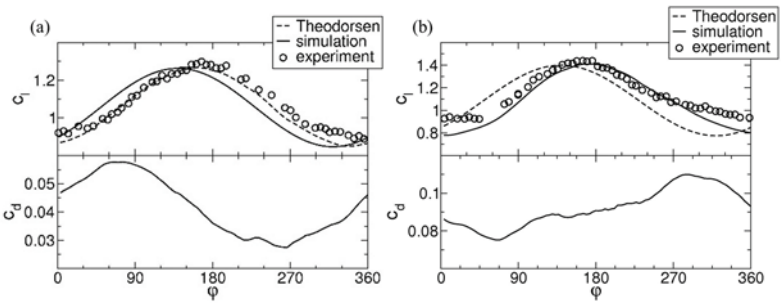

Figure 3. Lift and drag coefficient for a) α=10deg, k=0.7, h=0.032 and b) α=12deg, k=0.7, h=0.048.

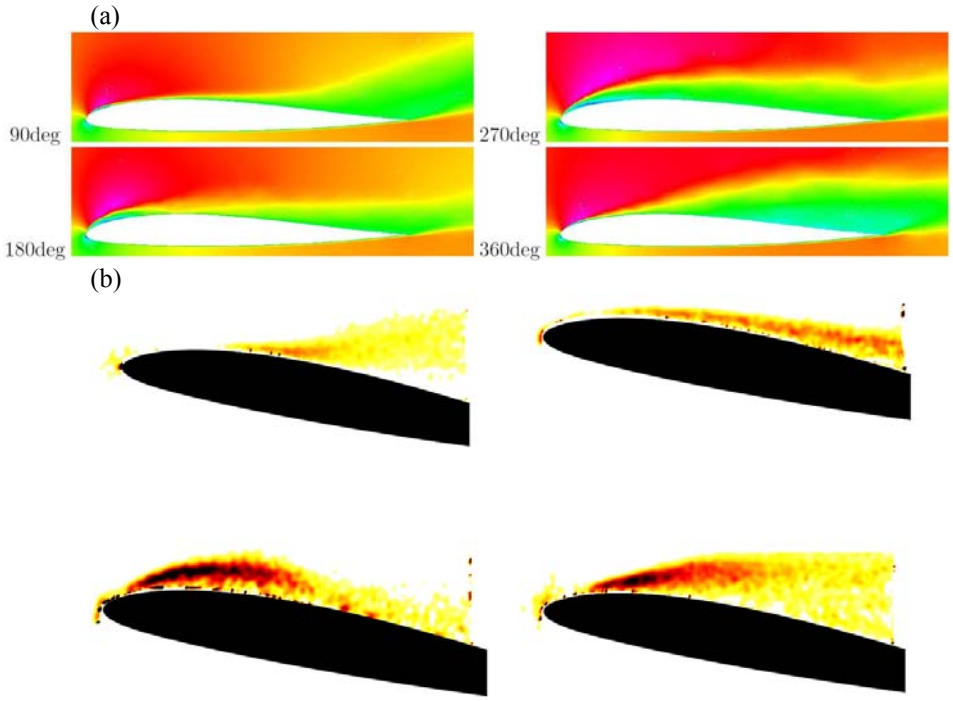

Figure 4. Flow visualiztion for α=12deg, k=0.7, h=0.048. (a) Iso-contours of u-velocity from simulations (phase and spanwise averages); (b) phase averaged vorticity (from PIV).

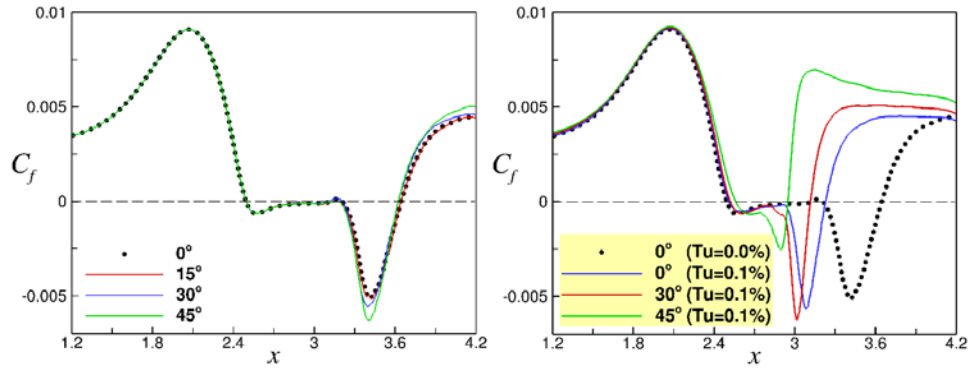

Figure 5. Time- and spanwise-averaged wall-skin friction for various sweep angles. Left: natural simulations (FSTI=0); right: FSTI=0.1%.

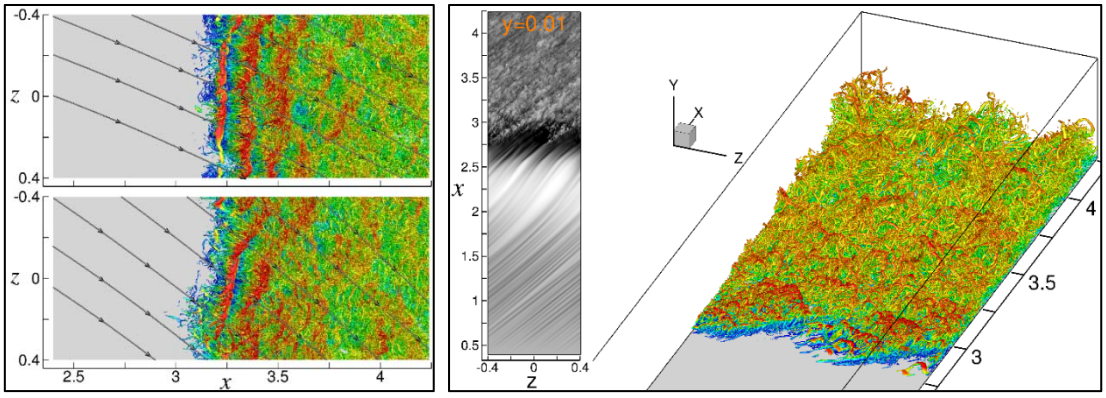

Figure 6. Instantaneous flow visualizations. Left: Top-down views of iso-surfaces of $\lambda_2 = -500$ colored by u-velocity together with inviscid streamlines for $\phi_\infty = 30^o$ (top) and $\phi_\infty = 45^o$ (bottom) for FSTI=0; right: Iso-surfaces of $\lambda_2 = -500$ colored by u-velocity together with contours of u-velocity at constant y-location for FSTI=0.1% and 45deg sweep.

Speed-to-Fly Theory #1: Insights on the implications of flying incorrect speeds with quadratic and non-quadratic polars

Michael Steckner, PhD, MBA
mks@steckner.net

Abstract: Speed-to-fly theory, based on quadratic polars, is considered robust against inter-thermal flight speed errors and consistently so across a broad range of sailplane performance and flight conditions. Modern sailplane polars may be sufficiently non-quadratic to have sailplane-unique robustness characteristics. Current quadratic error tolerance properties are expanded and non-quadratic polar properties are introduced.

***Keywords*:** *speed-to-fly, error sensitivity, quadratic, non-quadratic*

Introduction

Speed-to-fly (stf) theory, based on quadratic sailplane polars, has provided a strong foundation for sailplane flight optimization. It has long been understood that flying at the incorrect speed does not significantly degrade average cross-country speed performance, unless the speed error is significant. However, this understanding is premised on a few assumptions, specifically that sailplane polars are well described by a quadratic, that are investigated here in this and the companion papers in detail.

This paper reviews an excellent summary publication[1], but which may have only considered the case of no inter-thermal air mass movement, to establish a standard knowledge baseline. It is shown that inter-thermal air mass movement does have a small impact on error sensitivity. It has also been stated[1], that higher sailplane performance does not significantly impact stf theory robustness. This is confirmed and updated. Most importantly, this paper demonstrates that if the sailplane polar is not well described by a quadratic, flying the incorrect inter-thermal speed may have a significant (>1%) impact on achieved cross country speed and the robustness to incorrect flight speeds can be lower, or higher, than standard stf theory suggests. The non-quadratic polars are variously represented and tested to confirm results.

Figure 1 is the equivalent classic error plot for an ASW-15 vs the Standard Cirrus plot shown in Reichmann[1] as computed by Kauer and is an excellent summary of current understanding. Figure 2 shows a representative and unique error plot for a Discus.

Methodology

Non-quadratic polars were derived from sailplane vendor published data and/or flight test evaluations. Presently, there are no known simple curve fitting methods that can be applied uniformly to all sailplanes as quadratics are presently fitted to all sailplanes. Results presented in this series of papers variously used short straight line segments and higher order polynomials of various orders to evaluate the flight speed robustness properties of non-quadratic polars in the same manner quadratic polars have been evaluated.

Sensitivity to flight speed errors was computed over a range of lift expected vs actual ring settings and was presented as % error contour plots. In addition to repeating known results, quadratic polar results were further extended by considering the impact of inter-thermal air mass motion. Non-quadratic polar analysis was restricted to no inter-thermal air mass motion conditions.

Results

The sensitivity of quadratic sailplane polars to inter-thermal air mass movement is marginal. It will be shown that error contours are slightly more tightly bunched around the central diagonal in the case of air mass lift but slightly wider spaced in the case of air mass sink, but neither trend likely of practical consequence, except potentially in extreme inter thermal lift/sink conditions. It is reconfirmed that sailplane performance has a minor impact on error sensitivity.

The limited number of non-quadratic polars analyzed have unique shapes that cannot be consistently fit with one common function. Consequently, the robustness to inter-thermal flight speed errors is unique, as shown in Figure 2 for a Discus, and significantly different from the current quadratic based literature as represented by Figure 1 (ASW-15). The Discus polar results in increased sensitivity at lower climb rates which then rapidly transitions to a much more robust sensitivity at higher climb rates. ASW-24 results, not shown here, have a more uniform and highly robust sensitivity shape distinctly different than the Discus.

Conclusions

Anecdotal observation suggests that modern sailplane polars are non-quadratic. Analysis shows that the slight differences in polar shape do significantly change the robustness to inter-thermal speed errors.

References

[1] Reichmann, H., 1993: Cross-Country Soaring (Streckensegelflug), ISBN-13: 978-1883813017 Thomson Publications

[2] Steckner, M., 2017: Speed-to-Fly Theory #3: Potential issues with modern sailplanes with non-quadratic polars, OSTIV 2017

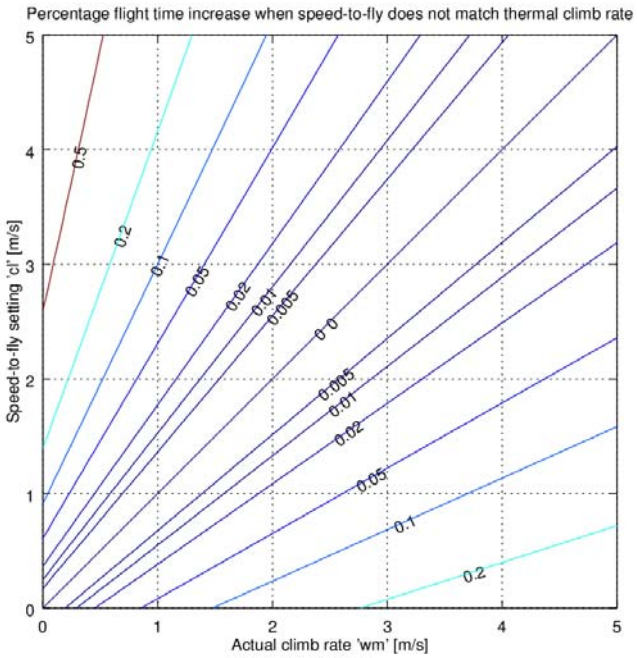

Figure 1. Contour intervals show percent flight time increase due to incorrect thermal climb rate prediction, with no inter-thermal airmass movement for an ASW-15.

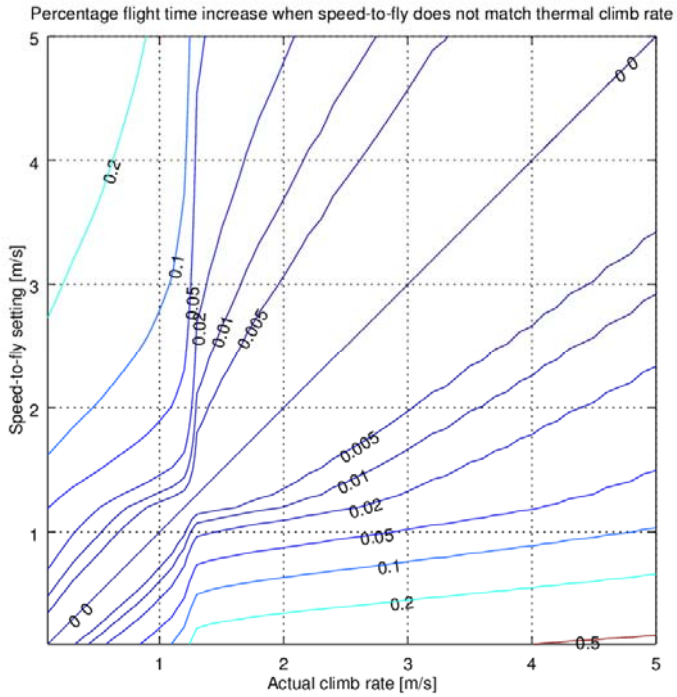

Figure 2. Contour intervals show percent flight time increase due to incorrect thermal climb rate prediction, with no inter-thermal airmass movement for a Discus

Speed-to-Fly Theory #2: Implications of flight test data variability

Michael Steckner, PhD, MBA
mks@steckner.net

Abstract: Deriving polars from flight test data presents unique challenges. Implications for speed-to-fly results and how to perform a test program to optimally produce accurate polars can be determined by Monte Carlo analysis. Such analysis requires a statistical signature of a flight test program for realistic Monte Carlo analysis. This paper is based on a special extraction of most Johnson test series data. Results suggest a slight positive bias in the Johnson summary results, but a scatter in the expected range. Results also show it is possible to slightly optimize a test program for quadratic polar curve fitting purposes and that if the fit passes simple quality checks, the impact on quadratic speed-to-fly theory is minimal.

Keywords**:** *speed-to-fly, flight testing, quadratic, non-quadratic, Monte Carlo*

Introduction

Speed-to-fly (stf) theory, based on quadratic polars, requires quality performance data. Given that flight testing is a difficult and expensive task, it is useful to investigate the impact of flight test data quality on stf results. Given a statistical understanding of experimental flight test evaluation (fte) data, as derived from a scatter analysis of most of the Johnson flight test series, Monte Carlo simulation methods are used to investigate how fte methodology impacts the quality of a polar fit and resultant errors in stf. Additionally, the same understanding of fte data and its stf impact can be used to optimize fte methods and generate specifications that support stf analysis. The analysis presented here uses the large and widely available Richard Johnson flight test evaluation (fte) reports[1].

Methodology

An accurate manual digitization process, with verification test points, extracted the Johnson fte data from published graphs. Each graph was fitted by Loess methods (some combination of "LOcally wEighted Scatterplot Smoothing" or "LOcal regrESSion") methods[2].

With a statistical signature of a representative fte program, Monte Carlo methods were applied to simulate various test procedures and the range of errors that could be produced by quadratic fits. Additional Monte Carlo analyses analyzed the consequences of fitting errors and supported simple quality assessment tools to characterize curve fits as useful, or not.

Results

Figure 1 is a residuals (differences between fitted and actual measurement) analysis from approximately 170 Johnson fte plots comprising nearly 6200 test points. The standard deviation of the residuals shown in Fig 1 varied at approximately 1/15 of the underlying sink rate. Monte Carlo analysis suggests testing fewer speeds more frequently slightly improved quadratic fits, and attempts to optimize the fte altitude testing budget by preferentially testing lower speeds more frequently produced worse results.

The Monte Carlo analysis methods determined that if the fte data scatter accuracy was improved to 1/25 the sink rate, then the curve fits were 95% likely to produce acceptable results, assuming the simple quality check metrics used (best LD and speed of best LD sanity check). Under the sanity check restrictions, a quadratic polar produced from fte test data would produce almost identical xc speed results compared to a known reference (e.g. Reichmann ASW-15 definition), assuming a classic quadratic based polar is the correct shape. In contrast, the 1/15 scatter/sink rate characteristic of the Johnson fte, in conjunction with the sanity checks, results in a 70% confidence level in the polar fit. Additional equivalent Monte Carlo simulations, using a sample Nimbus 4DM polar, derived similar quality metrics with sanity checks.

Lastly, a simple statistical analysis was made of the Johnson best LD analysis relative to the Loess fit estimates. In broad terms, the scatter in the Johnson results appear to be approximately consistent with 1/15 residual: sink rate Monte Carlo analysis. Figure 2 also shows that there was also a slight Johnson optimism bias.

Conclusions

On the assumption that a quadratic polar is the correct representation of sink rate, and given real experimental data from a test program with a known statistical quality signature, it is possible to show that simple quality checks on curve fits are sufficient to determine whether the curve fit results are useful, or not. No matter how good the data,

random scatter can distort the curve fit results. Data scatter reduction helps to make the output of an expensive test program more likely to be useful.

Loess has been demonstrated to be a powerful curve fit tool when the underlying form of the data is unknown. However, like any quantitative curve fit algorithm, the results are the best unbiased fit to the data with experimental scatter and is not guaranteed to be correct. A comparison of Loess based results with Johnson estimates suggests Johnson had a slight optimism bias, but the spread in his data appears to be consistent with the statistical signature of his test program.

References

[1] http://www.ssa.org/SoaringMagazine?show=blog&id=2395 (retrieved March 2016)

[2] https://en.wikipedia.org/wiki/Local_regression

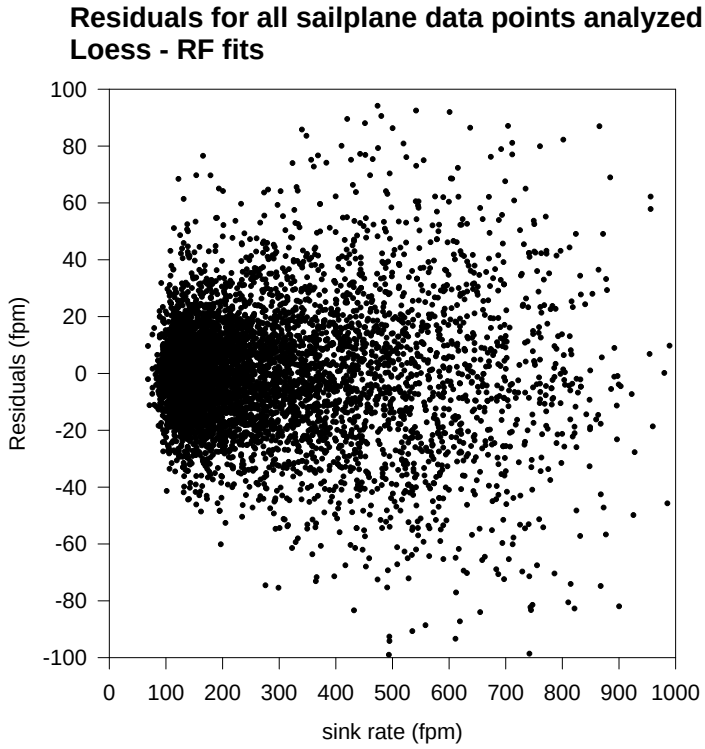

Figure 1. Scatter plot of all residuals as a function of the measured sink rate.

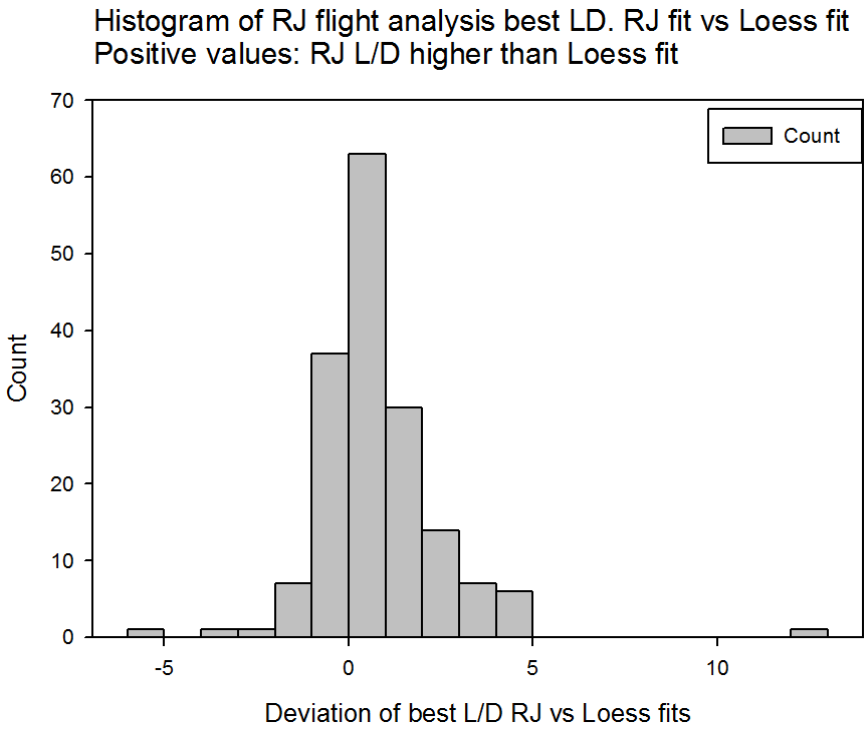

Figure 2. Histogram of the difference between the best LD assessment of Richard Johnson vs the Loess curve fit method.

Speed-to-Fly Theory #3: Potential issues with modern sailplanes with non-quadratic polars

Michael Steckner, PhD, MBA
mks@steckner.net

Abstract: A quadratic fit to a non-quadratic polar generates subtle errors in sink rate estimates and biases the appropriate speed-to-fly simultaneously. Presently, there is no generalized alternative fit recommendation. Significant effort is required to create unique and accurate fits. Two cases, while requiring different fits, show similar over/under sink estimate patterns resulting in similar impact on proper speed-to-fly, but with different robustness against inter-thermal flight speed errors. The sample cases show >1% degraded total cross-country performance. The prevalence of non-quadratic polars is unknown and assumed to be increasingly widespread in modern sailplanes since the 1980s.

Keywords**:** *speed-to-fly, data fitting, quadratic, non-quadratic*

Introduction

Modern sailplane polars may start to diverge sufficiently from the standard quadratic approximation such that optimal cruise speeds are different in certain climb conditions, with resultant significant (>1%) impact on achieved cross-country speed. This paper analyzes a Discus polar published by the vendor and an ASW-24 polar derived from a Johnson flight test[1] and reports errors of up to ~1.5% (Discus) and ~2.5% (ASW-24), depending on the lift conditions.

Methodology

Higher order polynomial fits were applied to the sailplane polar or associated LD plot (LD vs speed, back converted to a conventional sink polar) in conjunction with "brute force" point-by-point minimization searches. It is imperative that investigations of quadratic polars derive recommended stf from the quadratic, but true sink rates not be computed from the quadratic. Flight test evaluation and manufacturer published polars were variously evaluated.

Results

Figure 1 shows a digitized Discus polar from the manufacturer's marketing, the poor fit of a quadratic polar, and the excellent fit of a 7th order polynomial. Figure 2 is recommended stf for an ASW-24 polar derived from a Johnson data (5th order polynomial fit to the LD plot), which had fitting problems similar to Figure 1, when evaluated by standard quadratic and higher order polynomial fit. The unusual shape of the stf curve causes different sensitivity to flight speed errors, as discussed in the first paper of the series[2].

Figure 3 shows the cross country speed errors caused by non-quadratic polar for the Discus polar shown in Figure 1. While the higher order polynomial does not provide perfect results, the error is substantially reduced relative to standard quadratic polar treatment.

Conclusions

Modern sailplane polars may have non-quadratic polars to the degree that stf recommendations are not appropriate for the lift conditions, resulting in achieved xc speeds >1% from optimal.

It is unknown how many sailplanes may have polars that are not well fit with a quadratic. Published polars of advanced open class sailplanes (Concordia, eta) suggest more advanced curve fitting methods and stf analyses may be required to fully optimize their performance.

References

[1] http://www.ssa.org/SoaringMagazine?show=blog&id=2395 (retrieved March 2016)

[2] Speed-to-Fly Theory #1: Insights on the implications of flying incorrect speeds with quadratic and non-quadratic polars. OSTIV 2017 Australia

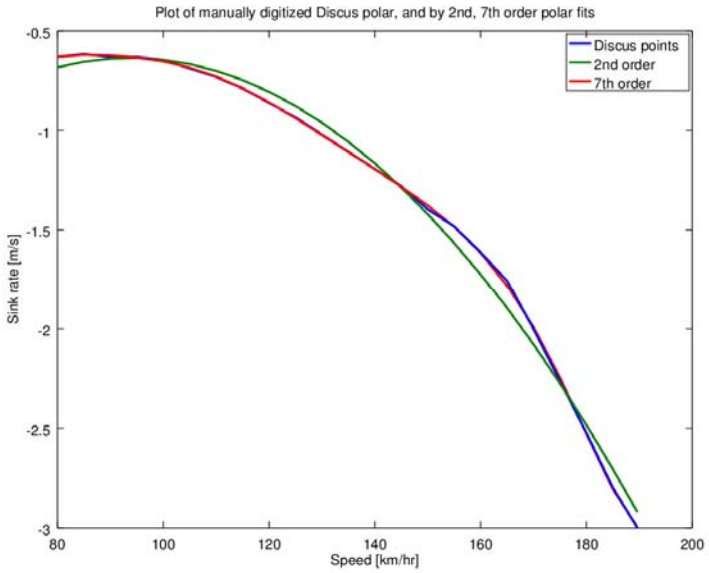

Figure 1. Digitized Discus polar with quadratic and 7th power polynomial representations

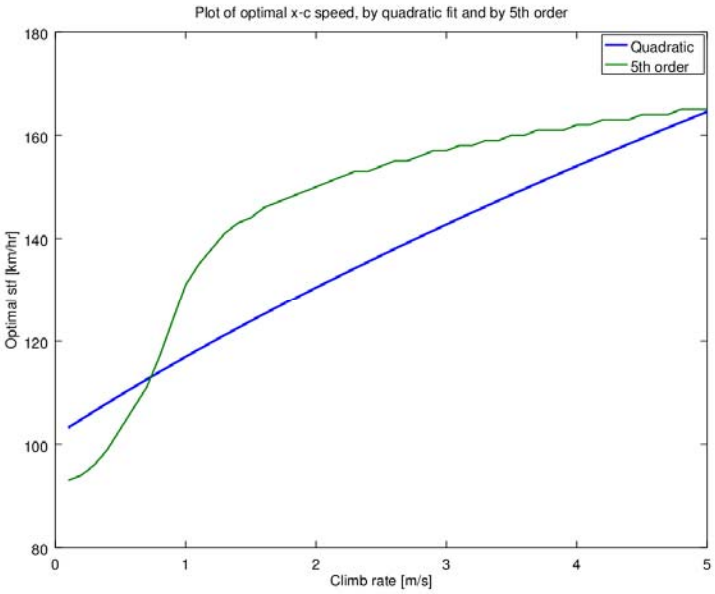

Figure 2. The recommended ASW-24 stf of a 2nd order polar vs 5th order LD fit

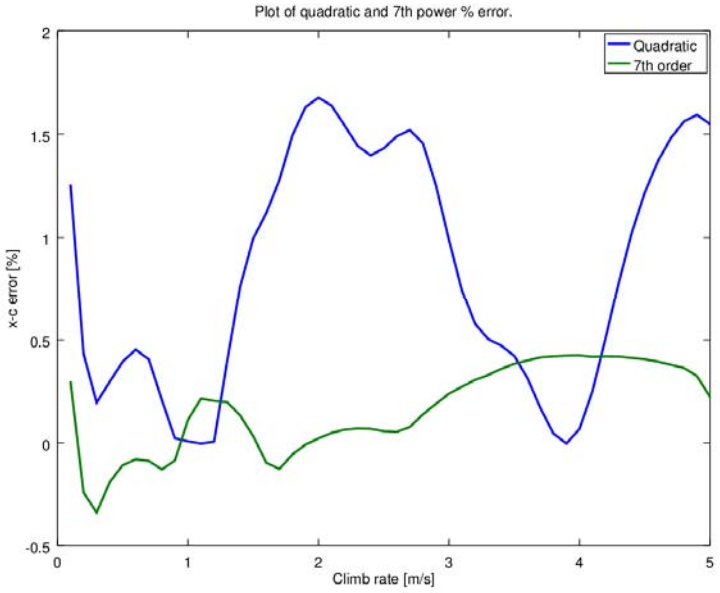

Figure 3. The Discus resultant errors in average cross country speed when flying at classic stf or higher order polynomial fits to the polar, as compared to stf derivations direct from the flight polar.

Using data from high-altitude sailplane flights to study atmospheric mountain waves

Rick Millane[1], Ni Zhang[1], Einar Enevoldson[2] and James Murray[2]
[1]*Computational Imaging Group, Department of Electrical and Computer Engineering*
University of Canterbury, Private Bag 4800, Christchurch, New Zealand
rick.millane@canterbury.ac.nz
[2]*NASA Armstrong Flight Research Center, Edwards, California 93524, USA*

Abstract: Sailplane flight data is potentially useful for studying the 3D wind fields in mountain waves. We have previously developed methods for extracting this information from limited sailplane flight data and applied them to a high altitude flight in the Andes. Here we further analyze the results in terms of potential errors and validation through comparison with reanalysis and radiosonde data.

***Keywords*:** mountain waves, wind field, sailplane, flight data.

Introduction

Mountain lee waves are atmospheric gravity waves that are triggered by the abrupt change in wind velocity occurring when air descends after flowing over elevated terrain [1,2]. The waves used for soaring are usually standing, or trapped, waves that are stationary relative to the terrain. Trapped waves exist when the atmospheric conditions are such that the atmosphere forms a horizontal waveguide and result from interference between different propagating waves. The boundary of the waveguide is generally associated with appropriate temperature, stability or wind speed profiles with altitude. However, even trapped waves can exhibit leakage and some vertical propagation. This can allow propagation high into the troposphere and even into the stratosphere. These high level waves have been utilized by the Perlan Project [3] to climb into the lower stratosphere.

Atmospheric waves, both in the troposphere and in the stratosphere, are important because they carry and transfer momentum and energy in the atmosphere. They produce drag that affects the general circulation, and can influence the vertical structure of wind speed and temperature, windstorms, clear-air turbulence and ozone abundance [4]. Despite their importance, measurement of the three-dimensional wind field in mountain wave systems is not without difficulty. Radiosondes and Doppler radar provide useful information, although the information form the former is limited and the latter method is expensive. An effective method is through the use of dedicated flights using specialized research aircraft. However, such field campaigns are very expensive.

Mountain waves are a common source of lift used by sailplane pilots. Such flights can cover large distances and altitudes. Therefore, sailplane flights present potential "sensors of opportunity" for measuring wind fields and other parameters in mountain waves. This potential has been explored in a number of studies [5-9]. One difficulty with attempting to use flight data from routine flights is that the instrumentation generally carried in such flights is quite limited. Even with modern flight computers, the data that is measured, and in particular that is logged, is limited. We have previously described methods for determining 3D wind velocities in mountain waves that use logs of only GPS position and airspeed [8,9]. Since these data are insufficient, by themselves, to estimate the 3D wind velocity, they are supplemented by the knowledge that the wind velocity in mountain waves is slowly varying in space and time. We have previously applied these methods to flight data from Perlan Project flights in California and Argentina. In particular, we have derived the 3D wind velocities for the altitude record breaking Perlan Project flight that reached an altitude of approximately 50,000 feet, well into the stratosphere. We have conducted a preliminary analysis of these results and compared them with some observational data from reanalysis. Here we describe some further analysis of the results including a study of the errors in our estimates and their effects, comparison with South American radiosonde data, and the relationship to the reanalysis data.

Methodology

Our methods for estimating the 3D vector wind field along the flight path for a sailplane wave flight, using a time series record of only GPS position and airspeed have been described previously [8,9], and the reader is referred to these two references for the details. The horizontal component of the wind velocity (magnitude and direction) is estimated first, and the vertical velocity second. Without aircraft heading data, the horizontal wind velocity cannot be estimated directly. We use the fact that in a wave flight, the wind velocity can be considered to be quasi-stationary in space and time to resolve the ambiguities and arrive at a horizontal wind speed estimate. As long as data are available for a variety of (unknown) headings within spatio-temporal regions that are smaller than the characteristic scale of the wind velocity field, the ambiguities can be resolved [8]. In this approach we use characteristic scales that are typically of the order of 2km horizontally, 100m vertically, and 10min temporally. We divide the flight path into spatio-temporal regions of these dimensions, and within each region use pairs of ground velocity and air speed data and a clustering analysis to derive consistent horizontal wind velocity estimates. The vertical wind speed estimate uses the logged GPS altitude data followed by correction for the sailplane sink

rate using the indicated air speed and the sailplane flight polar. The sailplane acceleration is calculated from the air speed and this is used to correct for the effects of potential-kinetic energy exchange.
Data were obtained from a Perlan Project flight that departed from El Calafate in Argentina in August 2006 using a specially equipped DG-505M. The flight duration was 4.8 hours and it reached an altitude of approximately 50,000 feet. 3D wind velocities were estimated along the flight path as described above. Reanalysis data was obtained from the NCEP/NCAR Global Reanalysis and a GEOS visible satellite picture. Radiosonde data was obtained for Ouerto Mott (Chile), Punta Arenas, and the Falkland Islands.

Results

The recorded temperature profile showed clear penetration into the stratosphere with the tropopause at approximately 11,000 m. The derived vertical wind speeds showed the positions of some main wave areas along the flight path and these allowed the wavelength to be estimated in the troposphere (~9 km) and the straosphere (~22 km) where the sailplane executed faily long either upwind or down wind flight segments. The wavelength seen in the straosphere is coinsistent with the spacing of cloud features seen in the GEOS picture. Comparison of the estimated horizontal wind velocity with the reanalysis data showed good agreement with the wind direction but some discrepencies with the wind speed. This was analysed further by a more detailed study of the errors in the wind velocity estimates and by comparison with radiosonde data from the sites described above. While not giving a firm explanation for the discrepencies seen, the variations between the reanalysis and the radiosonde data appear to explain much of the variation.

Conclusions

Sailplane flight data can provide useful information on mountain wave wind fields that is difficult to obtain by other methods. Even with limited data from conventional data loggers, useful information can be extracted. The methods appear to be effective, although validation can be difficult due to a paucity of independent data. More reliable, comprehensive and useful information could be obtained by using data from multiple flights in the same region and using more sophisticated data loggers.

References

1 Scorer, R. S., Dynamics of Meteorology and Climate, Academic Press, San Diego, 1997.
2 Etling, D., Atmospheric Gravity Waves and Soaring Flight, 2014. Available at www.schwerewelle.de.
3 www.perlanproject.org
4 Holton, J. R., 1983: The influence of gravity wave breaking on the general circulation of the middle atmosphere. J. Atmos. Sci., 40. pp. 186-201.
5 Hindman, E. E., R. L. McAnelly, W. R. Cotton, T. Pattist and R. M. Worthington, 2004: An unusually high summertime wave flight. Tech. Soar., 28, pp. 7-23.
6 Lindemann, C., R. Heise and W. Herold, 2008: Lee waves in the Andes region, mountain wave project (MWP) of OSTIV. Techn. Soar., 32, 93-96.
7 J. Dummann, J., 2009: A report on glider pilot activities to document lee wave events in northern German and their aims. Tech. Soar., 33, pp. 109-116.
8 Millane, R. P., G. D. Stirling, R. G. Brown, N. Zhang, V. L. Lo, E. Enevoldson and J. E. Murray, 2010: Estimating wind velocities in mountain waves using sailplane flight data. J. Atmos. Ocean. Technol., 27, pp. 147-158.
9 Zhang, N., R. P. Millane, E. Enevoldson and J. E. Murray, 2012: Measuring 3D wind fields in mountain waves using sailplane flight data. Tech. Soar., 36, pp. 57-66.

The Harz-Foehn-Project - empirical research on mountain waves in an northern German low mountain range

Karl-Heinz Dannhauer
Triftweg 69, D-04277 Leipzig, khdannha@t-online.de

Abstract: The Harz is well suited as a model system for the practical mountain wave research. This presentation will give some answers to important questions about the formation and the peculiarities of mountain waves in a northern German low mountain range. In the framework of the Harz Foehn Project temperature measurements were carried out in field campaigns to record the foehn effects.

Keywords**:** wave flights above low mountains**,** empirical mountain wave research, field campaigns of foehn activity, possibilities of long distance wave flights along low mountain ranges,

Introduction

We report about mountain wave flights we have done in the last 20 years in a low mountain range called the Harz. The Harz is a low and isolated mountain range in a flat country in Northern Germany. It extends 110 kilometers by 35 kilometers. The highest peak is the Brocken (height 1141 m above sea level). In the fall and winter months, the prevailing wind direction is SW with average wind speeds of over 50 km/h (HENTSCHEL 1953).
Mountain Waves develop in SW wind conditions with wind speed above 45 km/h perpendicular to the longitudinal direction of the mountain (DANNHAUER 2011).

Methodology and Results

The main method of the investigation was the consistent follow-up of the conducted mountain wave flights under SW wind conditions.
The weather conditions, the locations of the waves, the reached heights and the special features of the flight performance were documented.
During the wave flights above the Harz, temperature measurements were carried out in the framework of several field campaigns to record the foehn effects.

Weather conditions
Mountain waves above the Harz often occur before a cold front passage of an approaching low pressure area. A low pressure system in the northwest (northwest of the British Isles) and a high pressure area in the southeast (Slovakia-Eastern Europe) lead to a strong southwest flow in the area of the Harz. The resulting anticyclone isobar curvature at the edge of the area over Eastern Europe ensures a sinking inversion or stable layering conditions at the altitude level of 1300 m MSL. This effect creates high reaching mountain waves above the north eastern part of the Harz and also at the lee side of the Thueringer Wald, the Lausitzer Bergland and the Riesengebirge

Optimal parameters for mountain waves on the Harz are the following:

The wind direction should be 210 +/- 30 degrees 500 m above ground to 500 hPa (5500 m). The wind speed should be more than 25 kts on the ground and 35 to 50 kts in higher regions.
There should be an inversion layer of about 1-2 degree Celsius increase between 100 and 200 m above the ridge line or a stable stratification 1300-2200 m MSL.

Flight practice
The most spectacular flights with high reaching waves were carried out mainly during SW wind and south wind conditions. Carsten Lindemann reached a height of 7260 m above sea level in the lee of the Brocken on 30. October 2000 (fig. 1 *). He described the best requirements for the formation of waves on the Harz in a paper (LINDEMANN, 1999).

The entry into the mountain wave system is usually in the region of the lower Harz. The climbing areas can be entered at a relatively low altitude. This wave system is triggered by the lower Harz (750 m MSL) and the distances between the oscillation amplitudes are short. After climbing in the region of the lower Harz one can head towards the upper Harz. The aim is to reach the lee area of the Brocken via the wave system of the lower Harz. The diagram of Figure 2 summarizes the specific conditions in the wave formation and shows a cross section view the arrangement of the wave systems in the upper Harz.

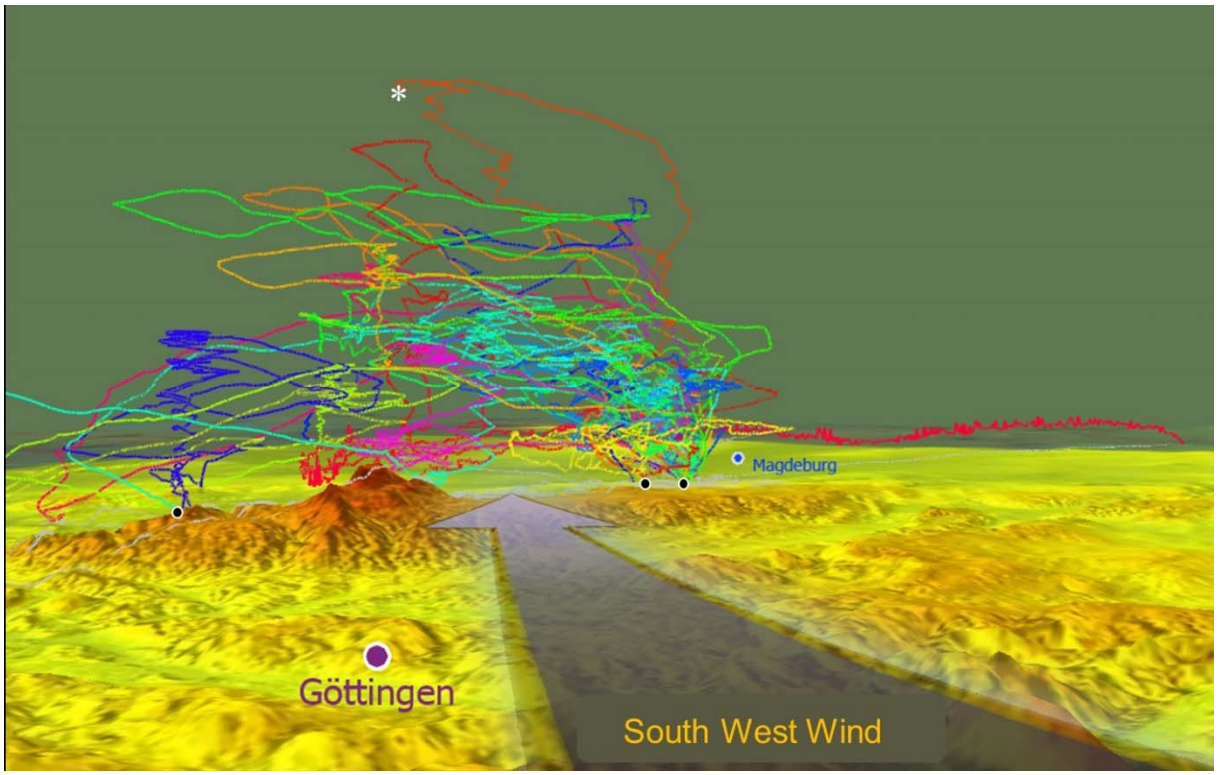

Fig. 1: The picture shows a compilation of representative flights in the lee of the Harz at southwest wind flow. The highest altitude so far was reached in a wave on 30 October 2000 in the lee of the Brocken (*).

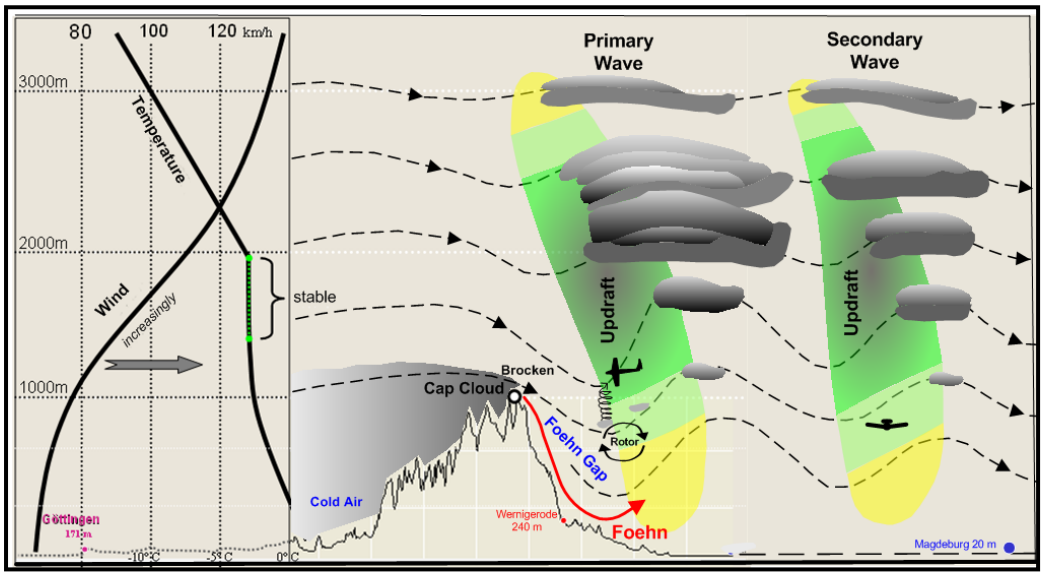

Fig. 2: The image shows a cross section through the center of the upper Harz windward (left) to the lee side (right) .

The Harz-Foehn-Project
In the search for possibilities for the description of the mountain wave activity in the lee of the Harz, temperature measurements were carried out for the detection of the foehn activity on the ground

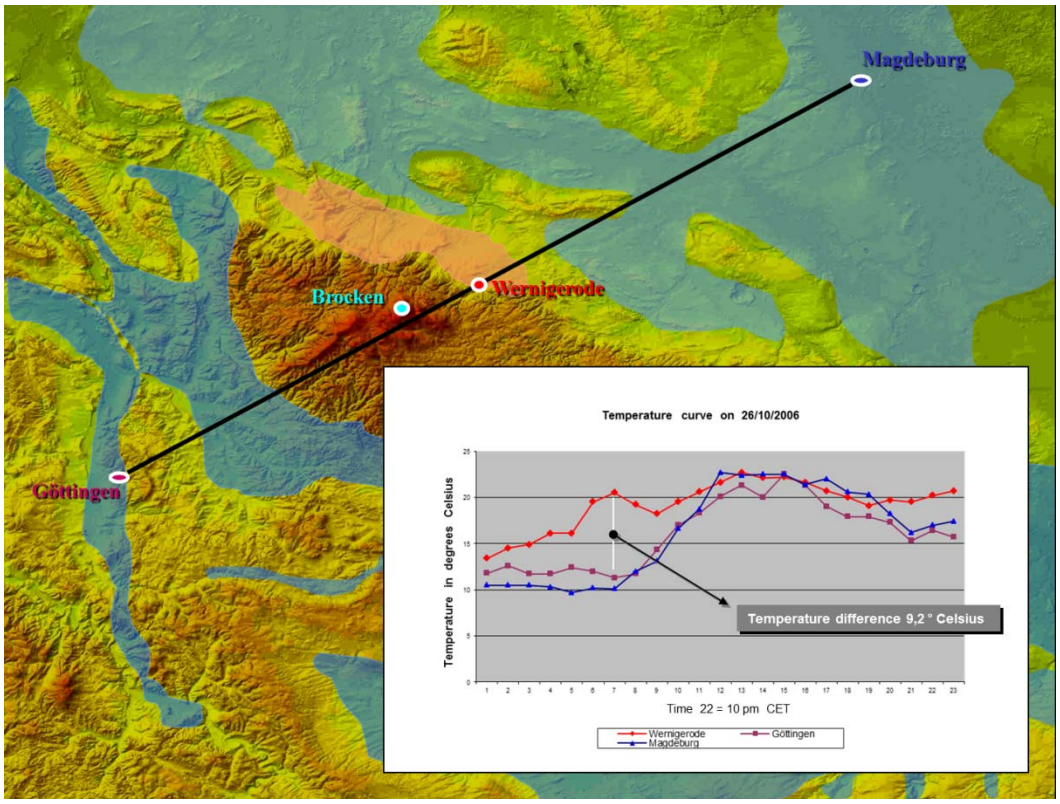

Fig. 3: Comparison of the temperature measurements of the DWD weather stations Goettingen - Wernigerode-Magdeburg. At 07.00 CET a temperature increase was measured in the Lee of the Brocken (SW wind 100 km / h) compared to the other stations of over 9 degrees Celsius.

Comparing temperature data of the climatological stations Goettingen (SW-luv, DWD), Wernigerode (close to SW-lee, private) and Magdeburg (distant SW-Lee, DWD), we found a significant warming of more than 9°C for the Wernigerode station relative to the other stations on the 26.10.06 at 7:00 CET (see fig. 3). The presumption of a foehn effect being the reason for this is supported by the fact that static pressure at this time reached a minimum value at Wernigerode, while wind speed at the Brocken reached a maximum.

In the vicinity of the Harz there are not only weather stations of the DWD, but also many private weather stations. This allows to investigate the wave effects and perhaps the changes in the wave activity as part of large field campaigns. The comparison of these measurements, for example, with satellite pictures could be a good way to describe the wave dynamics on the Harz even better.

Conclusion and Vision

The development of mountain waves in the low mountain ranges is a complex process. The empirical research of the Harz Foehn Project has shown some fundamental connections between the formation of mountain waves and the possibilities for using this phenomenon in gliding flight practice.

Field campaigns use the real atmosphere as a natural laboratory by measuring as many processes as possible at the same time. With the inclusion of private monitoring stations, which are often available in our investigation area, investigations can also be extended to larger areas.

In the future it may be possible to determine new flight routes through field campaigns.

References

Dannhauer, K.-H. (2011): Leewellenflüge am Harz. Segelfliegen pur, 2011
Hentschel, G. (1953): Das Föhngebiet des Harzes. Akademie-Verlag-Berlin 1953
Schulz, L. (1939): Einfluß des Harzes auf Wetter und Witterung im Frühjahr 1936. Springer Verlag, Berlin 1939
Lindemann, C. (1999): Bei Wernigerode wartet ein kräftiger Rotor, Der Lilienthaler, 1/1999
Lindemann, C. (1971): Leewellen in der Flugmeteorologie. Meteorol. Abhandlungen; Bd. 89, H. 4, 1971

Heat Transfer by Convection from the Ground to a typical Australian Thermal

David M Wilson BE, M Eng Sci, DAE
dwjcra@ozemail.com.au

Abstract: The parameters describing a typical Australian thermal are defined and used to calculate the surface velocity field around the thermal. Heat transfer from the hot ground to the thermal is then calculated using heat transfer theory. The significant effect of a Raleigh vortex, which is present in most thermals, is demonstrated.

***Keywords*:** Thermals, Convection, Heat transfer, Greenhouse, Radiation

Introduction

The sun does not heat the air in which we fly. It heats the ground. The soil is about 2500 times as dense as the air, has a specific heat up to four time higher than air and has the capacity to hold much thermal energy. It is the transfer of this energy to the air that creates thermals. For many years, and in many text books, you may have read about the development of "pools of hot air", or "superadiabatic layers" postulated as the source of the energy to drive a thermal. These ideas are wrong. A superadiabatic layer with enough energy to drive a thermal is a physical impossibility. This paper sets out the real way in which the ground heats the air for thermal generation. A typical Australian thermal is described in mathematical terms which enable later analysis of the heat transfer from the ground into the thermal. The thermal description is based on my observations over fifty years of flying in Australian thermals, mostly out over the plains. The description does not apply to thermals in the mountains.

Methodology

No two thermals are the same. I have chosen parameters which are reasonably typical. Some thermals are larger, some are smaller, some go much higher. The central core might be near one edge instead of the middle, or may even not be there. The overall diameter of a thermal, i.e. the area in which the air is going up is D, typically about 800m. The rate at which air is rising in the main thermal is denoted by L, typically about 2m/s. A glider circling in this air would show about 1.5m/s (3 knots) on the vario.

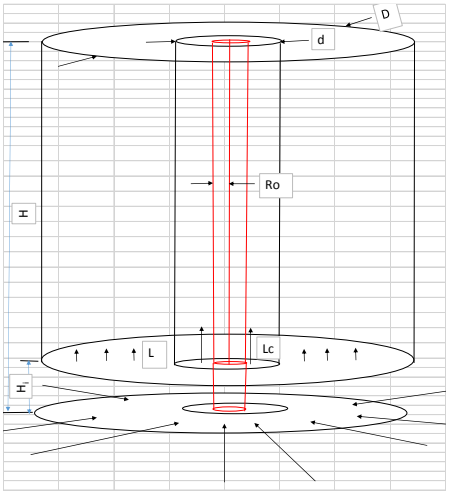

Figure 1 A typical thermal

The height of the thermal H will depend on the atmospheric temperature distribution with height. Typically, it is about 2000m. The thermal has an inner core where the air is rising much faster than the general air in the thermal. The rate of rise in this region is denoted by L_c. In a typical thermal it would be about 3.5m/s. A glider circling in the core would show about 3m/s (6 knots) on the vario. The diameter of this core is typically about d = D/4, or about 200m. The thermal has inside its core a Raleigh vortex, shown red in the diagram. The vortex is rotating, for reasons which will become obvious when you look at the convective heat transfer. In the outer part of the vortex, the velocity of rotation is inversely proportional to the distance from the centre according to the equation: $v = K/r$ where the constant K defines the strength of the vortex. This formula applies down to a relatively small radius R_o (typically about 10m). Inside R_o the velocity follows the formula: $v = Kr/R_o^2$, i.e. it reduces linearly to zero at the centre. The peak velocity of rotation in the vortex at $r = R_o$ is equal to K/R_o. A typical value for the strength of the vortex, K in an Australian thermal is about 210 m^2/s. That means that if you were observing the willy willy (or dust devil) at the base of a thermal you would see a dust column about 20m diameter, rotating so that it performed a complete revolution in about 3 seconds. At the bottom of the thermal there is an inflow zone of height H_i (taken to be D/10, or in a typical thermal 80m).

For there to be any thermal at all, the temperature of the ground surface must be higher than the temperature of the inflowing air. The temperature difference is denoted by ΔT. In the middle of the day over a dry brown ploughed paddock ΔT might be as much as 25°C. Thermals will be weak if ΔT is less that about 10°C.

Thus any thermal can be defined fully by the parameters H, D, d, L, L_c, K, R_o, H_i and ΔT. I will assume that ΔT is constant over the whole field of the base of the thermal and take a typical figure of $\Delta T = 20°C$

The heat transfer from the ground to the air is an example of forced convection. The rate of heat transfer is related to the horizontal velocity of the air flowing over the surface. Heat transfer calculations require the velocity field under and around the base of the thermal. There are three components of the velocity

1. Flow convergent towards the centre of the thermal, which decreases in intensity as you approach the centre.
2. Concentric flow around the centre arising from the action of the Raleigh vortex
3. Uniform flow created by the fact that the whole thermal is drifting with the prevailing geostrophic wind.

If you consider a curtain of any given radius hanging down for the full height of the inflow zone, and assume that the convergent flow velocity is constant over the full height of the curtain, then you can calculate the inflow velocity based on the observation that the air flowing in through the curtain must equal the air flowing out the top of the inflow zone enclosed within the curtain.

I have calculated the inflow velocity as described above out to the edge of the thermal, and have assumed that the inflowing air region extends out for a **further** distance of D/8, with the inflow velocity tapering to zero at the outer edge of D/8.

If there is no geostrophic wind, the inflow and vortex velocities are axisymmetric, and the result of the calculation is shown in Figure 2.

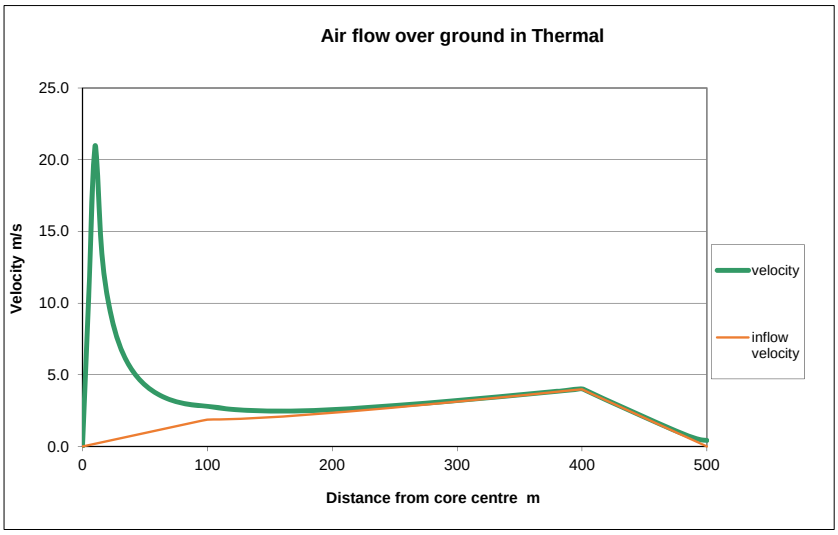

Figure 2

The orange line in the diagram shows the inflow velocity, and the green line shows the vector combination of the inflow velocity and the vortex rotation. Geostrophic wind is set to zero for this figure. The vortex significantly increases the velocity of the air over the ground at radiuses up to about 200m.

There is almost always a geostrophic wind. This can be anywhere from 1m/s to 10 m/s or more. At higher wind velocities, the thermals tend to be broken and hard to work. The vortex is distorted, with some parts leaning. At more gentle geostrophic winds, the main effect is to reduce the inflow velocity in the regions the thermal is drifting towards and increase the inflow velocity in the region the thermal has just passed over. It also introduces an asymmetry in the velocity near the vortex, with higher velocity on one side than the opposite side. This asymmetry is believed to be the source of the angular momentum which feeds the vortex and keeps it from dissipating.

Heat transfer

There are three mechanisms for heat transfer, radiation, convection and conduction. Conduction within the ground is important, but we can ignore conduction in the air because the air is an excellent insulator.

Energy from the sun all arrives by radiation through the vacuum of space. It arrives with nearly all of the energy in short wavelength radiation peak wavelength about 0.6µm. With the exception of ozone in the ozone layer, the air does not absorb any of this energy. Some is reflected by ice crystals in cirrus clouds and by smoke particles. The rest reaches the ground. The energy intensity reaching the top of the atmosphere is about 1150W/m^2. On a clear day with the sun overhead about 1100W/m^2 reaches the ground.

Dependent on the soil surface, between 20% and 40% of the sun's energy is reflected at the same wavelengths as the incoming radiation and is lost back into space. The rest is absorbed by the ground, heating the surface. Early in the day, some of the heat is conducted down into the lower layers to up to about 200mm down. Late in the day and overnight the conduction process is reversed, with the lower layers keeping the surface warmer as it loses heat.

Radiation from the ground

The earth's surface radiates heat continuously, even at night. The peak wavelength of the radiation from the earth is about 20µm.The equation for calculating the intensity of the radiation is $E = \sigma \zeta T^4$, where E is the intensity of radiation in W/ m^2, T is the absolute temperature of the surface in ^oK, σ is the Stefan Boltzmann constant $\mathbf{5.670367\times10^{-8}}$ W m^{-2} K^{-4}, ζ is the emissivity, which is 1 for a black body, but can be less than 1 for a grey body. For the earth surface ζ is about 0.95.

With no solar input, the earth surface cools down overnight. At dawn the surface temperature out in the desert will be near 0^oC, or 273^oK. Alternatively, by mid-afternoon, the temperature of a brown ploughed paddock or the sand in the desert could reach over 50^oC or 323^oK. The radiation from the Earth's surface near dawn is about 300 W/m^2, and by mid-afternoon, a brown paddock might be radiating energy at about 600 W/ m^2.

The "Greenhouse effect"

Modelling this effect is not the subject of this paper. The greenhouse effect does not create any thermals. Greenhouse gases in the atmosphere absorb about half of the energy radiated from the earth, getting warmer as a result. Water vapour, by far the most important greenhouse gas, will absorb nearly all of the energy in the wavelengths it can absorb, in the first 1000m of the atmosphere above the surface. The atmosphere also radiates energy, dependent on its temperature. Some of the emitted radiation from the air is absorbed by adjacent layers, and some reaches back to the ground, where the surface absorbs it and hence gets a little warmer.

Convection

Convection is a process where the air adjacent to a hot surface is transported away from the surface, to be replaced by cooler air, which is heated in turn and then transported away. The warm surface is the soil and as you can easily imagine, the rate of transport of warm air away from the surface will be higher when the wind is blowing harder. The equation for the rate of heat transfer from a horizontal flat plate with wind blowing over it is

$q = h \Delta T$

Where q is the rate of heat transfer per m2 of surface and h is a heat transfer coefficient.

h is a complicated function of the velocity of the air u_x, the distance of the path along which the air has travelled x, the density ρ, the specific heat of the air c_p, and the viscosity of the air μ. Our case is not exactly the same as air flowing over a flat plate. It is not easy to choose a value for x and for simplicity I have conservatively used the distance inwards from a circle 1.25 times the radius of the thermal, plus a nominal 1000m.

$$\mathbf{h} = \frac{\rho c_p C_f/2}{1+12.8(Pr^{0.68}-1)\sqrt{(C_f/2)}}\, u_x, \quad C_f = \frac{0.455}{(\ln(0.06\,\mathbf{Re_x}))^2}, \quad Re_x = \frac{\rho u_x x}{\mu}$$

where Pr is the Prandtl number, which for air is 0.71. For the source of these equations please refer to Ref 1 Chapter 6

Results

For the parameters I have chosen, the heat transfer from the ground into the air is shown in Figure 3. In the figure, the wind is blowing towards us, and the thermal vortex is rotating clockwise. The pale blue and orange area are where the geostrophic wind and the inflow velocity oppose each other and at the rear the higher transfer rate is where they are combining. The peak transfer rate near radius Ro is 394 W/m^2 on the side of the thermal where the geostrophic wind and the vortex wind combine. On the opposite side it is 305 W/m^2. More typical rates are about 130 W/m^2 behind the thermal and down to 30 W/m^2 on the left hand side.

Integrating the power input over the entire thermal base gives a total input of energy by convection to the thermal of 62.1 MW. This sound a lot, but the mass flow of air into the base of the thermal is 975 ton/s, so that the average rise in temperature is only $0.063\ ^oC$. The temperature rise near the centre of the core is probably about double this. No wonder attempts to centre thermals by measuring temperature at each wingtip did not work. Thermometers are not that accurate.

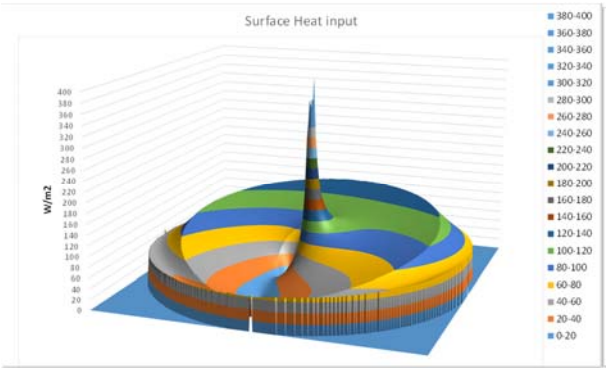

Figure 3 Heat transfer for a typical thermal

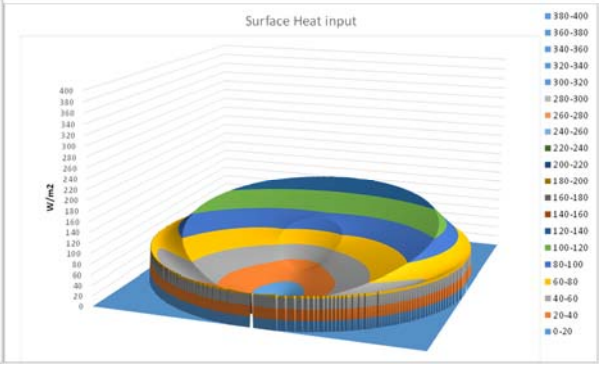

Figure 4 Heat transfer without the vortex

Thermal diameter	800	m	
Thermal core Diameter	200	m	
Vortex Core Diameter	20	m	
Time for one revolution	3	sec	
Vortex strength K	209		
Thermal updraft speed	1.5	m/s	
Thermal core updraft speed	3	m/s	
Height of inflow zone	80	m/z	
Tground - T air	20	m	
Geostrophic wind	3	m/s	
Total heat input	62.1	MW	
Total air inflow	975	Tonne/s	

Table 1 Parameters for Figure 3

Thermal diameter	800	m	
Thermal core Diameter	200	m	
Vortex Core Diameter	20	m	
Time for one revolution	3E+10	sec	
Vortex strength K	0		
Thermal updraft speed	1.5	m/s	
Thermal core updraft speed	3	m/s	
Height of inflow zone	80	m/z	
Tground - T air	20	m	
Geostrophic wind	3	m/s	
Total heat input	60.4	MW	
Total air inflow	975	Tonne/s	

Table 2 Parameters for Figure 4

To show the importance of the vortex in the total picture, I have set the time of one revolution to a very large value, effectively setting K = 0. In practice, this would reduce the rate of lift in the thermal, and probably mean that there would be no core. However, for this illustration I have only changed one variable. The result is shown in Figure 4.

The spike of high energy transfer in the middle of the thermal is gone. Most of the energy now comes from the area where the inflow and geostrophic winds combine, at the back of the thermal in Figure 4

Conclusions

The results of the calculations clearly confirm the assertion that the main store of the energy which drives thermals is energy stored in the layer of soil heated by the sun.

Although there is some uncertainty in applying heat transfer equations derived for flow over a hot flat plate to a situation where the free stream velocity is not constant and the starting point for the boundary layer is indefinite, the figures derived are clearly of the right order of magnitude.

The significance of the central vortex, frequently observed in thermals over dust country, has been shown

The variables H, D, d, L, L_c, K, R_o, H_i and ΔT have been treated as independent variables. Clearly there are interactions between them, and also with other variables. Considerably more work is needed before the interactions between these variables could be used as a method of predicting thermal strength.

References

1 Leinhard, John IV and Leinhard John V 2016: A Heat Transfer Textbook. Fourth Edition Phlogiston Press Cambridge Massachusetts Chapter 6. This text can be downloaded on line.

Investigation of the Vegetation Effects on Convection by Using COSMO-CLM

Nilcan Akataş[1], Serhan Yeşilköy[1,2], Zafer Aslan[3]
[1] *Istanbul Technical University, Faculty of Aeronautics and Astronautics, Department of Meteorological Engineering, Istanbul/Turkey, akatas@itu.edu.tr*
[2] *Atatürk Soil Water and Agricultural Meteorology Research Institute Directorate, Kırklareli/Turkey, yesilkoy@itu.edu.tr*
[3] *Istanbul Aydın University, Faculty of Engineering, Istanbul/Turkey, zaferaslan@aydin.edu.tr*

Abstract: Convection is affected by vegetation cover considering variation of water and heat retention of different soil surfaces. Vegetated area also changes the amount of incoming or outgoing components surface energy budget, therefore affects the atmospheric convection. In this study, vegetation effects on convection have been investigated by a non-hydrostatic limited-area atmospheric prediction model (COSMO-CLM) simulations using different land cover maps that use different vegetation fractions and normalized difference vegetation index (NDVI) values. Selected model domain covers especially forested regions from the northeastern part of Turkey and Black Sea to the eastern coasts of Caspian Sea. In this context, changes of atmospheric parameters considered as indicators of convection obtained by model simulations were investigated.

***Keywords*:** Vegetation cover, COSMO-CLM, convection

Introduction

Vegetation covered area promotes convection both by extraction of soil moisture and by shading the soil so that conduction of heat into the soil was reduced (thereby increasing the available energy).[1,2] Considering surface energy budget, vegetated area changes the amount of incoming or outgoing components of the budget. In order to understand the effects of vegetation on convection, fluxes over the surfaces should be examined. In this study, vegetation effects on convection has been investigated by COSMO-CLM simulations using different land cover maps covering especially forested regions.[3,4]

Data and Method

Vegetation effects were simulated by using COSMO-CLM. The COSMO model is the non-hydrostatic operational weather prediction model applied and further developed by the national weather services joined in the COnsortium for SMall scale MOdeling (COSMO) COSMO was developed from the Local Model (LM) of the German Meteorological Service by CLM-Community which is an open international network of scientists (URL-1). In 2005, The CLM-Community improved the COSMO-Model to be capable of long-term simulations so it is called COSMO model in CLimate Mode (COSMO-CLM or CCLM), then CCLM became the regional Community-Model for the German climate research. This model version has been applied on time scales up to centuries and spatial resolutions between 1 and 50 km in different regions of the world (URL-2). The COSMO model is based on primitive thermo-hydro-dynamical equations that define compressible flow in a moist atmosphere without using any scale approximations. The general aim is to be used for both operational numerical weather prediction (NWP) and research applications on meso-scale. GLC2000 and GLOBCOVER were used as land use cover maps for the simulations. They are differing from each other according to the satellites and sensors that they use. GLC2000 land cover map uses SPOT 4 satellite and has 1 km spatial resolution. GLOBCOVER land cover uses 300 m MERIT sensor of ENVISAT satellite.

Results

Model results were obtained as 6 hourly data and then converted to the daily values. The figures of model outputs show the monthly averages for temperature, sensible heat flux, latent heat flux and total cloud cover and the monthly total values for precipitation data. Analyses illustrates on both GLC2000 and GLOBCOVER land use maps. Land use maps shows different vegetation fractions and normalized difference vegetation index (NDVI) values. For GLC2000 land use, plant cover and leaf area index for the COSMO-Model and for a special day are produced by using only the data set for vegetation and an averaged NDVI ratio by NDVI type choosing. For GLOBCOVER land use plant cover, leaf area index and roughness length for the COSMO-Model and for a special day are produced by using 12 monthly climatological mean values for plant cover, leaf area index and roughness length. The difference for the vegetation area fractions for GCL2000 and GLOBCOVER are shown in Figure 1. Sensible heat flux and latent heat flux have not much difference for different land use maps but where vegetation fraction is high for GLOBCOVER, values are higher than GLC2000. Especially in summer times, over the sea and the eastern part of the sea, lower negative values can be seen. Sensible heat flux values are lowest in the eastern part and also in the southeast part of the Black Sea. Heat fluxes cannot be linked to only vegetation cover of the

surface. Sea-land distribution and topographic effects should also be considered. However, in winter times, heat fluxes have highest values where vegetation fractions also high.
Total cloud covers mainly affected by moisture sources. In this study, existence of sea triggers the convection by evaporation and air masses pass through the Black Sea. However, vegetation cover is also a source for connectivity by the gas exchange between plants and atmosphere.

Conclusions

The impacts of vegetation on convection occur as affecting surface fluxes by gas (CO_2, O_2, H_2O etc.) exchanges, affecting wind speed over the plant canopies and extracting of soil moisture. Surface fluxes over canopies have different behavior from bare soil. Because vegetation processes and change directly affect the surface energy and moisture fluxes into the atmosphere. Convection in the atmosphere depends on many other factors and causes the change of many other parameters. Thus, for the future studies, changes of other parameter like wind shear and wind shift can be examined. Beside monthly variation, daily and hourly variations can also be considered in the examinations. It is hard to examine the only vegetation effects, so atmosphere-ocean-cloud-agriculture coupled models can be applied for this kind of studies.

References

[1]Clark, C. A., & Arritt, P. W., 1995: Numerical simulations of the effect of soil moisture and vegetation cover on the development of deep convection. Journal of Applied Meteorology, 34(9), 2029-2045.
[2]Fitzjarrald, D. R., Acevedo, O. C., & Moore, K. E., 2001: Climatic consequences of leaf presence in the eastern United States. Journal of Climate, 14(4), 598-614.
[3]***URL -1 <http://www.cosmo-model.org***/> Retrieved in May 31, 2016.
[4]***URL -2 <http://www.clm-community.eu/>*** Retrieved in May 31, 2016.

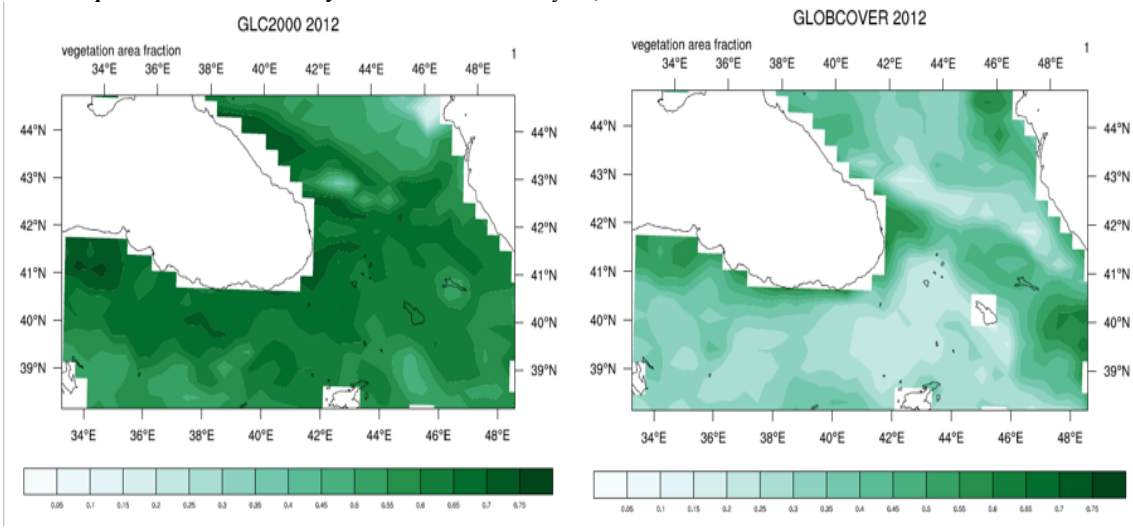

Figure 1. Vegetation area fractions for GLC2000 and GLOBCOVER land use maps

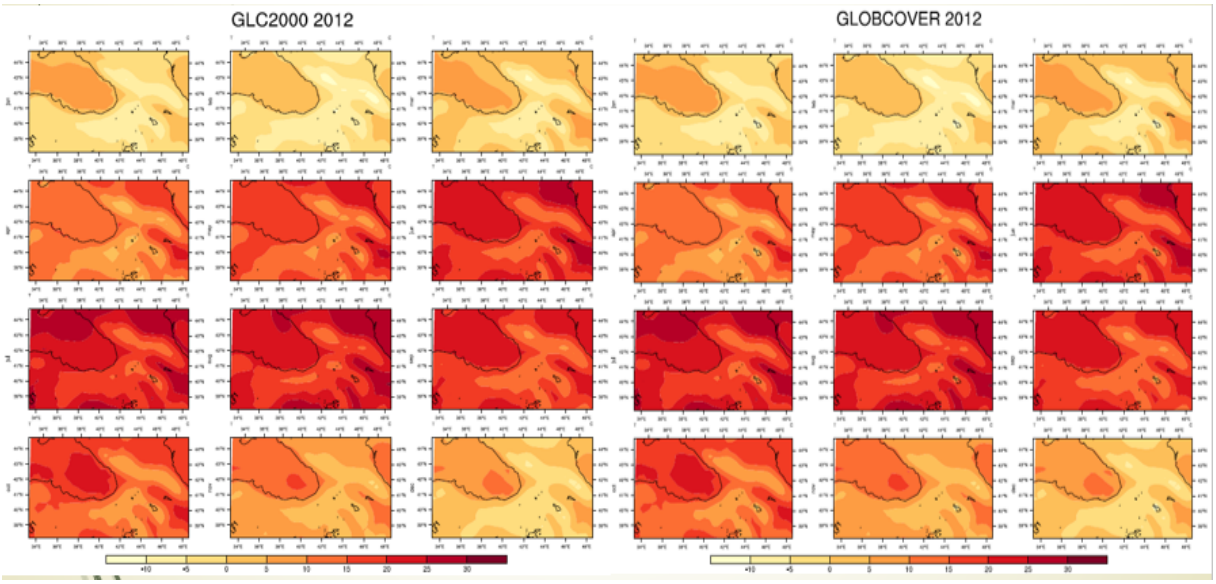

Figure 2. Monthly mean temperature for GLC2000 and GLOBCOVER land use maps

Sailplane Winglets: How Many Tips are Too Many Tips?

Travis Krebs[1], Dr. Goetz Bramesfeld[2]
[1]*tkrebs@ryerson.ca*

Abstract: An optimization process is developed to design wingtip devices for the Standard Cirrus, a high-performance sailplane. The process is first used to design winglets, with the purpose of increasing the maximum cross-country speed of the sailplane. The results of that study are compared to traditionally-designed winglets created with similar objectives in mind. The designs of the optimization process show competitive results when compared to these winglets. The process is then used to develop split-winglets for the same sailplane, with the purpose of determining their suitability for this application, as well as how they may work. There have been several effective split-winglet designs created with the process, with performance increases beyond what was capable with the conventional winglet design from the previous study.

***Keywords*:** Sailplane, winglet, optimization.

Introduction

The past 20 years has seen large advances in sailplane winglet design, as it is now known that winglets can provide a net benefit, even with the parasitic drag penalty at cruise conditions. Nowadays most modern sailplanes come equipped with winglets. Maughmer (1) provides an excellent in-depth review regarding the traditional sailplane winglet design process. In general, existing sailplane wingtip devices are almost exclusively winglets; little is known about the performance of other wingtip varieties. Therefore, in order to expand the understand of other wingtip geometries, the primary focus of the herein presented research focused on exploring the viability of split-tip designs for sailplanes. To investigate the performance of these split-tip designs, an optimization process from a previous study by Krebs and Bramesfeld (3) was used. In the previous study, this process was used to design conventional winglets for the Standard Cirrus. The final designs were compared to winglets designed for the same sailplane with similar objectives in mind. The performance difference between the optimized result and the existing winglet design was very small, with both benefiting the sailplane a similar amount across the flight envelope. For this current research, the optimization was repurposed to design split-tips, following very similar methodology as the previous study.

Methodology

The flight performance of the winglet designs is evaluated using a higher-order potential flow method that uses elements with distributed vorticity, and has viscous flow corrections. The method also includes a relaxed-wake model, as seen in Fig. 2. Results from this performance model, when analyzing the Standard Cirrus sailplane, are compared to empirical flight data and agree well. The geometry is inputted by defining panels. These panels then get discretized into distributed vorticity elements (DVEs), based on the panel density defined by the user. An example of this panel geometry can be seen in Fig. 2.

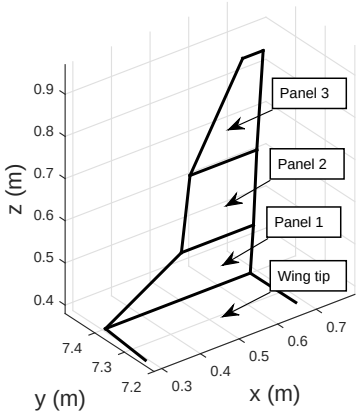

Figure 2. An example of a conventional winglet input geometry.

A typical winglet is shown in Fig. 3. For the conventional winglet optimization process, three panels were chosen to model the geometry. This allowed for one transition panel from the wing to winglet, and two panels for the program to explore main winglet geometry. The design variables for the optimization process were simply the

geometry of the winglet. Each panel in the performance model was defined by a triplet of (x,y,z) coordinates tracing the leading edge, which determined the sweep, cant and height of each panel. In addition, each panel could have been given a linear twist and taper distribution. The winglet was added to the wing by first removing the outboard 11 cm of wingtip, so that the wingspan would remain inside 7.5m for the standard class.

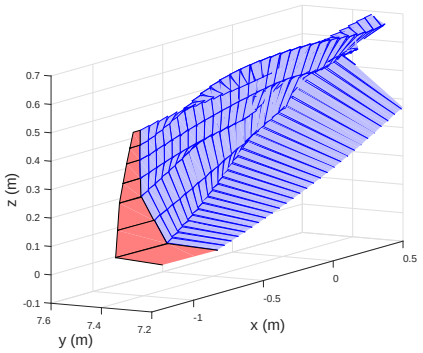

Figure 3. An example of a conventional winglet design, discretized into DVEs.

For the split-winglet analysis, an example can be seen in Fig. 4. Each of the tips was given two panels for the geometry, resulting in four panels for the entire wingtip device. These panels were subdivided into two DVEs each by the performance model. The inboard panels were rapidly tapered to form transition panels from the existing wing geometry, and the tips were staggered in the chordwise direction.

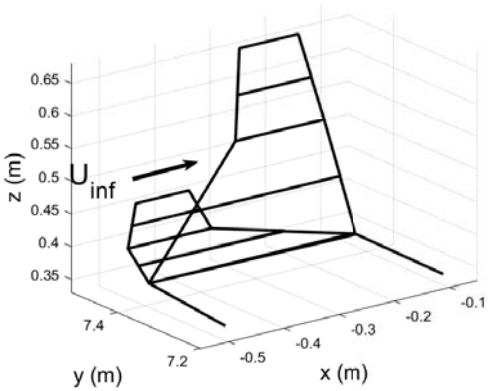

Figure 4. An example of a split-winglet design, discretized into DVEs.

Similar constraints from the previous design study were implemented in this process. Each of the two tips were forced to go outward, and they were forced to be staggered in the chordwise direction at the end of the transition panels, so they would not intersect. The lower tip was set to be aft of the upper panel. The lower, rear tip was allowed to, at its lowest bound, continue straight out in the plane of the main wing. The outboard edges of the transition panels were separated by a minimum of 9 cm, to account for airfoil thickness in that region. Both tips were not forced upwards outboard of the transition panel. Nevertheless, they were allowed to go downward provided they did not drop below the plane of the main wing.

The outboard edge of both tips were constrained to not exceed a total half-span distance of 7.5 m, so it could remain within the definition of a Standard Class sailplane. The amount of wingtip removed to create room for these split-winglet designs was a design variable. To add to this, experimentally it was noticed that removing too much of the wing for the split-winglets negatively impacted the potential cross-country performance of the Standard Cirrus. Further study of this parameter is needed to draw any further conclusions.

Results

Detailed results from the conventional winglet design study can be seen in Krebs and Bramesfeld (3), where the final design was predicted to increase the average cross-country speed of the Standard Cirrus a maximum of 4.5% in the weakest weather, with 2 m/s thermal core strength. In stronger weather, the benefits of the winglets were only slight, in the order of a tenth of a percent.

The split-tip design study is still on-going, though Fig. 5 shows a split-tip design from the optimization process that was chosen for further analysis. It has a pronounced, tall forward tip and a rear tip with greater chord that lies

in the plane of the wing. The projected span of this wingtip device is 21 cm. Even with the pronounced front tip, the maximum increase in wing-root bending was measured at 0.9% with respect to the Standard Cirrus. The high speed cruise drag coefficient increased from an estimated 0.0140 to 0.0141 with the addition of these particular split-tips.

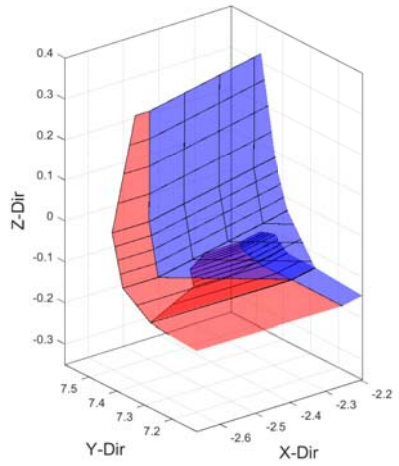

Figure 5. An example of a split-winglet design, discretized into DVEs.

Figure 6 shows the percent increase in average cross-country speed with respect to the Standard Cirrus with no winglets. An increase of approximately 5.4% is achieved in the weakest weather, with that benefit falling with the increasing strength of the weather. These split-tips, though sup-optimal as the study is still on-going, provide a performance increase beyond what was achieved in the previous conventional winglet design study.

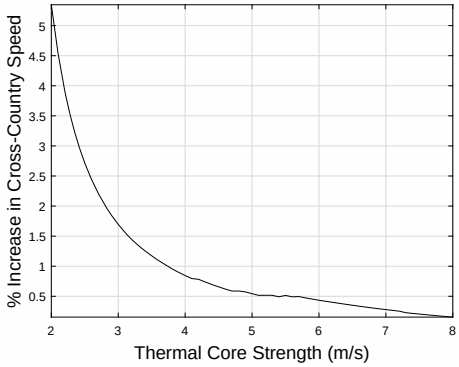

Figure 6. Chosen split-winglet design performance with respect to the Standard Cirrus.

Conclusions

An optimization process which was previously used to design conventional winglets for the Standard Cirrus was used to investigate split-tips, or split-winglets. Though the research continues to grow and evolve, a sample from the process was selected for further investigation. The chosen design has two tips, and is quite pronounced. It provides a maximum cross-country performance benefit over the Standard Cirrus of 5.4% in the weakest thermals, with minimal impact on the root-bending moment and the high-speed drag coefficient. This research is on-going, and will continue to explore split-tip devices in order to better understand how they work.

References

[1]Maughmer, M.D., 2003. Design of winglets for high-performance sailplanes. Journal of Aircraft, 40(6), pp.1099-1106.
[2]Smith, S.C., 1996. A computational and experimental study of nonlinear aspects of induced drag.
[3]Krebs, T. and Bramesfeld, G., 2016. Using an optimisation process for sailplane winglet design. *The Aeronautical Journal*, pp.1-20.

Investigating Designs of Autonomous Glider Exploration of Outer Solar System Atmospheres

Christopher Colletti[1] and Raymond P. LeBeau, Jr.[2]
[1]*Parks College, Saint Louis University, Saint Louis, MO 63103*

Goetz Bramesfeld[3]
Ryerson University, Toronto, ON

Abstract: AtmosPerf functions as an aircraft performance model that analyzes gliders in different atmospheric conditions. It generates 3D approximations and uses them in tandem with panel method approximations from FreeWake to generate mission profiles. This tool is intended to explore potential glider missions to other planetary atmospheres, maximizing flight range and endurance for each planet. The goal is to investigate the design of a cross-planetary mission platform. Preliminary results indicate the potential value for glider missions, however, the results between AtmosPerf and FreeWake vary enough that real glider flight data in the lower atmosphere is needed to further tune the solvers.

Keywords: Glider, Titan, Gas Giants, Performance Model, Planetary Atmospheres

Introduction

In 1989, the Galileo mission was launched on its six-year journey to Jupiter, where it would make observations for the next eight years. About five months before entering orbit around Jupiter, an atmospheric descent probe was released into the gas giant's atmosphere. The probe collected data as it dropped through the atmosphere, until it failed at about 22 bar (120 km below 1 bar) due to excess temperatures causing electronic failure [1]. This mission helped set the precedent for orbiter-probe combination missions being used to observe and take in-situ atmospheric data for the gas giants and their moons. In 1997 the Cassini-Huygens mission started its seven-year journey to Saturn. Similar to its sister mission, Galileo, the Cassini-Huygens mission consisted of an orbiter and an atmospheric entry probe. However, instead of descending through Saturn's atmosphere, the probe was aimed for Saturn's moon, Titan. Titan was chosen due to its thick atmosphere, which interfered with lower atmosphere and surface observations. Yet there were hints of a lower atmospheric meteorology that was uniquely Earth-like, composed of methane and other hydrocarbons and producing rain, clouds, and surface liquids.

Both of these missions provided valuable data about the behavior and properties of these atmospheres. The observations from these missions provided has promoted new atmospheric models and significantly improved insight into the nature of these planet's weather systems. Additionally, this data increased our understanding of how Earth's atmosphere has evolved into what it is today. Collectively, general atmospheric knowledge has been fundamentally improved by these orbiter-atmospheric probe missions.

Thus far, there have only been two orbiter-probe missions to the outer solar system. Continued exploration and collection of *in situ* data would provide additional unique insight into the nature of these atmospheres and the parallels that can be drawn between the behaviors of Earth's atmosphere and those of the gas giants and Titan. For such missions, it would be optimal for *in situ* data to be collected over an extended period of time. An alternative to a parachute drop probe would be an autonomous aircraft. An autonomous aircraft will cover a larger area of the atmosphere and can adjust to the changing conditions experienced throughout the atmosphere, making it ideal for more extensive atmospheric data collection.

Methodology

Basic methodology for this analysis includes the use of two different numeric approaches, a panel method (FreeWake) and 3D correction method (AtmosPerf), to evaluate the flight characteristics of a glider platform midflight. Aircraft specifications are imported into both solvers along with the atmospheric data for each planet. The solvers evaluate the general flight performance at various points throughout each atmosphere and select the best flight angle at each point for maximizing mission endurance and/or range. Estimated mission profiles associated with given aircraft platforms were collected from the two solvers to generate a general guideline for what can be expected when flying a glider on these planets. By using two different solvers, the limitations of each method can be covered by the other, which will give a more accurate representation of flight through another atmosphere. There are some key differences in the assumptions each solver makes that affect the overall range and endurance results. FreeWake does not perform any Mach corrections, as it assumes most of the flight regime will be in the incompressible region, and it only considers turbulent effects for the fuselage. AtmosPerf does include Mach corrections and turbulent mixing across the wings, but it does not consider separation drag, which becomes increasingly important as the solver selects higher angle of attacks for the optimum flight condition.

An incomplete understanding of these atmospheres means the general flight trends and characteristics for each glider platform are the most valuable results for this analysis. These results will demonstrate whether glider missions to the four gas giants and titan are worth the time and expense. Additionally, by focusing on trends seen from this analysis, it can be seen as to whether the same base glider configuration can be reasonably used for multiple missions on different planets, which would provide greater flexibility in mission selection and planetary exploration depending on current objectives.

Results

The main application of AtmosPerf is to develop a mission profile for a glider on the gas giants or Titan. Once the model was developed and tuned with FreeWake, so that results matched with some accuracy, various glider designs were analyzed. Using a constant platform, i.e. constant mass, payload, wingspan, and tail sizing, thirteen different airfoils where analyzed to determine a maximum possible mission range and endurance for each of the gas giants and Titan, see table 1 below. The airfoil configuration that gave the maximum range and endurance are listed for each solver and planet; here the airfoil similarity between all planets indicate that there could be a cross-planetary glider platform that would optimize data collection for each planet.

Table 1. Maximum Mission Range and Endurance Values for the Given Airfoil on Each Planet

	FreeWake			AtmosPerf		
Planet	Range (km)	Endurance (hr)	Airfoil	Range (km)	Endurance (hr)	Airfoil
Jupiter	9,000	35	Eppler 67	12,000	55	Aquila
Saturn	11,000	40	Eppler 67	16,500	65	Aquila
Uranus	10,000	60	Eppler 67	8,500	32	PSU 94-097
Neptune	7,000	40	Eppler 67	7,200	40	Aquila
Titan	4,400	95	Eppler 67 | PSU 94-097	7,000	160	Aquila

The table above illustrates the differences in the results due to assumptions each solver makes. Due to the difference in methodologies AtmosPerf estimates a lower flight velocity than that of FreeWake, which affects the overall drag and lift calculations, and therefore range and endurance. It is expected that the true values of the flight data lie between the results of the two solvers, so the next step in further verification would be to incorporate real flight glider data in lower Earth's atmosphere into the adjustment process so that both solvers can be further tuned with the same flight data. Depending on the results from the real flight data, various constants could be adjusted to match the data or a mixed solution could be developed, where the results of both solutions are combined to generate a solution that matches the real flight data.

Conclusions

Atmospheres of the four gas giants and Titan hold a particular interest to scientists due to their application in developing atmospheric models that can apply to earth. By observing the general circulation of an atmosphere as an outside, a better understanding can be developed of the internal machinations that moves the planet's atmosphere. Additionally, Titan holds a significant interest due to the fact that it is similar to what a young Earth's atmosphere is believed to have been like, an atmosphere composed of primarily diatomic nitrogen. Due to the unique aspect of these atmospheres and the contribution a better understanding of them would add, there is a desire to have a mission visit any number of these planets. In the past there have been probe-drop mission to Jupiter and Saturn, but a drop probe has a very limited mission range and endurance over which to collect atmospheric data. A more efficient mission could involve the use of a glider to collect atmospheric data over a longer range and endurance than what a drop probe could provide, while not being as complicated and costly as a powered flight in a relatively unknown atmosphere, millions of miles from Earth.

AtmosPerf functions as an aircraft prediction model that works to analyze flight characteristics of a glider under different atmospheric conditions, it generates 3D approximations for the lift and drag build-up based on 2D airfoil data and aircraft geometry. An optimum angle of attack is then selected in order to maximize mission endurance and range, finally a flight regime of the glider moving through the planet's atmosphere, along with flight performance estimations at each point in the atmosphere, are output. The AtmosPerf tool functions as a method to perform an initial flight analysis of a glider moving through the atmosphere of one of the four gas giants or Titan. It can be used to evaluate numerous glider geometries and try to narrow down a single aircraft platform for each planet to allow for more flexible mission options. As work continues on the performance prediction model, real time glider data from lower Earth's atmosphere can be used to provide additional verification and tuning of the solver results. Data collected from the glider would be used in tandem with the results from FreeWake to find the best mix of results and/or tweaked constants that are needed to reasonably recreate the real flight data.

References

[1]Jet Propulsion Laboratory., "Galileo Mission to Jupiter", NASA Facts Sheet. California Institute of Technology

The Use of Computational Fluid Dynamics Analysis in Wing-Winglet Design

Mark D. Maughmer[1], James G. Coder[2]
[1]*The Pennsylvania State University, mdm@psu.edu*
[2]*The University of Tennessee, jcoder@utk.edu*

Abstract: To better understand how computational fluid dynamics (CFD) methods can support sailplane design efforts, the design of the wing and winglet for a new 18-m high-performance sailplane (the new Schempp-Hirth Ventus) is performed in the classical manner using potential flow methods combined with viscous two-dimensional airfoil considerations. The final design is then analyzed using a computational fluid dynamics solver that incorporates a recently developed transition/turbulence model. Predictions made using CFD are compared to those obtained using the more traditional methodology, and then used to explore and refine the design in the areas in which the traditional approaches are less reliable.

Keywords: Sailplane design, winglet design, transition prediction, computational fluid dynamics

Introduction

While the benefits of using computational fluid dynamics (CFD) in the design and analysis of commercial transport types of aircraft are significant and noteworthy, this is not being the case for sailplanes. This is because until recently, CFD methodologies have been unable to accurately account for the effect of laminar- turbulent transition. For the operational Reynolds numbers of sailplanes, accurate transition prediction is necessary to correctly capture aerodynamics and performance, while for aircraft operating at much higher Reynolds number, transition as little impact and boundary-layer flows can be treated as fully turbulent. Clearly, for CFD to have a role in sailplane design, new methods of accounting for transition in the Reynolds averaged Navier-Stokes (RANS) equations framework are needed. Although there have been many efforts in the past two decades to do this, the watershed event for this technology was the development and public release of the local-correlation transition model developed by Langtry and Menter.[1] A more recent advancement in CFD transition modeling is the amplification factor transport equation developed by Coder and Maughmer.[2] This model is based on a transformation of the approximate envelope transition method used in XFOIL[3] and MSES[4] to a CFD-compatible transport equation that may be massively parallelized. CFD solutions using the amplification factor model predict two-dimensional profile drag more accurately than the Langtry-Menter model and thus, for the prediction of sailplane aerodynamics and performance, have comparable accuracy to what would be found in airfoil look-up tables.[2]

The goal of this paper is to explore the capabilities of CFD in predicting the aerodynamics of the wing and winglet for a recently designed sailplane, shown in Fig. 1, and investigate some of its more complicated flow features. Of particular interest is the flow around the winglet juncture, as this region not well predicted by traditional potential-flow-based methods.

Wing-Winglet Design Using Traditional Process

Prediction of Sailplane Performance

The accurate prediction of sailplane performance is an important component of the winglet design problem. This prediction must have sufficient resolution to account for the effect of small changes to the winglet geometry, but also be accurate and reliable in other aspects of the prediction, as any errors or inconsistencies here can easily overshadow those due to changes in the winglet. The accuracy necessary for successfully undertaking activities such as winglet design is achieved through the use of a performance prediction program that has been developed to predict sailplane straight- and turning-flight polars.[5] In addition to the drag contributions of the major components of the sailplane, the program accounts for the effects of airfoil characteristics, trim drag, static margin, flap geometry, and flap-deflection scheduling. Essential to the analysis method is the inclusion of accurate airfoil aerodynamics. Wing profile drag is a large portion of the overall drag and small errors in its determination can eclipse the effects of winglets. To accurately provide such data, it is necessary to interpolate the airfoil drag and moment data over operational ranges of lift coefficient, Reynolds number, and flap deflection.[3, 6]

The other essential component for predicting the planform aerodynamics is the determination of the span efficiency and lift distribution. The lift distribution directly affects the wing profile drag, and the planform efficiency dictates the induced drag of the wing. Because this is where the benefit of the winglet is quantified, accurate methods of determining these two items is of critical importance. In the present approach, use is made of a multiple lifting-line method, with and without a free wake.[7, 8] The multiple lifting-line method, which has been integrated directly into the performance program, makes use of a second-order vorticity distribution that sheds a continuous singularity-free sheet of vorticity into the wake. The method allows the spanwise lift distribution and induced drag of non-planar wing geometries to be predicted with reasonable accuracy and low computational effort.

The use of the multiple lifting-line program and the interpolation of airfoil characteristics allows the performance program to produce accurate straight- and turning-flight polars for any aircraft configuration. Comparisons of the method with flight-test results over a wide range of sailplane types have demonstrated that the method is able to resolve small enough differences between configurations to be of value in the winglet design effort.[5, 9]

The turning-flight performance of the sailplane is obtained by adjusting the straight-flight polar for bank angle and load factor. By these means, the minimum sink rate, optimal bank angle, and optimal flight velocity as a function of turning radius are determined. The effects of deflected ailerons and the rotational flow field are neglected.

Analysis of Cross-Country Performance

The metric for determining whether or not a particular design performs better or worse is the average cross-country speed. This task is accomplished by means of the MacCready average cross-country speeds for a given configuration using the straight- and turning-flight polars as generated by the performance program.[5, 9] In addition, for a design to be robust and suited for all operational situations in which the sailplane must perform, the winglets performance must be considered over a range of thermal strengths, wing loadings, and flap settings.

The thermal model used in this analysis has a distribution of vertical velocity that varies parabolically with thermal radius. Thus, the thermal profile is specified in terms of its radius and the magnitude of the vertical velocity of the rising air at the core. This profile has a significant impact on the cross-country performance of a sailplane and the most realistic performance index would result from a specific mix of thermal strengths and profiles, although there is certainly "some" varying strength model that would give equivalent results as the mix and, for the reason done here, greatly simplifies the interpretation of the outcome and still yields a meaningful comparison between sailplanes having different winglet geometries.

To obtain the optimal climb rate for a particular configuration, the thermal profile is superimposed over the predicted turning polars. The straight flight polar is then searched for the inter-thermal cruise speed to optimize the MacCready cross-country speed. The result is a trade-off of climb and cruise performance, properly weighted to account for the variations in soaring conditions over which the sailplane might be operated.

The current design methodology has been developed and validated with flight-test measurements, comparison flying, and a long record of competition results. It has been successfully applied to a large number of winglet designs, which generally satisfied their design goals without modification.[9]

Analysis Using Computational Fluid Dynamics

The geometry used for this study is the isolated wing and winglet of the new 18-meter sailplane. A single-domain O-O surface mesh was generated from the production IGES model of the geometry. The original IGES definition of the wing begins at the wing root; the surface mesh was subsequently extrapolated to the aircraft centerline. This allows a true symmetry plane to be applied while preserving the true span of the wing.

The flow solver used for the analyses is OVERFLOW 2.2f. OVERFLOW is a structured, overset solver developed and maintained by NASA and is capable of solving the three-dimensional Reynolds-Averaged Navier-Stokes (RANS) equations.[10] Closure for the turbulent Reynolds stresses is achieved using eddy-viscosity models, which typically consist of 0, 1, or 2 transport equations. This solver contains an implementation of the Langtry-Menter model which solves two additional transport equations to automatically predict transition;[1] however, for the current study, transition is predicted using the amplification factor, or N-factor, transport equation developed by the authors.[2] This model requires the solution of one transport equation.

Comparison of Results and Discussion

Modeling the Winglet Juncture

A region of the wing geometry that is of particular interest for CFD modeling is the wing-winglet juncture region. This region is typically not well predicted by typical potential-flow methods as the geometry changes very rapidly relative to the thickness of the wing and the effect of viscosity becomes very important.

The predicted upper-surface-streamlines (numerical "oil flow") in the juncture and on the winglet for $C_L = 0.3$ are shown in Fig. 2. The presence of a laminar separation bubble is visible on both the wing and winglet. The flow over the main wing is almost entirely two-dimensional, which confirms the design of the winglet itself. Through the juncture and along the winglet, there is some spanwise flow, especially aft of the laminar separation bubble. A subtle but important flow feature is a vortex in the juncture as revealed by the surface streamlines; this is indicated by the vortical convergence of several streamlines at the base of the winglet on the laminar separation line. The predicted streamlines on the lower surface are shown in Fig. 3, where it is observed that the winglet airfoil has fallen out of low-drag region. This deserves attention as to whether or not this case represents cruising flight that is faster than what should be expected, or if airfoil should be redesigned and/or, more simply, if the winglet toe angle should be adjusted to mitigate this issue.

Concluding Remarks

The key enabling technology in CFD for accurate prediction of sailplane performance has been the development and promulgation of automatic, accurate methods for predicting laminar-turbulent transition in the flow field. The N-factor transition model of Coder and Maughmer, as applied to the Spalart-Allmaras turbulence model, was used to predict the performance of the new Ventus wing. The transitional solutions were able to predict the presence of a laminar drag bucket in the drag polar and the presence of laminar separation bubbles as the primary means of transition on the wing, something clearly missing in the fully turbulent modeling as used in the past. It is unlikely that CFD will supplant potential-flow-based methods and airfoil look-up tables for sailplane wing and winglet design in the foreseeable future; however, modern CFD capabilities provide the means to explore aspects of the design that are not well predicted by potential flow

References

[1]Langtry, R. B. and Menter, F. R., "Correlation-Based Transition Modeling for Unstructured Parallelized Computational Fluid Dynamics Codes," *AIAA Journal*, Vol. 47, No. 12, 2009, pp. 2894-2906.

[2]Coder, J.G. and Maughmer, M.D., "CFD Compatible Transition Modeling Using an Amplification Factor Transport Equation," *AIAA Journal*, Vol. 52, No. 11, Nov. 2014, pp. 2506-2512.

[3]Drela, M. and Youngren, H., "XFOIL 6.9 User Primer," Massachusetts Institute of Technology, Cambridge, MA, 2001.

[4]Drela, M. and Giles, M. B., "Viscous-Inviscid Analysis of Transonic and Low-Reynolds Number Airfoils," *AIAA Journal*, Vol. 25, No. 10, 1987, pp. 1347-1355.

[5]Maughmer, M.D. and Kunz, P.J., "Sailplane Winglet Design," *Technical Soaring*, Vol. 22, No. 4, Oct. 1998, pp. 116-123.

[6]Eppler, R., Airfoil Program System "PROFIL07," User's Guide, Richard Eppler c. 2007.

[7]Horstmann, K.-H., "Ein Mehrfach-Traglinienverfahren und seine Verwendung für Entwurf und Nachrechnung nichtplanarer Flügelanordnungen," DFVLR, Institut für Entwurfs-aerodynamik, Braunschweig, DFVLR-FB 87- 51, 1987.

[8]Bramesfeld, G. and Maughmer, M.D., "A Free-Wake, Lifting-Surface Model Using Distributed Vorticity Elements," *Journal of Aircraft*, Vol. 45, No. 2, March-April 2008, pp. 560-568.

[9]Maughmer, M.D., "The Design of Winglets for High-Performance Sailplanes," *Journal of Aircraft*, Vol. 40, No. 6, Nov.-Dec. 2003, pp. 1099-1106. Reprinted in *Technical Soaring, An International Journal*, Vol. 27, No. 1 and 2, Jan. and April 2003, printed Oct. 2005, pp. 44-53.

[10]Nichols, R. and Buning, P., "User's Manual for OVERFLOW 2.1, Version 2.1t," NASA Langley Research Center, Hampton, VA, August 2008.

Fig. 1 The Schempp-Hirth "New" Ventus.
MTOW, 600 kg; Wing Area, 10.32 m^2; Aspect Ratio, 29.9.

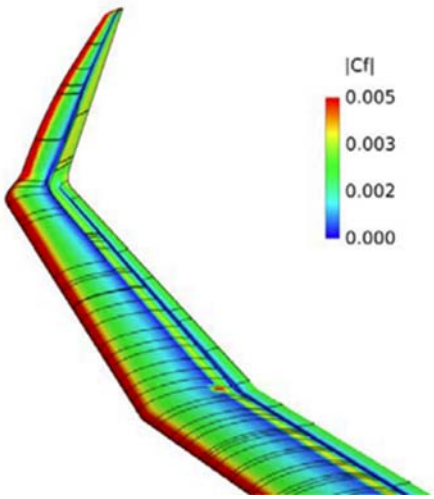

Fig. 2 Upper-surface streamlines of wing/winglet. C_L = 0.3.

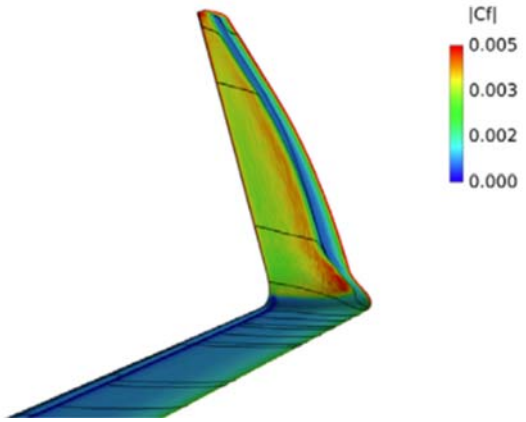

Fig. 3 Lower-surface streamlines of wing/winglet. C_L = 0.3.

On the gust loads of sailplanes

L.M.M. Boermans
TU Delft, Faculty of Aerospace Engineering, l.m.m.boermans@tudelft.nl

Introduction

The gust load determination in Certification Specifications for Sailplanes and Powered Sailplanes CS-22 and OSTIV Airworthiness Standards for Sailplanes and Powered Sailplanes OSTIVAS are based on theoretical and experimental investigations performed by NACA in 1959. The present paper clarifies that both in the theoretical work and in the data reduction of these gust tests, assumptions are applied that are not valid for sailplanes. In addition, calculations with a modern aerodynamic/structural/control simulation tool show that pitching and flexibility are essential parameters for gust load determination. These insights show the need for improved gust load determination for sailplane airworthiness requirement purpose.

Methodology and Results

The gust load determination in CS-22 and OSTIVAS is based on NACA reports 997 (1951)[1], 1206 (1959)[2] and the maximum gust velocity of 15m/s is defined in TN D-29 (1959)[3]. The first two reports deal with discrete gusts on large airplanes and do not cover the parameter range of sailplanes. As a result, the definition of the gust gradient distance of the (1-cos) shaped standard design gust, being 12.5 times the mean chord of the wing, is not applicable for sailplanes.
Pratt's formula for the gust alleviation factor, used in CS-22 and OSTIVAS and based on the prescribed gust length of 12.5 times the mean chord of the wing, can be generalized to be applicable for any airplane in any gust. Figure 1 shows the gust load factors calculated for a variety of sailplanes in (1-cos) gusts with maximum gust velocity of 15m/s calculated according to CS-22 and OSTIVAS, and for (1-cos) gusts with the steepest gust gradient measured with sailplanes in Russia leading to a gradient distance of 15m. The latter gust load factors are about 15% lower.

Airworthiness requirement codes for transport aircraft require that design loads include discrete gust dynamic loads because structural flexibility might cause higher loads. Since the dynamic response is sensitive to gust gradient distance, the atmospheric turbulence is assumed to consist of a series of discrete (1-cos) gusts with maximum gust velocity of 15m/s and varying gust gradient distance, which are investigated in order to tune the gust to give maximum response. This tuned discrete dynamic gust load analysis was applied by E. Lasauskas[4] on an 18m span 600kg MTOM sailplane, using ASWING, a code based on an integrated model for aerodynamic, structural, and control simulation of flexible aircraft with moderate or high aspect ratio wings in extreme flight situations, developed by M. Drela[5]. The calculations are performed for both a rigid wing and a flexible wing (with a given mass and bending stiffness distribution) and cg position at 42% of the mean aerodynamic chord. Time histories of several parameters are presented and the present paper shows the resulting maximum gust load factor plotted as a function of the gust gradient distance in comparison with the gust load factor obtained with Pratt's generalized expression. These calculation results clarify that the assumptions applied at the derivation of the formulas in CS-22 and OSTIVAS, being a rigid wing that flies with constant flight speed without pitching through the gusts, have to be revised. Pitching is related to the rearward cg position and causes a higher gust load factor for the rigid wing than the gust load factor obtained with Pratt's generalized expression, while flexibility alleviates the gust load in this case. Gust gradient lengths lower than 10m to 15m are too short for the sailplane's inert reaction, causing a decrease of the gust load factor.

The alternative for the discrete gust approach is the Power Spectral Density method, a continuous gust method where the turbulence data are covered by the von Kármán PSD function for isotropic turbulence. Similar to Pratt's development of a simple formula of the gust alleviation factor for the discrete gust method as described before, J. B. de Jonge[6] developed a simple formula of the spectral gust alleviation factor for the continuous gust approach. But the problems of this approach are similar as well: the appropriate atmospheric calibration of the method has not yet been established i.e. the standard design gust for sailplanes is not known yet. And the assumptions applied at the derivation of the formulas are the same as well: a rigid wing flying with constant flight speed without pitching through the continuous gusts.

Conclusion

The challenge to determine the gust loads of sailplanes for airworthiness requirement purpose is to find simple formulas which are based on the insight gained from sophisticated tools and imply the effects of the governing parameters of a flexible wing that flies plunging and pitching through specified gusts.

References

1. Donely, P., 1951: Summary of information relating to gust loads on airplanes. NACA Report 997.
2. Pratt, K.G. and Walker, W.G., 1954: A revised gust-load formula and re-evaluation of the V-G data taken on civil transport airplanes from 1933 to 1950. NACA Report 1206.
3. Walker, W.G. and Copp, M.R., 1959: Summary of VGH and V-G Data obtained from Piston-Engine Transport Airplanes from 1933 to 1950. NASA TN D-29.
4. Lasauskas, E., Dec. 2016: Influence of sailplane wing-bending flexibility on "1-cos" gust loads. The Aeronautical Journal, Vol. 120, No 1234.
5. Drela, M., 1999: Integrated Simulation Model for Preliminary Aerodynamic, Structural, and Control-Law Design of Aircraft. AIAA 99-1394.
6. J.B. de Jonge, J.B., 1970: A spectral gust alleviation factor for sailplanes. NLR MP 70002U.

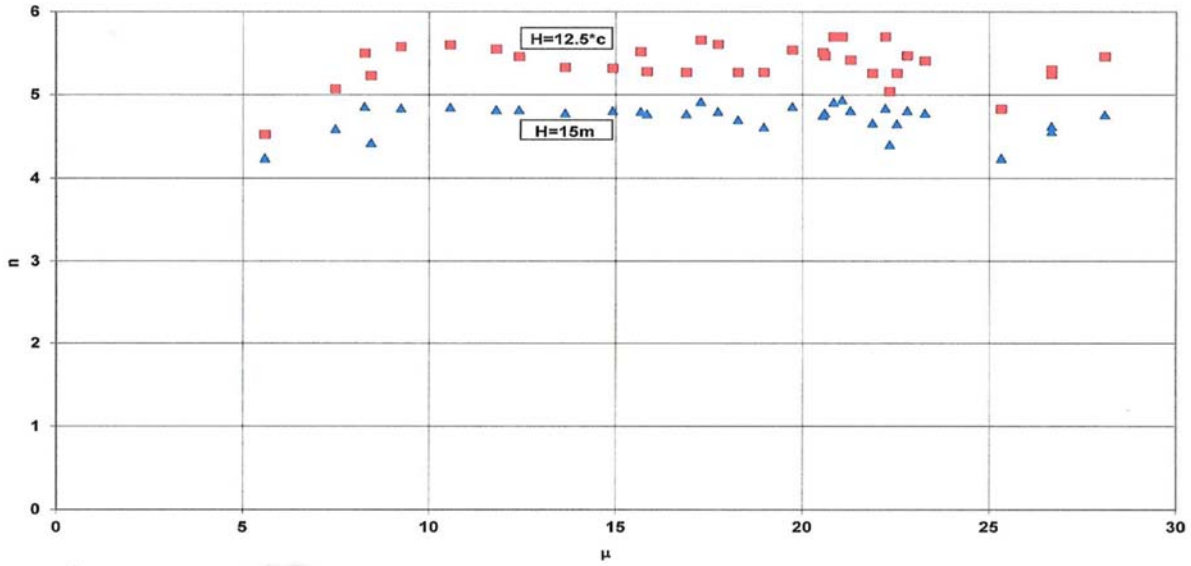

Figure 1. Gust load factor as a function of μ_g for 33 sailplanes in a (1-cos) gust with maximum gust velocity 15m/s and gradient distance of H=12.5*$\bar{c}$ m (red symbols, CS-22 and OSTIVAS) and 15m (blue symbols, Russian tests with gliders).

Lifetime Considerations on Sailplanes

Christoph Kensche, Jelmer Wassenaar
DG Flugzeugbau

Introduction

Historically, service life investigations on composite gliders in Germany started in the Sixties by developing a multi-step fatigue programme based on mainly theoretical assumptions on the various loadings during take-off, flight and landing. For many years, the resulting Franzmeyer-programme simulating 3.000 flight hours was then used for lifetime certification of glass- and carbon-fibre reinforced sailplanes.

Although not losing its validity it was replaced in the Eighties by the Kossira-Reinke- Spectrum which – with minor modifications – became then the KoSMOS-Standard. This service life programme representing 6.000 flight hours was established by measuring the strains on the wing of a Janus glider in flight. After digitizing the analogue data they were graded and stored in a 32x32 Markov transition matrix.

KoSMOS is now available as a time history in two versions which differ by the percentage of omission to be able to reduce the testing time of a certification test. Such investigations are nevertheless costly and, thus, gliders are generally just certified for a flight time of 12.000 h.

The data can, however, also be applied for a lifetime assessment. For this case we need additionally to the spectrum material-specific s-n data and a damage accumulation hypothesis like the simple Palmgren-Miner-rule which is widely used and accepted for lifetime calculations on Rotor blades of wind turbines, too. By means of a program developed at DLR, for composites a significantly higher lifetime could be demonstrated than is possible to shown by experiment on e.g. a wing structure by reason as explained before.

Evaluation of new flight measurements

This code was recently very helpful for comparison calculations between the damaging effects of KoSMOS and flight measurements carried out on DG-1000 sailplanes in their acrobatic configuration (18 m span). The goal of that campaign was to figure out whether pure acrobatic as well as basic training flights would cause higher damaging rates than KoSMOS.

For this purpose, accelerometers were placed in the centre of the cockpit and strain gauges were applied on the wing structure. Thus, after completing all flights, Markov transition matrices were established for the four different configurations strain-based flights in acrobatic and basic training mission as well as those with accelerometer measurements.

The cumulative frequency diagrams in Figure 1 show the KoSMOS spectrum in various stages of development in comparison to the basic and acrobatic flights of the DG-1000 campaign. From these plots, no objective conclusion can be drawn
on possible differences between the spectra.

However, by the calculations it could be demonstrated that in no configuration with strain measurements higher damage rates were achieved than allowed with KoSMOS as demonstrated clearly in Figure 2. Furthermore, it became evident that accelerometers placed in the cockpit of a sailplane with the high elasticity of the wing are not an appropriate means to replace a sound strain measurement

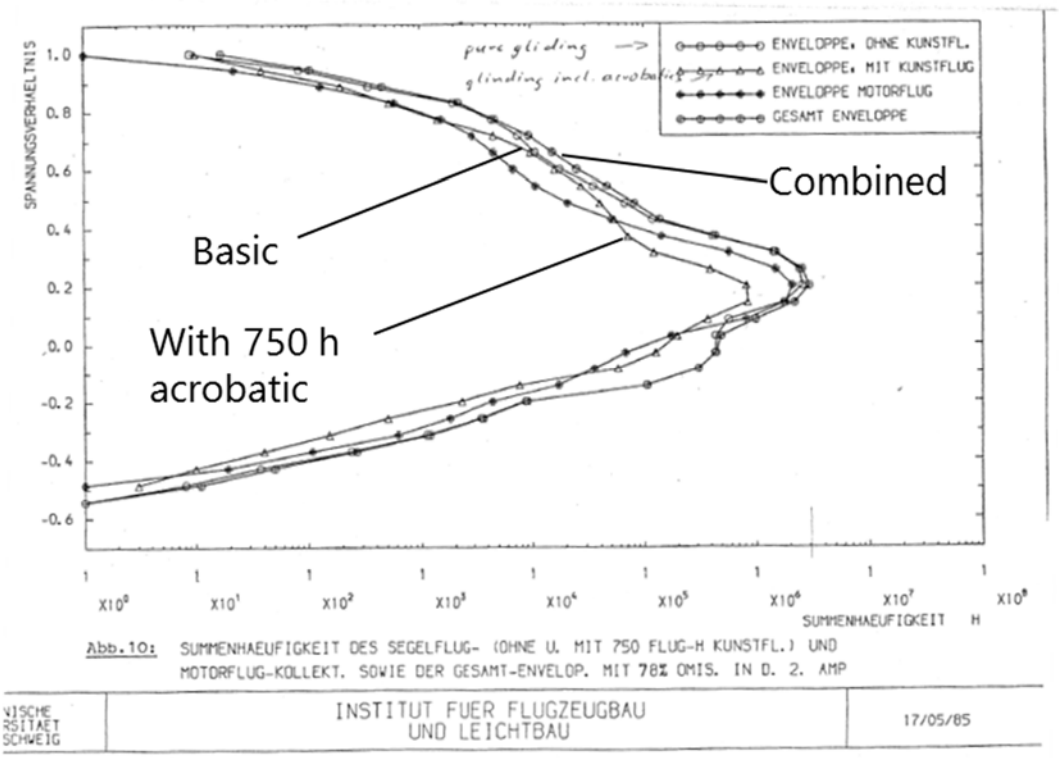

Figure 1: Cumulative frequency plot of KoSMOS

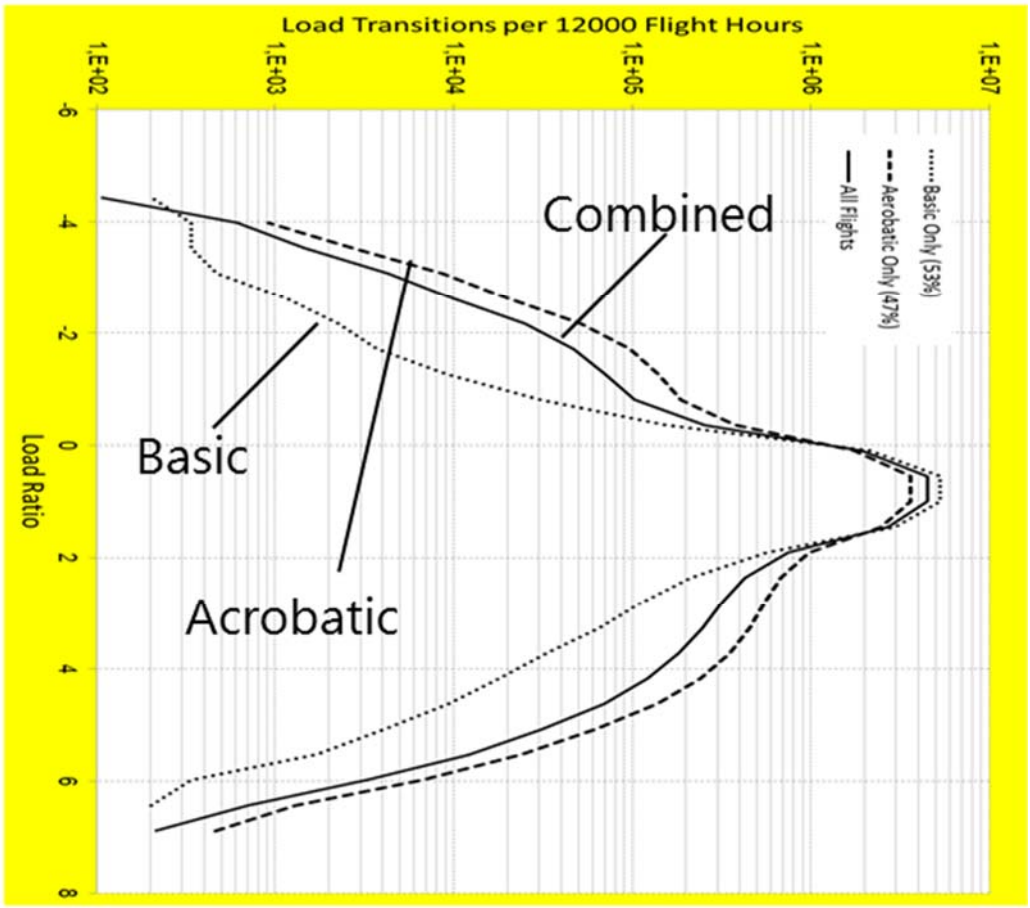

Figure 2: Measured DG 1000 spectrum

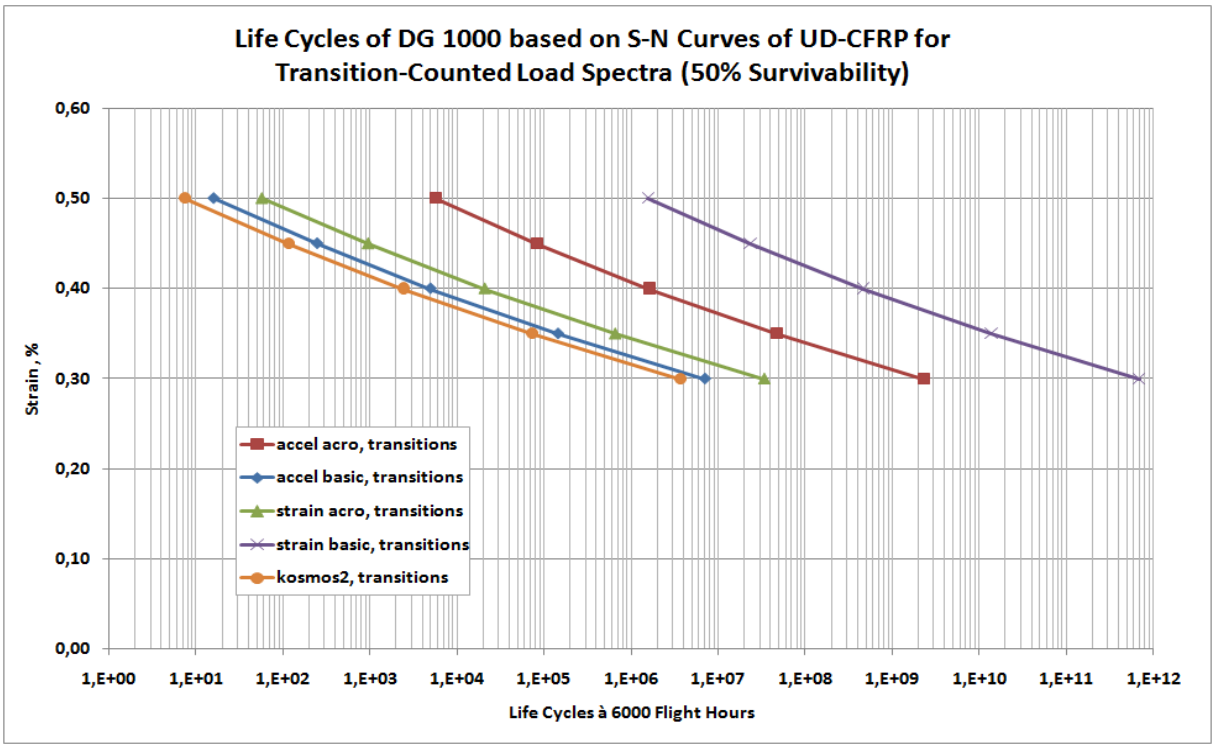

Figure 3: Damage calculation of KoSMOS and DG 1000 spectrum at different design strains in a CFRP spar cap

Do not get caught-on-top!

Em. Prof. Dr. Edward (Ward) Hindman
The City College of New York, New York, NY US 10031
hindman@sci.ccny.cuny.edu

Abstract: Climbing 5000 m in a glider to earn the *FAI* Altitude Diamond is most often achieved using lift generated by mountain waves. During these flights, a primary concern can be an undercast forming below the glider and/or a wave cloud enveloping the glider. These phenomena may (can?) be forecast by interpreting on-line atmospheric profiles (soundings, thermics) from numerical weather prediction (NWP) models. Profiles are presented from actual wave flight accidents caused by these instrument meteorological conditions (IMC).

Keywords: Safety, mountain-waves, soundings, thermics

Introduction

During my gliding career - which started in 1970 - as a way of progressing, I earned the *Fédération Aéronautique Internationale* Badges. I earned the Silver Badge in 1981, the Gold Badge in 1983 and the 300 km Diamond Goal flight in 1983, 500 km Diamond Distance flight in 1998 and the 5 km Diamond Altitude climb I have yet to achieve. I plan to make the climb using the stationary, rising-air produced downwind of a mountain barrier called the mountain wave. I've made attempts in the west and east of the US. Often the clouds forming in the wave have interfered with the climbs. Thus, I will describe the clouds, their behavior and how to forecast the behavior so that you **recognize**, **understand** and **act** to fly safe and achieve the climb.

Methodology

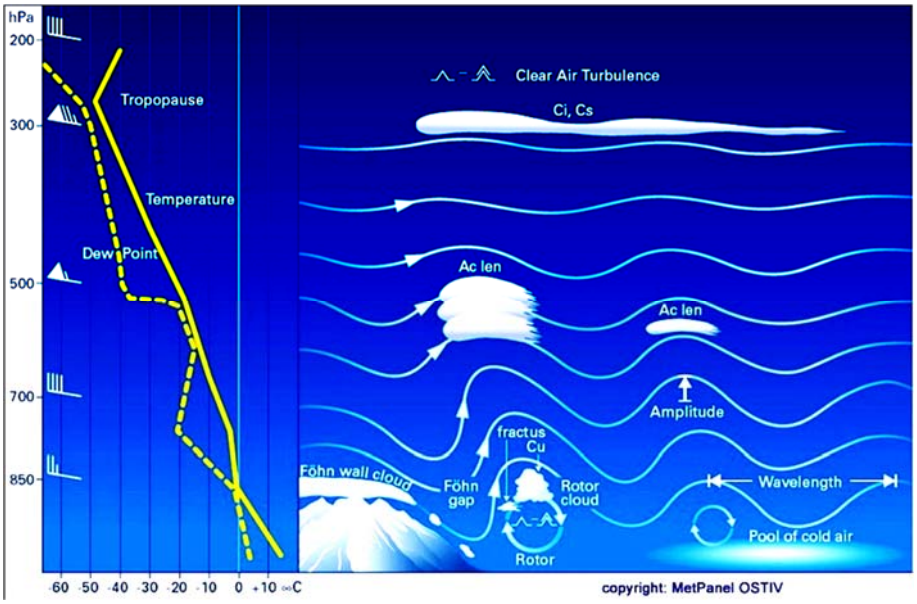

Figure 1. Common profile (left) and clouds during mountain-wave condition (based on Fig. 1.15 in [1])

The common mountain wave clouds are depicted in Fig. 1. Notice the clouds form in the rising air and dissipate in the sinking air. Most successful Diamond climbs occur in the rising air in the Föhn gap ahead of the fractus Cu and Rotor cloud and ahead of the Altocumulus-standing-lenticular clouds (Ac len). But, because of small fluctuations in the Temperature and Dew Point profiles and the air flow, these clouds can quickly increase and/or decrease in area and depth as illustrated in this video made downwind of the Rockies *www.youtube.com/watch?v=_roxFGsfzto*. For example, my greatest concern while climbing is the Föhn gap closing trapping me on top.

During the 2015 soaring season, at least two US pilots encountered IMC flying in the mountain wave. While descending in the Sierra wave near Reno NV on 5 April, Bob Spielman, apparently, was not far enough ahead of the rotor cloud, was enveloped and had to bail out when his ship disintegrated inside the turbulent cloud [2]. This incident reminds me of the infamous Edgar ship breakup and bail out during the Sierra Wave project [3]. Additionally, while descending in the Mt. Washington NH wave on 14 October, Chris Giacomo had the Föhn gap close, was enveloped and chose to bail out rather than continue the descent risking colliding with the mountain (*www.mtwashingtonsoaring.org/Documents.asp*).

Results

These incidents demonstrate the clouds can 'reach out and bite you'. What can we do in our pre-flight weather studies to anticipate such cloud behavior? Study the forecasted atmospheric profiles of temperature, dew point and winds.

The profiles are freely available from the Internet. I describe how to obtain the profiles and use them to forecast mountain wave conditions in [4]. The profiles that follow are from the NOAA-READY 'archived meteorology' section; the forecasted soundings are found in the 'current' meteorology' section. I do not know how to obtain forecasted soundings, after-the-fact. Nevertheless, I argue these profiles would have been close to the forecasted profiles if the pilots had performed their preflight briefing just a few hours prior to launch.

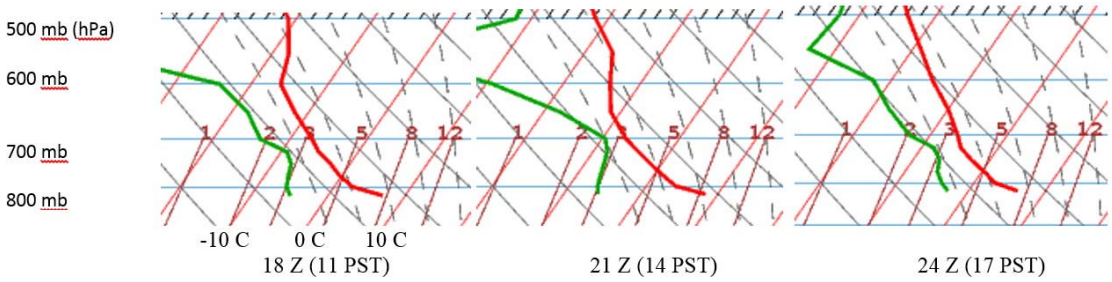

Figure 2. The actual atmospheric profiles during the Spielman flight; the bail out occurred around 15 PST.

It can be seen in Fig. 2 that the 700 mb level (about 10 kft MSL) moistened significantly between 11 and 14 PST (the gap diminished between the temperature (red) and dew point (green)) most likely causing the rotor cloud to expand engulfing Spielman.

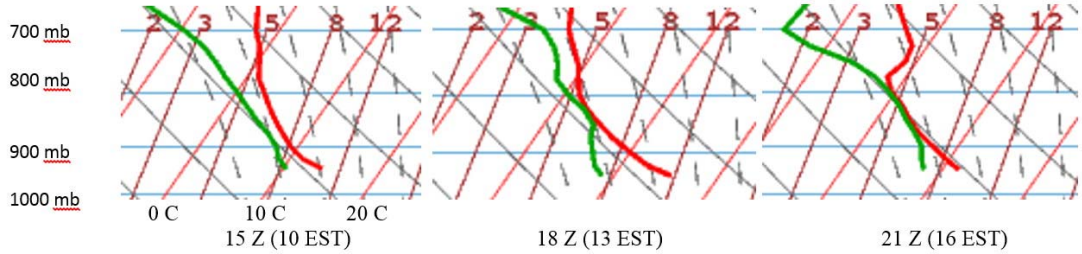

Figure 3. The actual atmospheric profiles during the Giacomo flight; the bail out occurred around 1230 EST.

It can be seen in Fig.3 that the 850 mb level became saturated (cloud-filled) between 10 and 13 EST causing the Föhn gap to close engulfing Giacomo. In fact, the cloud layer thickened between 13 and 16 EST. Notice the atmosphere was much colder and drier for the higher altitude Spielman flight than for the Giacomo flight. This difference, in part, explains why a pilot is less likely to get caught-on-top in a western US mountain wave.

What can we do during a wave flight to avoid 'getting bit'? From my eastern US wave flying experience, I watch the size of the Föhn gap below as I ascend. At the first signs that narrow cloud 'tentacles' begin almost to reach across the gap, I cease climbing, push ahead into the sinking air and get back down through the gap. If I continue to climb, I must have a downwind airport chosen for an emergency landing.

Conclusions

Interpreting forecasted atmospheric soundings, freely available on the Internet, can provide guidance to pilots to avoid being enveloped by IMC while climbing in mountain waves. However, a fact I learned from my studies of Mt. Everest weather for the ultimate ascent - using a sailplane [5], **getting to the top is optional, getting down is mandatory**!

Recognize, **understand** and **act** to fly safe!

References

[1] World Meteorological Organization, 2009: *Weather forecasting for soaring flight*. TN No. 203, 68 pp.
[2] Spielman, R., 2015: Jump. *Soaring*, December, pp 32-36.
[3] Kuettner, J., 1955: Jet Stream Project – II. *Soaring*, November-December, pp 2-6.
[4] Hindman, E. E., 2014: A free, on-line soaring weather forecasting system for world-wide use. *Technical Soaring*, **38**/3, 28-42.
[5] Hindman, E. E., O. Liechti and P. Lert, 2002: Soar Mt. Everest! *Technical Soaring*, **26**/4, 114-123.

Gravity wave over flat terrain

Daniel L. Johnson (MD)
Mayo Clinic Health System, drdan@wwt.net

Abstract: Wave is everywhere throughout the atmosphere, wherever shear exists. Standing gravity wave is important because of its predictability and spectacular physics. Reports of widespread, workable lift over flat terrain, even with overcast conditions, has been reported. Satellite photos show that wave-cloud phenomena are common, though evanescent, involve geographically small areas, and often in weather traditionally not considered "soarable."

This paper reviews such wave conditions, and reports flight results. A flight program was devised, from which a single flight was feasible, with interesting data that shows vertical movement to extend several hundred meters below cloud base.

Keywords: gravity wave, flat terrain, undular bore, cloud streets, thermal wave

Introduction

The research question concerns the conditions in which unusual soarable wave conditions may exist.

Atmospheric wave is everywhere; but not all wave is soarable. There is more wave that is generally realized, in conditions that seem poor for soaring, different from typical thermal soaring or mountain wave soaring.

Simplistically, the atmosphere is a stack of vast leaves of air moving across each other that differ in density (temperature, humidity), lapse rate, and/or velocity (speed or direction). These atmospheric leaves are relatively homogeneous; within them flow is generally laminar, and thus they have wide boundaries at which they interface.

Fluid flow is normally laminar unless disturbed. Soaring takes advantage of non-laminar flow. Consider water waves as analogous. A pond may be mirror smooth; then, a puff of breeze ripples the surface. The resulting wavelets have small breadth, short wavelength, and minimal height. They are not lined in rows. Consider flowing water: if it flows over a fixed irregularity, a standing wave is formed. Wave formed by wind moves with the flow.

Atmospheric wave is three-dimensional because of vertical displacement.

Where there's difference across a boundary, and relative motion, there is undulant wave. When atmospheric moisture saturation permits condensation, linear cloud forms of several types may develop.

There are several different forms of lined-up cloud.

- We are all familiar with thermal streets, in which clouds align with the wind in the boundary layer.
- Less well known is convective wave, in which lift aligns above cloud base across the cloud face, as above a mountain or hill.
- Sometimes thermal streets interact with sheer above, creating a checkerboard appearance on satellite photos.
- Sometimes clouds are lined up in rows due to roll convection, in which the lift is not connected to a ground source and the sky may be completely overcast.

Not all atmospheric wave forms undulations or rolls. Some weather phenomena are analogous to water waves, in which energy is propagated across the air-water interface independent of any horizontal movement of the water. For example, frontal thunderstorm development occurs ahead of evolving storms, as unstable conditions propagate through the atmosphere, and dissipate behind, so that the "radar echo speed" of the storm exceeds the air mass speed in which the storm is embedded. Thus a squall line represents a wave phenomenon without having an undular appearance. This research, is, however, focused on conditions that generate recognizable – and predictable – gravity wave where there are no orographic features to trigger or stabilize it. This may involve any of several types of atmospheric periodicity:

·0 Stable: no wave; laminar flow, eddies damp out.

·1 Shear wave: periodicity due to difference of wind velocity (speed, direction) across a boundary (of density, humidity, temperature, velocity)

·2 Thermal wave (streeting). This is strongly affected by wind velocity and atmospheric instability.

·3 Convection wave involves periodicity enhanced by thermal penetration from lower layer to upper. This is strongly affected by instability of lower and stability of upper layer.

·4 Convective roll. This is less appreciated by most soaring pilots because it occurs in conditions that are less easily predicted, that are less comfortable for pilots (stronger surface winds in particular), and that may be difficult to reach without self-sustaining motors. This is commonly seen on visible satellite photos in the overcast cloud disc behind cold fronts. The most famous convective roll is the Australian Morning Glory. Convective roll development requires vertical windspeed shear with little direction change.

·5 Boundary wave is waviness at the interface between atmospheric layers with velocity shear across the boundary. Horizontal shear with little difference in wind speed appears to produce lovely thin wavy clouds. This phenomenon is readily experienced in an airplane by flying just at the top of the haze layer. In this case, gentle pitch undulations, of about .10-.30 Hz at small-aircraft speed, may persist for many kilometers.

Authors have speculated that roll convection must be triggered by some vertical displacement: I propose that boundary wave, for example at the top of the haze layer, or at the condensation level, is sufficient. Convective roll must be triggered differently from the mechanisms causing thermal wave (in which thermals condense and penetrate the sheared layer above) because its phenomenology is completely different.

When satellite visible-light photos are studied, the cloud patterns near a low-pressure center often can be seen to contain, in different regions, patterns characteristic of all these types of atmospheric wave. A recent example:

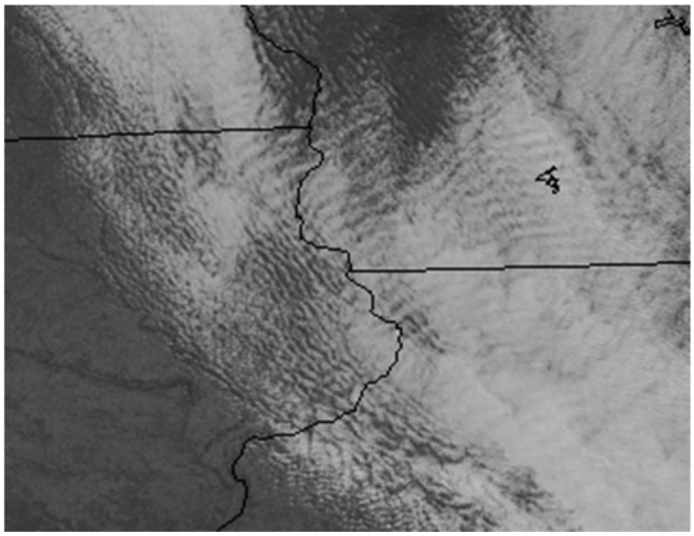

Figure 1 Cloud bands above Wisconsin, USA.

The broad cloud bands in this satellite photo above southwestern Wisconsin, USA, 19 November, 2016, 1300 UTC, the day following cold-front passage, are orthogonal to the gradient wind and represent convective roll. The narrower bands over eastern Iowa are thermal streets, aligned with the wind. 2-meter winds in this area were 15-25 kt with progressive speed shear to over 100 kt in the upper flight levels.

These conditions are typical after spring and fall cold-front passage over the flat terrain of the northern plains; one only needs to look at the southwest quadrant of low-pressure systems to find these patterns. Usability for soaring is mitigated by the strong winds involved and the difficulty predicting just where that quadrant will be located on any particular day.

They are sometimes a cause of annoying low-level turbulence to airline travelers.

In any case, the questions for the soaring pilot are whether this can be reached; whether it will endure long enough for flight; and whether the vertical velocities involved are enough to sustain flight. I propose that these conditions pertain more often than we expect, and that launching in windy overcast conditions and taking a high climb or tow, will sometimes turn out to be very interesting.

Thermal wave

Thermal activity creates vertical motion that in moderate wind velocities gathers thermals into rows-streeting, itself a complex wave phenomenon.

The base of cumulus clouds forms at the top of the haze layer. It was shown by Kuettner in 1957 and others, that the air lifted above cloud base preserves the velocity (speed, direction) it had in the boundary layer.

- If the wind above the boundary layer has a different speed, the cumulus presents a (malleable) boundary as a hill.
- If the wind in the boundary layer creates streeting, rows of cumulus act as ridges.
- If the wind above the boundary layer is approximately orthogonal to the wind below, this streeting will be augmented and thermal wave will be amplified. The challenge for soaring is that the required wind speeds are more than about 15 kt, a high-performance glider is preferred. Another challenge is that these conditions are rare.

Roll wave

If one studies post-frontal overcast, areas of wave are often seen. Sometimes there is no discontinuity; sometimes there are small clear breaks between long rolls. Typically, this is seen best far behind the cold front near the edge of the overdevelopment disc, where the roll clouds gradually fade, but presumably the rotor continues invisibly unless its mechanism requires the boost on the back side of the rotor that condensation would give.

If the wind above the boundary layer is approximately in line with the wind below, with a velocity difference that favors wave at the interface, streeting will be entrained by the wave and satellite photos may show a "checkerboard" cumulus array.

It is difficult to differentiate thermal wave from mountain lee wave when cumulus are being formed only a couple of hundred miles downwind from the range. In addition, lee wave would obviously augment thermal wave in ideal conditions.

A special situation that does not depend on actinic heating of the ground is the undular bore. This is a long, sausage-shaped, curved cloud that is most famous as the Australian Morning Glory. This situation requires vertical velocity shear of about 2 kt per thousand feet or 3m/s per km altitude. Visible cloud also requires suitable dew point conditions so that the lifted air cools below its dew point in the upward-flowing part of the rotor, accelerating upward movement.

Methodology

When waviness was observed in an overcast sky, and when work could be set aside, the airplane was launched: a Mooney 231 aircraft in which was mounted a GPS flight recorder. A stable climb was established at 2.5 M/S, 500 ft/min, into the gradient wind, to the base of the overcast. A 180-degree turn was then made, and the airplane flown near cloud base that had an undulating appearance, then turned crosswind. The flight trace was downloaded to See-You flight analysis software and climb rates shown graphically.

Figure 2: Clouds, ENE view

Results

On 13 March, 2016, wave conditions could be seen throughout the morning in the base of the overcast. Lift was encountered about 300 meters/1000 feet agl; and continued until near cloudbase at about 1500 meters/ 4800 feet agl – the depth of the roll convection was thus about 1200 meters/ 4000 feet, beginning just about at the usual launch altitude

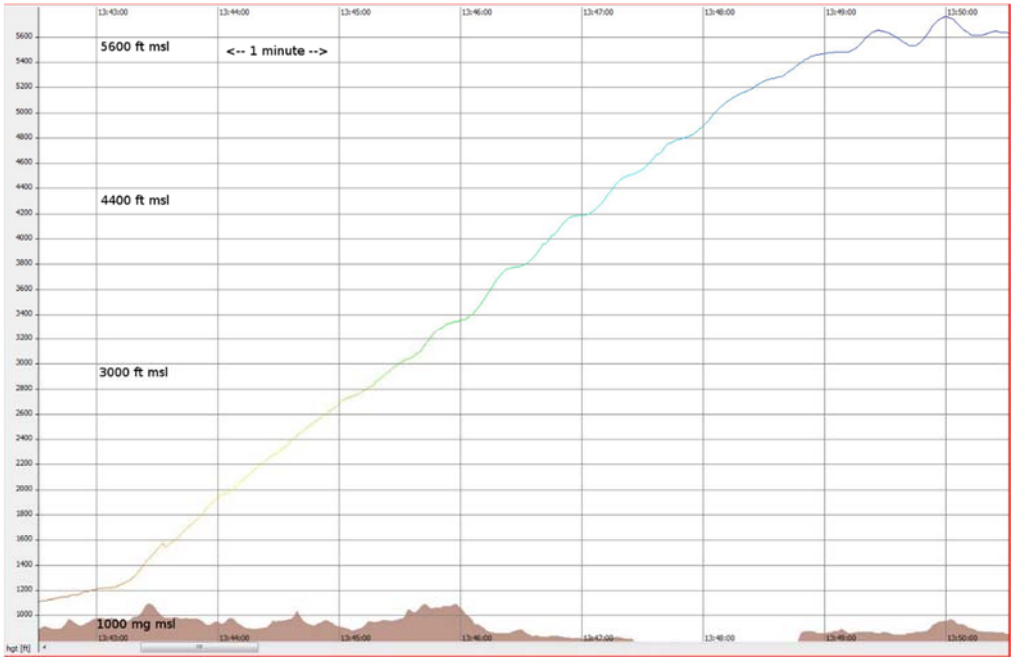

Figure 3: Climb profile

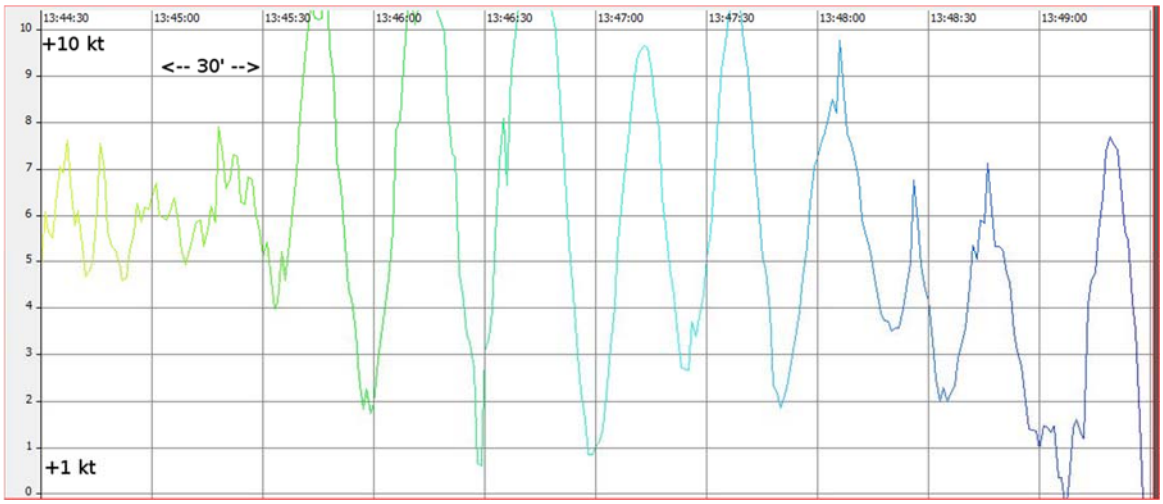

Figure 4: Vertical velocity during climb from ground to cloud base

The periodicity is short, about 30 seconds, related to the speed of the aircraft, about 100 knots. The aircraft's set climb rate of 500 ft/min (5 knots) means that the vertical air movement varied from -4 to +6 knots – very usable for soaring. (It was not possible to explore the lateral extent of this wave.)

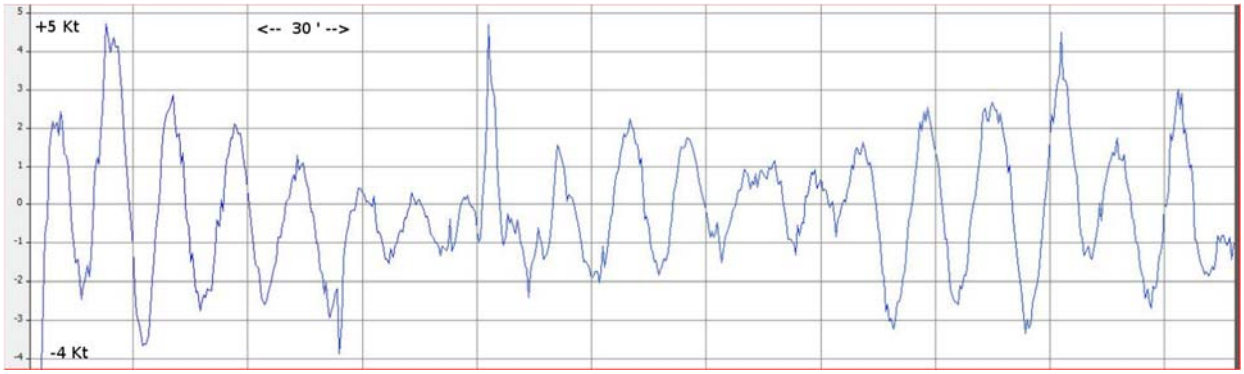

Figure 5: During level flight near cloud base, vertical velocities were similar: -2 to -3 kt to +2 to +4 kt.

Research flights that include cloud penetration has not yet been possible.

Conclusions

Organized lift of usable strength was encountered from a conveniently low altitude above ground to (and surely into) cloud. This lift extended across a wide local area, and the cloud base waviness persisted for several hours.

Additional flights that penetrate cloud and that explore the horizontal extent of this convective roll would be interesting. We already know from studying satellite photos that this lift is regional, and therefore will be more engrossing to pilots who want to extend their local and regional soaring-weather choices than to those wanting to set distance records by zipping back and forth over mountains. Still, oxygen masks or pressure suits won't be needed.

References

Kuettner, J. P., P. A. Hildebrand, T. L. Clark, 1987: Convection waves: observations of gravity wave systems over convectively active boundary layers. Quarterly Journal of the Royal Meteorological Society, 113, 445-467.

Bohme, T., Lane, T. P., Hallc, W. D. and Haufa,T., 2007: Gravity waves above a convective boundary layer: A comparison between wind-profiler observations and numerical simulations. Q. J. R. Meteorol. Soc. 133: 1041–1055.

Comparison of Field Measurements and MODIS Albedo Data and Its Effect on Latent Heat Flux

Serhan Yeşilköy[1,2], Nilcan Akataş[2], Levent Şaylan[2], Fatih Bakanoğulları[1], Zafer Aslan[3]
[1] *Istanbul Technical University, Faculty of Aeronautics and Astronautics, Department of Meteorological Engineering, Istanbul/Turkey, yesilkoy@itu.edu.tr, akatas@itu.edu.tr, saylan@itu.edu.tr*
[2] *Atatürk Soil Water and Agricultural Meteorology Research Institute Directorate, Kırklareli/Turkey, serhan.yesilkoy@tarim.gov.tr, fatih.bakanogullari@tarim.gov.tr*
[3] *Istanbul Aydın University, Faculty of Engineering, Istanbul/Turkey, zaferaslan@aydin.edu.tr*

Abstract: Determination of albedo and latent heat flux (LE) over agricultural lands plays a crucial role to better investigation of sustainable agriculture and food security which are related to evapotranspiration. LE is related to net shortwave (R_{ns}) and net longwave radiations (R_{nl}) which depend on surface conditions like surface albedo and climate of a region. Albedo is the reflectivity of the surface. There are many different crops in agriculture ecosystem. Thus, surface energy balance components vary by vegetation surfaces. Net radiation (Rn) is the most important component of surface energy balance which is difference between R_{ns} and R_{nl}. These are calculated by commonly used equations and applied to the LE equation using meteorological stations' data located in cities. However, there are differences between urban areas and agricultural ecosystems. This situation causes to the calculation errors. In this research, it is aimed to investigate the changes between estimated and measured surface energy balance components which are estimated by MODIS and meteorological stations' data in the urban area and measurements from a rural area over winter wheat surface 2014-2015 growing season in Thrace Region located in the Northwestern part of Turkey, Kırklareli city.

***Keywords*:** Albedo, MODIS, Latent Heat Flux, Kırklareli/Turkey.

Introduction

Surface energy balance depends on the energy transfer between land and atmosphere and it has considerable importance on occurrence of atmospheric phenomena. Crop, climate and meteorological factors intertwined especially in agricultural fields. Events which have occurred within the atmosphere are uncontrollable mechanisms. Albedo is not only an important component of these mechanisms but also a significant factor for energy balance. For many years, development of methods and technologies for the aim of determining albedo has been one of the focus points of researchers. In order to determine the albedo which occurs in plant surfaces, in other words reference LE, one of the most widely used methods in the world is "Penman-Monteith" equality. As a component of this equation, net radiation (Rn) is the most significant variable that controls the LE.[1,2]

The aim of this study is to investigate albedo difference from the satellite and in-situ measurements. Albedo is an important parameter that affects R_{ns}, R_{nl}, Rn and LE. In this context, within the framework of General Directorate of Agricultural Research and Policies (TAGEM) project, measurements of 2014-2015 growing period of winter wheat crops in Atatürk Soil Water and Agricultural Meteorology Research Station Directorate located in Kırklareli, Turkey were used. Also, MODIS albedo product time series are provided for the same growing period. Measured and calculated albedo, R_{ns}, R_{nl}, Rn were compared. In addition, effects of calculated and measured radiation values on LE were examined.

Data and Method

MODIS albedo data is downloaded for the case study area that is located northwestern part of Turkey. MODIS albedo data resolution is 500m x 500m area that is covers 250 acres. Figure 1 shows the MODIS data providing tool. Calculated albedo can be selected in MODIS land products for selected area. Date selection is applied between 17th of November and 26th of June, which covers in-situ measurements.

Moreover, root mean square error (RMSE), mean bias error (MBE), mean absolute error (MAE), relative error (RE) are evaluated for performance estimations of R_{ns}, R_{nl}, R_n, LE.

Results

Figure 1 shows the time series of MODIS and measurements albedo values. Both time series have the same pattern but close to the harvest date there is a difference between them (Figure 1). Scatter plot between satellite and measurements is shown on the right side. Determination coefficient is 0.61 (Figure 2).

Latent heat flux, also called evapotranspiration, time series is shown in Figure 13 for growing season of winter wheat. Both time series are closed each other and have the same pattern. Calculated LE is representative to measured LE and determination coefficient is 0.92 (Figure 3). Average calculated and measured LE is 21.39 and 23.73 W/m2, respectively.

Conclusions

Albedo data from MODIS satellite were compared in-situ measurements. MODIS albedo data and measurements have the same pattern but there are differences about 0.10. Net longwave, net shortwave, net radiation, and latent heat flux were calculated by using Turkish Meteorological Service (TSMS) meteorological data and MODIS albedo data. Also, they compared in-situ measurements over winter wheat canopy surface. Calculated fluxes from MODIS and TSMS data were underestimated than measurements except net longwave radiation. Determination coefficient MODIS and measurements albedo is 0.61. Error analysis between measurements and estimated R_{nl}, R_{ns}, R_n, and LE is shown in Table 1.

References

[1]Kabenge, I., Irmak, S., Meyer, G. E., Gilley, J. E., Knezevic, S., Arkebauer, T. J.,Woodward, D., Moravek, M., 2013: Evapotranspiration and surface energy balance of a common reed-dominated riparian system in the Platte River Basin, Central Nebraska. Transactions of the ASABE, 56(1), 135-153.

[2]Wever, L. A., Flanagan, L. B., Carlson, P. J., 2002: Seasonal and inter-annual variation in evapotranspiration, energy balance and surface conductance in a northern temperate grassland. Agricultural and Forest Meteorology, 112(1), 31-49.

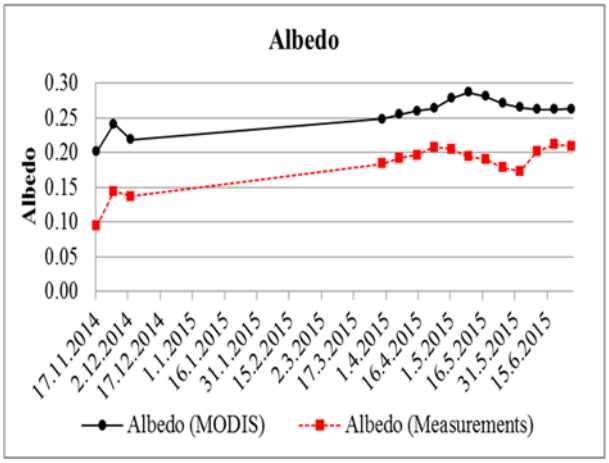

Figure 1. MODIS and Measurements of Albedo Time Series.

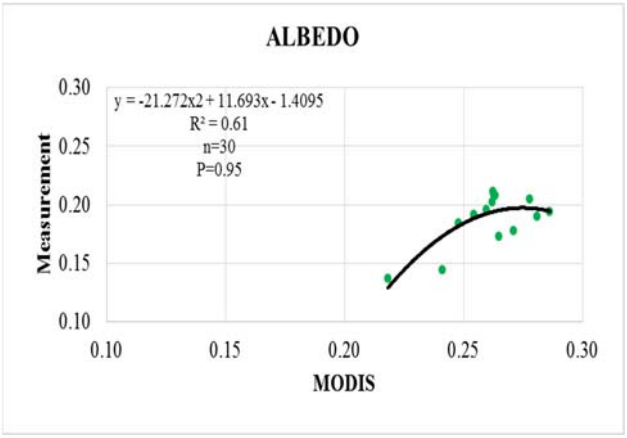

Figure 2. Comparison of MODIS and Measurements of Albedo.

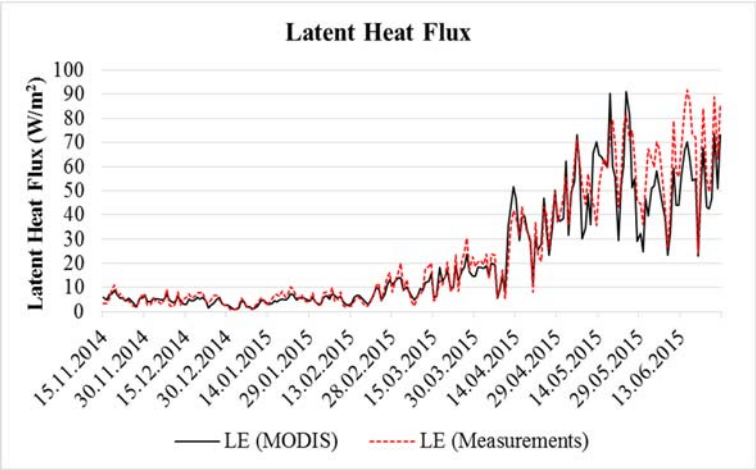

Figure 3. Latent Heat Flux Time Series for Winter Wheat Growing Season.

Atmospheric Convection and Sea Surface Temperature

İpek Osanmaz[1]
[1]*Istanbul Technical University, Maslak, Istanbul, Turkey*
osanmaz16@itu.edu.tr

Abstract: Over the past 60 years, both average daily precipitation intensity and extreme precipitation have increased in many regions.[1] Over the Black Sea and Marmara region, the potential for extreme spring convective precipitation has grown alongside substantial sea surface temperature increase.[2] A typical convective event experienced in that region was the 25th,26th,27th April 2016 precipitation extreme near the Marmara Sea and Black sea town of Istanbul. Here I study the effect of sea surface temperature (SST) increase on convective extremes within the region, taking the Istanbul event as a showcase example. The enhancement of lower tropospheric instability due to the current warmer Black Sea and Marmara Sea allows convection to be triggered. The research I identify indicates that Black Sea and Marmara Sea coastal regions may face convective precipitation under continued SST increase.

Keywords: Sea surface temperature, convection, precipitation extremes

Introduction

The relationship between sea surface temperature (SST) and large-scale convection has been studied in a variety of context during the 1960s and 1970s. Studying data from global tropics, Waliser *et al.*(1993) found that the characteristic of the relationship between SST and deep convection is such that at temperatures between 26 and 29°C, convection increases with increasing SST, but above 29°C, the intensity of convection observed tend to decrease with increasing SST.[3] He, however, has no explanation for the decrease in convection above SST of 29° as observed by Waliser *et al.* (1993). In my article, I have tried to understand the SST-convection relation by studying a typical spring days with thunderstorms, hailstone and rain of the Istanbul.

I carry out convection-permitting atmospheric model and show the crucial role of SST increase in the event. The enhancement of lower tropospheric instability due to the current warmer Black Sea and Marmara Sea allows convection to be triggered, increasing precipitation. Precipitation response to incremental SST increase suggests that the Black Sea and Marmara Sea has exceeded a regional threshold for the intensification of convective extremes.

I have summarized in introduction most of the observational studies available to date on the relation between SST and convection in the Black sea and Marmara region. In section 2, the data used in this study are described. Our observational studies on the relation among SST, surface wind and divergence (and also vertical velocity at 500hPa) and convection in the atmosphere on monthly and daily scales are given section 3. Comments gives a discussion of the various aspects of SST-convection relations found in observations.

Methodology

The NOAA 1/4° daily Optimum Interpolation Sea Surface Temperature (or daily OISST) is an analysis constructed by combining observations from different platforms (satellites, ships, buoys) on a regular global grid. A spatially complete SST map is produced by interpolating to fill in gaps. The *in situ* SSTs need to be checked for outliers, and then averaged onto the 1/4° grid, separately for ships and buoys.[4]

The Weather Research and Forecasting (WRF) Model is a next-generation mesoscale numerical weather prediction system designed for both atmospheric research and operational forecasting needs. WRF can generate atmospheric simulations using real data (observations, analyses) or idealized conditions.[5]

The Global Forecast System (GFS) is a global numerical weather prediction system containing a global computer model and variational analysis run by the United States' National Weather Service (NWS). The mathematical model is run four times a day, and produces forecasts for up to 16 days in advance, but with decreased spatial resolution after 10 days. [6]

Case Study: There are two basic precipitation generation types which are dynamic precipitation and convective precipitation.[7,8] Dynamic precipitation is also known as stratiform precipitation. Dynamic precipitation results from a forced lifting of air. Convective precipitation is also known as thermodynamic precipitation. While dynamic precipitation only needs saturated air and lift, convective precipitation requires an additional component called instability. Uplift due to instability release occurs when the air rises on its own after being lifting to a certain point in the troposphere. Instability is commonly assessed by examining the Lifted Index (LI) and CAPE (Convective Available Potential Energy). Both these indices can be used to assess the acceleration rate of air once air from the lower troposphere is brought to a level in the troposphere where it will rise on its own due to positive buoyancy. Instability causes the air to rise much faster than it would by forced lifting alone. The aim of this study is (1) To determine meteorological conditions supporting precipitation extreme, (2) To use OISST Optimum

Interpolation Sea Surface Temperature, WRF model, GFS model to track upper air activities and SSTs and finally (3) to find the interaction between sea surface temperature and atmospheric convection.

Results

The spring precipitation extreme of Istanbul, Turkey took place on April 26th and 27th 2016 with sudden hailstone, heavy rain and lightning. This case study analyses spring precipitation extreme of Istanbul, Turkey on April 26th, 2016 00 GMT, April 26th, 2016 12 GMT, April 27th, 2016 00 GMT.

Conclusion

It has moist, conditionally unstable layer with relative humidities >60% from the surface up to 7 km. The rainfall rate at a particular point is proportional to the magnitude of the upward, vertical moisture flux. This means rising air should have substantial water vapor content, and the ascent rate should be large. The atmosphere must be conditionally unstable, and there must be a mechanism by which the warm, moist air will rise to its level of free convection. Detection of convective activities in microscale requires specific radiosonde measurements. Between two regular measurements it is so much likely to miss out valuable convective pattern. There is no significant relationship SST and convection in İstanbul. Statistics show that there is a low negative correlation (Fig.1). However, especially in spring, negative temperature anomalies due to synoptic environment on relatively warm sea surface can result convective activities triggered. Sea surface temperature can vary on micro scale widely in Istanbul. There is a meaningful variation from Black sea to southern Marmara Sea locally. So it is so much likely to initiate local convective activities near sea surface more than land areas in suitable atmospheric conditions.

References

[1]Edmund P. Meredith, Vladimir A. Semenov, Douglas Maraun, Wonsun Park, Alexander V. Chernokulsky, 2015: Crucial role of Black Sea warming in amplifying the 2012 Krymsk precipitation extreme, Nature Geoscience, 8, 615-619.
[2] MGM, 2016 Türkiye çevresindeki denizlerin su sıcaklıkları parametresinin istatiksel analizi raporu (1970-2015).
[3]Waliser DE, Graham, Gautier C., 1993: Comparison of the highly reflective cloud and outgoing longwave data sets for use in estimating tropical deep convection. Journal of Climate 6: 331-353.
[4]https://www.ncdc.noaa.gov/oisst
[5]http://wrf-model.org/index.php
[6]https://en.wikipedia.org/wiki/Global_Forecast_System
[7]http://www.mgm.gov.tr/deniz/marinatahmin.aspx?m=17907#sfB
[8]http://www.theweatherprediction.com/habyhints/106/

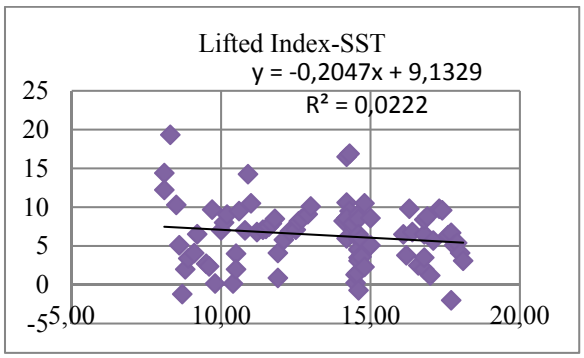

Figure 1. Lifted Index-SST Relationship

Climate Change, Aviation and Gliding

Ahmet Tokgözlü[1], Kadir Temurçin[1], Kamile Yasdiman Uysal[2]

[1] *Süleyman Demirel University, Department Of Geography Isparta / Turkey*
tokgozlu68@gmail.com, kadirtemurcin@sdu.edu.tr
[2]*THK. İnönü-Eskişehir/ Turkey, kamileyasdiman@gmail.com*

Abstract: According to the Intergovernmental Panel on Climate Change (IPCC), climate change refers to any change in climate over time, whether due to natural variability, or as a result of human activity. Global climate change is caused by the accumulation of greenhouse gases (GHG) in the lower atmosphere. The Greenhouse Gas of most concern is carbon dioxide (CO_2). Although aviation is a relatively small industry, it has large impact on the climate system. ICAO's initial estimate is that the total volume of aviation CO_2 emissions in 2006 (both domestic and international) is in the range of 600 million tons. At present, aviation accounts for about 2% of total global CO_2 emissions and about 12% of the CO_2 emissions from all transportation sources. Gliding is also a part of sportive aviation. It is such a clean and pleasing sport. But in recent years motorized gliding activities began to increase. So the fuel of moto-gliders creates air pollution and carbon emission. When the fuel is burned, the carbon in the fuel released and bonds with oxygen in the air to form carbon dioxide. So it increases the accumulation of carbon dioxide at lower atmosphere. Obviously, the easiest way to reduce CO_2 emissions from aviation is to reduce the amount of flights. For that, people can choice to fly with airlines with lower CO_2 performance figures. In gliding, glider pilots should fly with non-motorized gliders or can use the engine only in necessary situations. As a result, we have just one world and urgently need for an environmentally sustainable aviation policy.

Keywords: Aviation, Climate Change, Gliding, Global Warming

Introduction

Human activities release greenhouse gases into the atmosphere. The atmospheric concentrations of carbon dioxide, methane, chlorofluorocarbons and tropospheric ozone have all increased over the past century.[1-3] These rising levels of greenhouse gases are expected to cause climate change. By absorbing infrared radiation, these gases change the natural flow of energy through the climate system. The climate must somehow adjust to this "thickening blanket" of greenhouse gases to maintain the balance between energy arriving from the sun and energy escaping back into space. This relatively simple picture is complicated by increased amounts of surface aerosol from human activities that modulate incoming solar radiation and rend to cause a cooling effect on climate, at least on regional and hemispheric scales.

Methodology

Aviation is an integral part of the infrastructure of today's society. It plays an important role in a global economy; it supports both commerce (through business travel and air freight) and private travel. Aviation also plays an important role in military activity. As such, aviation effects the lives of citizens in every country in the world, regardless of whether they fly. The activities of the civil air transport industry have long been circumscribed by matters of public interest in addition to economic factors. Of most importance historically are matters related to safety and environmental issues associated with local noise and air pollution. Two global environmental issues have emerged for which aviation may have potentially important consequences: Climate change, including changes to weather patterns (i.e., rainfall, temperature, etc.), and for supersonic aircraft, stratospheric ozone depletion and the resultant increase in UV-B radiation at the Earth surface. Although, aviation is relatively small industry, it has a disproportionately lager impact on the climate system. It accounts for four to nine per cent of the total climate change impact of human activity.

Results

According to the Intergovernmental Panel on Climate Change (IPCC), climate change refers to any change in climate over time, whether due to natural variability, or as a result of human activity. Global climate change is caused by the accumulation of greenhouse gases (GHG) in the lower atmosphere. The Greenhouse Gas of most concern is carbon dioxide (CO_2). Although aviation is a relatively small industry, it has large impact on the climate system. ICAO's initial estimate is that the total volume of aviation CO_2 emissions in 2006 (both domestic and international) is in the range of 600 million tons. At present, aviation accounts for about 2% of total global CO_2 emissions and about 12% of the CO_2 emissions from all transportation sources.[1-3]

If we are talking about aviation, we should also think about sportive aviation. In recent years, gliding is one of the most important sportive aviation.[5-6] Actually, gliding is a non-powered aircraft but in the following years added motors on them with the development of technology and a new model emerged: motorized gliders. Their fuels are

generally two types: 95 octanes unleaded fuel and 110 octane avgas, so it's the same with an aircraft. When the fuel is burned, the carbon in the fuel released and bonds with oxygen (0_2) in the air to form carbon dioxide (CO_2). Burning the fuel also release water vapor, nitrous oxides, sulfate and soot. As a conclusion, we can say that motorized gliders also pollute the air.

Conclusions

What can we do?
- We can choose to fly less frequently whether for business or pleasure,
- We can consider taking a train as an alternative to domestic or short hop flights,
- We can investigate teleconferencing as an alternative to business flights,
- We can use motorized gliders to take altitude then stop the engine and find thermals. It'll be more cheap and environmental friendly.

References

[1]ICAO Environmental Report, 2007: ***http://www.icao.int/env/pubs/env_report_07.pdf***
[2]IPCC, Climate Change, 2007: The Physical Science Basis, Cambridge Univ. Press, Cambridge, UK.
[3]IPCC, 1999: Aviation and the Global Atmosphere, Cambridge Univ. Press, Cambridge, UK.
[4] Aviation Environment Federation, ***http://www.aef.org.uk/issues/climate/***
[5]David Suzuki Foundation, ***http://www.davidsuzuki.org/issues/climate-change/science/climate-change-basics/air-travel-and-climate-change/***
[6] *International Civil Aviation Organization, Air Transport Bureau (ATB), 2008:*Aircraft Engine Emissions, Retrieved 2008-03-19.

High Evapotranspiration and Humidity on the Aviation and Soaring

Funda Dökmen[1], Zafer Aslan[2]
[1]*Kocaeli University, Vocational School of Food & Agricultural School, Campus of Arslanbey, 41285 Arslanbey-Kartepe, Kocaeli-Turkey*
f_dokmen@hotmail.com & funda.dokmen@kocaeli.edu.tr
[2]*Istanbul Aydın University, Faculty of Engineering, Department of Computer, 34590 Istanbul-Turkey, zaferaslan@aydin.edu.tr*

Abstract: Evapotranspiration (ET) is the sum of evaporation and plant transpiration from the Earth's land and ocean surface to the atmosphere. Evaporation accounts for the movement of water to the air from sources such as the soil, canopy interception, and waterbodies. Factors that affect evapotranspiration include the plant's growth stage or level of maturity, percentage of soil cover, solar radiation, humidity, temperature, and wind. Isotope measurements indicate transpiration is the larger component of evapotranspiration. Where the evaporating surface is the soil surface, the degree of shading of the crop canopy and the amount of water available water content at the evaporating surface are other factors that affect the evaporation processes. Frequent rains, irrigation and water transported upwards in a soil from a shallow water table wet the soil surface. Turkey is among the countries at risk group in terms of the potential effects of high evapotranspiration and also humidity depends on climatic conditions. Generally, the most important changes observed increases in summer temperatures in Turkey. Summer temperatures often, on Turkey's Mediterranean and Southeast Anatolia regions are increasing in the last 50 years. This paper presents a study of the high evapotranspiration (ET) and humidity variation at agricultural regions. And also, all of these were discussed by their role on aviation and soaring over all on the long years of climate data.

***Keywords*:** Aviation, drought, global warming, out-landing, water management.

Introduction

Evapotranspiration as a major component of the water balance has been identified as a key factor in hydrological modeling and a wealth of methods have been developed for its calculation.[1-2] In general; the term potential evaporation and potential evapotranspiration are to be differentiated. The first one is a measure for the atmospheric demand, which is solely meteorologically driven under the assumption of unlimited water supply. Especially for irrigation scheduling, this definition was further specified to refer to a reference surface consisting of a hypothetical grass with specific characteristics, termed reference crop evapotarnspiration.[3-4] Turkey is located in a semi-arid region, where the average annual rainfall is 643 mm. The significant differences between regions that are observed worldwide in terms of the amount and distribution of precipitation have also been observed in our country. Some regions record up to 3000 mm rainfall, while others do not exceed 250 mm. In Southeastern Turkey, the annual rainfall is generally less than 350-400 mm and occurs mostly in disordered, unpredictable storms. Therefore, especially during periods of crop cultivation, plants do not provide enough water for their vegetal grow in terms of the desired amount of water. As a direct cause of global warming, forest fires, drought and desertification, and ecological degradation, will affect our water resources in particular, as well as our other natural resources.

Methodology

Potential evaporation or **potential evapotranspiration (PET)** is defined as the amount of evaporation that would occur if a sufficient water source were available. If the actual evapotranspiration is considered the net result of atmospheric demand for moisture from a surface and the ability of the surface to supply moisture, then PET is a measure of the demand side. Surface and air temperatures, insulation, and wind all affect this. A dryland is a place where annual potential evaporation exceeds annual precipitation.

Thornthwaite equation (1948),[5]

$$PET = 1.6\left(\frac{L}{12}\right)\left(\frac{N}{30}\right)\left(\frac{10T_a}{I}\right)^{a} \quad (1)$$

Where

PET is the estimated potential evaporation (mm/month)
T_a is the average daily temperature (degrees Celsius; if this is negative, use 0) of the month being calculated
N is the number of days in the month being calculated
L is the average day length (hours) of the month being calculated

$$\alpha = (6.75 \times 10^{-7})I^3 - (7.71 \times 10^{-5})I^2 + (1.792 \times 10^{-2})I + 0.49239 \quad (2)$$

$$I = \sum_{i=1}^{12} \left(\frac{T_{ai}}{5}\right)^{1.514} \quad (3)$$

is a heat index which depends on the 12 monthly mean temperatures T_{ai}.[5]

Somewhat modified forms of this equation appear in later publications (1955 and 1957) by Thornthwaite and Mather.[6]

Results

We can collect results on the below points as summary:

- Surface temperature shows increasing in Southeastern Anatolia Region of Turkey.
- Time variation of evapotranspiration level temperature shows increasing depend on agricultural cultivation and management of irrigation in Southeastern Anatolia Region of Turkey.
- Equivalent potential temperature increases depend on climate changes in agricultural area.
- Using of modern irrigation methods should support for agricultural areas.
-Main open irrigation channels should be converted to closed channels in a short time due to high evaporation.
- Furrow irrigation (wild irrigation) must not use for agricultural region and also cultivation due to high evapotranspiration.
- Using of drip irrigation and subsoil irrigation systems proper to agricultural activities.
-Selection is governed by season of the year, crop, and farming techniques.
-Color and texture best determine suitability. It may help to have an order of preference during field selection.
- Avoid fields with high crops, such as rape, sunflowers and root crops. These are usually either bright or dark colored.

Conclusion

The type of vegetative cover is not as important in the evapotranspiration process as is solar radiation if the vegetative cover is dense and sufficient soil moisture is available.[7] The reflective characteristics of the land surface also have an effect on the magnitude of evapotranspiration. The average annual evapotranspiration for irrigated lands varies is dependent on the grass or crop type, quantity of water applied, and length of the growing season. Evaporation is one of the main variables in the humidity budget equations which govern heat fluxes.

References

[1]Brutsaert, W., 1982: Evaporation into the atmosphere. Theory, History, and Applications, Kluwer Academic Publisher, Dordrecht, Boston, London.
[2]Jensen, M.E., Burman, R.D. and R.G. Allen, 1990: Evapotranspiration and irrigation water requirement, New York.
[3]Allen, R.G., Pereira, L.S., Raes, D., and M. Smith, 1998: Crop evapotranspiration, Guidelines for computing crop water requirements, FAO, Rome.
[4]Wright, J.l., 1981: Crop coefficients for estimates of daily crop evapotranspiration, irrigation scheduling for water and energy conservation in the 80's, Am. Soc. of Agric. Engrs. Dec.
[5]Thornthwaite, C.W., 1948: An approach toward a rational classification of climate," geographical review, Vol. 38, pp. 55-94.
[6]Thornthwaite, C.W., and J.R. Mather, 1957: Instructions and tables for computing potential evapotranspiration and the water balance: Center on, N.J., Laboratory of Climatology, Publication in Climatology, Vol. 10, no. 3, pp. 185-311.
[7]Kozlowski, T.T., 1964: Water metabolism in plants: New York, Harper and Row, Biological Monographs, p: 227.

The First Year in Argentina for the Perlan 2

Morgan Sandercock
Perlan Project, morgan@sandercock.com

Abstract: A report on the first year's operation of the Perlan 2 high-altitude glider

***Keywords*:** Polar Vortex, Stratosphere, Flutter

Introduction

The Perlan 2 glider took nine years to build. This paper will describe the results of the first year's operation from the first test flight to test flights in Minden Nevada and the expedition to El Calafate, Argentina.

The glider has not yet reached any significant new altitude, so there is no new data but the mission is still underway to explore the atmosphere, aerodynamics and inspire future generations of engineers and scientists.

Methodology

The unique features of this glider are (1) the airfoil section designed for high altitude, (2) the pressurized cabin and (3) in-flight flutter excitation and measurement. Supporting those features are the (a) carbon pre-preg construction, (b) custom rebreather oxygen system and (c) onboard data network and telemetry.

The Perlan 2 follows the success of the Perlan 1 glider, which achieved the current World Record altitude of 50,722 ft. (15,460 m). That flight proved that the Polar Vortex does produce significant vertical motions in the stratosphere. It also proved the impracticality of using pressure suits in a standard sailplane cockpit. The design of the Perlan 2 was intended to overcome the difficulties found by the Perlan 1 and achieve a higher altitude.

After the first test flight of the Perlan 2 in September 2015, there was a series of test flights conducted in Minden Nevada. During this time, the high altitude systems were installed and tested. Success for this phase of testing was defined as 2 hours duration above 25,000ft. This was achieved in June 2016.

The glider was then shipped to El Calafate, in southern Argentina. This is the site of the successful flight of the Perlan 1. The peak season for the southern Polar Vortex is August and September. Due to shipping delays and damage repairs, we were not able to fly on the 10th anniversary of the previous record flight, with our first flight in Argentina taking place on the 9th of September 2016.

This year's Polar Vortex seemed smaller than previous years. There were fewer occasions when the vortex core moved overhead El Calafate. On those occasions, the low-level wind was much less than required to initiate the mountain wave. One of the unknowns that we were testing was how often low-level cloud and rain would prevent the glider from launching or landing safely. This year there were very few days where visibility was a problem.

Without the right weather conditions to fly to extreme altitude, we were unable to test our systems any higher than the Minden test flights. However simply flying safely and legally in Argentina was a great step forwards to setting another record. We always expected (and budgeted) for several years' operations to set a new record.

Results

The maximum altitude achieved to date is 26,000ft (8,000m) and the maximum altitude achieved in Argentina was 23,000ft (7000m.)

Flutter data was taken in flight, transmitted to the ground and then analyzed by offsite engineers to return a flutter clearance to the glider while it was still flying.

The Minden testing identified deficiencies in moisture control inside the cabin, with windows fogging up and water dripping from the cabin roof. Cabin temperatures were relatively high, even with low outside temperatures.

Conclusions

The glider was shipped and flown safely, with no injuries to anyone. The local air traffic control was willing to work with us. The federal government was willing to work with us to give us the airspace. Everyone from the tow plane manufacturer to the local taxi drivers will be happy to see us again next year.

In-flight flutter measurement has been proven to be possible with a limited budget. The rebreathers and pressurization met expectations. Further work is required on cabin temperature and moisture control.

Figure 1. Perlan 2 glider soaring in Argentina

Table 1. Test Flight Log

Flight No.	Location	Date	Duration (h)	Altitude (ft)
1	Redmond, OR	23 Sept 2015	0.6	8,100
2	Minden, NV	15 Jan 2016	0.7	10,800
3	Minden, NV	15 Jan 2016	0.7	10,700
4				
5				
6				
7	Minden, NV	13 Feb 2016	0.6	10,700
8	Minden, NV	13 Feb 2016	0.6	9,500
9				
10				
11	Minden, NV	13 Apr 2016	0.8	11,400
12				
13	Minden, NV	7 May 2016	0.2	6,900
14	Minden, NV	11 May 2016	0.7	10,700
15				
16	Minden, NV	19 May 2016	1.1	24,200
17	Minden, NV	20 May 2016	2.1	20,800
18	Minden, NV	16 Jun 2016	3.7	26,200
19	El Calafate	9 Sept 2016	0.4	4,100
20	El Calafate	11 Sept 2016	0.7	6,700
21	El Calafate	13 Sept 2016	1.8	11,400
22	El Calafate	18 Sept 2016	2.2	14,600
23	El Calafate	21 Sept 2016	2.3	22,400
24	El Calafate	23 Sept 2016	3.0	12,200
25	El Calafate	25 Sept 2016	0.5	6,300
26	El Calafate	25 Sept 2016	1.6	11,400

Reference: Sandercock, 16 Jan 2016

Electric Propulsion in Gliders is more than an Alternative to Traditional Combustion Engines

Rainer Klein
Baden-Wuerttemberg Cooperative State University (DHBW),
rainer.klein@mosbach.dhbw.de

Abstract: The paper describes the development process of an electric propulsion system for gliders, serving as self-retriever (Turbo) for a double seater. The project goal was focused on improved environmental protection, improved inherent safety and easy handling, even under stress. Due to costs and related customer acceptance most of the required components should been proven and free available on the market.

***Keywords*:** elelctric propulsion, glider, safety, sailplane, lithium-ion battery

Introduction

Due to the fact, that more than 80% of actual fabricated and sold gliders have a motor (either self-launch or self-retrieve) the disadvantages and risks of this combustion propulsion becomes more and more evident in the accident statistics[1]. According to the BFU (the German equivalent to the American NTSB) between 2005 and 2012, nearly 30% of the reported accidents of motorized sailplanes with dead or injured persons are directly related to the failure of the propulsion. This evaluation leads to a special safety guideline for motorized gliders by the German BFU[1]. Without taking into account the propulsion failure that fortunately did not lead to accidents. An impressive summarization of failure experiences with combustion propulsion in gliders can be found in the presentation of Jean Marie Clement[2]. Most of the problems with the combustion propulsion are direct related to the permanent vibrations caused by the two stroke combustion engine. Rotary engines replace vibrations by thermal problems. Both propulsions require high attention, intensive checking and high maintenance and service costs.

The electric propulsion has the potential avoid all immanent disadvantages of combustion propulsion. The electric propulsion is well suited to the usage profile of a motorized glider, where the engine will be used only for a few minutes for take-off and optionally usage for self-retrieve. Additionally, it offers the chance to increase the safety by avoiding the immanent disadvantages of combustion propulsion such as:

- much less moving/no oscillating parts,
- nearly no vibration
- much lower mechanical complexity
- significant less mechanical wear, (only two bearings)
- due to much higher efficiency (>90%) lower thermal problems

Never the less, electric Propulsion has also some disadvantages. First and obviously the lower energy density compared to gasoline. This will be partly compensated by a much higher efficiency. Due to increasing energy density with time of R&D activities, this will become less significance. One other disadvantage is higher cost, mainly caused by the batteries.

Based on our experiences in other electric mobility projects at the mechatronic department, DHBW-Mosbach, we intend to increase the availability of gliders with electric propulsion systems. At the beginning of the project only the Antares by Lange Aviation was commercial available on the market. The Arcus electric has been under development in cooperation between Schempp Hirth and Lange Aviation, but we did not know that at this time. We contacted the well-known German producers of gliders and presented our project idea. At Alexander Schleicher und Michael Greiner, we found fertile soil and a competent well motivated partner. The consortium was completed by the University of Kassel and a producer and supplier of batteries. The whole project was funded by the German state of Hessen via Loewe Agency.

Methodology

Components and required specifications

- Brushless DC Motor
  - 25-30kW at 2500 rpm
  - air cooled
  - low weight/ low cross section
- Battery/BMS
  - Low weight max. 60kg
  - Max. capacity (range 100km), ~ 8kWh
  - Electric power 30 kW
  - 400V/92 A
  - no cooling required
  - BMS for cell-voltage and -temperature monitoring
  - CAN Bus
- Power Electronic
  - Power > 30kW
  - Low weight and volume
  - High efficiency
  - Air cooled
- Man Machine Interface (MMI)
  - CAN Bus
  - Serving as main controller for the whole System
  - Monitoring all relevant Parameters
    - Cell-Voltage, Cell-Temperature
    - State of Charge (SOC)
    - Power Setting
    - Switching high voltage contactor
  - Display relevant parameter
    - State of Charge (%)
    - Propeller Speed (rpm)
      - Current Motor Power (kW)
      - Temperature Power Electronic
      - Temperature Battery
      - Temperature Motor
      - Position of Propeller Tower

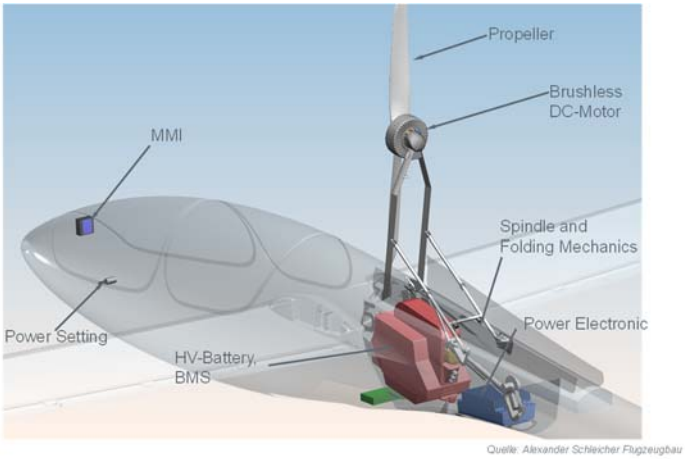

Fig. 1 Sketch of System Layout

Brushless DC Motor

Different motors, available on the market have been identified, evaluated and some tested on the test bench. Selection criteria were cost, power, weight, (power density) efficiency, thermal behaviour, cooling and outer dimension. Due to our experiences with the validity of technical data from data sheets, we made or own measurements with some selected motors. Only the EMRAX 228 fulfils all requirements. An overall (motor + power electronic) efficiency of > 90% could be measured.

Power Electronic

The power electronics / frequency converter converts the DC voltage provided by the battery into a three-phase alternating voltage, which is variable in frequency and amplitude, driving directly the BLDC motor. Motor status parameters (speed, angular position of the rotor, temperature) are feedback via rotary encoder and temperature sensor into the power electronic.

After market analysis and evaluation, a suited power electronic has been identified, but because it was only available in water-cooled version, and due to the heavy housing, it has been necessary to modify. The cooling has been changed to air-cooling and a new and lighter housing has been developed.

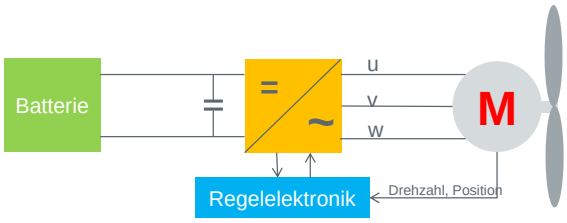

Fig. 2 Power electronic converts DC voltage into a three-phase alternating voltage

Battery

The weakest link in the chain is the energy supply, the battery. The Battery has to fulfil many contradictory requirements; it has to be lightweight, high energy density, high power density, long life time and low cost! Under these circumstances, it is obvious that all possible solutions are compromizes.

The most limiting factor is weight. 60kg for the whole energy storage, including battery cells, battery management system (BMS), contactors, fuse and housing. An additional limiting factor was available space within the fuselage. The Battery has to be placed near the center of gravity within the motor compartment. To reduce problems concerning electromagnetic compatibility by interference with other electronic components. The power lines between battery and power electronic (DC) and between power electronic and motor (AC) have to keep as short as possible.

Many different battery types are available, but due to the above-mentioned requirements, only lithium-ion batteries are suitable. Lithium-ion batteries differ in energy density, power density, cell-chemistry (LiFePO4) ,(LiCoO2), (LiNiO2), (LiMn2O4) ...., internal resistance, allowed temperature range, outer dimensions, shape, cost, availability,...

Fig.10 shows the most common different typical shapes of lithium-ion battery cells. They are either cylindrical, or prismatic, or pouch cells, all with different outer dimension, and different contacts.

Unfortunately, the most important parameters of a mobile energy storage, energy density and power density, behave oppositely

We decided to use cylindrical 18650 lithium ion cells. 18650 means a diameter of 18mm and lenght of 65mm they are well known as Laptop cells.

One further specification requirement, it should be possible to climb with maximum power until the battery is discharged down to the minimum allowed voltage level. Due to costs and reduced complexity of the battery we intend to fulfil this requirement without cooling of the battery. So only the heat capacity of the battery serve as a heat sink for the energy loss at the internal resistance of the battery.

With an adjustable external electronic load (max. 400A) we tested load induced temperature behavior of different cell configurations. We discharged a package 12p/1s with a constant load of 275W (representing 27,5kW for the complete battery) Fig.3 shows the increase of battery temperature with time. The maximum temperature remains below 54°C. The different colored infrared pictures show the measured temperature distribution on the surface of the cell package. It shows a homogenous temperature distribution without any hotspots. The battery has an allowed temperature range from -30°C to 60°C (discharge)

The battery management system (BMS) integrated in the battery housing, is an electronics, monitoring all cell-voltages and cell-temperatures of each parallel stack. The BMS is via CAN-Bus connected to the Man Machine Interface (MMI) representing the main controller for the whole System. In case of exceeding or falling below specified values for cell-voltage or temperature the MMI will produce a hierarchized cascade of optical and acoustic warnings for the pilot.

Due to safety aspects of the battery, we have to answer the question what could happen in a malfunction or accident. The maximum current thru battery, and phase current in motor and power electronic will be measured by sensors in the power electronics and monitored by the MMI. In case of exceeding maximum allowed currents, the power can be reduced or the main contactors could be switched off by the MMI. If both fails, a thermal, non-reversible, fuse in the internal power line of the battery disconnects the power line.

However, a short-circuit on cell level; will not be detected this way! Therefore, we have to answer the question: Could a short-circuit on cell level initiate a chain reaction, leading to thermal runaway of other cells or the whole battery? To answer this question, we made different “nail-tests”.

In a nail-test, a steel nail will be driven through a cell, producing an internal short-circuit and a thermal runaway with a lot of heat production. First, we made the nail-test with a single 18650 cell, with high energy density (Panasonic 18650PD) after the short-circuit, the internal overpressure fuse has disconnected the plus pole and opened the housing, to avoid explosion by venting the reaction gases.

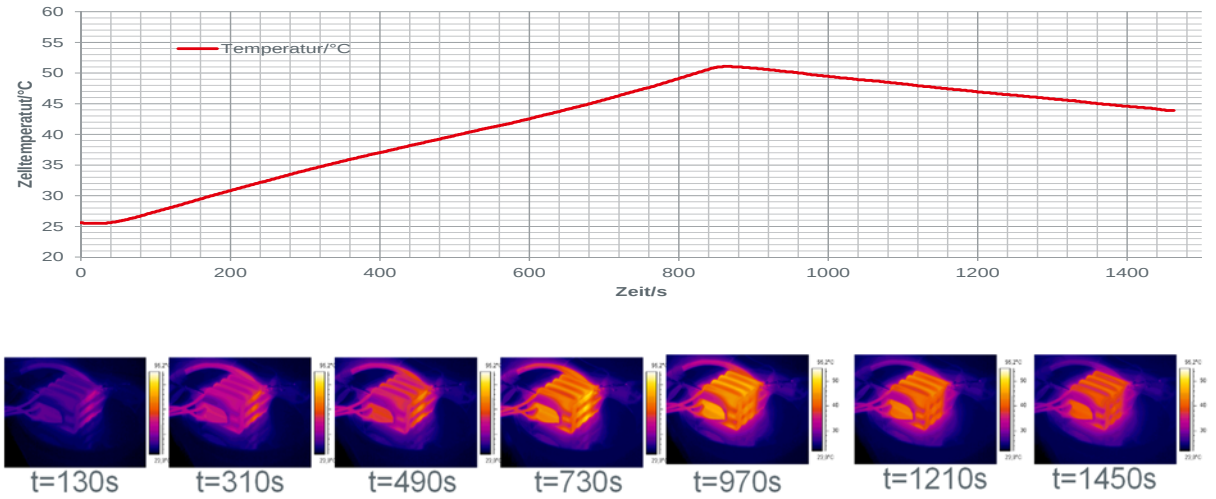

Fig.3 Temperature of cell package during discharge with maximum load

Fig.4 18650 cell packages after nail-tests

In further tests, we nailed a single cell within a cell package, where all cells electrically connected parallel and therefore each cell is in direct thermal contact to the neighbour cells. The nailed cell was in the centre of the package, surrounded by other cells. The same impressive reaction with much heat and flames. The temperature near the nailed cell had been measured with a thermocouple, indicating > 500°C. This tests have been made several times, at no time there was a chain reaction leading to thermal runaway or short-circuit of surrounding cells. The voltage level of the cell package after the test was nearly the same as before. Fig.4 shows different cell packages after nail test.

Man Machine Interface (MMI)

The Man Machine Interface (Fig.5) has been developed within the project it consists of a microcontroller-display unit, only one single control organ, single lever operation for power setting (throttle control) and moving out or retract the motor/propeller, and additional security switch to avoid maloperation. The electric motor is stopped by pulling the lever down. The MMI serves as user interface and main controller for the whole system. The MMI monitors and displays all relevant system parameters such as:

Results

The electric propulsion integrated in the new ASG32 EL was first presented at the Aero 2015 in Friedrichshafen, Germany. Maiden flight was 16 of June 2016. All expectations were fulfilled. “A runtime of 20 minutes under full power and a climb performance of 1,3m/s (256 ft/min) results in a range of 100km (62mi, 54nm) using the climb and glide method with two pilots on board” [5].

- Cell-Voltage, Cell-Temperature via BMS
- State of Charge (SOC)
- Power Setting (kW)
- Propeller/Motor Speed (rpm)
- Current Motor Power (kW)
- Temperature Power Electronic (°C)
- Temperature Battery (°C)
- Temperature Motor (°C)
- Position of Propeller Tower

Fig.5 Display of MMI and control organ (power Setting)[5]

Fig.6 Maiden flight of ASG32 EL[5]

Conclusions

An electric propulsion for gliders has been developed and realized. The electric propulsion offers many advantages compared to combustion propulsion.

- Much lower noise level in and outside of the cockpit
- No fumes or toxic gases caused by gasoline and exhaust gases
- Nearly no vibrations
- Much lower wearing
- Much higher life time
- No noticeable climb rate drop with increasing altitude
- Increased safety by single lever operation
- Less service and maintenance cost

References

1. BFU-Flugsicherheitsinformationen “Risiko Klapptriebwerk”,V177, Mai 2012 http://www.bfu-web.de/DE/Publikationen/Flugsicherheitsinformationen/Berichte/V177%20-%20Flugsicherheitsinfo%20-%20Klapptriebwerke%20ein%20Risiko.pdf?__blob=publicationFile

2. Jean Marie Clement “Problems in Engines for Self-Launching Gliders”, Sport Aviation Symposium, Milan, October 21-26, 2005 (download on http://www.streckenflug.at/download/motorprobleme.pdf).

3. http://www.enstroj.si/

4 http://www.hybrid-autos.info/images/stories/Technik/Energiespeicher/Ragone_Diagramm_elektrische_Energiespeicher.jpg

5. Alexander Schleicher Flugzeugbau, http://www.alexander-schleicher.de/flugzeuge/asg-32-el/

Investigations into the Design of a Two-Seat Self-Launching Motor Glider

Rosemary Taouk[1], Dr KC Wong[2]
[1]*University of Sydney, School of Aerospace Engineering, rtao9062@uni.sydney.edu.au*
[2]*University of Sydney, School of Aerospace Engineering, kc.wong@sydney.edu.au*

Abstract: This paper presents the findings of an extensive market survey that was conducted across the 65 gliding clubs in Australia to potentially come up with an Australian glider design. While Australia enjoys a relatively active gliding scene, gliding clubs across the nation are having to import gliders from overseas, thus driving up their acquisition costs, as there is no Australian glider currently in production. The purpose of the survey was to ask clubs, their acquisitions teams, as well as their members what their preferences were with regards to the configuration of the gliders that they fly. The project targeted the design of a two-seat self-launching motor glider, and subsequently, the questions were about things pertaining to the layout and materials that the glider was comprised of. The questions in the market survey scratched the surface on some very basic preferences that the design clubs entailed may have, such as seating preference, openness to new and alternative materials, like or dislike of electric propulsive systems, and whether or not gliding clubs valued cost over performance. As with any engineering design firm, starting a dialogue with the target market prior to beginning the iterative design process is highly valuable.
With over 230 respondents, the survey was very well-received and presents statistically meaningful data on which to base design decisions and to prove the marketability of the resulting glider. Some of the main findings were that the majority of gliding clubs did not possess a two-seat glider at all, and that most gliders in operation were over 25 years old. The preferred seating configuration was tandem seating, which makes for a more streamlined design and is what most glider pilots are accustomed to. Additionally, 68% of respondents stated that they would want to acquire a two-seat motor glider, and over 95% stated that they would be open to electric propulsion systems for the self-launching stage. There was a slight aversion in the market for materials that aren't composites, with storage capabilities being rated as important, and 79% of respondents being open to the purchase of such an Australian glider at lower costs than its European counterparts. A question also asked respondents to rate the importance of each individual glider attribute, thus providing quantitative results and a numerical weighting for each consideration. Performance was found to be only marginally less important than cost, with durability and ease of maintenance being the main two concerns of gliding clubs. Alternative solutions were also assessed to see if there truly is a need for an indigenous glider, with the present circumstances and market survey findings encouraging this endeavour.

Introduction

Australia currently enjoys an active gliding scene, consisting of approximately 65 clubs spread across the nation. A gap in the market was identified in the form of no Australian gliders being in production at the present time. This project has as its main focus the investigation into the market desire and overall feasibility of a two-seat self-launching motor glider. A survey was sent out, and yielded over 230 respondents, thus rendering the data statistically significant and providing insight as to the present market wants. After consideration of market need, manufacturing methods, and the results outlined in the survey, the outcome for the concept was a two-seat self-launching motor glider that was made out of composites due to weight saving and its subsequent impact on cost savings. The implementation of vacuum bag infusion was also preferred for more streamlined aircraft parts at reasonable costs, and electrical propulsion was selected for the self-launch phase.

Methodology

The methods implemented in this body of work were firstly the review of relevant literature on glider performance and cost-effective materials. Australian gliding clubs, being the target market, were surveyed in order to understand the needs of clubs and glider pilots, and in order to preface design decisions with an understanding of what would make the glider marketable. Aircraft materials and corresponding manufacturing techniques were evaluated in order to select what would be optimal in terms of acquisition, weight reduction, and tooling and manufacturing costs. Weight calculations were carried based on design methodology, and in relation to formulae for metal vs composite aircraft. Weight also impacts tooling costs, and cost calculations were then conducted to make inferences with regards to the impact of weight (i.e. material) on the overall aircraft cost. Manufacturing techniques were then evaluated in order to factor in the effect of tooling on the final cost, and to research a method that would be cost-effective but able to produce high-performing aircraft. The subsequent step was to begin the design process, after having assessed market preference for glider configuration and having decided the material and manufacturing technique, both of which drive the design. Preliminary sizing was conducted and design methodology was applied.

Results

The outcome of the comprehensive and well-received market survey was the determination that the majority of gliding clubs did not possess a two-seat glider at all, and that most gliders in operation were over 25 years old. The preferred seating configuration was tandem seating and 68% of respondents stated that they would want to acquire a two-seat motor glider. Over 95% stated that they would be open to electric propulsion systems for the self-launching stage. There was a slight aversion in the market for materials that aren't composites, with storage capabilities being rated as important, and 79% of respondents being open to the purchase of such an Australian glider at lower costs than its European counterparts. A question also asked respondents to rate the importance of each individual glider attribute, thus providing quantitative results and a numerical weighting for each consideration which indicated that gliding clubs value cost only marginally more than performance. The main two considerations for clubs were found to be durability and ease of maintenance.

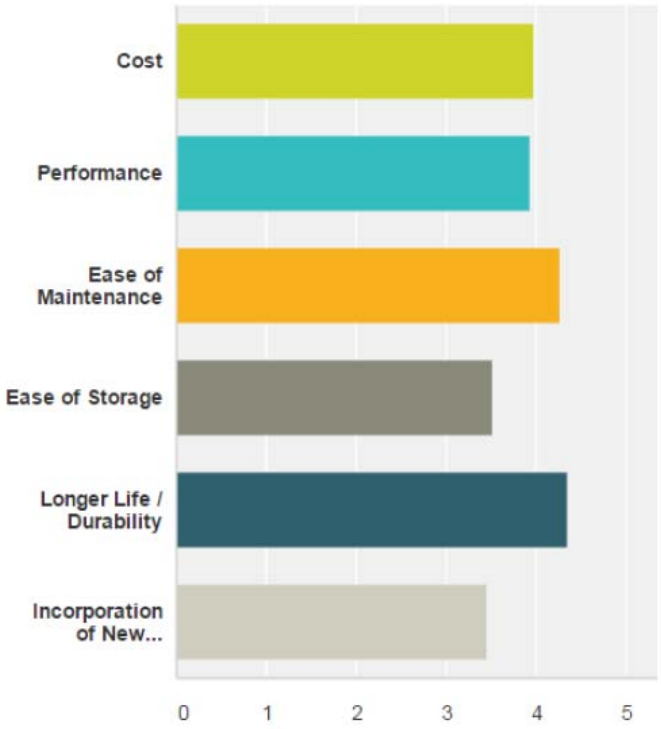

Figure 1. Statistical Distribution of Glider Attribute Rating

The outcome of the design, evaluation, and survey process is a composite glider with tandem seating and an electric engine for the self-launch stage, given the efficiency of electric starting and its appropriateness given the required power and operational ceiling of a glider. The glider would also be manufactured using the vacuum infusion process, which eliminates the need for an autoclave whilst retaining the ability to create streamlined aircraft parts. Additionally, this glider has a tapered 18m wingspan, a T-Tail, a glide ratio of 35, and Level 1 handling qualities across most flight phases.

Conclusions

Having assessed the needs of the Australian market, the market climate demonstrates a genuine problem and a real need for an indigenous glider that can cater to Australian clubs. The market is open to and supportive of a national glider design that would eliminate the need for the high acquisition and importing costs of foreign gliders. The glider that has been produced out of this work has demonstrated its marketability, appeal, performance capabilities, and feasibility. Some future work could involve making the glider more sustainable, via the addition of solar panels to recharge the engine batteries and using greener manufacturing materials, such as natural fibre composites.

Soaring meets Cruising – optimal strategies in powered flight

Mörsel, T.[1], Scheffel, P.[2]
APUS - Aeronautical Engineering GmbH
[1]t.moersel@apus-aero.de [2]p.scheffel@apus-aero.de

Abstract: The present abstract compares different strategies during electrical powered flight under consideration of the aerodynamic characteristics and the propulsion system behavior. This comparison is done for the classical retractable self-sustainer engine (RE) as well as for the Front Electric Sustainer (FES) both equipped with electric engines. Conclusions were drawn concerning the optimal strategies and optimal design for the analyzed propulsion concepts.

***Keywords*:** Electric, Strategy, Front Electric Sustainer, retractable power plant.

Introduction

In most times, the propulsion system in a powered sailplane is a trade-off of integration and available propulsion power. For electric propulsion systems, this conflict is expanded to the amount of usable energy on board due to the high mass of energy source (batteries). Focusing on high efficiency of such propulsion system is more essential than for classical, piston engine driven systems, to reach a maximum range or flight time. The pure efficiency of the overall system is mainly influenced by the engine, the propeller, the integration and the aerodynamic characteristics of the aircraft. Nevertheless, the efficiency of the aim related to the used energy could be significantly influenced by the flight strategy.
When thinking about optimal strategies in powered flights, not only the horizontal flight has to be analyzed. Alternative strategies are the saw-tooth flight and the trapezoid flight path (see Figure 3). The saw-tooth flight consists of several climb and glide sections. During the climb, primary energy is transformed to potential energy which is used in the following glide section to reach maximum range or time. This method seems to be most efficient, if the single efficiencies of the detour via the potential energy are in sum higher than the direct way (see Figure 4). The trapezoid flight path can be justified by the fact, that some system characteristics depends on the equivalent airspeed (EAS) while others are a function of the true airspeed (TAS) which deviates with increasing altitude from the EAS. For powered sailplanes, which are subjects of the present analysis, the effects are neglectable so that this strategy is excluded in the present report.
The present report compares the different flight strategies for the gliders equipped with the a RE system or a FES system. For powered sailplanes, mainly three aims are interesting for normal usage. The most important one is to maximize the possible range of the glider with a given amount of energy. The second aim is the maximization of flight time and the third is to get the maximum altitude from the given primary energy source.

Methodology

The present analysis is done for a single-seated reference sailplane with a 15 m flapped wing (S = 10 m²). In clean configuration, this aircraft has a best glide ratio of 1:45 @ 110 km/h with a take-off mass of approximately 400 kg. For estimating the aerodynamic effects of the FES, the results from IDAFLIEG measurements[1] were used. These describe an additional amount of drag coefficient due to the FES installation, slightly increasing linear with the lift coefficient. In powered flights with the FES, a further degradation of aerodynamic properties is assumed. For the effects of a RE on the aerodynamic characteristics approved information are rare. Corresponding to other publications[2], a constant increase of drag coefficient is assumed for the present analysis. Being conservative, a value of $\Delta C_W = 7.8 \cdot 10^3$ is calculated. Using these estimations, the aerodynamic power demand P for a steady flight state, described by the airspeed and the climb angle, can be computed. Integration of this power leads to a term of energy consumption per time E/T. Regarding the groundspeed this expression can be transformed to an energy consumption per range E/R. Taken the vertical speed into account an energy consumption per reached height E/H is calculated.
For the horizontal flight strategies, the expressions for E/R and E/T are sufficient to evaluate the efficiency of the flight. Regarding the saw-tooth flight path, a superposition of the energy consumption per height and the glide characteristics of the aircraft is necessary. Depending on the aim of the flight, the speed of best glide ratio or the speed for minimum sink rate must be chosen for the glide section. The lift-to-drag ratio at this speed defines the possible range or time based on a reached altitude during the climb section. Finally, a cumulative specific energy consumption for a flight with this strategy can be computed to compare it with the pure horizontal flight.
The methodology described in the previous paragraphs analyzes only the aerodynamic characteristics of the powered sailplane in the different states and strategies. When evaluating the efficiency of the complete system, the propulsion system behavior is regarded by an efficiency η which relates the aerodynamic power demand to the primary energy power demand. This efficiency is the product of engine efficiency, propeller efficiency and integration efficiency.

Results

The methodologies described in the last section were used to analyze the different propulsion system and strategies for their aerodynamic behavior. The resulting specific energy consumptions are visualized as a function of the true airspeed for the horizontal flight strategy and different values of climb rate for the saw-tooth strategy.
Figure 5 shows the range specific (aerodynamic) energy consumption and the power demand for the different states. These values include only the aerodynamic characteristics and neglect the propulsion system characteristics. The following conclusions can be stated:

- For the saw-tooth strategy the efficiency increases with higher vertical speeds during climb section. The effect is much more pronounced for the RE system (+10% from 1 m/s to 4m/s) than for the FES system (+1.2% from 1 m/s to 4 m/s). Nevertheless, both types show a convergence of the effect. For the FES system, the convergence emerges faster than for the RE-system. The increase in efficiency is coupled to a higher power demand (~170%) which is nearly similar for both propulsion types.
- Even for smaller climb rates, the reachable specific consumption with the saw-tooth strategy is lower than for the horizontal flight. With 1 m/s climb rate at saw-tooth flight, the efficiency is increased about 16,8% for the RE system and 2.8% for the FES system. Both systems need for that an approximately 2.4 times higher power demand.
- The glider equipped with a RE system needs a minimum climb rate of 3 m/s to reach the range specific energy consumption of the FES equipped glider in horizontal flight. To achieve that state, the RE has a 7 times higher power demand. This implies that gliders with RE systems needs enough power to enable high climb speeds for reaching a higher efficiency.
- The curves for the specific energy consumptions of the saw-tooth strategy are nearly flat around the minimum. This makes the system efficiency tolerant for off- optimal designed propulsion systems and deviations during the flight. In contrast to that, the optimum for the horizontal flight is very pronounced so that there is only a small margin of tolerance.

In Figure 6 the time specific (aerodynamic) energy consumption and the power demand is shown for the same conditions as discussed above. In addition to the facts listed above, the following can be stated:

- The principle behavior of the saw-tooth strategy is identical when regarding the time specific energy consumption. A difference is the reachable increase in efficiency. For the FES system, the effect is nearly the same (+1.3% from 1 m/s to 4 m/s) while the gain for the RE system is much smaller (+5.3% from 1 m/s to 4 m/s). Also, the convergence emerges faster when analyzing the time specific consumption.
- In contrast to the range analysis, the RE system needs only minimum 1 m/s at saw-tooth flight to reach the efficiency of the FES system in horizontal flight. Therefore, also weak RE systems are competitive for acceptable time specific energy consumptions

Summarizing the knowledge of the aerodynamic analysis, different setups of propulsion systems are possible. For a rough comparison study, a virtual propulsion system consisting of a EMRAX 207 and a propeller with 1 m diameter were designed for the two principle systems. For the saw-tooth profile, a setup with maximum shaft power seems to bring the maximum efficiency. Regarding the EMRAX 207 properties[3], a rotational speed of 5000 1/min is necessary for that, so that the propeller must be optimized for a rate of advance of J = 0.35. The second setup should be optimal for the horizontal flight of the FES system. The highest possible efficiency of the engine is reached for that power setting at a rotational speed of 1000 1/min so that the propeller must be optimized for a rate of advance of J = 1.8. The third power setting is defined by a medium power setting at a point of maximum engine efficiency. This is reached at approximately 3300 1/min so that the propeller must be optimal at J = 0.53. For the present analysis, it is assumed that the propeller of each setup reaches the same maximum efficiency.
Using these three different setups of propulsion system for the FES and RE equipped reference aircraft the specific primary energy consumption can be computed. The results for the optimal range specific values for each setup are shown in Table 1. For the FES system, the lowest range specific consumption is reached with the medium power setup while the RE system reaches the lowest value for the maximum power setup. Due to the lower engine and aircraft efficiency, the optimal range specific energy consumption in horizontal flight with setup #2 is 6% higher than with medium power setup. As already known from the aerodynamic analysis, only 3.9% are ascribed by the aerodynamic behavior. This implies that the EMRAX 207 engine is not optimal for the FES system with a horizontal flight strategy. On the other hand, this engine equipped with an optimal propeller for setup #2 leads to the best efficiency of the FES system using the saw-tooth strategy. Regarding the RE system, the selected engine seems not to have enough power for optimal specific consumption. Even with maximum power and lower engine efficiency the resulting overall efficiency is higher due to the better aerodynamic behavior. This implies that aircraft and propulsion system optimal points are still not harmonized so that the overall system has potential for optimization.

Conclusions

The analysis has shown that the strategy used for a flight has significant influences to the efficiency of the aircraft, expressed by the specific energy consumptions.

For the FES powered reference glider, the range and time specific energy consumption could only be reduced about 6% using the saw-tooth strategy instead of a pure horizontal flight. This reduction is associated with an increased power demand by about 520% (range) and 650% (time) compared to the horizontal flight. The higher power demand corresponds to larger engines with higher mass and high-discharge-rate batteries with lower energy density. These disadvantages have more negative effects on the efficiency than the reduction of specific energy consumption so that for a FES with defined propulsion system mass a low power system should be chosen with maximum battery capacity. The optimal strategy for such a powered sailplane is the pure horizontal flight. The propeller should be designed for a horizontal flight at the best engine operating point. In most cases this operating point is not identical with the maximum power so that even in such a propulsion setup a slight climb would be possible, albeit with low efficiency.

Regarding the reference glider equipped with a RE system, the slogan "short and sweet" describes the optimal strategy very well. The range specific energy consumption can be decreased about 26%, the time specific consumption about 16% using the saw-tooth strategy instead of a pure horizontal flight. The power demand for the saw-tooth flight is about 520% (range) and 550% (time) higher than for the horizontal flight. The selection of the optimal propulsion system depends for the RE mainly on the propulsion system characteristics: If the higher energy density of low-discharge-rate batteries and a lower engine weight compensate the poor efficiency of the aircraft in horizontal flight by more possible engine time from the defined propulsion system mass than the low power system could be the most efficient. Unless this situation is achieved, a propulsion system with high power and good climb performance is the best way to reach maximum efficiency with the saw-tooth flight.

For already existing FES and RE propulsion systems, the optimal strategy seems to be the saw-tooth flight if the drive system is able to provide sufficient climb speed. Nevertheless, this statement is mainly true if the propeller is designed for maximum climb rate at the engines sweet spot. Therefore, the optimal strategy must be computed for each aircraft type and propulsion system.

Acknowledges

Parts of the research described in the present abstract are funded by the German Federal Ministry for Economic Affairs and Energy under the Grant 20Q1512B.

References

[1] Pätzold, F., 2014: Results of Flight Performance Determination of the Lak-17a FES (S5-3117) using the comparison flight method in Aalen-Heidenheim-Elchingen, August 20th and 21st 2012. Technische Universität Braunschweig, Institut für Flugführung.

[2] Galvão, F. L.: A Note on Glider Electric Propulsion. Technical Soaring, Vol. 36, No. 4.

[3] Enstroj d.o.o: EMRAX 207 Technical Data Table. http://www.enstroj.si/ 14.11.2016

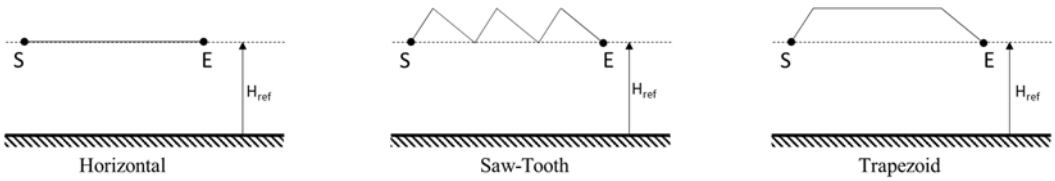

Figure 3 Different strategies for powered flights

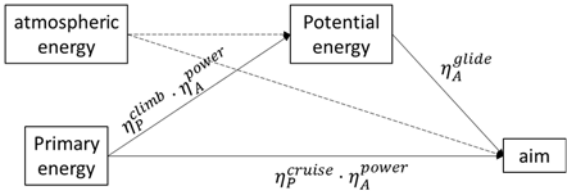

Figure 4 Principles of energy flow for powered sailplanes

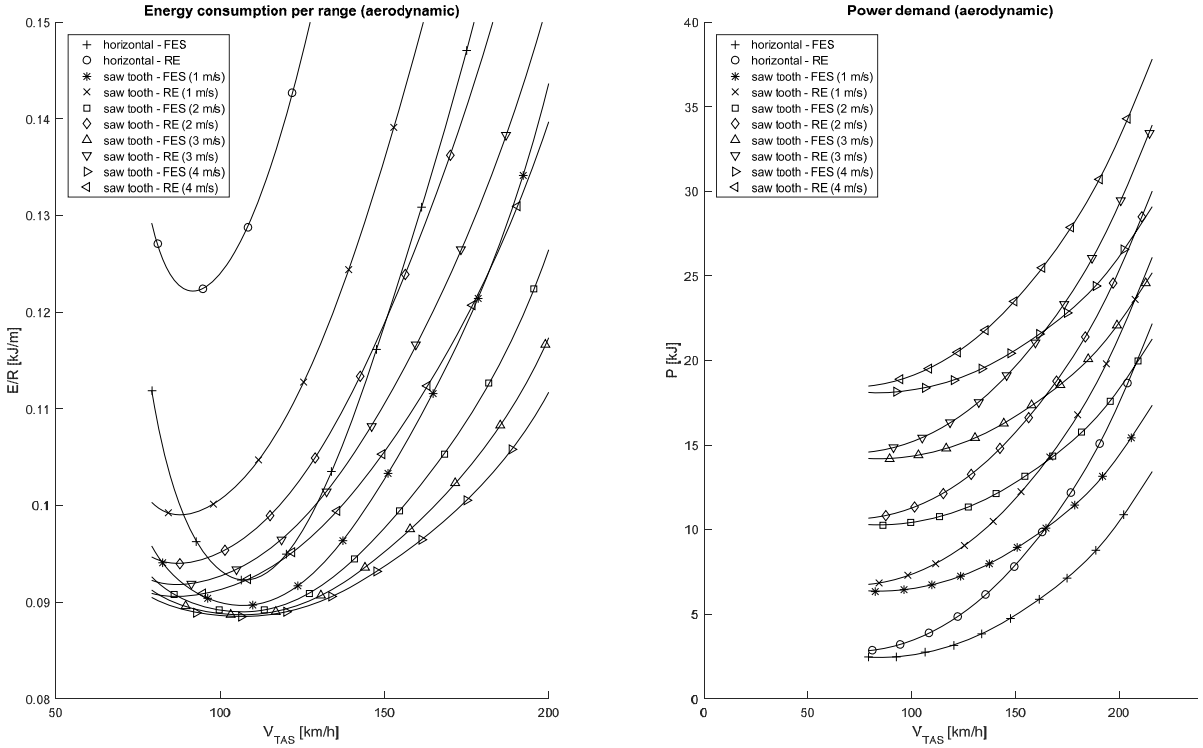

Figure 5 Range specific energy consumption and power demand (aerodynamic)

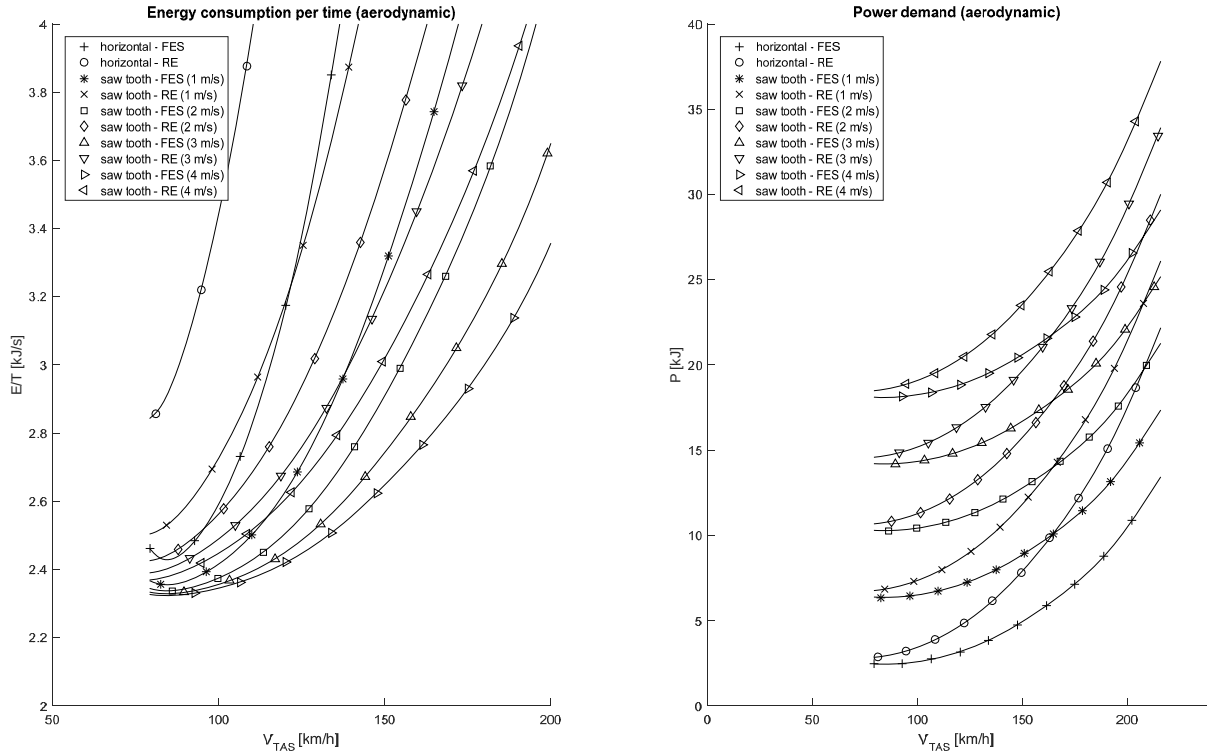

Figure 6 Time specific energy consumption and power demand (aerodynamic)

Table 1 Optimal range specific primary energy consumptions for different setups

		Setup #1		Setup #2		Setup #3	
		E/R [J/m]	P_{PE} [kW]	E/R [J/m]	P_{PE} [kW]	E/R [J/m]	P_{PE} [kW]
FES	Horizontal	194.1	4.6	**151.0**	4.5	166.1	4.9
	Saw Tooth 1 m/s	165.6	11.2	194.0	15.5	150.6	10.8
	Saw Tooth 2 m/s	153.6	17.1	---	---	144.0	16.8
	Saw Tooth 3 m/s	148.1	23.1	---	---	**142.3**	23.4
	Saw Tooth 4 m/s	**145.4**	29.3	---	---	145.0	30.7
RE	Horizontal	230.8	5.3	**203.2**	5.3	214.7	5.5
	Saw Tooth 1 m/s	174.0	11.7	---	---	161.8	11.2
	Saw Tooth 2 m/s	156.6	17.7	---	---	150.8	17.3
	Saw Tooth 3 m/s	149.5	23.6	---	---	**149.5**	24.4
	Saw Tooth 4 m/s	**146.8**	30.0	---	---	---	---

Measurement and Simulation of Potential Electromagnetic Interference Sources in Small Aircraft

Maike Fröhner, Robert Geise, Björn Neubauer
Institute for Electromagnetic Compatibility, TU Braunschweig, m.froehner@tu-braunschweig.de

Abstract: Electronic equipment used in aircraft for research or flight test must be adapted to function properly in the electromagnetic environment of these aircraft. This requires a detailed description of the existing fields. Based on simulations and measurements, the present work provides a characterization of the individual interference sources and corresponding field conditions occurring in small aircraft. A method for measuring transient fields on-site under conditions uncommon to standard EMC testing procedures is described.

Keywords: Electromagnetic Interference, Field Strength Measurements

Introduction

For the development of electronic devices, knowledge of the electromagnetic environment in which the device shall be used is essential. Compliance with the requirements described in EUROCAE ED-14 (RTCA DO-160) [1] usually guarantees the electromagnetic compatibility of certified avionics. Complete certification, as required in ED-14, is often not required for equipment temporarily installed in an aircraft. This primarily includes measuring equipment for research purposes, but may also be true for personal navigation systems and other systems. Here, a more explicit description of the electromagnetic environment is desirable.

The potential sources of interference need to be identified and, if practicable, characterized individually to facilitate the estimation of the surrounding electromagnetic fields in any particular aircraft. In the event of an interference, good knowledge of the source will simplify the process of eliminating the interference. The emitters determining the electromagnetic environment of general aviation aircraft can be divided into three groups: on-board transmitters, engine and associated components, and external influences.

On-board transmitters include radios, FLARM®, and transponders in most of the larger aircraft. The radiation is well defined in terms of transmission power, frequency, and antenna type and consequently qualifies for simulation with an appropriate computer program. The resulting fields inside and outside of the fuselage have proven to be strongly dependent on the material of which the aircraft is built.

Engine components include the ignition system in gasoline engines, starter and generator in both gasoline and diesel engines, and electric fuel pumps in most fossil fuel burning engines. Measurements were performed on a gasoline powered aircraft to examine the influence of these components on the electromagnetic fields inside the cabin. An overview of the transient nature, bandwidth, and intensity of the emissions was obtained. For future research remains the investigation of power electronics, the most relevant interference source in electric motors.

The last group, external influences, encompasses transmitters from outside the aircraft, including cellular phones of crew members, and natural influences. These have been addressed by previous works, namely [2] and [3].

Methodology

The software CST Microwave Studio® was employed to simulate the electromagnetic fields radiated by on-board transmitters. Fuselages of gliders (wooden and carbon fiber airframes) and powered aircraft (wooden and metal airframes) were modeled including the antennas. Carbon fiber as used by the aircraft industry is not part of the simulation tool's materials library and was therefore replaced by an isotropic carbon material with a conductivity of 10^5 S/m and a dielectric constant of 12. With this simulation tool, the power is introduced into the model at the feeding point of an antenna and then radiated according to the design of the antenna. Therefore, the antennas were adjusted in an iterative process to properly radiate at the applicable frequency. The propagation of the field originating from the antenna was then computed by the simulation tool within a bounding box.

The electromagnetic fields caused by the engine and its accessories do not qualify for simulation because they are neither defined in pattern, frequency, nor power. A regular field strength measurement can only be considered if the polarization and the direction of propagation is known beforehand. Therefore, a different approach is needed for the assessment of these disturbance sources. In the worst case of electromagnetic interference, the receiving device would act as a resonant antenna toward the surrounding field. It would then receive at most the voltage an actual antenna of the same size and orientation would generate at its feeding point. Hence, a loop antenna with a circumference of 80 cm was set up at the location of the copilot's seat as a generic substitute for a poorly designed device, and the received voltage was recorded by a digital storage oscilloscope.

Where possible, the sources were switched on separately to relate potential findings to specific emitters. During each measurement, the antenna was successively set up in the three directions of a Cartesian coordinate system to gain information about the approximate direction of the field. The location of the antenna remained the same. The time domain recording and subsequent Fourier transform allows the examination of transient field disturbances as may occur, for example, during an ignition event.

Results

The simulation results show that wooden airframes have little influence on the fields propagating from the antennas of radios and transponders. Carbon fiber and metal airframes, however, reflect the electromagnetic field, and thereby cause shielded areas on the inside and areas of high field intensities on the outside of the aircraft. Inside the tail boom of a glider, with the radio antenna modeled at the tail of the aircraft and the transmission power set to 10 W, an electric field strength of 2 V/m was computed for carbon fiber aircraft, whereas 28 V/m were computed for non-conductive aircraft. On the outer skin of the same boom, the field strength remains unchanged for the non-conductive aircraft, while amounting to 95 V/m on the carbon fiber aircraft. Comparable results were computed for the fields transmitted by the transponder.

In conductive airframes, resonances may occur at places were the structure forms a cavity, yet opens far enough for the waves to intrude. The vicinity of the cockpit is therefore the most likely, but not the only, position of resonances from radio signals. For a metal airframe, an electric field strength of 70 V/m was computed for a test point 3 m away from the antenna with the transmission power set to 10 W. Resonances of transponder signals arise in smaller cavities than the cockpit and require a smaller opening due to their shorter wavelength.

The electromagnetic fields emitted by the radio were measured inside the cabin of a wooden aircraft using the setup described in the methodology section. The deviation of the computed field strength from the measured field strength is 4%. Noticeably, harmonics of the carrier frequency have been found to build up in the electromagnetic spectrum within the first 50 ms after the beginning of the transmission.

Measurement of field effects inside the aircraft revealed transient electromagnetic fields originating from ignition, starter, generator and fuel pump. The voltage amplitude recorded at the feeding point of the receiving antenna varied from 1.5 mV (fuel pump) to 7 mV (ignition). The frequencies measured in the pulse of the ignition range up to 1 GHz, the maximum slew rate is $2.6 \cdot 10^6$ V/s. In the other transients, slew rates range from $5 \cdot 10^4$ V/s (fuel pump) to $6 \cdot 10^6$ V/s (generator). The duration of the pulses varies between 2.5 µs (fuel pump) and 0.1 µs (generator).

Conclusions

The description of the electromagnetic fields transmitted by radios and transponders in non-conductive airframes is sufficient for the required characterization. At the position of the receiving antenna, the computed and the measured field coincide. The propagation of FLARM® signals has not yet been simulated.

For conductive airframes, the simulation results illustrate the presence of electromagnetic resonances within the structure. The location of these resonances depend on the exact shape of the airframe. Consequently, no general statement as to their position and strength is possible. It can be asserted, however, that electromagnetic fields of high intensities are to be expected in unshielded areas. Spaces well enclosed by conductive structures usually contain very low field intensities compared to similar spaces in non-conductive airframes. To which extent this is true for real carbon fiber, as opposed to the isotropic substitute, is yet to be determined. The intensity, approximate direction, and in some cases the bandwidth of the field disturbances caused by the engine and its components at the location of the receiving antenna can be estimated from the measured results. Additional data on the electromagnetic fields at multiple test points and in other type of aircraft is needed for a sufficient characterization of the electromagnetic environment. An initial description encompassing many of the interference sources typical for small aircraft is presented with this contribution.

References

[1] Environmental Conditions and Test Procedures for Airborne Equipment, EUROCAE ED-14G, 2011.
[2] Schmidt, I., Junge, A., Schwark, M., Pötsch, S., Enders, A., and Kebel, K.: Successful Certification of WLAN Systems in Commercial Passenger Aircraft. EUROEM, Magdeburg, 2004, July 12-16.
[3] Oppermann, L., 2014: Analyse der PED-Emissionen bei einem Praxistest im Airbus A320. Bachelor Thesis, Institute for Electromagnetic Compatibility, TU Braunschweig.
[4] Balanis, C. A.: Antenna Theory, Analysis and Design. John Wiley & Sons, 2005.

The Use of Simulation in Gliding: Current State and Future Directions

Gerard Robertson
Australasian representative, OSTIV Board
gerard@xtra.co.nz

Abstract: This paper examines the results of an international survey conducted to identify the extent of the use of simulation, its possible benefits and barriers to its adoption. It concludes with the view that many of the elements of the "one best way" already exist, but are dispersed around the world, and that more co-operative effort internationally is needed to share best practice and reap the benefits possible.

Keywords: Simulation, Condor, training

Introduction

This study reviews the use of simulation in gliding, with the goals of understanding why simulation has not been widely adopted, discovering where it has been applied – successfully or otherwise – so that best practice can be identified and shared.

Simulation has several elements: the teacher, the student, the teaching material plus the combination of hardware and software that makes up the simulator itself. In addition to the teaching approach (the pedagogy), there must be some means of validating the effectiveness of the teaching and equally, of ensuring that there is no negative transfer (i.e. bad habits learnt on the simulator and transferred to real life).

Simulation has more potential applications than just teaching in the club environment e.g. the ability to train at any time of day, in any weather and to even bring the simulator to the student(s), in place of what can be a long trip to the gliding club.

Simulation can also overcome the tyranny of distance by making it possible to have instructor and student in separate, even distant locations but connected via the Internet.

As well as training, simulation also has potential as a marketing tool, showing off the sport by bringing the product to the potential club member rather than the other way around, thereby removing one barrier to attracting new members.

Even with a comprehensive survey, this study is simply the start of a voyage of discovery whereby what is discovered is used as a building block for future work.

Methodology

Information about current applications of simulation – plus the potential applications outlined above - was sought by creating and distributing a detailed survey, comprised of 40 questions, to gliding movements, clubs and simulation practitioners around the world.

Notwithstanding the co-operation of various gliding bodies, getting respondents proved challenging, possibly due to language barriers. It is hoped that more sharing will be facilitated by the publication of the results of this study.

The survey responses were analysed for common themes.

Interim results

The results are varied, but can be summarised as:

- France is the only country to have formally adopted simulation, by building about 50 forward fuselages and distributing them around the clubs. The Centre National de Vol a Voile at St Auban has also produced an outstanding guide[1] for the instructor using a simulator
- On an individual basis, the United States has some instructors[2] who have used simulation very effectively, including over the Internet, with coaching done on a commercial basis
- Simulation was used by just under half of the respondents, while just over half those not using simulation had considered it
- Amongst those who use simulation, the lack of a structured link between simulator training and actual flying was identified as the major single reason for simulation not becoming part of the club's standard practices
- Only half the clubs using simulation had done so for longer than 12 months
- The introduction of simulation in clubs has generally been the result of a single champion
- Instruction is often given by experienced pilots, not just by instructors
- Both strengths and weaknesses of simulation were identified
- Condor is the overwhelming favourite choice of software

[1] Centre National de Vol a Voile St Auban, 2014, Guide Practique de l'instructeur simulateur

[2] Paynter, F., 2011, Cross Country Soaring With Condor

Conclusion

The gliding movement is not realising the possible benefits of simulation, due to:

- the absence of a clear strategy for the use of simulation by national organisations, be it for training or marketing etc., leaving the initiative to individuals within clubs
- the lack of a clear pedagogical approach to teaching using simulation
- the time and effort involved in developing material
- studies that show that the change in thinking will deliver results (noting that there is a lot of anecdotal evidence).

This can be remedied by an international collaborative effort, under the auspices of OSTIV, to share experience and best practice. The most advanced training material, as noted, is that of the French CNVV, which the survey author is translating.

More work is thus required, which the author is happy to be part of.

Flight Performance Measurement of Gliders with GNSS-System

Kai Rohde-Brandenburger
Institute of Aerodynamics and Flow Technology; German Aerospace Center (DLR e.V)
kai.rohde-brandenburger@dlr.de

Abstract: For flight performance measurements of sailplanes at the German Aerospace Center (DLR), a new reference glider was procured and a new measurement system has been developed. The talk will give an overview of the methods used in the past and today, the new reference glider and measurement system. The system utilizes differential GNSS (Global Navigation Satellite System) solutions and measures the position and speed of two gliders relative to each other. Together with pressure and temperature sensors, the relative sink speed of the gliders can be measured very precisely and at a high rate. First stationary measurement of drag polars with the Glider Comparison Method were conducted at the annual summer meeting of the idaflieg in August 2015. The new reference glider, a modified Schempp-Hirth Discus-2C, was compared to the old reference, the „holy" DG300/17. Thereafter the polars of several other gliders were assessed. Measurement data will be used to demonstrate the analysis and the evaluation method of the new system, the validation and its advantages

***Keywords*:** *Performance, Measurement, GNSS, Glider, idaflieg*

Introduction

Since the beginning of aircraft design flight performance is an important factor for engineers. Therefore, engineers developed calculation methods to predict the performance of a new design, but because of its complexity, up to now each prediction method has its errors. For evaluating the amount of error, only flight tests can be used to compare the theory to the real glider with all construction tolerances. Even wind tunnel tests have errors, especially if the design makes use of laminar flow technology and is thus very sensible to Reynolds number effects and free stream turbulence. The performance especially for gliders is usually expressed by the best glide ratio. But nowadays it is not the only value that counts. The glide ratio at different airspeeds can show how the glider will perform on competitions, but the handling qualities will express if it is possible to achieve this performance over hours of flying without fatigue the pilot too much.

Methodology

The aerodynamic performance of an aircraft can be expressed by the glide ratio, which is the ratio of lift over drag at a given speed in calm air. Without an engine or moving air masses, to add energy in the amount of the drag, the aircraft has to sink or decelerate, only using kinetic and potential energy. For measuring a drag polar of gliders several methods can be used. Some ways to measure the performance in flight without engine are to measure the deceleration at changing speeds, the sinking of the glider at constant speed or the angle of the glide path to the earth. Since 1961 the DLR and its predecessor research institutions together with the idaflieg student groups are measuring drag polars of gliders. For this application different methods have been tested the last decades.

1. Deceleration method:

The measuring of the deceleration is highly unsteady and so the requirements for the measurement equipment are very challenging. The height has to be kept very exactly by the pilot and weather error cannot be obtained (**Figure 1**).

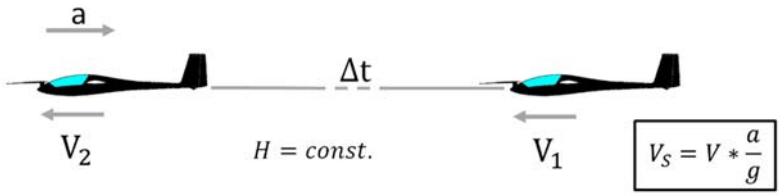

Figure 1: Deceleration method

2. Timed Descent method

Measuring of the sink speed by flying at constant speed is easier to fly and the measuring is quasi static. So the measurement equipment only has to deliver the speed, the height and the temperature. Small changes in speed can be taken into account. But the weather error of moving air masses can only be estimated by a high number of flights and statistic calculations. Therefore, a lot of flights at different weather conditions have to be done and to get a polar of one standard-class glider would take up to one week, if the weather conditions are perfect.

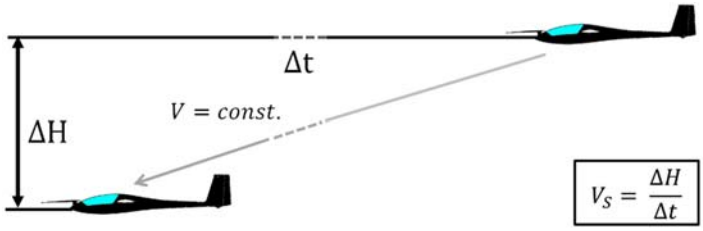

Figure 2: Timed Descent method

3. Glide Path method:

To measure the correct glide path, the angle of attack, the airspeed, the temperature and the angle to the earth's coordinate system theta have to be measured very exactly. Therefore a nose boom has to be mounted, which, in turn, affects the performance of the glider. Due to very small angle changes, the measurement errors are very high.

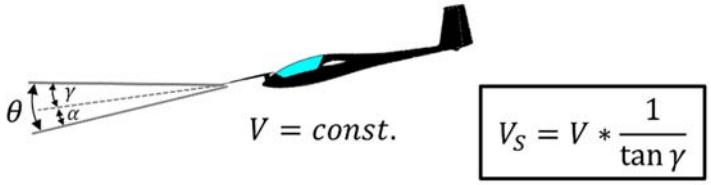

Figure 3: Glide Path method

4. Comparison method

A fast way to measure the sink speed of various gliders is to measure the relative sinking in comparison to a "reference" glider. If both planes are flying in formation, the weather error is nearly zero, because both planes are influenced in the same amount. Only the reference glider has to be measured by the time consuming method no.2. So the time for measuring the whole speed polar of a standard-class glider can be done in one day and because of its efficiency this method is used since the beginning of the DLR-/idaflieg-measurements. At the beginning the pilots were estimating the relative height, since 1973 measuring was done with the photogrammetric method taking pictures at the beginning and the end of each speed interval. With the actual sensor measurement system based on GNSS the relative position between both gliders and the whole flight is recorded and can be analyzed.

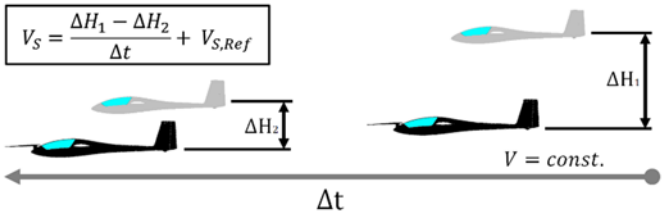

Figure 4: Glider comparison method

Over the past decades the performance of new glider designs has increased, resulting in decreased sink speed of the measured planes and thus the influence of measurement error gained prominence. The precondition of flying in formation necessitates a small difference in sinking speed of both gliders and therefore a new reference glider was procured to increase the measurement time of each speed step by decreased sinking even at higher speeds. For this new glider the DLR developed a new measurement system with very exact relative position measurement based on GNSS-Receiver. The relative position error of the new system is in range of +/- 1cm at a sampling rate of up to 10Hz, due to the Moving-Base-method. Now this can be used to decrease systematic errors, indicate random errors caused by pilot actions and to take into account plane caused speed changes (e.g. phugoid).

Results

The aim of all these efforts is the sink speed polar. From the speed polar the glide ratio polar can be derived. With the mass and wing area of the measured airplane the aerodynamic coefficients can be calculated and shown in the drag polar. While the sink speed polar is important e.g. for calculating the theoretically cross country speed in handicap systems, the glide ratio polar L/D is the most wanted by the pilot, showing even small changes in performance and gives a direct information about how many kilometers you can get from 1km of height in calm air. For the designers the aerodynamic coefficient graphs can indicate problems with laminar separation bubbles and help to determine the correct turbulator position.

To get this sink speed polar from the comparison method, every measurement segment for a flown airspeed is evaluated. At first this only results in the relative sinking speed to the reference glider. These values are converted to a height of zero meters in the standard atmosphere; therefore, the density has to be calculated with the measured temperature and static pressure. At the measured airspeed of the reference glider and its previously good determined speed polar, the related sink speed is added to the measured relative sinking and marked in the graph.

As an example, Figure 5 shows measured points of three flights in one graph. With those points a curve is fitted to improve the understanding of the course of the graph. The sinking of the reference glider and of the measured plane are plotted, the difference between both polars is the relative sinking measured with method no. 4, calculated to zero meter of height in standard atmosphere.

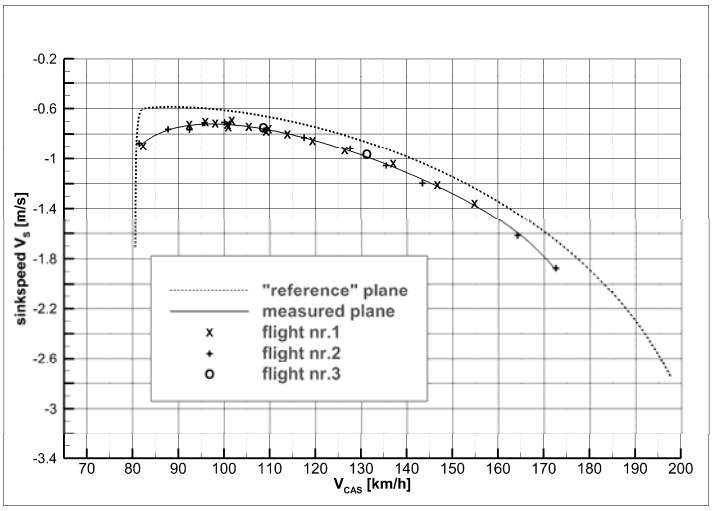

Figure 5: sink speed over calibrated airspeed of three flights

The glide ratio is calculated and shown in Figure 6. In this type of presentation all measurement deviations are better resolved.

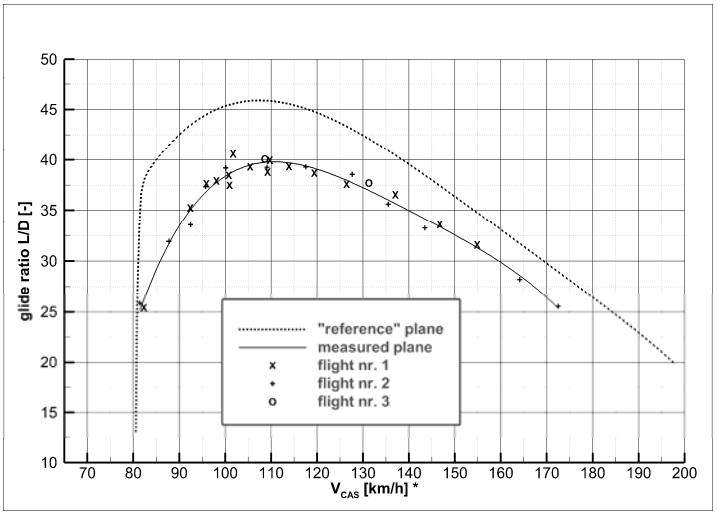

Figure 6: glide ratio over calibrated airspeed of three flights

In order to evaluate if the change from the photogrammetric method with the “holy” Cirrus as reference to the actual method with the Discus as reference changed the results, some measurements where done with older aircrafts, which have been measured years ago. Typically changes of the performance have to be expected because of worn out painting or small damages and repairs. In Figure 7 the new measurement of the SB 12 is shown and overlaid to the measured polar of 1981. During such period of time the fuselage was repainted. The wings are in good shape, but some small dents can be seen on the wing, so maybe the wing shape today is not in the same good condition. In 1981 the measurement was done with and without blowing for boundary layer control. In 2016 the SB 12 was measured again with and without blowing. The pneumatic system was deactivated by a thin tape on the blowing holes.

For comparison the results from 2016 were transformed to the same wing loading like in 1981. The graph shows nearly the same shape of the glide ratio, with a loss of 1-1.5 points at best glide ratio. Without blowing it shows the same behavior like in 1981.

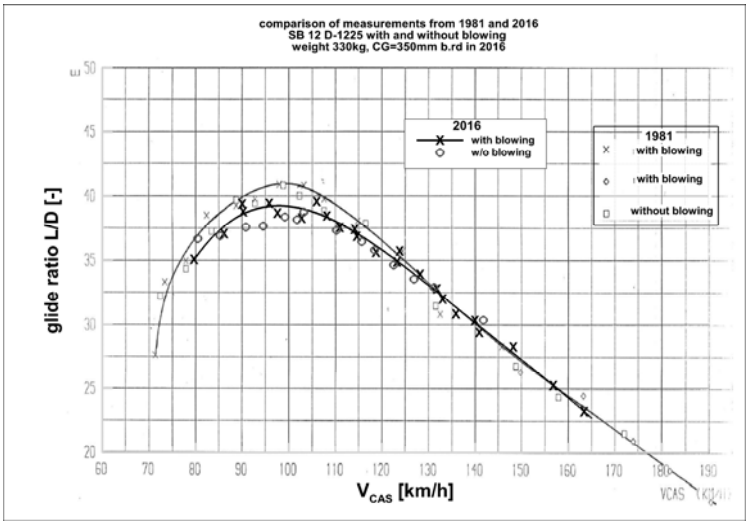

Figure 7: comparison of the measurements 1981 vs. 2016

Conclusions

Some concepts for evaluating the performance of a sailplane are presented and rapidly discussed. The used method of DLR/idaflieg is possible to measure fast and without too many influences of the pilot and the atmosphere. Therefore, some measurements are shown, to illustrate the process of the evaluation and why the same data is plotted in different graphs. Since 1961 over 300 speed polars of different sailplanes and motor gliders have been measured and collected. This data collection is used to

- improve sailplane design
- improve aerodynamic calculation methods
- to evaluate new designs and improve handbooks for engineers
- make different gliders comparable in competitions (handicap systems)
- base for the glide computing and navigation system in nearly all actual gliders
- etc…

Measurements of the SB 12 from 1981 and 2016 are overlaid in the same graph and compared. Even though there are 35 years between the measurements, the curves have the same shape and the same behavior when the blowing is switched off. The difference in best L/D may result in the new measurement system and reference plane, but it appears likely that the condition of the plane after 35years or a different CG are the cause, which is not documented in 1981.

For the new method, a detailed error calculation will be done in the future. To improve the method, several projects are planned. An experimental autopilot was built into the new reference glider to reduce error by the pilot and in speed shift. If this works, the same system will be tested for measuring turning flights for validating the calculation tools and improve turning flight performance for new glider designs.

Reinforcement Learning Algorithms for Soaring Flight in Turbulent Environments

Gautam Reddy[1], Jerome Wong-Ng[1], Antonio Celani[2], Terrence Sejnowski[3,4], and Massimo Vergassola[1]

[1]*Department of Physics, University of California at San Diego, La Jolla, CA 92093, USA*
[2]*The Abdus Salam International Centre for Theoretical Physics (ICTP), Strada Costiera, 11, I-34014, Trieste, Italy*
[3]*Howard Hughes Medical Institute, The Salk Institute of Biological Studies, La Jolla, CA 92037, USA*
[4]*Division of Biological Sciences, University of California at San Diego, La Jolla, CA 92093 USA*

Abstract: Birds and gliders exploit warm, rising atmospheric currents (thermals) to reach heights comparable to low-lying clouds with a reduced expenditure of energy. This strategy of flight (thermal soaring) is frequently used by migratory birds. Soaring provides a remarkable instance of complex decision-making in biology, and requires a long- term strategy to effectively utilize the ascending thermals. The formation of thermals unavoidably generates strong turbulent fluctuations, which constitute a significant element of soaring. Here, we approach soaring flight as a problem of learning to navigate complex, highly fluctuating turbulent environments. We simulate the atmospheric boundary layer by numerical models of turbulent convective flow and combine them with model-free, experience-based, reinforcement learning algorithms to train the gliders. For the learned policies in the regimes of moderate and strong turbulence levels, the glider adopts an increasingly conservative policy as turbulence levels increase, quantifying the degree of risk affordable in turbulent environments. Reinforcement learning uncovers those sensorimotor cues that permit effective control over soaring in turbulent environments. The algorithms require minimal processing power and are easily implementable on remote-controlled gliders equipped with a microcontroller chip.

***Keywords*:** Thermal Soaring, Reinforcement Learning, Turbulent Navigation

Introduction

Thermals are convective plumes that are created due to the formation of strong temperature gradients in the atmospheric boundary layer. The hydrodynamic processes that result in the formation of a thermal are unstable and the resulting environment around a thermal is characterized by erratic turbulent fluctuations. Local quantities such as temperature and wind speeds that could be sensed by soaring birds and gliders are thus subject to large fluctuations. Extracting information about ascending currents in such an environment is non-trivial, particularly for smaller soaring birds and remote-controlled (RC) gliders. Furthermore, the sensory observables that provide the most information about the presence of a thermal and its location within a turbulent environment are unknown. The present work attempts to find simple, general rules for soaring based on observables that can be measured by birds and RC gliders.

Techniques of thermal soaring rely on a bag of heuristics collected over decades of hobby and competitive soaring. One such heuristic, the Reichmann rules[1], states that the rate of climb rate (i.e., the vertical acceleration of the plane) is the observable that should be used to control the orientation of the glider. Other heuristics specify flight patterns that maximize the amount of air explored in the search for regions with lift. To explore a wide variety of strategies in a controlled setting, we first approached the problem of thermal soaring with numerical simulations. In the past, numerical simulations have indeed been used to learn strategies of soaring. However, past simulations[2-4] have considered the case of soaring with no turbulence or fluctuations modeled as Gaussian white noise. The simulations in Wharington et al[2] recover the Reichmann rules, however, Akos et al[5] have shown that these simple rules fail with the inclusion of modest amounts of fluctuations. We train virtual gliders in a simulated environment using modern machine learning techniques and analyze the strategies learned by the algorithms. The implications for soaring strategies and studies on soaring birds are discussed.

Methodology

Virtual gliders that follow basic aerodynamic constraints are simulated in a turbulent environment. The gliders are trained using reinforcement learning algorithms. A full description of the methodology used is described in Reddy et al[6]. Here, we summarize the key points:

Modeling the turbulent environment: Wind turbulence and thermal formation is modeled as Rayleigh-Bénard convection. Thermals are formed due to a temperature gradient created due to the sun's heating of the earth. The buoyant convection associated with thermal formation is captured in Rayleigh-Bénard convection. The corresponding equations form a set of coupled equations for the temperature and velocity fields and are derived using the Boussinesq approximation on the full Navier-Stokes equations. Full details on Rayleigh-Bénard convection are given in Ahlers et al[7]. We performed direct numerical simulations of the equations in the high-

Rayleigh number regime. In this regime, convective forces dominate and the flow is unstable, leading to turbulence. The statistics in steady state were verified with previous works.
To ensure that the strategy is robust to changes in the qualitative aspects of the environment and are not specific to Rayleigh-Bénard convection, we considered an alternative model of the atmospheric boundary layer. The model is kinematic i.e., the velocity field is specified directly, and the statistics of the velocity field are tuned so as to match the statistics observed in the atmospheric boundary layer. Specifically, Kolmogorov and Richardson laws[8] of turbulence are captured. Further, the scaling of the root-mean-square velocity[9] in the free convection layer ($v^2_{rms} \sim z^{2/3}$) and the mixed layer ($v^2_{rms} \sim$ constant) were reproduced successfully. We observed that the strategy learned in the two cases differed minimally.
Glider mechanics: We use a simplistic model of a glider in mechanical equilibrium, except for centripetal forces while turning. A glider experiences a lift force perpendicular to its velocity and a drag force antiparallel to it. The magnitudes of the lift and drag depend on the speed, angle of attack, the density of air and the surface area of the wing. The equations can be used to derive the relationship between the glide angle for different speeds and angles of attack. The turning rate of the glider is also found. The kinematics of the glider is determined by the wing loading and the dependence of the lift and drag coefficients on the angle of attack. Changing the bank angle and the angle of attack of the glider can alter the orientation and speed of the glider.

Reinforcement Learning Algorithms: The glider has to search for regions of lift, while also using the lift when it has found it. The reinforcement learning framework is particularly well poised to deal with problems involving a tradeoff between exploration and exploitation. We train gliders using the SARSA algorithm[10], which falls under the general class of reinforcement learning algorithms. The theory of reinforcement learning is phrased in the framework of a Markov Decision Process (MDP). An MDP consists of an agent traversing a state space by performing picking actions. The action to choose at each state is given by a policy. A Markovian transition matrix specifies the probability of jumping from one to state to another upon performing an action. There is a reward associated to each transition that depends on the current state, the action performed, and the future state. The goal of a reinforcement learning problem is to find the policy that maximizes the expected long-term reward. Given the transition matrix i.e., by specifying a model of the environment, an optimal solution can be obtained using dynamic programming. In other words, the expected long-term reward can be calculated explicitly and the policy is derived as the action that maximizes the expected long-term reward for each state. In our simulations, we assume that the glider does not have a model of the environment, and therefore has no *a priori* information about the dynamics of the turbulent fluctuations. The SARSA algorithm is a model-free, online algorithm that updates the expected long-term reward for each state based on the observed reward. As training progresses, the agent gets can accurate estimate of the expected long-term reward and the policy can be derived henceforth.

Experimental Setup: The learned strategies using reinforcement learning were implemented on remote-controlled (RC) gliders. The RC gliders are equipped with a Pixhawk microcontroller chip. The chip is specialized for RC plane and copter applications and can be equipped with peripheral devices such as a GPS, compass and airspeed sensors. The open-source ArduPlane codebase can be used to precisely control the ailerons, rudder, throttle and elevator via the Pixhawk. A variety of autopilot modes are available within the Pixhawk-ArduPlane system. We introduced our own soaring autopilot mode with the ArduPlane system that implements the policies learned through reinforcement learning in the simulations. The experiments were performed using a ParkZone Radian Pro soaring glider in the Poway area of San Diego.

Results

The virtual glider has control over its bank angle and angle of attack i.e., at each step it can choose to increase, decrease or keep the same bank angle/angle of attack. The gliders can sense different local quantities such as wind velocities, wind acceleration and torques on the wings (the lift on the right wing minus the lift on the left wing), which are included in the state space of the learning algorithm. The glider can sense whether the above quantities are positive high, low or negative high. The gliders are trained for 500 trials of 2.5 minutes each and the learned policy is tested on an independent test set. The criterion for good soaring performance was the average height gained in every test trial of 2.5 minutes each.
Observables for effective learning: Various observables were experimented to test which observables are needed for the best soaring performance. We learned that wind acceleration, which is approximately the rate of climb rate (at low sink rates of the glider), and the torques on the wings lead to the largest average gain of height per trial. Interestingly, wind velocities and temperature were found to not produce any improvement in the gain of height.
Control over angle of attack: The control of angle of attack was found to be unnecessary for good soaring performance. The control over angle of attack on the other hand can indeed be useful for gliders to cover large horizontal distance during cross-country soaring or bird migration as evidenced by MacCready theory[11]. We confirmed that is true in another test case of a glider traversing a two-dimensional track consisting of a series of ascending and descending columns of air with fluctuating velocities. We found that in this case, giving the gliders control over angle of attack indeed improves the soaring performance significantly.

Optimal policy: As mentioned previously, the expected long-term reward calculated using the SARSA algorithm was used to obtain the optimal policy. Since wind acceleration and torques were found to be the quantities that were most useful and the control over bank angle was the only action that is relevant, we show the optimal policy only in this case. Figure 1 shows the optimal policy in two environmental conditions– the case where the wind speeds are much smaller than the speed of the glider, and the case where the wind speeds are much larger than the speed of the glider. We observed that the policies of the glider in the two cases are mostly similar and lend themselves to simple interpretations. Careful analysis of the differences in the policies reveals that the glider is typically more conservative when the wind speeds are much larger than the glider's speed. In other words, the glider preferred to turn less in windy conditions and reacted only when it detected a particularly strong thermal.
Experimental results: The policy shown in Figure 1 was implemented on a glider and tested in an airfield at Poway, California. Preliminary results are encouraging, with the autonomous glider in certain instances gaining a height of 500 meters within six minutes. A sample trial in the field is shown in Figure 2. The glider can compute the wind acceleration using its GPS. The torque on the wings is computed by precise measurements of the fluctuations in bank angle of the glider.

Conclusions

The reinforcement learning methods described above learn policies that can cope with turbulent fluctuations. The observables and the actions that the glider could use were kept particularly simple in order to connect to what birds are likely to sense and control. The discretization of the states and action was also kept purposefully simple. Despite the simplicity of the algorithms used, we notice that the glider learns a policy that copes well with turbulent fluctuations. The policy in windy and less windy conditions can be contrasted and the differences in policy can be clearly demarcated. The learned policy is consistent with known heuristics such as the Reichmann rules but is also more general. The major advantage of our method is that any number of new observables and test situations can be tested with relative ease. For instance, our results suggest that the usage of a temperature sensor on gliders can be spared.

From a practical point of view, the policies can be easily implemented on gliders i.e., require minimal computational power and preliminary results using RC gliders show encouraging results. An exciting possibility is the implementation of the learning algorithm on the microcontroller chip so that the glider learns the policy online while gliding in real atmospheric conditions. Finally, our predictions about useful observables and the learned policy can be compared to the behavior of soaring birds and could reveal the elusive strategy that birds use to soar.

References

[1]Reichmann H. ,1988, Cross-Country Soaring (Thomson Publications, Santa Monica, CA) .
[2]Wharington J., Herszberg I., 1998, Control of a high endurance unmanned aerial vehicle. Proceedings of the 21st Congress of International Council of the Aeronautical Sciences (International Council of the Aeronautical Sciences, Bonn, Germany), Paper 98-3.7.1.
[3]Lawrance NRJ, et al., 2014, Long endurance autonomous flight for unmanned aerial vehicles. AerospaceLab 8(5):1–15.
[4]Woodbury T., Dunn C., Valasek J., 2014, Autonomous soaring using reinforcement learning for trajectory generation. Proceedings of the AIAA Aerospace Sciences Meeting (American Institute of Aeronautics and Astronautics, Reston, VA), AIAA Paper 2014-0990.
[5]Akos Z., Nagy M., Leven S., Vicsek T., 2010, Thermal soaring flight of birds and un-manned aerial vehicles. Bioinspir Biomim, 5(4):045003.
[6]Reddy G., Celani A., Sejnowski T., Vergassola M., 2016, Learning to soar in turbulent environments, Proc. Natl. Acad. Sci., vol.113, no. 33, E4877-E4884.
[7]Ahlers G., Grossmann S., Lohse D., 2009, Heat transfer and large scale dynamics in turbulent Rayleigh–Benard convection. Rev Mod Phys 81:503.
[8]Frisch U, 1995, Turbulence: The Legacy of A. N. Kolmogorov (Cambridge Univ Press, Cambridge, UK).
[9]Garrat J. R., 1994, The Atmospheric Boundary Layer. Cambridge Atmospheric and Space Science Series (Cambridge Univ Press, Cambridge, UK).
[10]Sutton R. S., Barto A. G., 1998, Reinforcement Learning: An Introduction (MIT Press, Cambridge, MA).
[11]MacCready P. B. J., 1958, Optimum airspeed selector. Soaring 1958(1):10–11.

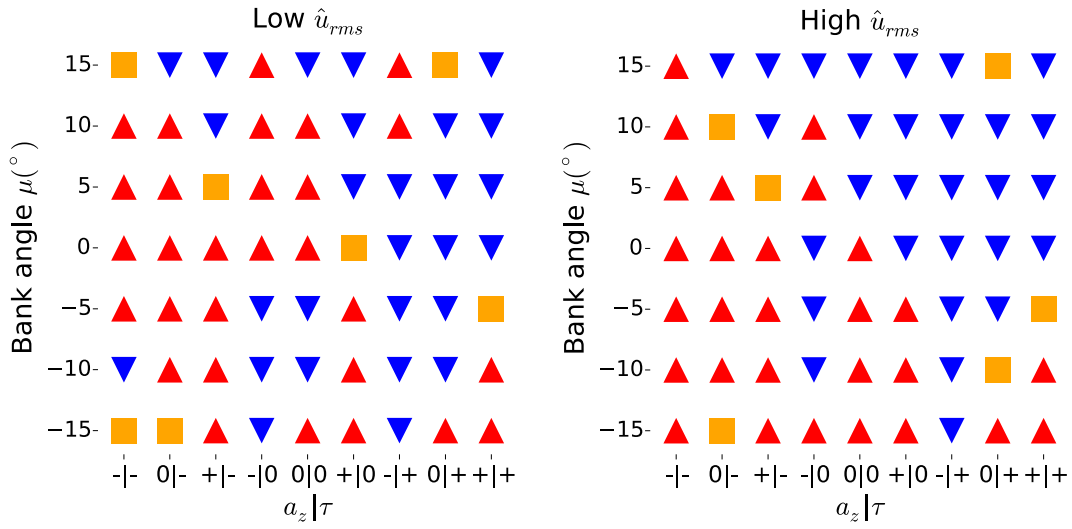

Figure 1. Learned policies

Policies of flight for different levels of turbulent fluctuations i.e., less windy (left) and windy (right) with $\hat{u}_{rms}$ defined as the ratio of average wind speed and glider speed. The plot shows the optimal action on the bank angle μ upon receiving a given sensorimotor cue of vertical acceleration and torques a_Z , τ. Here +, −, and 0 denote positive high, negative high, and low values for a_Z, τ as discussed in the text. The red upward arrow, blue downward arrow and orange square indicate that the optimal policy is to increase, decrease, or maintain the same bank angle, respectively. The figure and caption are modified versions from ref. 6.

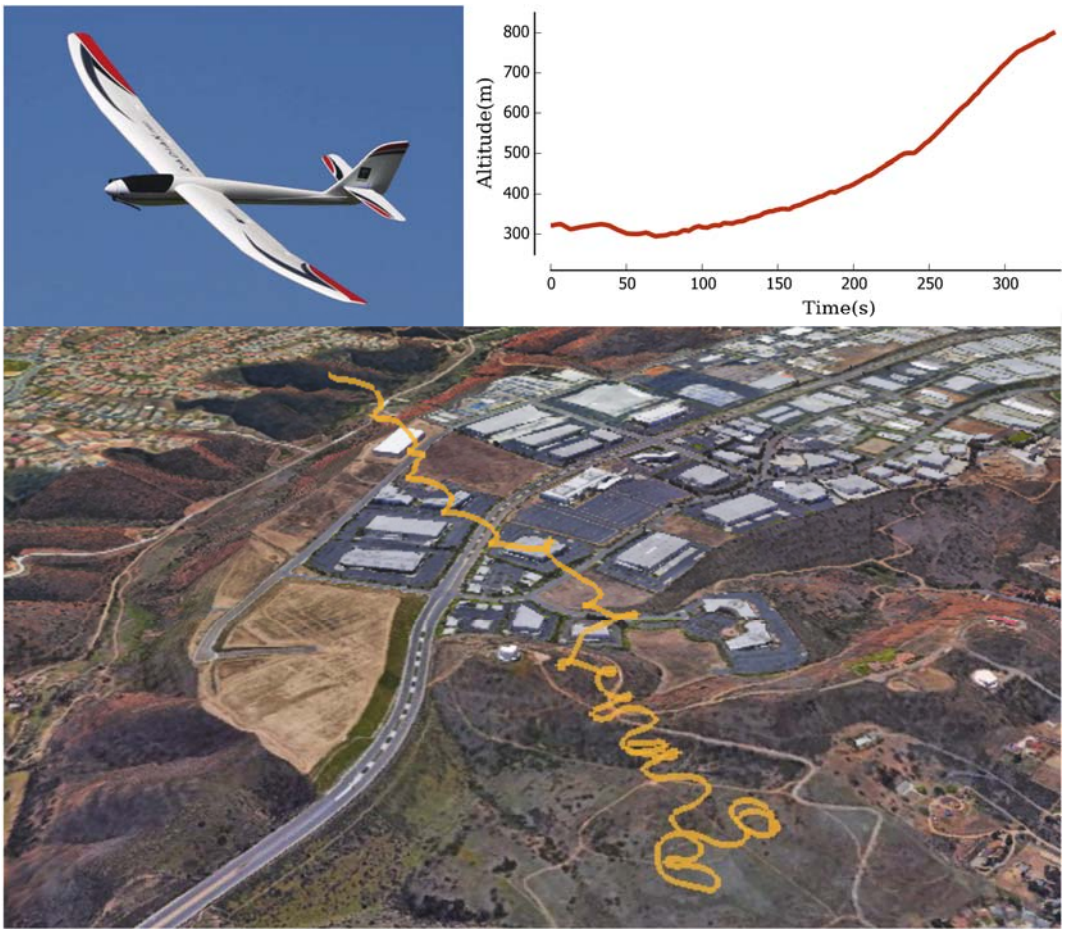

Figure 2. Sample flight trajectory of the RC glider

The policy was implemented on a Radian Pro glider using a Pixhawk flight controller. The figure shows a sample trajectory overlaid on a Google Earth image of the airfield. The plot shows the gain in relative altitude (w.r.t launch position) with time. The glider gains about five hundred meters in six minutes.

Aspects of FAI 13.5 m Class

Helmut Fendt
Braunschweig, Germany, Helmut.Fendt@lba.de

Abstract: IGC is searching technical advice for promotion of a racing class of small gliders (b = 13.5 m). Idea was to provide a racing home for microlight motor gliders, that fall below the floor of EASA regulations (300 kg takeoff mass). OSTIV Sailplane Development Panel (SDP) was approached to supply their advice and opinions about the best way to define a class of small racing gliders. Special attention should be given to the question, if a limitation of the wing loading, or the definition of a maximum takeoff mass should be preferred. In the presentation, the regulatory frame set by airlaw for such a class is highlighted. Existing airworthiness requirements, applicable for sailplanes operated outside governmental administration, are discussed. Comparison is made to internationally accepted airworthiness standards, especially in regard to safety provisions and crashworthiness requirements. Resulting from theses inputs, technical considerations and recommendations are given for introduction of such a class.

***Keywords*:** FAI 13.5 m racing class, microlights, technical definition, airlaw regulations, airworthiness requirements, safety, technical recommendations.

Introduction

IGC is currently struggling with the promotion of a racing class of small gliders (b = 13.5m). At present the class is restricted to 35 kg/m2 wing loading. Idea was to provide a racing home for the microlight motor gliders that fall below the floor of EASA regulations (currently: 300 kg takeoff mass). The wing loading limit was intended to encourage the development of new gliders by preventing the simple "sawing off" the wingtips of existing gliders. Advent of new materials, new construction techniques, and new power plants has opened up interesting possibilities for small racing gliders, and the imposition of a wing loading limit is now viewed by some as a mistake. OSTIV was requested by IGC for advice and opinions about the best way to define a class of small racing gliders.

Methodology

IGC's request was distributed by email to the members of the OSTIV SDP for preparation of the technical discussion during their meeting in Bern, Switzerland, in October 2016. During this meeting, technical, operational and legal considerations were discussed. OSTIV's President, Prof. Rolf Radespiel, reported from his talk to IGC members in Lausanne and the request for technical advice. Besides the pro's and con's regarding the technical limitations for a 13,5-m-racing class, a great part of the SDP's discussion in Bern was taken upon safety of the gliders and related certification standards. Contributions of the discussion were noted and put together to draw a picture of SDP's position.

Results

Aspects of 13,5 m class rules were considered. Wing loading limits appear as a severe restriction to the designer & manufacturer. Wing loading is difficult to measure during competition, puts uncertainty on equally designed aircraft. Wing loading limits exclude heavier pilots from competition. The use of certification standards to produce safe sailplanes is highly recommended. OSTIV SDP views class limits based on combinations of MTOM/stall speed technically preferable versus combinations of max wing loading/stall speed. At present there is no justified technical limit for MTOM or max wing loading.

Conclusions

Further technical advices of OSTIV to IGC should be based on precise requests issued by IGC.

List of Authors

Join us!

How to become an OSTIV Member ...

Visit us online at **http://www.ostiv.org** and click on **Join us!** in the menu bar.

Just load down the Application Form, fill it in and send it to the OSTIV Secretariat.

What you get ...

1. TECHNICAL SOARING, published quarterly, containing papers presented at OSTIV Congresses, reports of other OSTIV meetings and other articles dealing with the scientific and technical aspects of soaring. Digital copies of TECHNICAL SOARING are immediately available to all OSTIV members.
2. Active and Scientific/Technical members each receive a free copy of any OSTIV publication published.
3. Organizing OSTIV Congresses for the reading of scientific and technical papers during and on the World Gliding Championships.
4. Organizing and assisting training courses devoted to scientific and technical aspects of soaring.
5. Distribution of OSTV-Letters, informing members, institutions, organisations and all interested persons about the ongoing activities and matters regarding OSTIV's constitutional objectives.

... and what you give

Students under 25 years of age	free
Individual Membership	EUR 25,-- per year
Scientific/Technical Membership	EUR 80,-- per year
Active Membership	EUR 250,-- per year